frontiers | Research Topics

Advances in heart valve imaging

Edited by
Luigi P. Badano, Mani Vannan, Matteo Cameli, Konstantinos Papadopoulos, Anna Palmisano, Francesco Ancona and Antonio Esposito

Published in
Frontiers in Cardiovascular Medicine

ISSN 1664-8714
ISBN 978-2-8325-5213-1
DOI 10.3389/978-2-8325-5213-1

About Frontiers

Frontiers is more than just an open access publisher of scholarly articles: it is a pioneering approach to the world of academia, radically improving the way scholarly research is managed. The grand vision of Frontiers is a world where all people have an equal opportunity to seek, share and generate knowledge. Frontiers provides immediate and permanent online open access to all its publications, but this alone is not enough to realize our grand goals.

Frontiers journal series

The Frontiers journal series is a multi-tier and interdisciplinary set of open-access, online journals, promising a paradigm shift from the current review, selection and dissemination processes in academic publishing. All Frontiers journals are driven by researchers for researchers; therefore, they constitute a service to the scholarly community. At the same time, the *Frontiers journal series* operates on a revolutionary invention, the tiered publishing system, initially addressing specific communities of scholars, and gradually climbing up to broader public understanding, thus serving the interests of the lay society, too.

Dedication to quality

Each Frontiers article is a landmark of the highest quality, thanks to genuinely collaborative interactions between authors and review editors, who include some of the world's best academicians. Research must be certified by peers before entering a stream of knowledge that may eventually reach the public - and shape society; therefore, Frontiers only applies the most rigorous and unbiased reviews. Frontiers revolutionizes research publishing by freely delivering the most outstanding research, evaluated with no bias from both the academic and social point of view. By applying the most advanced information technologies, Frontiers is catapulting scholarly publishing into a new generation.

What are Frontiers Research Topics?

Frontiers Research Topics are very popular trademarks of the *Frontiers journals series*: they are collections of at least ten articles, all centered on a particular subject. With their unique mix of varied contributions from Original Research to Review Articles, Frontiers Research Topics unify the most influential researchers, the latest key findings and historical advances in a hot research area.

Find out more on how to host your own Frontiers Research Topic or contribute to one as an author by contacting the Frontiers editorial office: frontiersin.org/about/contact

Advances in heart valve imaging

Topic editors

Luigi P. Badano — University of Milano Bicocca, Italy
Mani Vannan — Piedmont Heart Institute, United States
Matteo Cameli — University of Siena, Italy
Konstantinos Papadopoulos — Interbalkan Medical Center, Greece
Anna Palmisano — San Raffaele Scientific Institute (IRCCS), Italy
Francesco Ancona — Servizio di Imaging Cardiovascolare, Ospedale San Raffaele (IRCCS), Italy
Antonio Esposito — San Raffaele Hospital (IRCCS), Italy

Citation

Badano, L. P., Vannan, M., Cameli, M., Papadopoulos, K., Palmisano, A., Ancona, F., Esposito, A., eds. (2024). *Advances in heart valve imaging*.
Lausanne: Frontiers Media SA. doi: 10.3389/978-2-8325-5213-1

Table of contents

frontiers | Frontiers in Cardiovascular Medicine

TYPE Editorial
PUBLISHED 11 July 2024
DOI 10.3389/fcvm.2024.1450661

OPEN ACCESS

EDITED AND REVIEWED BY
Elena Aikawa,
Harvard Medical School, United States

*CORRESPONDENCE
Konstantinos Papadopoulos
papadocardio@gmail.com

RECEIVED 17 June 2024
ACCEPTED 01 July 2024
PUBLISHED 11 July 2024

CITATION
Papadopoulos K, Badano LP, Vannan MA, Cameli M, Palmisano A, Ancona F and Esposito A (2024) Editorial: Advances in heart valve imaging.
Front. Cardiovasc. Med. 11:1450661.
doi: 10.3389/fcvm.2024.1450661

Editorial: Advances in heart valve imaging

Konstantinos Papadopoulos[1]*, Luigi P. Badano[2,3], Mani A. Vannan[4], Matteo Cameli[5], Anna Palmisano[6,7], Francesco Ancona[8] and Antonio Esposito[6,7]

[1]Echocardiography Department, European Interbalkan Medical Center, Thessaloniki, Greece, [2]Department of Medicine and Surgery, University of Milano Bicocca, Milan, Italy, [3]Department of Cardiology, Istituto Cardiologico Italiano, IRCCS, Milan, Italy, [4]Structural and Valvular Center of Excellence, Marcus Heart Valve Center, Piedmont Heart Institute, Atlanta, GA, United States, [5]Department of Medical Biotechnology, University of Siena, Siena, Italy, [6]School of Medicine, Vita Salute San Raffaele University, Milan, Italy, [7]Unit of Advanced Imaging for Personalized Medicine, IRCCS Ospedale San Raffaele, Milan, Italy, [8]Unit of Cardiovascular Imaging, IRCCS San Raffaele Scientific Institute, Milan, Italy

KEYWORDS

heart valves, imaging, transcatheter interventions, artificial intelligence, structural heart diseases

Editorial on the Research Topic
Advances in heart valve imaging

Heart valve diseases (HVD) pose significant challenges for imaging specialists, especially when combined with other cardiac pathologies. The advent of transcatheter interventions necessitates a multidisciplinary "heart team," including a skilled multi-modality imaging department. This team assesses patient suitability for various treatments, guides operations, and evaluates final results. It is now recognized that beyond the anatomical characteristics of the valves, parameters such as ventricular and atrial dimensions and performance, pulmonary pressures, and other comorbidities must be evaluated during pre-operative screening for valvulopathies.

Recent advances in three-dimensional echocardiography, 2D speckle-tracking, and cardiac CT and MRI have enhanced our understanding of the pathophysiology of a severe valvulopathy. Additionally, artificial intelligence (AI) and machine learning are becoming significant in screening and managing patients with HVD. This special issue explores the advances in imaging for HVD and the potential role of AI in the near future (Table 1).

Transcatheter Aortic Valve Implantation (TAVI) is the most common transcatheter intervention with expanding indications, garnering attention from the cardiology community. Xiao et al. studied a small cohort of patients with type-0 bicuspid aortic valve and identified predictors of success after TAVI. They found that the ellipticity index of the aortic root and bulky calcifications of aortic commissures differed between success and failure subgroups. Bulky calcifications were determined by visual assessment using multidetector CT transverse planes and maximum intensity projections. Multivariate analysis revealed though that only bulky calcifications had negative correlation with device success post-TAVI. This study highlights the importance of calcification degree and distribution in managing patients with bicuspid aortic valve, suggesting that a larger patient series could further improve TAVI outcomes for this group.

TABLE 1 Summary of all articles with authors and main findings included in this special issue.

Authors	Title	Summary
Aortic Stenosis – TAVI		
Xiao et al.	Determinants of device success after transcatheter aortic valve replacement in patients with type-0 bicuspid aortic stenosis	Bulky calcifications of AOV commissures play a negative role in the device success after TAVI in type-0 BAV
Parasca et al.	Right ventricle to pulmonary artery coupling after transcatheter aortic valve implantation-Determinant factors and prognostic impact	RV-PA coupling is improving after TAVI except for patients with persistent pulmonary hypertension. Baseline measurements of RV-PA coupling can provide information about patients' outcomes
De la Torre Hernandez et al.	First description and validation of a new method for estimating aortic stenosis burden and predicting the functional response to TAVI	LVOT flow velocity and aortic pressure loops can predict the functional improvement after TAVI through the parameter "[P (Vmax) – P (Vo)]/Vmax and lead to better quality-of life post-procedure
Pestiaux et al.	3D histopathology of stenotic aortic valve cusps using ex vivo microfocus computed tomography	High-resolution microfocus-CT can define the AOV calcification burden and cusps thickness. Aortic valves have thinner cusps with less calcium in low-gradient stenosis rather in high-gradient.
Namasivayam et al.	Machine learning prediction of progressive subclinical myocardial dysfunction in moderate aortic stenosis	AI identified peak AOV gradient, dimensionless index, baseline GLS and energy loss as predictors of subclinical myocardial dysfunction progression in moderate AS.
Mitral valve pathology		
Apostolou et al.	Case report: Aborted sudden cardiac death as a first presentation of severe mitral annulus disjunction-a case series and review of the literature	Cardiac MRI is important in detecting fibrosis as a cause of malignant arrhythmias and SCD in MAD syndrome
Papadopoulos et al.	The added value of three-dimensional transthoracic echocardiography in mitral annular disjunction: a case report	Three-dimensional echocardiography can provide most echocardiographic features of MAD syndrome and detect the presence of fibrosis through 4D strain analysis.
Zheng et al.	Understanding post-surgical decline in left ventricular function in primary regurgitation using regression and machine learning models	AI can detect the decline of EF after MV repair in patient with primary MR. EF, Sphericity index, LV end-systolic diameter and circumferential strain rate detected a post-operative EF < 50% in the random forest model.
Mihos	Left ventricular remodeling, mechanics, and the COAPT trial	COAPT criteria should be followed in patients with SMR and HFrEF but baseline GLS can further predict the LV remodeling after TEER and should be evaluated
HVD and coronary artery disease		
Molenaar et al.	The impact of valvular heart disease in patients with chronic coronary syndrome	A thorough echocardiographic examination should be conducted in all patients with CAD since HVD and especially moderate TR indicate myocardial damage and a poorer prognosis in these patients
Multimodality imaging and complex cardiac surgery		
Huenges et al.	Case report: The woman with the big heart-an imaging-guided attempt of surgical reduction	Multimodality imaging guided a complete pre-operative planning of a case that demanded atrial reduction along with MV replacement and CABG with a successful result

Right ventricular (RV) dysfunction and pulmonary hypertension are crucial in determining TAVI outcomes. Parasca et al. showed that RV-pulmonary artery (PA) coupling improves after TAVI, except in patients with persistent pulmonary hypertension. They emphasized the importance of evaluating RV-PA coupling during TAVI screening. A baseline RV-free wall longitudinal strain (FWLS)/pulmonary artery systolic pressure (PASP) cutoff of 0.63 was able to differentiate between normal and impaired RV-PA coupling, providing valuable prognostic information and guiding treatment decisions to improve patient outcomes.

Predicting the response after TAVI is vital since 20% of patients continue to experience poor quality of life post-procedure. De la Torre Hernandez et al. validated a new method to assess aortic stenosis (AS) burden and functional outcome after TAVI. This method integrates left ventricular outflow tract flow velocity and aortic pressure, focusing on parameters like "[P (Vmax) – P (Vo)]/Vmax," an independent predictor of functional improvement post-TAVI. This approach offers a more comprehensive hemodynamic assessment, potentially leading to better patient outcomes and quality of life post-procedure.

Understanding aortic stenosis mechanisms is crucial for treatment and patient outcomes. Pestiaux et al. analyzed the microstructure of calcified aortic valve cusps using high-resolution microfocus CT, demonstrating the calcification burden and cusp thickness. They found that aortic valves have thinner cusps with significantly less calcium in low-gradient vs. high-gradient patients. While not routine, this examination can enhance *in vivo* imaging protocols and clinical data interpretation.

AI plays a significant role in diagnosing structural heart diseases. Namasivayam et al. applied artificial neural networks to echocardiographic data from patients with moderate AS, identifying predictors of subclinical myocardial dysfunction progression. Key factors include peak gradient, dimensionless index (DI), baseline left ventricular global longitudinal strain (GLS), and energy loss. These parameters should be closely monitored in patients with moderate AS.

Mitral valve pathology, including new entities like mitral annular disjunction (MAD), is also under extensive research. Apostolou et al. described cases of aborted sudden cardiac death in patients with mitral valve prolapse and MAD, investigated using cardiac MRI, which revealed fibrosis associated with

malignant arrhythmias. This highlights the significance of multimodality imaging and interdisciplinary collaboration for managing such patients. Papadopoulos et al. suggested that three-dimensional transthoracic echocardiography and 4D strain analysis might suffice to demonstrate MAD features and fibrosis presence, but this needs validation through larger studies.

AI has been tested in mitral valve diseases as well. Zheng et al. used regression and machine learning models to predict postoperative ejection fraction (EF) decline in primary mitral regurgitation (PMR) patients. The random forest model accurately detected patients with postoperative EF < 50%, including predictors like LVEF, LV sphericity index, LV end-systolic diameter (LVESD), and LV mid-systolic circumferential strain rate. Although further research is needed, this study suggests a more accurate preoperative assessment for these patients.

LV mechanics are crucial for outcomes after transcatheter edge-to-edge repair (TEER) in secondary mitral regurgitation (SMR) patients. Mihos emphasized the importance of GLS in predicting left ventricular remodeling, crucial for patient prognosis. Following the echocardiographic criteria from the COAPT trial, which demonstrated TEER benefits in heart failure with reduced ejection fraction (HFrEF) and SMR, is recommended. However, deformation metrics might provide additional data on TEER responders. Heart teams managing these patients should also consider guideline-directed medical therapy and cardiac resynchronization therapy (CRT) when indicated.

In a study of about 2,000 patients, Molenaar et al. found that HVD affect prognosis in coronary artery disease (CAD) patients. LV dysfunction and moderate or severe HVD were the main indicators of higher mortality. Moderate tricuspid regurgitation (TR) was the strongest mortality predictor in multivariable regression analysis. HVD often indicates a higher atherosclerotic burden and more significant CAD, leading to more common myocardial damage and poorer prognosis. A thorough echocardiographic examination should be conducted when screening CAD patients.

Cardiac surgery has also progressed, allowing for the efficient management of complex cases. Huenges et al. described treating a patient with a gigantic left atrium requiring mitral valve replacement and coronary artery bypass grafting (CABG). Thorough multi-modality imaging with echocardiography and cardiac CT facilitated a successful operation, including atrial reduction techniques and MV replacement.

In summary, advances in imaging and AI are transforming the management of HVD and improve patients' outcomes through more accurate preoperative assessments and innovative treatment approaches.

Author contributions

KP: Writing – original draft. LB: Writing – review & editing. MV: Writing – review & editing. MC: Writing – review & editing. AP: Writing – review & editing. FA: Writing – review & editing. AE: Writing – review & editing.

Conflict of interest

The authors declare that the research was conducted in the absence of any commercial or financial relationships that could be construed as a potential conflict of interest.

The author(s) declared that they were an editorial board member of Frontiers, at the time of submission. This had no impact on the peer review process and the final decision.

Publisher's note

frontiers | Frontiers in Cardiovascular Medicine

TYPE Opinion
PUBLISHED 31 January 2023
DOI 10.3389/fcvm.2023.1124727

OPEN ACCESS

EDITED BY
Anna Palmisano,
San Raffaele Scientific Institute (IRCCS), Italy

REVIEWED BY
Stephan Stöbe,
Leipzig University, Germany
Yasufumi Nagata,
Massachusetts General Hospital and Harvard Medical School, United States

*CORRESPONDENCE
Christos G. Mihos
✉ christos.mihos@msmc.com;
✉ drcmihos@gmail.com

SPECIALTY SECTION
This article was submitted to Heart Valve Disease, a section of the journal Frontiers in Cardiovascular Medicine

RECEIVED 15 December 2022
ACCEPTED 16 January 2023
PUBLISHED 31 January 2023

CITATION
Mihos CG (2023) Left ventricular remodeling, mechanics, and the COAPT trial. *Front. Cardiovasc. Med.* 10:1124727. doi: 10.3389/fcvm.2023.1124727

Left ventricular remodeling, mechanics, and the COAPT trial

Christos G. Mihos*

Echocardiography Laboratory, Division of Cardiology, Columbia University Irving Medical Center, Mount Sinai Heart Institute, Miami Beach, FL, United States

KEYWORDS

echocardiography, edge-to-edge repair, global longitudinal strain (GLS), left ventricular remodeling, mitral valve repair (MV repair), secondary mitral regurgitation (SMR), speckle-tracking echocardiography

1. Introduction

Symptomatic mitral valve (MV) regurgitation is a common cause of morbidity amongst cardiovascular disease patients, with a 1.3-fold increase in prevalence per decade of life past 60 years of age (1). More specifically, secondary mitral regurgitation (SMR) remains a troubling sequela of ischemic heart disease, dilated cardiomyopathy, and atrial myopathy. The mechanisms of SMR are complex, interrelated, and centered on left ventricular (LV) dilatation and abnormal geometry, papillary muscle displacement, MV leaflet tethering, and altered annular shape and mechanics (2, 3). Surgical mitral valve repair (MV repair) has resulted in disappointing long-term outcomes in the SMR population, while replacement predisposes to continued adverse LV remodeling, peri-operative morbidity, and prosthetic valve complications (4, 5).

Conversely, the Cardiovascular Outcomes Assessment of the MitraClip Percutaneous Therapy for Heart Failure Patients with Functional Mitral Regurgitation (COAPT) trial showed that in carefully selected patients with moderate-to-severe SMR, MV transcatheter edge-to-edge repair (TEER) improves heart failure symptoms and survival, and decreases heart failure hospitalizations at 2-year follow-up when compared with medical therapy alone (6). In a recent post-hoc analysis the COAPT investigators analyzed risk of death or heart failure hospitalization according to baseline LV global longitudinal strain (GLS), which is a robust, reproducible, and sensitive marker of myocardial function. Between 10 and 24 months of follow-up, patients with a GLS $<-13.2\%$ had a lower risk of death or heart failure hospitalization when compared with those having a GLS $>-10.8\%$, although all patients receiving TEER garnered clinical benefit when compared with medical therapy alone (7). Herein we discuss the importance of LV remodeling and mechanics assessed by 2D and speckle-tracking echocardiography in patients with cardiomyopathy, and its application in the SMR and TEER population.

2. Left ventricular deformation, shape, and mechanics

The ventricular myocardium is composed of a surrounding basal loop with circumferential fibers in a transverse orientation, and an inner apical loop helix with oblique fibers oriented at approximately 60° angles (8). The interaction between the basal and apical loops results in systolic ejection, diastolic relaxation, and ventricular torsion. Essential to proper mechanics is the elliptical shape of the LV, which supports the oblique orientation of the apical loop limbs. In this state, a normal 15% myofiber shortening results in a LV ejection fraction of 60% through efficient myocardial contraction, shortening, and dispersed shearing forces. Conversely, in the

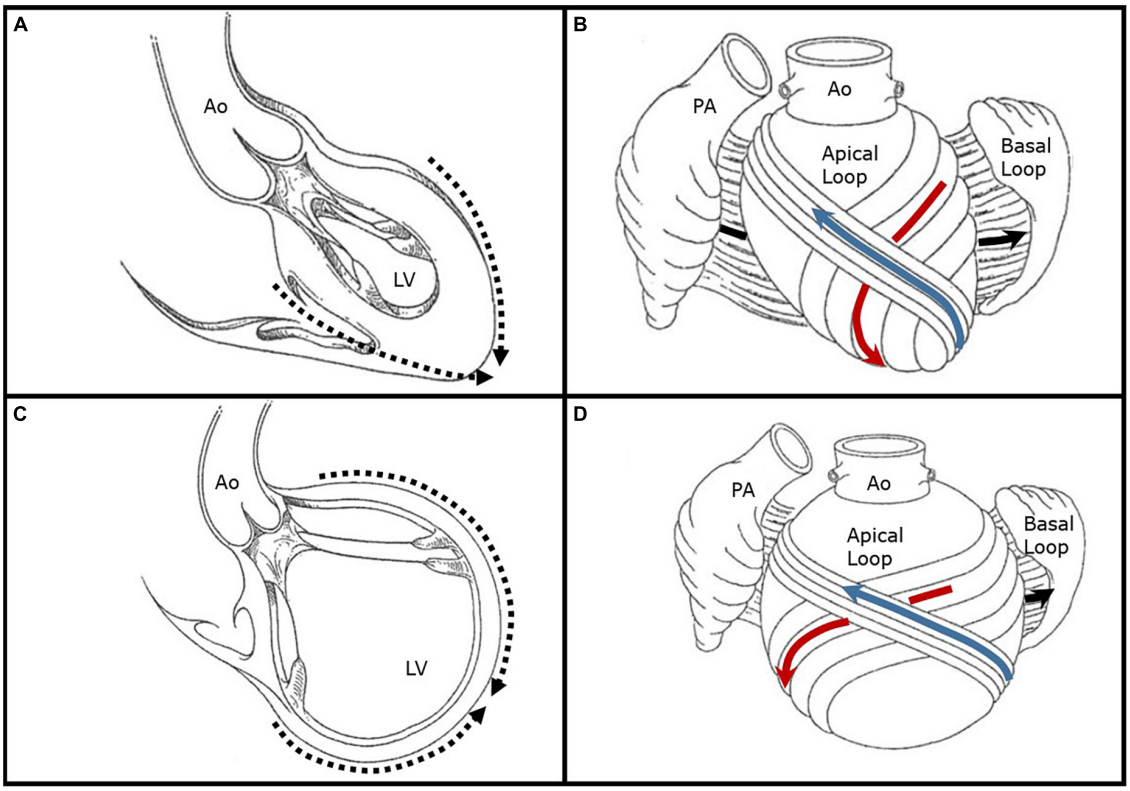

FIGURE 1
Illustrative representations of left ventricular remodeling and alteration in chamber shape and myofiber orientation. **(A)** Depicted is a left ventricle with a normal elliptical shape forming an apical cap (dashed arrows) with preserved papillary muscle orientation. **(B)** The basal ventricular loop is depicted open with circumferential fibers in a transverse orientation (black arrow) which surround an inner apical loop helix. The descending limb of the apical loop (red arrow) converges into a vortex at the apical cap which then crosses superficially to form the ascending limb (blue arrow). The myofibers of the apical loop limbs are oriented obliquely at approximately 60° angles, and their normal shortening of 15% produces an ejection fraction of 60%. **(C)** Depicted is a remodeled left ventricle with a spherical shape and lack of a true apex (dashed arrows). The chamber is markedly dilated and there is papillary muscle displacement. **(D)** In the setting of left ventricular dilatation and sphericity, the apical loop myofibers are stretched and adapt a transverse orientation similar to the basal loop. Transverse, or circumferential, fiber shortening generates an LV ejection fraction closer to 30%. Figures are adapted with permission from Buckberg et al. (19). Ao, aorta; LV, left ventricle; PA, pulmonary artery.

setting of LV dilatation and sphericity, the myofibers are stretched and adapt a transverse orientation similar to the basal loop; transverse, or circumferential, fiber shortening generates an LV ejection fraction closer to 30% (9). This latter LV remodeling provides the substrate for papillary muscle displacement, incomplete MV systolic closure, and SMR (**Figure 1**).

The electromechanical activation of the apical loop results in longitudinal ventricular shortening, which can be assessed by measuring GLS using speckle-tracking echocardiography. Importantly, full wall GLS takes into account the pivotal transmural mechanical interaction between the subendocardial, mid-wall, and subepicardial myofibers (10). GLS is useful in detecting subclinical myocardial dysfunction in the setting of preserved LVEF, while in dilated and ischemic cardiomyopathy it can provide insight into the degree of myocardial impairment (11). In a large study by Namazi et al. (12) of 650 patients with moderate or greater SMR, a GLS $>-7\%$ was independently associated with increased all-cause mortality (HR 1.34, 95% CI 1.04–1.72, $p = 0.02$) at a median follow-up of 56 months. When compared with patients who had a GLS $<-7\%$, those with GLS $>-7\%$ had more extensive LV remodeling with larger end-diastolic (124 vs. 92 ml/m^2, $p < 0.001$) and end-systolic volume (96 vs. 63 ml/m^2, $p < 0.001$) indices, and higher filling pressures (12).

3. The COAPT study and LV remodeling

The impact of LV remodeling on the performance of TEER is critical in interpreting the results of the COAPT study, and in translating its success to clinical practice. The inclusion criteria for enrollment in COAPT were: (1) symptomatic heart failure and moderate to severe SMR despite optimal guideline-directed medical therapy; (2) LVEF 20–50%; (3) LV end-systolic diameter <70 mm; (4) pulmonary artery systolic pressure <70 mmHg; and, (5) no evidence of significant right ventricular dysfunction. The 614 patients enrolled in COAPT had a mean LV end-diastolic volume index, LVEF, and GLS of 101 ml/m^2, 31%, and −11.9%, respectively. These characteristics are in sharp contrast to the Multicentre Study of Percutaneous Mitral Valve Repair MitraClip Device in Patients with Severe Secondary Mitral Regurgitation (MITRA-FR) trial, which showed no benefit of TEER in 307 patients randomized to percutaneous MR correction vs. medical therapy (13). The main inclusion criteria for MITRA-FR were: (1) symptomatic heart failure and severe SMR with guideline-directed medical therapy per "real-world" practice; and, (2) LVEF 15–40%. The mean LV end-diastolic volume index and LVEF in MITRA-FR were 135 ml/m^2 and 33%, with no data on GLS reported.

It is hypothesized that the discrepancy between COAPT and MITRA-FR regarding the benefits of TEER in patients with SMR was influenced by the extent of LV remodeling and alteration of mechanics. An important caveat to consider when interpreting the study results and emphasizing LV remodeling is that different echocardiography core labs were utilized by the respective trialists, which could potentially introduce uncontrollable confounding. Nevertheless, the patients in COAPT were reported to have a significantly smaller LV size and had to meet a specific cut-off for inclusion based on the maximum systolic chamber dimension, despite a similar LVEF when compared with MITRA-FR patients. It is well established in the surgical literature that the extent of pre-operative LV remodeling is one of the most powerful predictors of a durable MV repair and that there is a threshold beyond which the LV damage and fibrosis is irreversible (14). Important echocardiographic LV parameters that predict MV repair failure include an LV end-diastolic diameter >65 mm or a systolic sphericity index ≥0.7 (15, 16). GLS has been shown to perform well as surrogate marker for LV replacement fibrosis detected by cardiac magnetic resonance imaging in patients with dilated cardiomyopathy, with a value of >−7.9% having an area under the curve of 0.74 ($p < 0.05$) (17). In patients undergoing TEER, a baseline GLS >−9.3% predicts lack of LV reverse remodeling and persistent LV dilatation and sphericity at 2-year follow-up (AUC 0.84, $p < 0.001$) (18). A fair interpretation of this data within the context of the GLS observations from COAPT and the study by Namazi et al. (12), is that similar to patients undergoing surgical MV repair, TEER in the setting of advanced LV remodeling and fibrosis provides minimal clinical benefit at the expense of procedural risk and healthcare-related costs.

4. Conclusion

While the aforementioned hypothesis regarding LV remodeling and GLS in patients with SMR undergoing TEER requires prospective and external validation, it provides important insights into appropriate patient selection and factors contributing to the success and application of this relatively new therapy. Pure SMR is primarily a ventricular disease with concomitant histopathologic mitral leaflet remodeling, and as such, it is advisable that our inclusion criteria when selecting candidates for TEER be modeled strictly after those applied in the COAPT trial. Significant GLS impairment may be considered as a risk factor for a lack of LV reverse remodeling and suboptimal outcomes after TEER, with specific cut-off values for clinical use to be determined. Additionally, maximally tolerated guideline-directed medical therapy, as well as cardiac resynchronization therapy when appropriate, are of paramount importance. Taking these factors into account may allow for appropriate risk stratification, expectant management, and a pathway to improved patient outcomes.

Author contributions

The author confirms being the sole contributor of this work and has approved it for publication.

Conflict of interest

CM received research grants and speaker honorarium from GE Healthcare.

The author declares that the research was conducted in the absence of any commercial or financial relationships that could be construed as a potential conflict of interest.

Publisher's note

References

1. Coffey S, Roberts-Thomson R, Brown A, Carapetis J, Chen M, Enriquez-Sarano M, et al. Global epidemiology of valvular heart disease. *Nat Rev Cardiol.* (2021) 18:853–64. doi: 10.1038/s41569-021-00570-z

2. Silbiger J. Mechanistic insights into ischemic mitral regurgitation: echocardiographic and surgical implications. *J Am Soc Echocardiogr.* (2011) 24:707–19. doi: 10.1016/j.echo.2011.04.001

3. Tibayan F, Rodriguez F, Zasio M, Bailey L, Liang D, Daughters G, et al. Geometric distortions of the mitral valvular-ventricular complex in chronic ischemic mitral regurgitation. *Circulation.* (2003) 108(Suppl 1):II116–21. doi: 10.1161/01.cir.0000087940.17524.8a

4. Goldstein D, Moskowitz A, Gelijns A, Ailawadi G, Parides M, Perrault L, et al. Two-year outcomes of surgical treatment of severe ischemic mitral regurgitation. *N Engl J Med.* (2016) 374:344–53. doi: 10.1056/NEJMoa1512913

5. Virk S, Sriravindrarajah A, Dunn D, Liou K, Wolfenden H, Tan G, et al. A meta-analysis of mitral valve repair versus replacement for ischemic mitral regurgitation. *Ann Cardiothorac Surg.* (2015) 4:400–10. doi: 10.3978/j.issn.2225-319X.2015.09.06

6. Stone G, Lindenfeld J, Abraham W, Kar S, Lim D, Mishell J, et al. Transcatheter mitral-valve repair in patients with heart failure. *N Engl J Med.* (2018) 379:2307–18. doi: 10.1056/NEJMoa1806640

7. Medvedofsky D, Milhorini Pio S, Weissman N, Namazi F, Delgado V, Grayburn P, et al. Left ventricular global longitudinal strain as a predictor of outcomes in patients with heart failure with secondary mitral regurgitation: the COAPT Trial. *J Am Soc Echocardiogr.* (2021) 34:955–65. doi: 10.1016/j.echo.2021.04.003

8. Torrent-Guasp F, Buckberg G, Clemente C, Cox J, Coghlan H, Gharib M. The structure and function of the helical heart and its buttress wrapping. I. The normal macroscopic structure of the heart. *Semin Thorac Cardiovasc Surg.* (2001) 13:301–19. doi: 10.1053/stcs.2001.29953

9. Buckberg G, Coghlan H, Torrent-Guasp F. The structure and function of the helical heart and its buttress wrapping. V. Anatomic and physiologic considerations in the healthy and failing heart. *Semin Thorac Cardiovasc Surg.* (2001) 13:358–85. doi: 10.1053/stcs.2001.29957

10. Ünlü S, Mirea O, Duchenne J, Pagourelias E, Bézy S, Thomas J, et al. Comparison of feasibility, accuracy, and reproducibility of layer-specific global longitudinal strain measurements among five different vendors: a report from the EACVI-ASE strain standardization task force. *J Am Soc Echocardiogr.* (2018) 31:374–80. doi: 10.1016/j.echo.2017.11.008

11. Collier P, Phelan D, Klein A. A test in context: myocardial strain measured by speckle-tracking echocardiography. *J Am Coll Cardiol.* (2017) 69:1043–56. doi: 10.1016/j.jacc.2016.12.012

12. Namazi F, van der Bijl P, Hirasawa K, Kamperidis V, van Wijngaarden S, Mertens B, et al. Prognostic value of left ventricular global longitudinal strain in patients with secondary mitral regurgitation. *J Am Coll Cardiol.* (2020) 75:750–8. doi: 10.1016/j.jacc.2019.12.024

13. Obadia J, Messika-Zeitoun D, Leurent G, Iung B, Bonnet G, Piriou N, et al. Percutaneous repair or medical treatment for secondary mitral regurgitation. *N Engl J Med.* (2018) 379:2297–306. doi: 10.1056/NEJMoa1805374

14. Nappi F, Avtaar Singh S, Padala M, Attias D, Nejjari M, Mihos C, et al. The choice of treatment in ischemic mitral regurgitation with reduced left ventricular function. *Ann Thorac Surg.* (2019) 108:1901–12. doi: 10.1016/j.athoracsur.2019.06.039

15. Mihos C, Santana O. Mitral valve repair for ischemic mitral regurgitation: lessons from the Cardiothoracic Surgical Trials Network randomized study. *J Thorac Dis.* (2016) 8:E94–9. doi: 10.3978/j.issn.2072-1439.2016.01.27

16. Bouma W, van der Horst I, Wijdh-den Hamer I, Erasmus M, Zijlstra F, Mariani M, et al. Chronic ischaemic mitral regurgitation. Current treatment results and new mechanism-based surgical approaches. *Eur J Cardiothorac Surg.* (2010) 37:170–85. doi: 10.1016/j.ejcts.2009.07.008

17. Ota S, Hozumi T, Tanimoto T, Takemoto K, Wada T, Kashiwagi M, et al. Global longitudinal strain evaluated by speckle-tracking echocardiography as a surrogate marker for predicting replacement fibrosis detected by magnetic resonance-late gadolinium enhancement in patients with nonischemic cardiomyopathy. *J Clin Ultrasound.* (2021) 49:479–87. doi: 10.1002/jcu.22983

18. Citro R, Baldi C, Lancellotti P, Silverio A, Provenza G, Bellino M. Global longitudinal strain predicts outcome after MitraClip implantation for secondary mitral regurgitation. *J Cardiovasc Med.* (2017) 18:669–78. doi: 10.2459/JCM.0000000000000526

19. Buckberg G, Coghlan H, Torrent-Guasp F. The structure and function of the helical heart and its buttress wrapping. VI. Geometric concepts of heart failure and use for structural correction. *Semin Thorac Cardiovasc Surg.* (2001) 13:386–401. doi: 10.1053/stcs.2001.29959

frontiers | Frontiers in Cardiovascular Medicine

TYPE Original Research
PUBLISHED 17 April 2023
DOI 10.3389/fcvm.2023.1150039

OPEN ACCESS

EDITED BY
Francesco Ancona,
Ospedale San Raffaele (IRCCS), Italy

REVIEWED BY
Erberto Carluccio,
Division of Cardiology and Cardiovascular Pathophysiology, Heart Failure Unit, Italy
Davide Margonato,
San Raffaele Hospital (IRCCS), Italy

*CORRESPONDENCE
Catalina A. Parasca
✉ catalina.parasca@gmail.com
Bogdan A. Popescu
✉ bogdan.a.popescu@gmail.com

‡These authors have contributed equally to this work and share first authorship

†Deceased

SPECIALTY SECTION
This article was submitted to Cardiovascular Imaging, a section of the journal Frontiers in Cardiovascular Medicine

RECEIVED 23 January 2023
ACCEPTED 27 March 2023
PUBLISHED 17 April 2023

CITATION
Parasca CA, Calin A, Cadil D, Mateescu A, Rosca M, Botezatu SB, Enache R, Beladan C, Ginghina C, Deleanu D, Chioncel O, Bubenek-Turconi S, Iliescu VA and Popescu BA (2023) Right ventricle to pulmonary artery coupling after transcatheter aortic valve implantation—Determinant factors and prognostic impact. Front. Cardiovasc. Med. 10:1150039. doi: 10.3389/fcvm.2023.1150039

Right ventricle to pulmonary artery coupling after transcatheter aortic valve implantation—Determinant factors and prognostic impact

Catalina A. Parasca[1,2*‡], Andreea Calin[1,2‡], Deniz Cadil[1], Anca Mateescu[2], Monica Rosca[1,2], Simona Beatrice Botezatu[1], Roxana Enache[1,2], Carmen Beladan[1,2], Carmen Ginghina[1,2†], Dan Deleanu[2], Ovidiu Chioncel[1,2], Serban Bubenek-Turconi[1,2], Vlad A. Iliescu[1,2] and Bogdan A. Popescu[1,2*]

[1]Cardiothoracic Department, University of Medicine and Pharmacy "Carol Davila", Bucharest, Romania, [2]Cardiology and Cardiovascular Surgery Department, Emergency Institute for Cardiovascular Diseases "Prof. Dr. C. C. Iliescu", Bucharest, Romania

Introduction: Right ventricular (RV) dysfunction and pulmonary hypertension (PH) have been previously associated with unfavorable outcomes in patients with severe aortic stenosis (AS) undergoing transcatheter aortic valve implantation (TAVI), but little is known about the effect of right ventricle (RV) to pulmonary artery (PA) coupling. Our study aimed to evaluate the determinant factors and the prognostic value of RV-PA coupling in patients undergoing TAVI.

Methods: One hundred sixty consecutive patients with severe AS were prospectively enrolled, between September 2018 and May 2020. They underwent a comprehensive echocardiogram before and 30 days after TAVI, including speckle tracking echocardiography (STE) for myocardial deformation analysis of the left ventricle (LV), left atrium (LA), and RV function. Complete data on myocardial deformation was available in 132 patients (76.6 $\pm$ 7.5 years, 52.5% men) who formed the final study population. The ratio of RV free wall longitudinal strain (RV-FWLS) to PA systolic pressure (PASP) was used as an estimate of RV-PA coupling. Patients were analyzed according to baseline RV-FWLS/PASP cut-off point, determined through time-dependent ROC curve analysis, as follows: normal RV-PA coupling group (RV-FWLS/PASP $\geq$0.63, $n = 65$) and impaired RV-PA coupling group (RV-FWLS/PASP < 0.63, $n = 67$).

Results: A significant improvement of RV-PA coupling was observed early after TAVI (0.75 $\pm$ 0.3 vs. 0.64 $\pm$ 0.3 before TAVI, $p < 0.001$), mainly due to PASP decrease ($p < 0.001$). LA global longitudinal strain (LA-GLS) is an independent predictor of RV-PA coupling impairment before and after TAVI (OR = 0.837, $p < 0.001$, OR = 0.848, $p < 0.001$, respectively), while RV diameter is an independent predictor of persistent RV-PA coupling impairment after TAVI (OR = 1.174, $p = 0.002$). Impaired RV-PA coupling was associated with a worse survival rate (66.3% vs. 94.9%, p-value < 0.001) and emerged as an independent predictor of mortality (HR = 5.97, CI = 1.44–24.8, $p = 0.014$) and of the composite endpoint of death and rehospitalization (HR = 4.14, CI = 1.37–12.5, $p = 0.012$).

Conclusion: Our results confirm that relief of aortic valve obstruction has beneficial effects on the baseline RV-PA coupling, and they occur early after TAVI. Despite significant improvement in LV, LA, and RV function after TAVI, RV-PA coupling remains impaired in some patients, it is mainly related to persistent pulmonary hypertension and is associated with adverse outcomes.

KEYWORDS

aortic stenosis, TAVI, coupling, right ventricle, pulmonary hypertension

Introduction

The treatment of severe aortic stenosis (AS) is guided by evidence-based recommendations (1–3). Transcatheter aortic valve implantation (TAVI) has become the preferred treatment of severe symptomatic AS in patients who are at high risk for surgery, with continuous expansion towards use in intermediate and low-risk patients (4–7). Although providing excellent short-term results, post-TAVI-associated 1–5 year mortality varies widely between 8.3% and 67.8% according to patients' risk profiles (5–7). This calls for a detailed examination of patient-related factors that have an impact on long-term survival (8). Among these, right ventricular (RV) dysfunction and pulmonary hypertension have been shown to have a negative prognostic impact after TAVI (9–11). Only a few studies have analyzed the synergic impact of these factors on mortality, by evaluating the RV to pulmonary artery (RV-PA) coupling, which integrates the RV systolic performance at a given degree of afterload through a non-invasive parameter, but using different parameters or in chronic heart failure patients (12, 13). Our study aims to assess the determinant factors and the prognostic value of RV-PA coupling, by using the ratio between right ventricle free wall longitudinal strain (RV-FWLS) and pulmonary artery systolic pressure (PASP), in patients undergoing TAVI.

Methods

Study population and procedure

Patients with severe symptomatic AS scheduled to undergo transfemoral TAVI in our center were prospectively enrolled between September 2018 and May 2020. Selection criteria included: age >40, severe AS [aortic valve area (AVA) < 1.0 cm^2, indexed AVA < 0.6 cm^2/m^2, peak aortic jet velocity ≥4 m/s, or mean gradient ≥40 mmHg]. Exclusion criteria included: hypertrophic cardiomyopathy, prosthetic aortic valve, non-transfemoral TAVI, and poor acoustic window. All patients underwent Heart Team evaluation and were deemed eligible for TAVI based on current guideline recommendations. All procedures were performed in a hybrid operating room with participation of both interventional cardiologist and cardiovascular surgeon.

All patients underwent percutaneous transfemoral TAVI with balloon-expandable valve. The procedure was performed under general anesthesia and invasive hemodynamic monitoring. Transesophageal echocardiography was used during the procedure for additional guidance and assessment. Clinical, biological, and procedural data were collected. Coronary artery disease (CAD) was defined as the presence of coronary artery lesions, previously treated (PCI or CABG) or not requiring treatment at the time of procedure. The primary outcome was a composite endpoint of major adverse cardiac events (MACE) consisting of cardiac-related rehospitalization (obtained through a search in our institutional database and a telephone questionnaire), and all-cause mortality (obtained through a query of the National Register of population records), both performed 3 years after TAVI. No event was registered in the interval between intervention and follow-up echocardiography. The study was reviewed and approved by the institutional Ethics Committee.

Definitions and data collection—echocardiographic evaluation

All patients underwent a comprehensive echocardiogram performed by experienced echocardiographers both before and 30 days after TAVI using a Vivid E95 ultrasound system (General Electric Healthcare, Horten, Norway). Data were digitally stored for offline analysis using commercially available software (EchoPac version 203; GE Medical Systems, Horten, Norway) and images were analyzed by a single trained cardiologist according to current guidelines (14). Evaluation included standard parameters used to assess AS severity: peak aortic jet velocity, peak and mean pressure gradients across the aortic valve (using modified Bernoulli equation), and AVA (using continuity equation). In the parasternal long-axis view, LV dimensions were assessed, and LV mass was calculated using Devereux's formula and indexed to body surface area (14). LV end-diastolic and end-systolic volumes were measured in the apical 4-chamber and 2-chamber views and indexed to body surface area (14). LV ejection fraction (EF) was calculated according to the Simpson's biplane method (14). Left atrial volumes were measured by the biplane method of disks and indexed for body surface area (14). Transmitral flow was assessed by PW Doppler to measure the peak early (E) and late (A) diastolic velocities, and tissue Doppler imaging of the mitral annulus on the apical 4- chamber view was used to measure the e' velocities at both the lateral and septal sites to calculate the E/e' ratio.

Myocardial deformation analysis using speckle tracking echocardiography (STE) was performed to assess LV and LA function. Evaluation included STE analysis for LV function: LV global longitudinal strain (GLS); LA function: LA global

longitudinal strain (LAϵ, reservoir function), LA systolic strain rate (SSr, reservoir function), LA early diastolic strain rate (ESr, conduit function), late diastolic LA strain rate (ASr, contractile function). Complete myocardial deformation analysis was possible in 132 out of 160 patients. Negative values of strain parameters are used as moduli (positive numbers) for ease of analysis. RV function was assessed by measuring TAPSE, the peak systolic myocardial velocity at the lateral site of the tricuspid annulus (S'RV), RV fractional area change (FAC) and RV longitudinal strain parameters by STE: peak values of global RV strain (RV-GLS), RV free wall longitudinal strain (RV-FWLS) and the interventricular septum longitudinal strain (RV-IVS). The right ventricular systolic pressure was calculated from the peak velocity of the tricuspid regurgitant jet using the Bernoulli equation and the right atrial pressure (determined by the diameter and inspiratory collapse of the inferior vena cava) was added (14). Mean pulmonary arterial pressure was derived from pulmonary arterial systolic pressure (PASP) (15). The ratio of RV-FWLS to PASP was used as an estimate of RV-PA coupling. Patients were divided according to baseline RV-FWLS/PASP ratio as follows: RV-FWLS/PASP ≥ 0.63 as normal RV-PA coupling group ($n = 65$) and RV-FWLS/PASP < 0.63 as impaired RV-PA coupling group ($n = 67$) and were analyzed accordingly.

Statistical analysis

Continuous variables are given as mean ± standard deviation and compared using the Student *t*-test. Discrete variables were expressed as counts and percentages, and comparisons between groups were done with the χ^2 or Fisher`s exact test, when appropriate. For comparisons between subgroups, Kruskal–Wallis test, Wilcoxon rank sum tests using pairwise comparisons and Chi-square test for comparing proportions (of categorical variables) between >2 groups have been used. Bonferroni method was used to adjust *p*-values for multiple comparisons.

Long-term clinical outcomes were estimated using the Kaplan-Meier method, with comparisons made using the log-rank test (overall or pair wise as appropriate).

Univariable analysis (linear and binary logistic) was used to identify potential predictors of RV-PA coupling from baseline characteristics. After careful selection of variables based on clinical judgment, univariable assessment ($p < 0.05$), exclusion of variables showing collinearity (Pearson's coefficient >0.6), and multiple testing to ensure stability, a multivariable model has been fitted (by stepwise multivariable regression analysis, linear and binary logistic).

Univariable predictors of all-cause mortality were determined using Cox proportional hazards (Enter). Multivariable analysis was also performed in a similar fashion (Forward Wald). A two-sided *p*-value of 0.05 was considered statistically significant for all tests. Time-dependent receiver operating characteristic (ROC) analysis was used to determine the associations between individual and combined surrogate parameters of RV-PA coupling and 3-year mortality (**Figure 1**). The baseline RV-FWLS/PASP cut-off point of 0.63 to discriminate between normal and impaired RV-PA coupling was determined through time-dependent ROC curve analysis based on the highest sum of sensitivity and specificity (death—AUC 0.650, CI 0.60–0.70, $p = 0.001$; sensitivity 86%, specificity 57%;) and is within the same range of previous studies associated with survival in AS or heart failure patients (12, 16, 17). Time-dependent ROC curve analysis was performed using SAS, version 9.3, software (Cary, NC). The rest of the analyses were conducted using SPSS 21.0 (SPSS, Inc., Chicago, IL, USA).

Results

Baseline characteristics

Patients with impaired baseline RV-PA coupling were younger, had more often atrial fibrillation, prior myocardial infarction, angina, and higher NYHA functional class compared to patients with normal RV-PA coupling (**Table 1**). There were no differences between groups regarding comorbidities. Even though there were no significant differences between groups regarding peak aortic jet velocity and mean transvalvular gradient (**Table 2**), there was a higher incidence of bicuspid valve and smaller AVAi in the group with impaired RV-PA coupling as compared to patients with normal RV-PA coupling ($p = 0.031$, and $p = 0.008$, respectively). Impaired LVEF was more frequent, and the impairment was more severe in patients with impaired RV-PA coupling ($p < 0.001$). Additionally, patients with impaired RV-PA coupling had more advanced cardiac damage as suggested by larger LA dimension and lower LA-GLS, larger RA and RV dimensions, and lower parameters of RV function compared to normal RV-PA coupling group ($p < 0.001$).

Echocardiographic changes after TAVI

All echocardiographic parameters describing AS severity improved significantly after the procedure (**Table 3**). Compared with baseline, there was a significant improvement of LVEF after TAVI ($p = 0.008$) and decrease of LV mass index ($p < 0.001$). Additionally, mitral valve regurgitation decreased after TAVI ($p = 0.003$) and there was also a decrease of LA volume ($p = 0.007$), and an improvement of LA function ($p < 0.001$). We found a significant improvement in RV-PA coupling after TAVI ($p = 0.007$), mainly driven by a decrease in PASP ($p < 0.001$).

Significant improvement of echocardiographic parameters describing AS severity after TAVI were further noted regardless of group (**Table 4**). LV remodeling and LV function improvement were significant after the procedure regardless of baseline RV-PA coupling status. LA function and volume significantly improved after TAVI in both groups. RA diameter significantly decreased after TAVI in the impaired RV-PA coupling group ($p = 0.046$). RV function improved after TAVI in the impaired RV-PA coupling group as measured by RV-GLS ($p = 0.001$), RV-FWLS ($p = 0.003$),

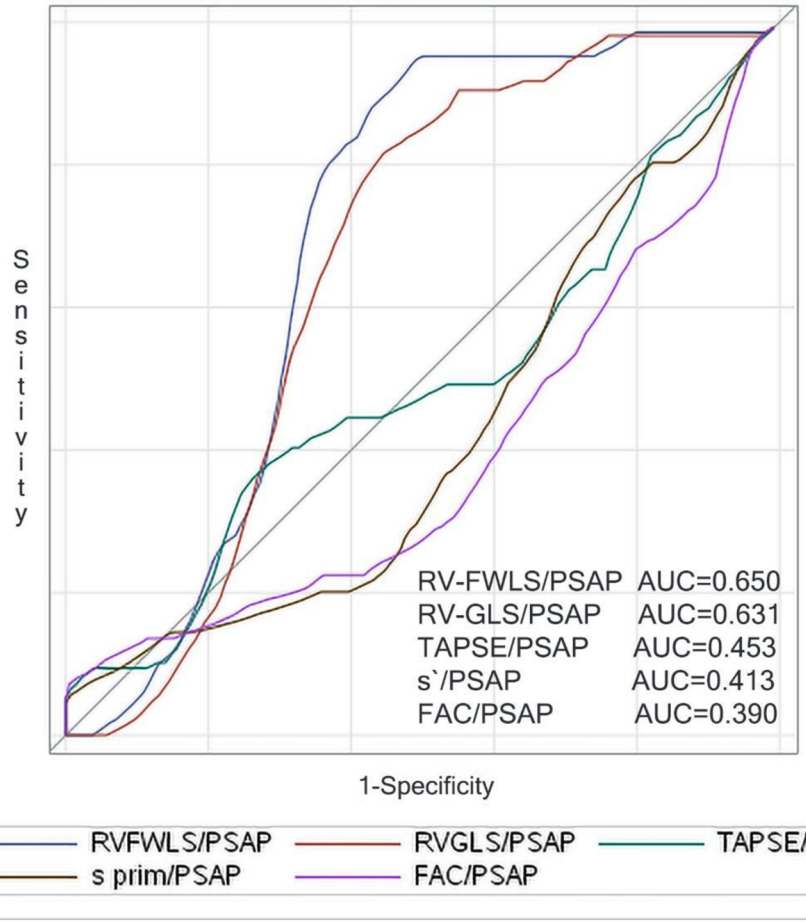

FIGURE 1
Right censored ROC curves for 3-year mortality of the parameters reflecting surrogates of baseline RV-PA coupling.

TABLE 1 Clinical characteristics.

Demographic and clinical characteristics	All patients ($n = 132$)	Normal baseline RV-PA coupling RVFWLS/PASP ≥0.63 ($n = 65$)	Impaired baseline RV-PA coupling RVFWLS/PASP <0.63 ($n = 67$)	*p*-value
Age (years)	76.6 ± 7.5	78.0 ± 5.7	75.1 ± 8.6	0.024
Gender (female)	76 (47.5%)	30 (46.2%)	37 (55.2%)	0.297
BMI (kg/m^2)	27.2 ± 4.5	26.8 ± 4.4	27.5 ± 4.6	0.375
Symptoms				
Angina	78 (59.1%)	44 (67.7%)	34 (50.7%)	0.048
NYHA functional class	2.7 ± 0.6	2.6 ± 0.6	2.7 ± 0.6	0.191
Class 2	39 (29.5%)	26 (40.0%)	13 (19.4%)	0.035
Class 3	86 (65.2%)	36 (55.4%)	50 (74.6%)	
Class 4	7 (5.3%)	3 (4.6%)	4 (6.0%)	
Comorbidities				
Atrial fibrillation	41 (31.1%)	11 (16.9%)	30 (44.8%)	0.001
CAD	74 (56.1%)	40 (61.5%)	34 (50.7%)	0.212
Prior PCI	35 (26.5%)	15 (23.1%)	20 (29.9%)	0.378
Obesity	45 (34.1%)	20 (30.8%)	25 (37.3%)	0.428
Type 2 DM	38 (29.0%)	21 (32.3%)	17 (25.8%)	0.402
COPD	13 (9.8%)	5 (7.7%)	9 (13.4%)	0.284
Anemia	57 (43.2%)	23 (35.4%)	34 (50.7%)	0.075
CKD (≥3)	31 (23.5%)	16 (24.6%)	15 (22.4%)	0.763
Frailty	54 (40.9%)	28 (43.1%)	26 (38.8%)	0.618

BMI, body mass index; DM, diabetes mellitus; CAD, coronary artery disease; CKD, chronic kidney disease; COPD, chronic obstructive pulmonary disease; NYHA, New York Hear Association Class; PCI, percutaneous coronary intervention.
Values are mean ± SD, *n* (%), or median (interquartile range).

TABLE 2 Echocardiographic characteristics.

Echocardiographic characteristics	All patients ($n = 132$)	Normal baseline RV-PA coupling RVFWLS/PASP ≥0.63 ($n = 65$)	Impaired baseline RV-PA coupling RVFWLS/PASP <0.63 ($n = 67$)	*p*-value
Aortic stenosis severity				
Vmax, m/s	4.67 ± 0.8	4.8 ± 0.8	4.6 ± 0.8	0.106
Mean gradient, mmHg	57.6 ± 19.3	59.7 ± 19.4	55.6 ± 19.3	0.233
AVAi, cm^2/m^2	0.4 ± 0.2	0.44 ± 0.2	0.37 ± 0.1	0.008
Bicuspid valve	19 (14.4%)	5 (7.7%)	14 (20.9%)	0.031
Aortic regurgitation	1.2 ± 0.7	1.3 ± 0.7	1.2 ± 0.7	0.742
Left ventricle				
LVEF, %	51.8 ± 12.2	55.0 ± 7.9	48.6 ± 14.9	0.001
LV-GLS, %	−12.4 ± 4.3	−14.2 ± 3.9	−10.5 ± 3.7	<0.001
LVMi, g/m^2	180.3 ± 50.9	174 ± 47	187 ± 53	0.154
E/A	1.2 ± 0.8	0.84 ± 0.4	1.8 ± 0.9	<0.001
Mitral regurgitation	1.3 ± 0.6	1.28 ± 0.6	1.27 ± 0.6	0.934
Left atrium				
LAAi, cm^2/m^2	15.2 ± 3.3	14.2 ± 2.4	16.3 ± 3.6	<0.001
LAVi, ml/m^2	55.2 ± 19.0	49.3 ± 13.4	61.3 ± 21.6	<0.001
LA-GLS, % (LA_ε)	12.4 ± 6.9	16.1 ± 5.9	8.6 ± 5.6	<0.001
Right ventricle				
TAPSE, cm	2.0 ± 0.4	2.2 ± 0.4	1.9 ± 0.4	<0.001
S`RV, cm/s	10.4 ± 2.8	11.5 ± 2.5	9.4 ± 2.6	<0.001
FAC, %	0.59 ± 0.3	42.6 ± 6.5	38.9 ± 9.1	0.009
PASP, mmHg	40.5 ± 15	30.9 ± 8.4	49.2 ± 15.1	<0.001
PAPm, mmHg	26.3 ± 9.2	20.9 ± 5.2	32.0 ± 9.2	<0.001
RA, mm	0.41 ± 0.1	33.8 ± 6.7	41.4 ± 8.5	<0.001
RV, mm	37.7 ± 8.4	32.0 ± 4.7	36.6 ± 6.4	<0.001
Tricuspid regurgitation	0.98 ± 0.87	0.85 ± 0.83	1.2 ± 0.90	0.014
RV-GLS, %	34.3 ± 6.1	−21.2 ± 4.3	−13.6 ± 4.9	<0.001
RV-FWLS, %	−17.4 ± 6.0	−27.0 ± 4.9	−16.9 ± 6.1	<0.001
RV-IVS, %	−22.0 ± 7.5	−13.4 ± 6.1	−8.6 ± 5.7	<0.001

Values are mean ± SD, *n* (%), or median (interquartile range).
Vmax, maximum aortic velocity; AVA, aortic valve area; AVAi, aortic valve area index; LVEF, left ventricle ejection fraction; LV-GLS, left ventricle global longitudinal strain; LA, left atrium; LAAi, LA area index; LAVi, LA volume index; LVMi, LV mass index; LA-GLS, LA global longitudinal strain; TAPSE, tricuspid annular plane systolic excursion; S`RV, peak systolic myocardial velocity at the lateral site of the tricuspid annulus; PASP, systolic pulmonary artery pressure; PAPm, mean pulmonary artery pressure; FAC, right ventricle fractional area change; RA, right atrium; RV, right ventricle; RV-GLS, RV global longitudinal strain; RV-FWLS, RV free wall longitudinal strain; RV-IVS, RV interventricular septum strain.

RV-IVS ($p = 0.003$), S`RV ($p = 0.026$), but not by TAPSE ($p = 0.187$) and FAC ($p = 0.060$).

Predictors of impaired RV-PA coupling

RV-PA coupling correlates at univariable and multivariable logistic regression analysis are presented in Table 5. Before TAVI, LA-GLS and RA diameter were independent predictors of RV-PA coupling impairment. Age, LA-GLS and RV diameter emerged as independent predictors of impaired RV-PA coupling after TAVI.

Clinical outcomes

Follow-up data were available for all patients, mean follow-up lasting 2.47 years (903 ± 216 days, range: 134–1,095 days). During follow-up, MACE occurred in 38 patients (24.4%), of which rehospitalization in 19 patients (11.9%), and death in 25 patients (15.6%). At 3-year follow-up the survival rate was 82.1%. Kaplan Meier analysis revealed that impaired baseline RV-PA coupling was associated with worse outcomes: lower freedom from MACE (54.8% vs. 85.6% in normal RV-PA coupling, *p*-value = 0.001) and lower survival rate (66.3% vs. 94.9% in normal RV-PA coupling, *p*-value < 0.001) (Figure 2). Impaired baseline RV-PA coupling as quantified by RV-FWLS/PSAP emerged as an independent predictor of both mortality (HR = 5.97, CI = 1.44–24.8, *p*-value = 0.014) and MACE (HR = 4.14, CI = 1.37–12.5, *p*-value = 0.012) (Table 6).

Discussion

Our study provides evidence that baseline RV-FWLS/PASP ratio, as a non-invasive surrogate of RV-PA coupling in patients with severe AS undergoing TAVI, is a novel parameter that refines risk assessment and independently predicts outcomes. The main findings of our study are: 1. Baseline RV-PA coupling impairment is influenced by persistent pulmonary hypertension and is associated with a greater burden of cardiac damage; 2. cardiac damage is only

TABLE 3 Echocardiographic changes after TAVI.

All patients ($n = 132$)	Baseline	post-TAVI	*p*-value
Aortic stenosis severity			
Vmax, m/s	4.67 ± 0.8	2.2 ± 0.5	<0.001
Mean gradient, mmHg	57.6 ± 19.4	12.1 ± 5.0	<0.001
AVA, cm^2	0.72 ± 0.3	1.7 ± 0.6	<0.001
AVAi, cm^2/m^2	0.4 ± 0.2	1.0 ± 0.3	<0.001
Aortic regurgitation	1.2 ± 0.7	0.8 ± 0.6	<0.001
Left ventricle			
LVEF, %	51.4 ± 12.1	55.1 ± 10.0	0.008
LV-GLS, %	−12.3 ± 4.2	−13.9 ± 4.0	0.002
LVMi, g/m^2	180.8 ± 50.5	155.8 ± 42.7	<0.001
E/A	1.2 ± 0.8	0.9 ± 0.4	0.001
Mitral regurgitation	1.3 ± 0.6	1.1 ± 0.5	0.003
Left atrium			
LAAi, cm^2/m^2	15.3 ± 3.2	14.2 ± 3.2	0.007
LAVi, ml/m^2	55.3 ± 19.0	49.1 ± 18.2	0.007
LA-GLS, % (LA_ε)	12.4 ± 6.9	15.6 ± 7.3	<0.001
Right ventricle			
TAPSE, cm/s	2.0 ± 0.4	2.1 ± 0.4	0.374
S'RV, cm/s	10.4 ± 2.8	12.3 ± 6.8	0.004
FAC, %	0.41 ± 0.1	0.42 ± 0.1	0.017
PASP, mmHg	40.2 ± 15	33.7 ± 11	<0.001
PAPm, mmHg	26.3 ± 9	22.1 ± 7	<0.001
RA, mm	37.7 ± 8.4	36.3 ± 7.9	0.178
RV, mm	34.3 ± 6.1	33.7 ± 5.9	0.378
Tricuspid regurgitation	0.98 ± 0.86	0.97 ± 0.77	0.944
RV-GLS, %	−17.3 ± 6.0	−18.6 ± 5.7	0.083
RV-FWLS, %	−21.9 ± 7.5	−23.2 ± 7.7	0.168
RV-IVS, %	−11.1 ± 6.2	−13.0 ± 5.1	0.010
TAPSE/PASP, cm/mmHg	0.59 ± 0.3	0.71 ± 0.3	<0.001
RV-GLS/PSAP	0.51 ± 0.27	0.61 ± 0.26	0.002
RV-FWLS/PSAP	0.64 ± 0.34	0.75 ± 0.33	0.007

Values are mean ± SD. TAVI, transcatheter aortic valve implantation.
Vmax, maximum aortic velocity; AVA, aortic valve area; AVAi, aortic valve area index; LVEF, left ventricle ejection fraction; LV-GLS, left ventricle global longitudinal strain; LA, left atrium; LAAi, LA area index; LAVi, LA volume index; LVMi, LV mass index; LA-GLS, LA global longitudinal strain; TAPSE, tricuspid annular plane systolic excursion; S`RV, peak systolic myocardial velocity at the lateral site of the tricuspid annulus; PASP, systolic pulmonary artery pressure; PAPm, mean pulmonary artery pressure; FAC, right ventricle fractional area change; RA, right atrium; RV, right ventricle; RV-GLS, RV global longitudinal strain; RV-FWLS, RV free wall longitudinal strain; RV-IVS, RV interventricular septum strain.

partially reversible, despite significant improvement of LV, LA, and RV function after TAVI; 3. Baseline impaired RV-PA coupling improves early after the procedure but continues to present a higher mortality risk in the long term.

RV-PA coupling and aortic stenosis severity

Although some studies reported no correlation between AS severity and the presence of PH or RV dysfunction, we found that patients with impaired baseline RV-PA coupling had more severe AS with lower AVAi and had more often bicuspid valves (13, 18, 19). The fact that there were no significant differences between groups regarding peak aortic jet velocity, peak and mean transvalvular gradients, should be interpreted in the context of impaired LVEF and low-flow low-gradient AS, which was more frequent in patients with impaired baseline RV-PA coupling. Moreover, AS severity traditionally quantified by transvalvular gradient and AVA has recently suffered a paradigm shift, resulting in the concept of AS-related cardiac damage or injury according to the reversibility potential (20, 21). As this model better translates AS severity into prognosis, in depth analysis of each component of cardiac damage/injury is required to improve treatment strategies and timing with respect to reversibility of injury (22, 23).

RV-PA coupling and left ventricular function in aortic stenosis

Even though the impact of impaired LVEF on RV-PA coupling has not been extensively studied, it has been previously reported that impaired LVEF is an independent predictor of PH (24). Due to ventricular interdependence, a significant fraction of developed pressure and RV volume outflow depends on LVEF, resulting in frequent RV dysfunction in patients with AS and is associated with reduced survival (25). Our study population included patients with impaired LVEF, more than a quarter, with a higher prevalence in the group with impaired RV-PA coupling. While LVEF and LV-GLS predicted to some extent baseline RV-PA coupling impairment, they failed to be independent predictors in the multivariable analysis. This could suggest that ventricular interdependence plays only a secondary role in the equation of RV-PA coupling. In our study we observed that baseline RV-PA coupling correlated with LV diastolic dysfunction but failed to independently predict it, which could indicate that despite reversible LV injury, impairment of upstream cardiac components could have different reversibility.

RV-PA coupling and left atrial function in aortic stenosis

Although LA function and dimensions have been previously shown to have an impact on morbidity and mortality in AS, little is known about the link between RV-PA coupling and LA function (26–28). In the context of AS, LA enlargement is a marker of longstanding increased LV filling pressures, and has been further correlated with upstream increased pressures in the pulmonary circulation (29).

In our study impaired baseline RV-PA coupling was associated with larger LA dimensions and impaired LA function, especially the reservoir and booster-pump. Atrial fibrillation was also correlated with impaired baseline RV-PA coupling, indicating loss of LA booster-pump. LA-GLS was associated with impaired RV-PA coupling before and after TAVI, suggesting that persistently impaired RV-PA coupling may be linked to irreversibility of atrial dysfunction. From a clinical point of view, improvement of left atrial function in the context of impaired RV-PA coupling failed to offer a significant benefit in terms of morbidity and mortality. While

TABLE 4 Echocardiographic changes after TAVI according to baseline RV-PA coupling impairment (short-term effect of TAVI on RV-PA coupling).

Echocardiographic parameters	Normal RV-PA coupling baseline RVFWLS/PASP ≥0.63 ($n = 65$)			Impaired RV-PA coupling baseline RVFWLS/PASP <0.63 ($n = 67$)		
	Baseline	1 m post-TAVI	*p*-value	Baseline	1 m post TAVI	*p*-value
Aortic stenosis severity						
Vmax, m/s	4.8 ± 0.8	2.3 ± 0.5	<0.001	4.6 ± 0.8	2.2 ± 0.5	<0.001
AVAi, cm^2/m^2	0.44 ± 0.2	0.98 ± 0.4	<0.001	0.37 ± 0.1	0.92 ± 0.3	<0.001
Aortic regurgitation	1.3 ± 0.7	0.9 ± 0.6	<0.001	1.2 ± 0.7	0.8 ± 0.6	<0.001
Left ventricle						
LVEF, %	55.0 ± 7.9	57.5 ± 6.3	0.041	48.0 ± 14.4	52.8 ± 12.4	0.042
LV-GLS, %	−14.2 ± 3.9	−15.3 ± 3.6	0.098	−10.5 ± 3.7	−12.6 ± 3.9	0.002
LVMi, g/m^2	174 ± 47	151 ± 41	0.003	187 ± 53	160 ± 44	0.002
E/A	0.84 ± 0.4	0.75 ± 0.3	0.167	1.8 ± 0.9	1.1 ± 0.6	<0.001
Mitral regurgitation	1.28 ± 0.6	1.05 ± 0.4	0.007	1.27 ± 0.6	1.12 ± 0.5	0.111
Left atrium						
LAAi, cm^2/m^2	14.2 ± 2.4	13.3 ± 2.5	0.047	16.3 ± 3.6	15.0 ± 3.7	0.032
LAVi, ml/m^2	49.3 ± 13.4	44.5 ± 12.9	0.042	61.3 ± 21.6	53.5 ± 21.3	0.037
LA-GLS, % (LA_e)	16.1 ± 5.9	19.1 ± 6.3	0.007	8.6 ± 5.6	12.1 ± 6.5	0.001
Right ventricle						
TAPSE, cm/s	2.2 ± 0.4	2.2 ± 0.4	0.936	1.9 ± 0.4	2.0 ± 0.4	0.187
S`RV, cm/s	11.5 ± 2.5	12.4 ± 2.2	0.020	9.4 ± 2.6	12.1 ± 9.3	0.026
FAC, %	42.6 ± 6.5	44.6 ± 6.7	0.084	38.9 ± 9.1	41.7 ± 8.2	0.060
PASP, mmHg	30.9 ± 8.4	29.1 ± 7.0	0.191	49.2 ± 15.1	38.1 ± 13.1	<0.001
PAPm	20.9 ± 5.2	19.8 ± 4.3	0.191	32.0 ± 9.1	25.3 ± 8.0	<0.001
RV-GLS, %	−21.2 ± 4.3	−20.9 ± 5.1	0.732	−13.6 ± 4.9	−16.5 ± 5.5	0.001
RV-FWLS, %	−27.0 ± 4.9	−26.1 ± 6.7	0.424	−16.9 ± 6.1	−20.6 ± 7.5	0.003
RV-IVS, %	−13.4 ± 6.1	−14.6 ± 4.5	0.244	−8.6 ± 5.2	−11.5 ± 5.1	0.003

Values are mean ± SD, *n* (%), or median (interquartile range).
Vmax, maximum aortic velocity; AVA, aortic valve area; AVAi, aortic valve area index; LVEF, left ventricle ejection fraction; LV-GLS, left ventricle global longitudinal strain; LA, left atrium; LAAi, LA area index; LAVi, LA volume index; LVMi, LV mass index; LA-GLS, LA global longitudinal strain; TAPSE, tricuspid annular plane systolic excursion; S`RV, peak systolic myocardial velocity at the lateral site of the tricuspid annulus; PASP, systolic pulmonary artery pressure; PAPm, mean pulmonary artery pressure; FAC, right ventricle fractional area change; RA, right atrium; RV, right ventricle; RV-GLS, RV global longitudinal strain; RV-FWLS, RV free wall longitudinal strain; RV-IVS, RV interventricular septum strain.

both indexed LA area and volume decreased after the procedure, persistence of LA dilation predicts the persistence of RV-PA coupling impairment. This clinically translated into the fact that the degree of decrease in LA dimensions only marginally impacted outcomes. These data are consistent with previous studies which suggest that LA active emptying is impaired in the presence of severe LA dilation, and propose the exceeding of optimal Frank-Starling mechanism as the explanation (30).

RV-PA coupling in aortic stenosis

Baseline pulmonary hypertension (PH) is common in patients with AS undergoing TAVI and has been linked to increased morbidity and mortality (31–33). Although more controversial regarding evaluation, quantification and impact, baseline RV dysfunction is also associated with adverse outcomes (21, 34, 35). The connection between PH and RV function has complex underlying pathophysiologic mechanisms that can be partly expressed through RV-PA coupling (36). Several studies have shown that TAPSE/PASP ratio as a non-invasive surrogate of RV-PA coupling offers prognostic information in patients with severe AS (12, 13). While PH can improve after TAVI and is associated with improved survival, similar to patients without PH, persistent PH is strongly associated with increased mortality and may require further treatment (33). Our study indicates an improvement in RV-PA coupling after TAVI, mainly through decrease in PASP values. Although not reflected by all RV function parameters, early improvement of RV function was noted, as assessed by tricuspid lateral annulus systolic velocity, FAC, RV-GLS and RV-FWLS. Acute improvements in RV function after TAVI have been previously demonstrated and can be partly explained by the LV-RV systolic interaction (37, 38). A study on HFrEF patients, where both RVGLS and RV-FWS have prognostic value, has shown that RV-FWS better predicts outcome, mainly because it is less influenced by LV longitudinal dysfunction (39). The results of our study, together with previous findings, support the idea that baseline RV-FWLS better refines risk assessment when used as a surrogate parameter for RV function normalized to baseline PASP value in the RV-PA coupling equation.

Limitations

This is a prospective study conducted on consecutive AS patients meeting the eligibility criteria for TAVI, resulting in a heterogenous population in terms of associated comorbidities, but resembling the real-life clinical setting. More than half of the

TABLE 5 Univariable and multivariable predictors of RV-PA coupling impairment (binary logistic regression).

Univariable regression analysis	Pre TAVI		Post TAVI	
	OR	*p*-value	OR	*p*-value
Age	0.940	0.028	0.952	0.044
Atrial fibrillation	3.980	0.001	9.389	<0.001
AVAi	0.048	0.009	0.406	0.102
Bicuspid	3.170	0.001	3.786	0.999
LVMi	1.005	0.129	1.009	0.043
LVEF	0.947	<0.001	0.951	0.008
LV-GLS*	1.305	<0.001	1.290	<0.001
E/A*	14.46	<0.001	4.689	0.020
LAVi	1.051	<0.001	1.046	0.001
LAAi	1.315	<0.001	1.251	0.001
LA-GLS	0.803	<0.001	0.845	<0.001
TAPSE	0.820	<0.001	0.900	0.030
S'RV*	0.715	<0.001	1.003	0.902
FAC*	0.942	0.011	0.897	<0.001
PASP*	1.156	<0.001	1.140	<0.001
PAPm*	1.267	<0.001	1.239	<0.001
RA	1.149	<0.001	1.107	<0.001
RV	1.179	<0.001	1.139	<0.001
Tricuspid regurgitation	1.687	0.017	1.750	0.024
RV-GLS*	1.483	<0.001	1.480	<0.001
RV-FWLS*	1.434	<0.001	1.361	<0.001
RV-IVS*	1.181	<0.001	1.227	<0.001
Multivariable regression analysis—Model 1 (Pre TAVI)				
LA-GLS	0.837	<0.001		
RA	1.111	0.003		
Multivariable regression analysis—Model 2 (Post TAVI)				
Age			0.931	0.040
LA-GLS			0.848	<0.001
RV			1.174	0.002

AVA, aortic valve area; AVAi, aortic valve area index; LVEF, left ventricle ejection fraction; LV-GLS, left ventricle global longitudinal strain; LA, left atrium; LAAi, LA area index; LAVi, LA volume index; LVMi, LV mass index; LA-GLS, LA global longitudinal strain; TAPSE, tricuspid annular plane systolic excursion; S`RV, peak systolic myocardial velocity at the lateral site of the tricuspid annulus; PAPS, systolic pulmonary artery pressure; PAPm, mean pulmonary artery pressure; FAC, right ventricle fractional area change; RA-right atrium; RV, right ventricle RV-GLS, RV global longitudinal strain; RV-FWLS, RV free wall longitudinal strain; RV-IVS, RV interventricular septum strain.

Model 1—Multivariable analysis (Backward Wald)—variables: age, atrial fibrillation, AVAi, bicuspid, LAVi, LA-GLS, LVEF, RA, RV, tricuspid regurgitation.

Model 2—Multivariable analysis (Backward Wald)—variables: age, atrial fibrillation, LAVi, LV mass index, LA-GLS, LVEF, RA, RV, tricuspid regurgitation.

*Variables highly correlated with another variable (Pearson coefficient > 0.6), not included.

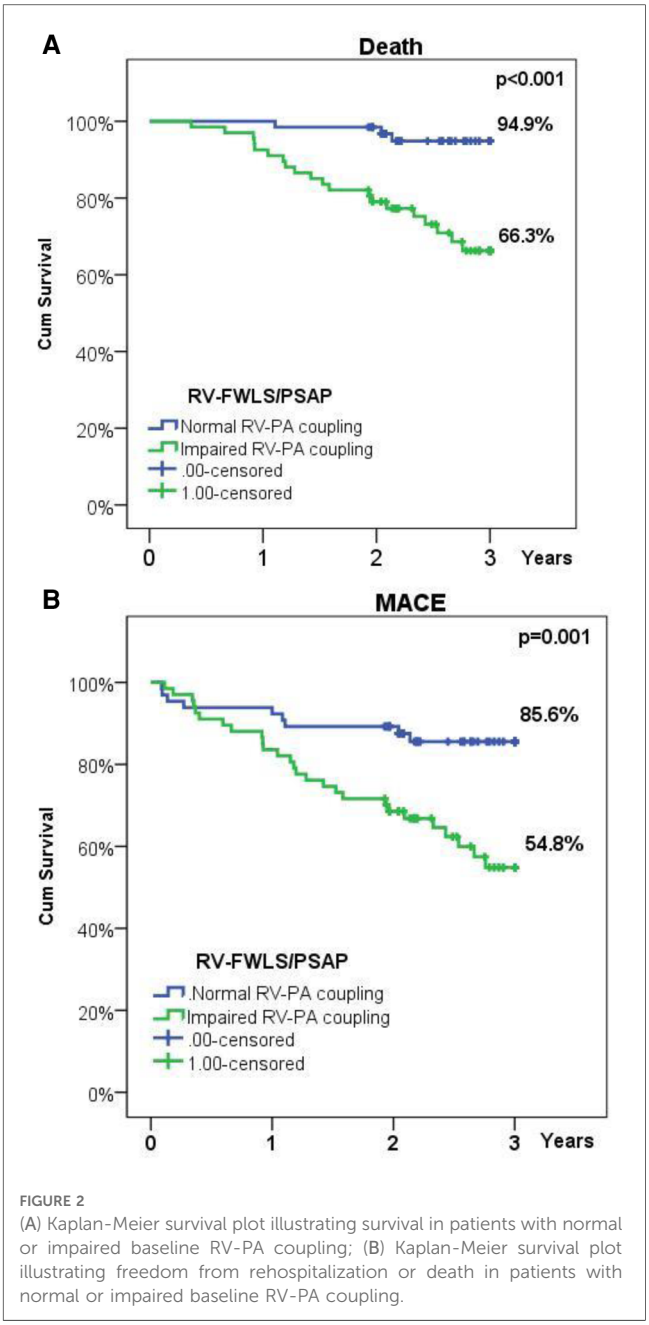

FIGURE 2
(A) Kaplan-Meier survival plot illustrating survival in patients with normal or impaired baseline RV-PA coupling; (B) Kaplan-Meier survival plot illustrating freedom from rehospitalization or death in patients with normal or impaired baseline RV-PA coupling.

included patients had associated CAD (of which half underwent previous coronary revascularization), as CAD is the most common comorbidity in AS (40).

One limitation of the study consisted in the short follow-up period as comprehensive echocardiographic evaluation was not routinely performed after the 1-month follow-up visit. Another limitation of the study is the lack of invasive measurements for comparison, but RV-FWLS/PASP has already been validated as a surrogate of RV-PA coupling as Ees/Ea in other populations (12, 41, 42) While mortality at 3-years was obtained through queries of the National Register of population records, no data regarding cause of death was available. Nonetheless, all-cause mortality represents an objective and relevant outcome. The pathophysiologic relations outlined in our study need to be interpreted in the context of a relatively small number of patients, but with comprehensive advanced echocardiographic assessment, and require further confirmation in larger studies.

Conclusion

Our results confirm that relief of aortic valve obstruction by TAVI has beneficial effects on the RV-PA coupling, that occur early after the procedure. This is accompanied by a significant improvement in LV, LA, and RV function. The results show a significant correlation between LA function and RV-PA coupling before TAVI, suggesting

TABLE 6 Predictors of MACE and mortality (Cox regression analysis).

Univariable analysis	MACE			Death		
Baseline parameters	HR	95% CI	*p*-value	HR	95% CI	*p*-value
Atrial fibrillation	2.18	1.14–4.16	0.018	2.27	1.02–5.07	0.044
LAVi	1.01	0.99–1.02	0.110	1.02	0.99–1.03	0.059
LAVi > 44*	2.40	1.01–5.73	0.049	3.11	0.94–10.4	0.065
LA-GLS	0.96	0.91–1.01	0.110	0.96	0.90–1.02	0.160
LA-GLS > 14*	0.42	0.19–0.91	0.027	0.31	0.11–0.91	0.032
LAAi	1.07	0.99–1.16	0.097	1.10	1.00–1.21	0.047
LAAi > 14*	2.67	1.23–5.82	0.013	2.67	1.20–10.2	0.021
PASP	1.03	1.01–1.05	0.007	1.03	1.00–1.05	0.030
PASP > 60*	3.06	1.39–6.71	0.005	3.63	1.44–9.15	0.006
TAPSE/PASP	0.26	0.66–1.06	0.061	0.50	0.10–2.55	0.401
TAPSE/PASP < 0.36*	3.12	1.64–5.92	0.001	2.41	1.07–5.42	0.034
RV-FWLS	1.03	0.99–1.08	0.128	1.05	0.99–1.10	0.082
RV-FWLS/PASP	3.77	1.25–11.4	0.019	5.51	1.32–23.0	0.019
RV-FWLS/PASP < 0.63*	3.27	1.54–6.97	0.002	7.39	2.19–24.9	0.001
Multivariable analysis	**MACE**			**Death**		
RV-FWLS/PASP	4.14	1.37–12.5	0.012	5.97	1.44–24.8	0.014

MACE, major adverse cardiac events; LAVi, LA volume index; LAAI, LA area index; LA-GLS, LA global longitudinal strain; TAPSE, tricuspid annular plane systolic excursion; PAPS, systolic pulmonary artery pressure; PAPm, mean pulmonary artery pressure; RV-FWLS, RV free wall longitudinal strain; RV-GLS, RV global longitudinal strain.
Multivariable analysis (Backward Wald)—variables: atrial fibrillation, LAVi, LAAi, LA-GLS, RV-FWS/PSAP.
*Cut-off values determined by ROC analysis.

the contribution of LA function in modulating right heart function in patients with AS. Persistence of impaired RV-PA coupling after TAVI is mainly influenced by persistent pulmonary hypertension and is associated with long-term adverse outcomes. The complex underlying mechanisms of RV-PA coupling impairment require further analysis of cardiac injury reversibility.

Data availability statement

Requests to access these datasets should be directed to bogdan.a.popescu@gmail.com.

Ethics statement

The studies involving human participants were reviewed and approved by Institute for Cardiovascular Diseases "Prof. Dr. C. C. Iliescu", Bucharest, Romania. The patients/participants provided their written informed consent to participate in this study.

Author contributions

CAP, AC, and BAP contributed to conception and design of the study. AC, MR, DC, SBB, RE and CB organized the database. CAP and AC performed the statistical analysis. CAP and AC wrote the first draft of the manuscript. DC, AM, MR, SBB, RE, CB wrote sections of the manuscript; CG, DD, OC, SB-T, VAI and BAP made critical revisions of the paper. All authors contributed to the article and approved the submitted version.

Acknowledgments

We gratefully acknowledge the support of our colleagues who have referred patients for this study. Publication of this paper was supported by the University of Medicine and Pharmacy Carol Davila, through the institutional program Publish not Perish.

Conflict of interest

BAP has received research support and lecture honoraria from GE Healthcare and Hitachi-Aloka. The remaining authors declare that the research was conducted in the absence of any commercial or financial relationships that could be construed as a potential conflict of interest.

Publisher's note

References

1. Harris AW, Pibarot P, Otto CM. Aortic stenosis: guidelines and evidence gaps. *Cardiol Clin*. (2020) 38(1):55–63. doi: 10.1016/j.ccl.2019.09.003

2. Vahanian A, Beyersdorf F, Praz F, Milojevic M, Baldus S, Bauersachs J, et al. 2021 ESC/EACTS guidelines for the management of valvular heart disease. *Eur Heart J*. (2021) 43(7):561–632. doi: 10.1093/eurheartj/ehab395

3. Nishimura RA, Otto CM, Bonow RO, Carabello BA, Erwin JP, Fleisher LA, et al. 2017 AHA/ACC focused update of the 2014 AHA/ACC guideline for the management of patients with valvular heart disease: a report of the American college of cardiology/American heart association task force on clinical practice guidelines. *J Am Coll Cardiol*. (2017) 70(2):252–89. doi: 10.1016/j.jacc.2017.03.011

4. Popma JJ, Deeb GM, Yakubov SJ, Mumtaz M, Gada H, O'Hair D, et al. Transcatheter aortic-valve replacement with a self-expanding valve in low-risk patients. *N Engl J Med*. (2019) 380(18):1706–15. doi: 10.1056/NEJMoa1816885

5. Mack MJ, Leon MB, Smith CR, Miller DC, Moses JW, Tuzcu EM, et al. 5-year outcomes of transcatheter aortic valve replacement or surgical aortic valve

replacement for high surgical risk patients with aortic stenosis (PARTNER 1): a randomised controlled trial. *Lancet*. (2015) 385(9986):2477–84. doi: 10.1016/S0140-6736(15)60308-7

6. Leon MB, Smith CR, Mack MJ, Makkar RR, Svensson LG, Kodali SK, et al. Transcatheter or surgical aortic-valve replacement in intermediate-risk patients. *N Engl J Med*. (2016) 374(17):1609–20. doi: 10.1056/NEJMoa1514616

7. Mack MJ, Leon MB, Thourani VH, Makkar R, Kodali SK, Russo M, et al. Transcatheter aortic-valve replacement with a balloon-expandable valve in low-risk patients. *N Engl J Med*. (2019) 380(18):1695–705. doi: 10.1056/NEJMoa1814052

8. Price J, Bob-Manuel T, Aymond J, Amoran O, Almusawi H, Kelly J, et al. Low risk TAVR: long- term considerations and appropriate patient selection. *Prog Cardiovasc Dis*. (2020) 63(3):377–82. doi: 10.1016/j.pcad.2020.04.002

9. Cavalcante JL, Simon MA, Chan SY. Comprehensive right-sided assessment for transcatheter aortic valve replacement Risk stratification: time for a change. *J Am Soc Echocardiogr*. (2017) 30(1):47–51. doi: 10.1016/j.echo.2016.11.006

10. Schwartz LA, Rozenbaum Z, Ghantous E, Kramarz J, Biner S, Ghermezi M, et al. Impact of right ventricular dysfunction and tricuspid regurgitation on outcomes in patients undergoing transcatheter aortic valve replacement. *J Am Soc Echocardiogr*. (2017) 30(1):36–46. doi: 10.1016/j.echo.2016.08.016

11. Grevious SN, Fernandes MF, Annor AK, Ibrahim M, Saint Croix GR, de Marchena E, et al. Prognostic assessment of right ventricular systolic dysfunction on post–transcatheter aortic valve replacement short-term outcomes: systematic review and meta-analysis. *J Am Heart Assoc*. (2020) 9(12):e014463. doi: 10.1161/JAHA.119.014463

12. Iacoviello M, Monitillo F, Citarelli G, Leone M, Grande D, Antoncecchi V, et al. Right ventriculo-arterial coupling assessed by two-dimensional strain: a new parameter of right ventricular function independently associated with prognosis in chronic heart failure patients. *Int J Cardiol*. (2017) 241:318–21. doi: 10.1016/j.ijcard.2017.04.051

13. Sultan I, Cardounel A, Abdelkarim I, Kilic A, Althouse AD, Sharbaugh MS, et al. Right ventricle to pulmonary artery coupling in patients undergoing transcatheter aortic valve implantation. *Heart*. (2019) 105(2):117–21. doi: 10.1136/heartjnl-2018-313385

14. Lang RM, Badano LP, Mor-Avi V, Afilalo J, Armstrong A, Ernande L, et al. Recommendations for cardiac chamber quantification by echocardiography in adults: an update from the American society of echocardiography and the European association of cardiovascular imaging. *Eur Heart J Cardiovasc Imaging*. (2015) 16(3):233–70. doi: 10.1093/ehjci/jev014

15. Chemla D, Castelain V, Humbert M, Hébert JL, Simonneau G, Lecarpentier Y, et al. New formula for predicting mean pulmonary artery pressure using systolic pulmonary artery pressure. *Chest*. (2004) 126(4):1313–7. doi: 10.1378/chest.126.4.1313

16. Habibzadeh F, Habibzadeh P, Yadollahie M. On determining the most appropriate test cut-off value: the case of tests with continuous results. *Biochem Medica*. (2016) 26(3):297–307. doi: 10.11613/BM.2016.034

17. Vizzardi E, Gavazzoni M, Sciatti E, Dallapellegrina L, Bernardi N, Raddino R, et al. Right ventricular deformation and right ventricular-arterial coupling in patients with heart failure due to severe aortic stenosis undergoing TAVI: long-term results. *Am J Cardiovasc Dis*. (2020) 10(3):150–63. PMID: 32923096; PMCID: PMC7486529.

18. Ahn HS, Chang SA, Kim HK, Kim SJ, Lee SP, Park SJ, et al. Determinants of pulmonary hypertension development in moderate or severe aortic stenosis. *Int J Cardiovasc Imaging*. (2014) 30(8):1519–28. doi: 10.1007/s10554-014-0498-5

19. Casaclang-Verzosa G, Nkomo VT, Sarano ME, Malouf JF, Miller FA, Oh JK. E/Ea is the major determinant of pulmonary artery pressure in moderate to severe aortic stenosis. *J Am Soc Echocardiogr*. (2008) 21(7):824–7. doi: 10.1016/j.echo.2007.12.002

20. Capoulade R, Le Ven F, Clavel MA, Dumesnil JG, Dahou A, Thébault C, et al. Echocardiographic predictors of outcomes in adults with aortic stenosis. *Heart*. (2016) 102(12):934–42. doi: 10.1136/heartjnl-2015-308742

21. Généreux P, Pibarot P, Redfors B, Mack MJ, Makkar RR, Jaber WA, et al. Staging classification of aortic stenosis based on the extent of cardiac damage. *Eur Heart J*. (2017) 38(45):3351–58. doi: 10.1093/eurheartj/ehx381

22. Maeder MT, Weber L, Weilenmann D, Haager PK, Joerg L, Taramasso M, et al. Invasive hemodynamic staging classification of cardiac damage in patients with aortic stenosis undergoing valve replacement. *Can J Cardiol*. (2020) 36(10):1667–74. doi: 10.1016/j.cjca.2020.02.004

23. Schewel J, Kuck KH, Frerker C, Schmidt T, Schewel D. Outcome of aortic stenosis according to invasive cardiac damage staging after transcatheter aortic valve replacement. *Clin Res Cardiol*. (2021) 110(5):699–710. doi: 10.1007/s00392-021-01835-w

24. Kapoor N, Varadarajan P, Pai RG. Echocardiographic predictors of pulmonary hypertension in patients with severe aortic stenosis. *Eur J Echocardiogr*. (2008) 9(1):31–3. doi: 10.1016/j.euje.2007.01.005

25. Khaddi S, Kharbouche K, Habbal R, Azouzi L, Drighil A. Prevalence and determinants or right ventricular dysfunction in severe aortic stenosis. *Arch Cardiovasc Dis Suppl*. (2018) 10(1):67. doi: .org/10.1016/j.acvdsp.2017.11.269

26. De Rosa R, Murray MI, Schranz D, Mas-Peiro S, Esmaeili A, Zeiher AM, et al. Short-term decrease of left atrial size predicts clinical outcome in patients with severe aortic stenosis undergoing TAVR. *Catheter Cardiovasc Interv*. (2020) 96(3):E341–47. doi: 10.1002/ccd.28542

27. Imanishi J, Tanaka H, Sawa T, Motoji Y, Miyoshi T, Mochizuki Y, et al. Association of left atrial booster-pump function with heart failure symptoms in patients with severe aortic stenosis and preserved left ventricular ejection fraction. *Echocardiography*. (2015) 32(5):758–67. doi: 10.1111/echo.12733

28. Galli E, Fournet M, Chabanne C, Lelong B, Leguerrier A, Flecher E, et al. Prognostic value of left atrial reservoir function in patients with severe aortic stenosis: a 2D speckle-tracking echocardiographic study. *Eur Heart J Cardiovasc Imaging*. (2016) 17(5):533–41. doi: 10.1093/ehjci/jev230

29. Calin A, Mateescu AD, Rosca M, Beladan CC, Enache R, Botezatu S, et al. Left atrial dysfunction as a determinant of pulmonary hypertension in patients with severe aortic stenosis and preserved left ventricular ejection fraction. *Int J Cardiovasc Imaging*. (2017) 33(12):1939–47. doi: 10.1007/s10554-017-1211-2

30. Pagel PS, Kehl F, Gare M, Hettrick DA, Kersten JR, Warltier DC. Mechanical function of the left atrium: new insights based on analysis of pressure-volume relations and Doppler echocardiography. *Anesthesiology*. (2003) 98(4):975–94. doi: 10.1097/00000542-200304000-00027

31. Abdelkarim I, Althouse AD, Thoma FW, Lee JS, Schindler JT, Gleason TG, et al. The importance of invasive hemodynamics for pulmonary hypertension screening in TAVR patients. *J Am Coll Cardiol*. (2017) 70(4):510–11. doi: 10.1016/j.jacc.2017.04.061

32. Ujihira K, Kohmoto T, Gimelli G, Raval A, Jacobson K, Wolff M, et al. The impact of increased pulmonary arterial pressure on outcomes after transcatheter aortic valve replacement. *Catheter Cardiovasc Interv*. (2020) 96(7):E723–34. doi: 10.1002/ccd.28862

33. Masri A, Abdelkarim I, Sharbaugh MS, Althouse AD, Xu J, Han W, et al. Outcomes of persistent pulmonary hypertension following transcatheter aortic valve replacement. *Heart*. (2018) 104(10):821–27. doi: 10.1136/heartjnl-2017-311978

34. Medvedofsky D, Koifman E, Jarrett H, Miyoshi T, Rogers T, Ben-Dor I, et al. Association of right ventricular longitudinal strain with mortality in patients undergoing transcatheter aortic valve replacement. *J Am Soc Echocardiogr*. (2020) 33(4):452–60. doi: 10.1016/j.echo.2019.11.014

35. Ito S, Pislaru SV, Soo WM, Huang R, Greason KL, Mathew V, et al. Impact of right ventricular size and function on survival following transcatheter aortic valve replacement. *Int J Cardiol*. (2016) 221:269–74. doi: 10.1016/j.ijcard.2016.07.085

36. Kubba S, Davila CD, Forfia PR. Methods for evaluating right ventricular function and ventricular–arterial coupling. *Prog Cardiovasc Dis*. (2016) 59(1):42–51. doi: 10.1016/j.pcad.2016.06.001

37. Eleid MF, Padang R, Pislaru SV, Greason KL, Crestanello J, Nkomo VT, et al. Effect of transcatheter aortic valve replacement on right ventricular–pulmonary artery coupling. *JACC Cardiovasc Interv*. (2019) 12(21):2145–54. doi: 10.1016/j.jcin.2019.07.025

38. Schwarz K, Singh S, Dawson D, Frenneaux MP. Right ventricular function in left ventricular disease: pathophysiology and implications. *Heart Lung Circ*. (2013) 22(7):507–11. doi: 10.1016/j.hlc.2013.03.072

39. Carluccio E, Biagioli P, Lauciello R, Zuchi C, Mengoni A, Bardelli G, et al. Superior prognostic value of right ventricular free wall compared to global longitudinal strain in patients with heart failure. *J Am Soc Echocardiogr*. (2019) 32(7):836–44.e1. doi: 10.1016/j.echo.2019.02.011

40. Beach JM, Mihaljevic T, Svensson LG, Rajeswaran J, Marwick T, Griffin B, et al. Coronary artery disease and outcomes of aortic valve replacement for severe aortic stenosis. *J Am Coll Cardiol*. (2013) 61(8):837–48. doi: 10.1016/j.jacc.2012.10.049

41. Focardi M, Cameli M, Carbone SF, Massoni A, De Vito R, Lisi M, et al. Traditional and innovative echocardiographic parameters for the analysis of right ventricular performance in comparison with cardiac magnetic resonance. *Eur Heart J Cardiovasc Imaging*. (2015) 16(1):47–52. doi: 10.1093/ehjci/jeu156

42. Schmeisser A, Rauwolf T, Groscheck T, Kropf S, Luani B, Tanev I, et al. Pressure-volume loop validation of TAPSE/PASP for right ventricular arterial coupling in heart failure with pulmonary hypertension. *Eur Heart J Cardiovasc Imaging*. (2021) 22(2):168–76. doi: 10.1093/ehjci/jeaa285

frontiers | Frontiers in Cardiovascular Medicine

TYPE Original Research
PUBLISHED 21 April 2023
DOI 10.3389/fcvm.2023.1112797

OPEN ACCESS

EDITED BY
Matteo Cameli,
University of Siena, Italy

REVIEWED BY
Jiandong ZHOU,
University of Oxford, United Kingdom
Michal Jasinski,
Wrocław University of Science and Technology, Poland
Bharath Ambale Venkatesh,
Johns Hopkins University, United States

*CORRESPONDENCE
Louis J. Dell'Italia
louis.dellitalia@va.gov

SPECIALTY SECTION
This article was submitted to Heart Valve Disease, a section of the journal Frontiers in Cardiovascular Medicine

RECEIVED 30 November 2022
ACCEPTED 28 March 2023
PUBLISHED 21 April 2023

CITATION
Zheng J, Li Y, Billor N, Ahmed MI, Fang Yu-Hua D, Pat B, Denney TS and Dell'Italia LJ (2023) Understanding post-surgical decline in left ventricular function in primary mitral regurgitation using regression and machine learning models.
Front. Cardiovasc. Med. 10:1112797.
doi: 10.3389/fcvm.2023.1112797

Understanding post-surgical decline in left ventricular function in primary mitral regurgitation using regression and machine learning models

Jingyi Zheng[1], Yuexin Li[1], Nedret Billor[1], Mustafa I. Ahmed[2], Yu-Hua Dean Fang[3], Betty Pat[2,4], Thomas S. Denney[5] and Louis J. Dell'Italia[2,4]*

[1]Department of Mathematics and Statistics, Auburn University, Auburn, AL, United States, [2]Division of Cardiovascular Disease, University of Alabama at Birmingham, Birmingham, AL, United States, [3]Department of Radiology, University of Alabama at Birmingham, Birmingham, AL, United States, [4]Birmingham Veterans Affairs Health Care System, Birmingham, AL, United States, [5]Department of Electrical and Computer Engineering, Samuel Ginn College of Engineering, Auburn University, Auburn, AL, United States

Background: Class I echocardiographic guidelines in primary mitral regurgitation (PMR) risks left ventricular ejection fraction (LVEF) < 50% after mitral valve surgery even with pre-surgical LVEF > 60%. There are no models predicting LVEF < 50% after surgery in the complex interplay of increased preload and facilitated ejection in PMR using cardiac magnetic resonance (CMR).
Objective: Use regression and machine learning models to identify a combination of CMR LV remodeling and function parameters that predict LVEF < 50% after mitral valve surgery.
Methods: CMR with tissue tagging was performed in 51 pre-surgery PMR patients (median CMR LVEF 64%), 49 asymptomatic (median CMR LVEF 63%), and age-matched controls (median CMR LVEF 64%). To predict post-surgery LVEF < 50%, least absolute shrinkage and selection operator (LASSO), random forest (RF), extreme gradient boosting (XGBoost), and support vector machine (SVM) were developed and validated in pre-surgery PMR patients. Recursive feature elimination and LASSO reduced the number of features and model complexity. Data was split and tested 100 times and models were evaluated *via* stratified cross validation to avoid overfitting. The final RF model was tested in asymptomatic PMR patients to predict post-surgical LVEF < 50% if they had gone to mitral valve surgery.
Results: Thirteen pre-surgery PMR had LVEF < 50% after mitral valve surgery. In addition to LVEF ($P = 0.005$) and LVESD ($P = 0.13$), LV sphericity index ($P = 0.047$) and LV mid systolic circumferential strain rate ($P = 0.024$) were predictors of post-surgery LVEF < 50%. Using these four parameters, logistic regression achieved 77.92% classification accuracy while RF improved the accuracy to 86.17%. This final RF model was applied to asymptomatic PMR and predicted 14 (28.57%) out of 49 would have post-surgery LVEF < 50% if they had mitral valve surgery.

Abbreviations
AUROC, area under the Receiver Operating Characteristic (ROC) curve; AUPRC, area under Precision-Recall (PR) curve; CMR, cardiac magnetic resonance; LV, left ventricle; LA, left atrium/atrial; LASSO, least absolute shrinkage and selection operator; LA EF, left atrial emptying fraction; LVEDD, left ventricular end-diastolic dimension; LVEF, left ventricular ejection fraction; LVESD, left ventricular end-systolic dimension; PMR, primary mitral regurgitation; RF, random forest; ROC, receiver operating characteristic; SHAP, Shapley Additive exPlanations; SVM, support vector machine; XGBoost. extreme gradient boosting; XO, xanthine oxidase.

Conclusions: These preliminary findings call for a longitudinal study to determine whether LV sphericity index and circumferential strain rate, or other combination of parameters, accurately predict post-surgical LVEF in PMR.

KEYWORDS

machine learning, mitral regurgitation (MR), predictive models, LV circumferential strain rate, post-surgical LVEF

Introduction

Patients with primary mitral regurgitation (PMR) and left ventricular ejection fraction (LVEF) > 60% have a 20% chance of LVEF < 50% after mitral valve repair or replacement (1–3). Current Class I guidelines include conventional echocardiography-derived LVEF < 60%, LV end-systolic dimension > 4.0 cm or symptoms for surgical intervention (4). These guidelines were based on postoperative survival with less emphasis on postoperative LV function (1). We have demonstrated severe cardiomyocyte ultrastructural damage in patients with moderate to severe PMR and echocardiographic LVEF > 60% in PMR patients (5–7). These findings reinforce the concept that unrecognized cardiomyocyte ultrastructural damage may in part explain the decrease in post-operative LVEF.

Given the risk of waiting too long for surgery, current Class IIa indication for asymptomatic patients with severe PMR and LVEF > 60% recommends mitral valve repair at a Heart Valve Center of Excellence with a greater than 95% likelihood of a successful and durable repair without residual mitral regurgitation and expected mortality rate of less than 1% (4). However, outcomes among these asymptomatic patients are heterogeneous, and models to select the subset of asymptomatic patients with LVEF > 60% who will benefit from early surgery remains elusive. The impetus for the current study is to identify cardiac magnetic resonance (CMR) markers of LV function and remodeling to optimize timing of surgical intervention to reduce the likelihood of post-surgical decline in LVEF.

The advantages of machine learning models are their ability to integrate predictors extracted from multiple sources and to model both linear and nonlinear interactions amongst them (8). An important advantage of machine learning over conventional statistical methods (e.g., logistic regression) is that various machine learning algorithms do not require data to conform to statistical assumptions. Thus, machine learning models can identify unexpected predictors not accounted for by linear models and interactions that have prognostic value. With recursive feature elimination and repetitive testing, machine learning models are now being used in pilot analyses even in smaller data sets (9, 10).

Recent studies employ machine learning and regression methods to achieve optimal analytical goals with multiple potential predictors (**Figure 1**) (11). The current study employs Random Forest (RF) (12), Support Vector Machine (SVM) with Radial Basis Function Kernel (13), extreme gradient boosting (XGBoost) (14), in addition to a standard least absolute shrinkage and selection operator (LASSO) penalized logistic regression (15). These models are trained, re-trained based on a reduced number of features and validated in data from pre-surgical PMR patients to predict six-month post-surgery LVEF < 50%. The final model is then applied to predict LVEF < 50% in a cohort of asymptomatic PMR patients if they had gone to mitral valve surgery.

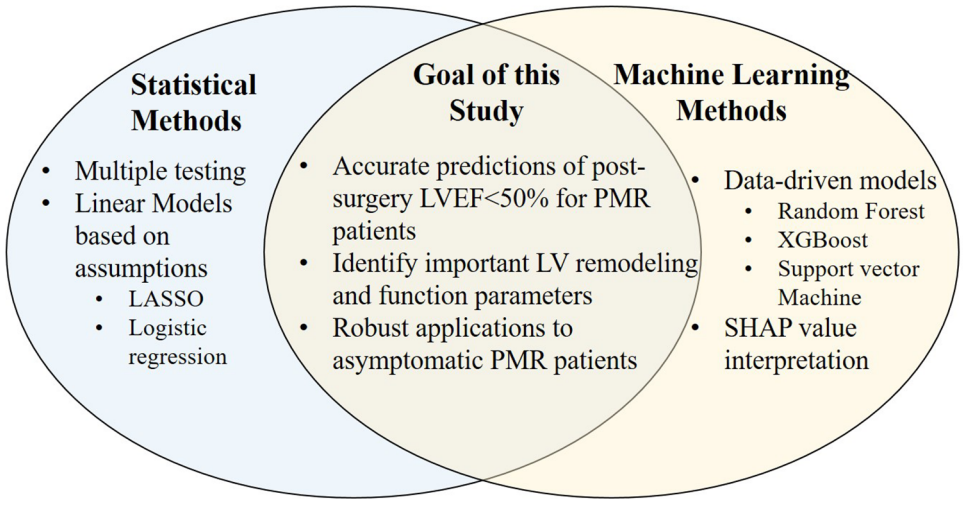

FIGURE 1
Application of regression and machine learning methods to achieve optimal analytical goals.

Materials and methods

Study population

This single-center study includes 49 asymptomatic and 51 pre-surgery PMR patients recruited between 2006 and 2010 under NHLBI Specialized Centers of Clinically Oriented Research grant (5, 6, 16). Primary degenerative mitral valve prolapse characterized by echocardiographic evidence of thickened, redundant leaflets with excessive motion and prolapse. Patients were excluded for evidence of: (1) aortic valve > trace aortic regurgitation or mean gradient of >10 mmHg, (2) mitral stenosis (mean gradient > 5 mmHg, valve area < 1.5 cm^2), (3) endocarditis, (4) iatrogenic MR (ergot, radiation induced), (5) hemodialysis, (6) pregnancy, (7) presence of coronary artery disease (stenosis > 50%), 8) positive exercise tolerance test with myocardial perfusion. The Institutional Review Boards of the University of Alabama at Birmingham and Auburn University approved the study protocol. All participants gave written informed consent.

Data collection

All data from patients' baseline and return visits were obtained prospectively and recorded in electronic health data records. Cardiac magnetic resonance (CMR) imaging with tissue tagging was performed in control volunteers who had no prior history of cardiovascular disease or medical illness, no history of smoking, and no cardiovascular medications. Asymptomatic PMR patients had Class I status, with moderate/severe PMR by color flow Echo/Doppler, LVEF > 60%, LV end-systolic dimensions (ESD) < 40 mm, leaflet thickening and prolapse, and normal maximal exercise myocardial perfusion imaging (17). At baseline, PMR patients (asymptomatic, $n = 49$ and pre-surgery, $n = 51$), plasma xanthine oxidase (XO) activity and carboxy-terminal propeptide of procollagen type I (PICP), a marker of type I collagen synthesis, and carboxy-terminal telopeptide of collagen type I (ICTP) levels, a marker of type I collagen degradation were measured. Post-surgical CMR was performed six months after the surgical procedure in all pre-surgery patients.

Cardiac magnetic resonance

Table 1 lists all CMR-derived LV and left atrial volumes, strains and twist as previously described in our laboratory (5, 6, 16, 17).

Xanthine oxidase measurement

Peripheral venous XO activity was measured by the rate of uric acid production in the presence of xanthine (75 μM) without NAD^+ as described previously in our laboratory (16).

Collagen homeostasis

Baseline levels of PICP and ICTP were measured with commercially available immunoassays (Quidel Corporation, USA and Orion Diagnostic, Finland). Detection limits were 0.2 ng/ml for PICP and 0.3 ng/ml for ICTP as described previously in our lab (16).

Statistical analysis

Data in Tables are presented as number (% of total) or median (interquartile range). Statistical differences between two groups are tested *via* Mann-Whitney U test for continuous variables and chi-square test for categorical variables (**Tables 1**, **2** and **Supplementary Table S1**). Comparisons between 3 groups are tested by Kruskal-Wallis and the *p*-values adjusted by false

TABLE 1 Features included in predictive models ($N = 37$).

Category (No. of Features)	Features
Demographics (9)	Age, Race, Gender, Weight, Height, BMI, BSA, Hypertension, Atrial Fibrillation
CMR	*Pre-surgery and Post-surgery (6 months)*
- LV function (6)	LV end-diastolic volume, LV end-systolic volume, LV end-diastolic dimension, LV end-systolic dimension, LVEF, LV Stroke Volume,
- LV remodeling (4)	LV end-diastolic mass, LV mass/volume, LV Sphericity Index (SI), LV mass/volume x SI
- Regurgitation (1)	Regurgitant Volume
- LA remodeling (3)	LA maximum and minimum volumes, Total LA emptying fraction
- RV parameters (1)	RV ejection fraction
LV CMR tissue tagging (9)	LV mid Systolic Circumferential Strain
	LV mid Systolic Longitudinal Strain
	LVES Maximum Strain
	LV mid Systolic Circumferential Strain Rate
	LV Systolic Longitudinal Strain Rate
	LV Peak Systolic Twist
	LV Systolic Twist-per-Volume Slope
	CL-Shear Angle
	LV Systolic Torsion
Biomarkers (4)	XOCM, PICP, ICTP, PICP/ICTP

CL, circumferential-longitudinal; CMR, cardiac magnetic resonance; ICTP, Carboxy-terminal telopeptide of collagen type I, a marker of type I collagen degradation; LA, left atrial; LV, left ventricle; RV, right ventricle; LVEF, LV ejection fraction; PICP, Carboxy-terminal propeptide of procollagen type I, a marker of type I collagen synthesis; XO, xanthine oxidase normalized to plasma protein (XOCM).

TABLE 2 Pre-Surgery baseline demographic and CMR data separated by LVEF≥ or <50% at 6 months post-surgery ($N = 51$).

	LVEF ≥ 50% ($N = 38$)	LVEF < 50% ($N = 13$)	*P* value	FDR adjusted *P*-value
Age	56 (46, 62)	51 (43, 66)	0.85	0.91
Female/Male	8 (21%)/30 (79%)	7 (54%)/6 (46%)	**0.025**	0.204
BMI (kg/m^2)	27 (24, 29)	25 (23, 30)	0.53	0.699
BSA (m^2)	2.02 (1.89, 2.12)	1.80 (1.68, 2.04)	0.06	0.223
Hypertension (Y/N)	15 (39%)/23 (61%)	3 (23%)/10 (77%)	0.29	0.459
Atrial Fibrillation (Y/N)	5 (13%)/33 (87%)	5 (38%)/8 (62%)*	**0.047**	0.204
LVEF (%)	65 (62, 68)	58 (53, 64)*	**0.005**	0.146
LVED Volume (mL/m^2)	104 (88, 128)	104 (96, 122)	0.91	0.91
LVES Volume (mL/m^2)	36 (29, 45)	44 (36, 54)*	**0.036**	0.204
LV Stroke Volume (mL/m^2)	69 (55, 82)	64 (54, 70)	0.23	0.459
LVED Diameter (mm)	57 (53, 62)	59 (55, 66)	0.30	0.459
LVES Diameter (mm)	44 (40, 47)	49 (40, 55)	0.13	0.376
LVED Mass/Volume (g/mL)	0.6 (0.6, 0.7)	0.6 (0.5, 0.7)	0.54	0.669
LV Sphericity Index (SI)	1.58 (1.43 1.78)	1.47 (1.29, 1.65)*	**0.047**	0.204
LVED Mass/Volume x SI	1.0 (0.8, 1.3)	0.9 (0.8, 1.1)	0.17	0.425
LV Systolic Twist/Volume slope (°/ml)	−0.07 (−0.09, −0.05)	−0.07 (−0.10, −0.05)	0.81	0.91
LV Systolic Circumferential Strain rate (1/s)	−0.69 (−0.77, −0.64)	−0.59 (−0.74, −0.51)*	**0.024**	0.204
Peak LV Torsion (°/cm)	2.05 (1.62, 2.55)	1.97 (1.34, 2.18)	0.30	0.459
Circumferential L-Shear Angle (°)	7.4 (6.5, 9.4)	7.1 (5.3, 8.8)	0.27	0.459
LVES Circumferential Strain	−0.15 (−0.16, −0.13)	−0.14 (−0.16, −0.12)	0.23	0.459
LVES Longitudinal Strain	−0.13 (−0.14, −0.11)	−0.11 (−0.16, −0.10)	0.89	0.91
LVES Maximal Strain	−0.20 (−0.21, −0.19)	−0.19 (−0.21, −0.18)	0.42	0.575
LA Max Volume (mL/m^2)	58 (49, 81)	58 (53, 79)	0.76	0.898
LA Min Volume (mL/m^2)	37 (22, 47)	38 (31, 47)	0.41	0.575
LA Emptying Fraction (%)	46 (37, 51)	42 (38, 46)	0.18	0.425
Regurgitant Volume (mL)	68 (49, 85)	57 (36, 70)	0.07	0.228

LV, left ventricle; LVED, LV end-diastolic; LVES, LV end-systolic; LVEF, LV ejection fraction; LA, left atrial; XO, xanthine oxidase normalized to plasma protein (XOCM) or plasma volume (XOCV); PICP, Carboxy-terminal propeptide of procollagen type I, a marker of type I collagen synthesis; ICTP, Carboxy-terminal telopeptide of collagen type I, a marker of type I collagen degradation.
Bold values indicate significance of $p < 0.05$.

discovery rate (FDR) for multiple testing, reported in **Supplementary Table S2**. Univariate and multivariate logistic regression are fitted to predict the probability of post-surgical LVEF < 50% using 4 pre-surgical parameters (LVEF, LVESD, LV sphericity index, and LV systolic circumferential strain rate (**Supplementary Tables S3, S4**).

Model development in pre-surgical patients

This study employed a standard LASSO (15) logistic regression and three machine learning models: random forest (RF) (12), support vector machine (SVM) with Radial Basis Function (RBF) Kernel (13), and extreme gradient boosting (XGBoost) (14). The models are trained to predict a binary response variable with two levels: LVEF < 50% or >50% at 6 months after mitral valve surgery in pre-surgery PMR patients. The models were initially developed using 37 features including demographics, CMR parameters, and biomarkers for predictive modeling (**Table 1** and **Figure 2**).

Feature selection

To avoid overfitting and to increase the reproducibility of the models, we attempted to include the most relevant features in predicting post-surgery LVEF < 50%. LASSO, which is a regression model penalized on l_1 penalty, performs both feature selection and regularization by itself to enhance the interpretability and accuracy of the linear model. Therefore, LASSO does not require extra feature selection. However, for RF, SVM, and XGBoost models, the most relevant features are selected by recursive feature elimination algorithm (18, 19). This fits machine learning models with all features at the beginning and excludes the least important features based on their importance rank, resulting in a model with a reduced number of features (**Figure 2**). This elimination process is then iterated by updating the feature importance rank using the model from the previous iteration, thus updating the model with a fewer number of features. The recursive feature elimination stops when the highest area under the ROC curve (AUROC) is achieved, and the final feature sets is the optimal feature set for our final models (**Figure 3A**).

For RF and XGBoost, the feature importance is measured by a mean decrease in Gini index, which reflects the contribution of each feature to the purity of the nodes or leaves in the tree-based models. The greater the mean decrease in Gini index, the more important the feature is in the model. For SVM, the feature importance is measured using the AUROC value. To compare the feature importance returned by different models, we scale the importance scores to the same scale (0–1) for each model

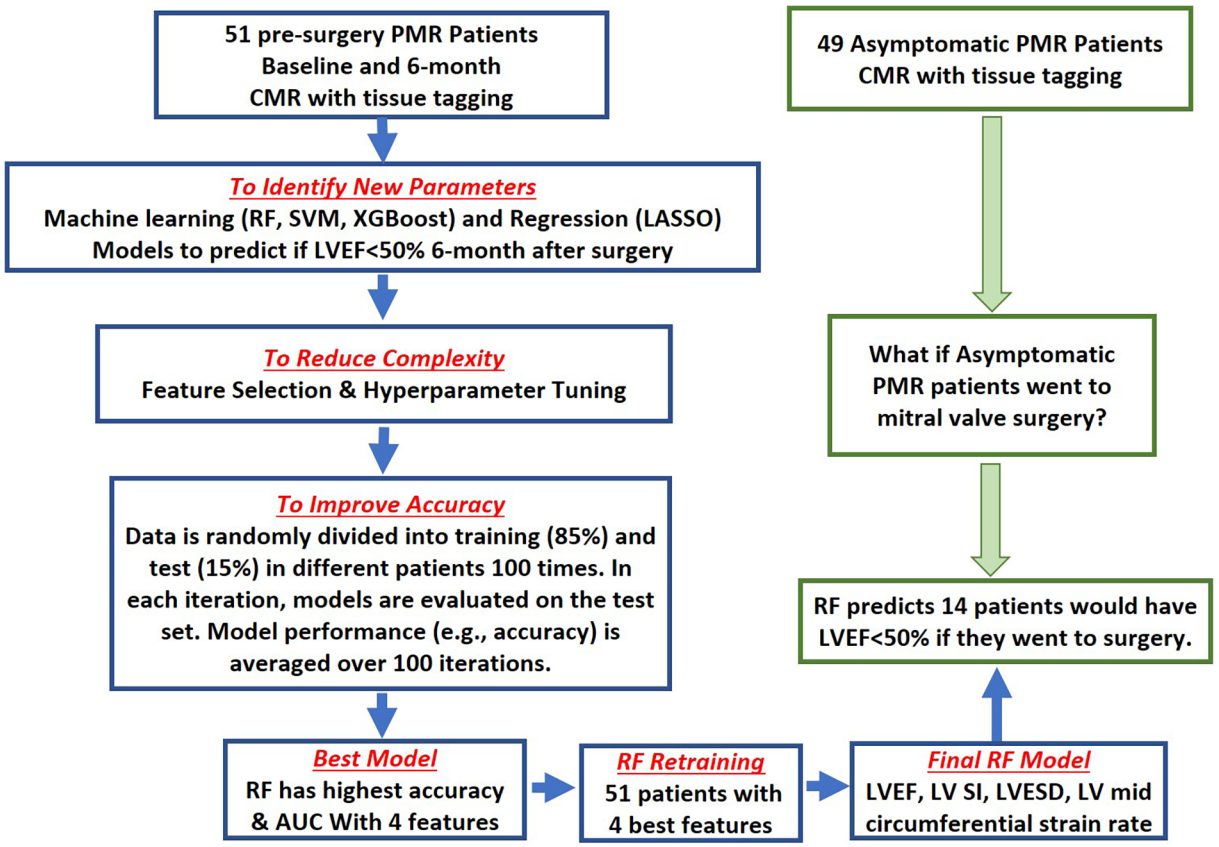

FIGURE 2
Flow chart of proposed model training and validation process. 51 pre-surgery and 49 asymptomatic PMR patients were recruited between 2005 and 2010. Random sampling was performed in pre-surgical patients to generate balanced data. Training ($n = 43$) and Testing Sets ($n = 8$) were established (blue flow chart). For each model, feature selection identified a subset of features relevant in predicting post-surgical LVEF <50% using LASSO, or the machine learning models: random forest (RF), support vector machine (SVM), and extreme gradient boosting (XGBoost) models. Random forest had the highest area under the curve and accuracy and was chosen as the best predictive model. Based on the top 4 predictive features [LVEF, LV Sphericity Index (SI), LVESD and LV systolic circumferential strain rate], the RF model was retrained on the 51 pre-surgery PMR patents then applied to 49 asymptomatic PMR patients to predict LVEF < 50% (14 patients—28%) if they were to have mitral valve surgery (green flow chart).

separately as follows:

$$Imp_{i,scaled} = \frac{Imp_i - Imp_{min}}{Imp_{max} - Imp_{min}}, i = 1, 2, \ldots, 37$$

where Imp is the raw importance score, Imp_{max} is the maximum importance score among 37 features, and Imp_{min} is the minimum importance score among 37 features. Figure 3C shows the top features selected by the four models.

Model training and testing process

Fifteen percent of pre-surgical PMR patients are randomly selected as an independent testing set ($n = 8$), and the remaining 85% are used to train the initial machine learning models ($n = 43$) using the initial 37 features (Table 1). During each iteration in recursive feature elimination, hyper-parameter tuning and cross-validation are performed to obtain the model with a reduced feature set and optimal hyper-parameters. For the LASSO and machine learning methods, the corresponding models with the optimal feature sets that result in the highest AUROC were selected as final models. Subsequently, the four final models are further evaluated and compared *via* cross-validation. To eliminate the potential sampling bias and to obtain a robust model performance, we repeated the splitting, training, and testing process 100 times (i.e., using a different testing patient set of $n = 8$ vs. the training set of $n = 43$), and record the averaged model performance across iterations in the results.

The LASSO and machine learning models are evaluated *via* six metrics: classification accuracy, area under the receiver operating characteristic curve (AUROC), area under Precision-Recall (PR) curve (AUPRC), sensitivity, specificity, precision, and F1 score in the 51 pre-surgical PMR patients who have an actual known outcome of LVEF < 50% at 6 months post-surgery (Figure 3D). Among the six metrics, AUROC was used to choose the final prediction model for post-surgical LVEF < 50%.

$$Accuracy = \frac{TP + TN}{TP + TN + FP + FN}$$

$$Sensitivity = \frac{TP}{TP + FN}$$

$$Specificity = \frac{TN}{TN + FP}$$

$$Precision = \frac{TP}{TP + FP}$$

$$F1\ score = \frac{2TP}{2TP + FP + FN}$$

Where TP, TN, FP, and FN = true positive, true negative, false positive, and false negative.

Interpretation of machine learning model

To interpret the final predictive model, we compute the Shapley Additive exPlanations (SHAP) (14) value, which is developed from the Shapley value in cooperative game theory. The Shapley value in game theory quantifies the contribution that each player brings to the game. Similarly, the SHAP value quantifies the contribution of each feature to the model prediction. In our case, one game is one patient, and the players are the optimal feature sets in the final predictive model. The SHAP value of a particular feature is computed by weighting the marginal contributions of the feature. For pre-surgery PMR patient or asymptomatic PMR patient, we compute the SHAP value to evaluate the contribution of each feature to prediction of the post-surgical LVEF < 50%. Therefore, the SHAP value provides a local (i.e., patient-level) interpretation of the decision made by the final machine learning model. Moreover, by averaging the absolute SHAP values, we can obtain the overall feature importance, which provides an overall (i.e., group-level) interpretation of the machine learning model. In addition, the sign of the SHAP value implies the directional impact of each feature on the prediction (i.e., a positive SHAP implies positive impact on the probability of post-surgical LVEF < 50%).

Results

Baseline characteristics of asymptomatic and pre-surgical PMR patients

There is a significantly higher incidence of episodic atrial fibrillation and medications, LV end-diastolic dimension (LVEDD), LVESD, and pulmonary artery systolic pressure (by Echo/Doppler) in pre-surgery vs. asymptomatic PMR. Forty seven per cent of pre-surgical patients are Class I, and all patients had normal renal function. Median pulmonary systolic pressure and median pulmonary artery wedge pressure are 38 and 16 mmHg, respectively, in pre-surgical patients (**Supplementary Table S1**).

CMR in asymptomatic and pre-surgery patients with moderate to severe PMR

LVEF does not differ among normal and both PMR groups. LV end-diastolic volume, LV stroke volume, LVEDD, LVESD, and regurgitant volume and XO activity are greater in pre-surgery vs. asymptomatic PMR. However, LVED mass/volume, Sphericity Index, and LVED 3-dimensional radius of curvature/wall thickness at mid LV do not differ in asymptomatic and pre-surgery PMR patients. Asymptomatic and pre-surgery patients have decreased LV systolic twist/volume slope (°/mL) vs. controls. The increase in plasma ICTP and decrease in the PICP are consistent with net collagen degradation in pre-surgery PMR patients. There is an increase in LA maximum and minimum volumes in asymptomatic PMR compared to normal and they are higher in pre-surgical PMR patients. However, only pre-surgical PMR patients have a decrease in total LA emptying fraction (**Supplementary Table S2**).

CMR in pre-surgery PMR patients with LVEF < 50% at 6 months post-surgery

Among the 51 pre-surgical patients, 13 patients (25.49%) had a decrease in CMR LVEF < 50% at 6 months post-surgery. Patients with LVEF < 50% were more likely to have a median baseline LVEF < 58% by CMR and a greater incidence of atrial fibrillation. Those with a decrease in LVEF had a higher LV end-systolic volume index and lower LV sphericity index and LV mid systolic circumferential strain rate, prior to surgery. However, FDR-adjusted *p*-values indicated no significant differences between the two groups (**Table 2**).

Statistical and machine learning modeling in pre-surgery PMR patients

Four predictive models: a standard linear model - LASSO, and three machine learning models: RF, SVM, and XGBoost were trained to predict a binary response variable with two levels: LVEF < 50% or >50% at 6 months after mitral valve surgery in the 51 pre-surgery PMR patients (**Figure 2**). The models were initially developed using 37 features including demographics, CMR parameters, and biomarkers for predictive modeling (**Table 1**). To reduce the complexity of the model, feature selection (**Figure 2**) identifies a subset of features that are relevant in predicting a post-surgical LVEF < 50% using LASSO for the linear model and recursive feature elimination for the machine learning models. **Figure 3A** shows the ROC and precision-recall curves (PRC) (**Figure 3B**) and the top important features selected by LASSO and the machine learning models (**Figure 3C**) and lists the model performance (**Figure 3D**) for all four models including: AUROC, AUPRC, accuracy, sensitivity, specificity, precision, and F1 score along with the 95% confidence

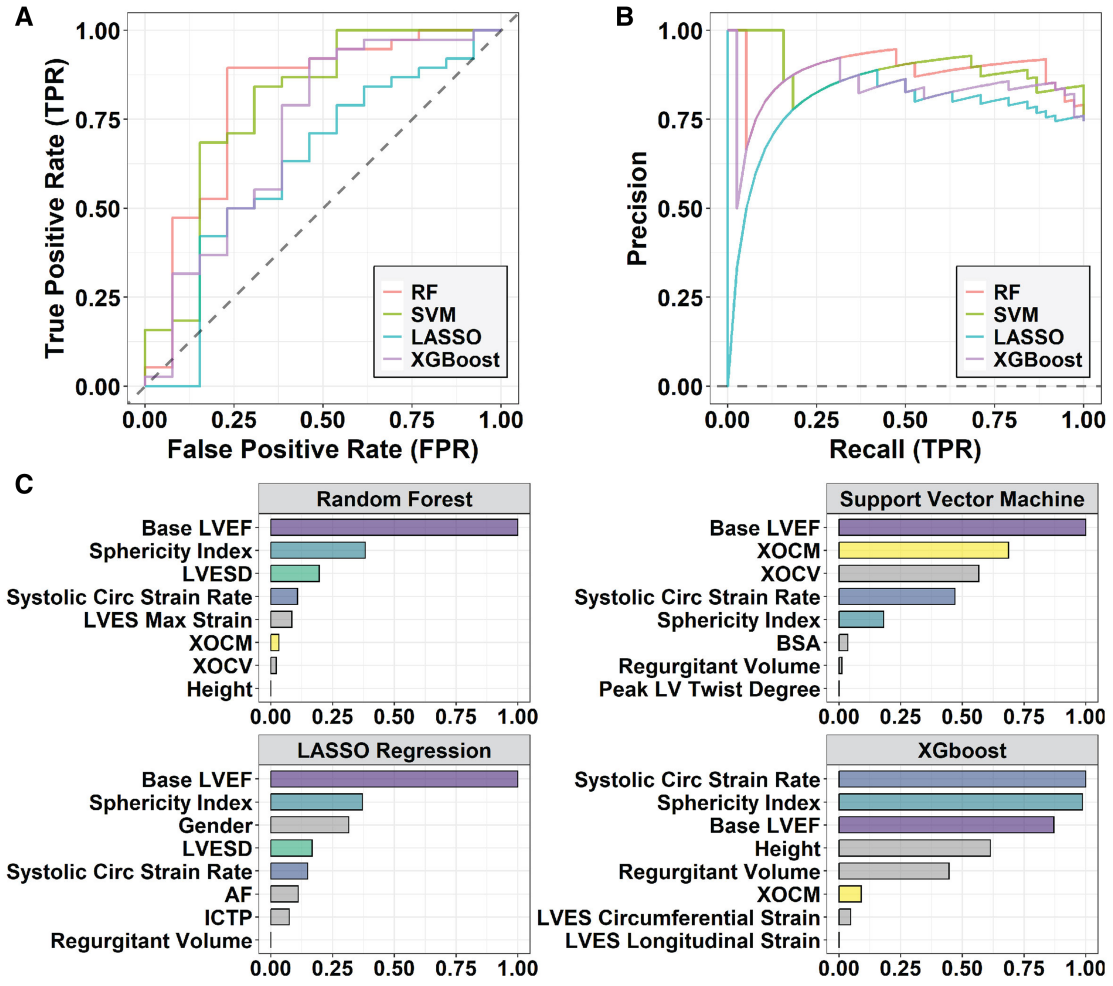

D

Linear and Machine Learning Model Performance Metrics (95% Confidence Intervals)							
	AUROC	AUPRC	Accuracy	Sensitivity	Specificity	Precision	F1
RF	0.846 (0.791,0.901)	0.958 (0.941,0.976)	0.862 (0.835,0.888)	0.904 (0.878,0.930)	0.650 (0.555,0.745)	0.936 (0.918,0.954)	0.913 (0.896,0.930)
SVM	0.834 (0.780,0.888)	0.958 (0.942,0.974)	0.858 (0.835,0.882)	0.940 (0.919,0.961)	0.450 (0.351,0.549)	0.904 (0.886,0.921)	0.916 (0.901,0.931)
XGBoost	0.801 (0.743,0.859)	0.949 (0.932,0.967)	0.863 (0.840,0.887)	0.920 (0.897,0.943)	0.580 (0.482,0.678)	0.926 (0.908,0.943)	0.916 (0.901,0.931)
LASSO	0.638 (0.572,0.704)	0.902 (0.879,0.925)	0.768 (0.743,0.794)	0.884 (0.856,0.912)	0.190 (0.112,0.268)	0.849 (0.833,0.864)	0.859 (0.842,0.877)

FIGURE 3
(A) the receiver operating characteristic (ROC) and (B) precision-recall curves (PRC) for logistic regression with LASSO, random forest (RF), SVM, and XGBoost models. (C) Feature selection identifies a subset of features that are relevant/important in predicting a post-surgical LVEF < 50% using LASSO for the linear model and Recursive Feature Elimination for the RF, SVM, and XGBoost models. XOCM is XO activity in μUnits/mg protein; XOCV is XO activity in μUnits/ml plasma. (D) Table of Model Performance for each Predictive Model with 95% confidence intervals in parentheses.

interval generated *via* bootstrapping. Overall, the machine learning models outperform the LASSO regression model. Based on the top features, the RF model provided the highest AUROC and AUPRC and was chosen to re-train the 51 pre-surgical patients using the four most relevant features identified by RF, for predicting LVEF < 50%: baseline LVEF, LV Sphericity Index, LVESD, and LV Systolic circumferential strain rate to improve predictability of the final model (Figure 2).

Random forest model interpretation

The SHAP value interprets the contribution of the four important features of the RF model that predict post-surgery LVEF < 50% for both pre-surgery (Figure 4A) and asymptomatic PMR patients (Figure 4B). The directional impact of each feature is represented by the sign (negative or positive) of the SHAP value. A positive SHAP for each feature has a positive

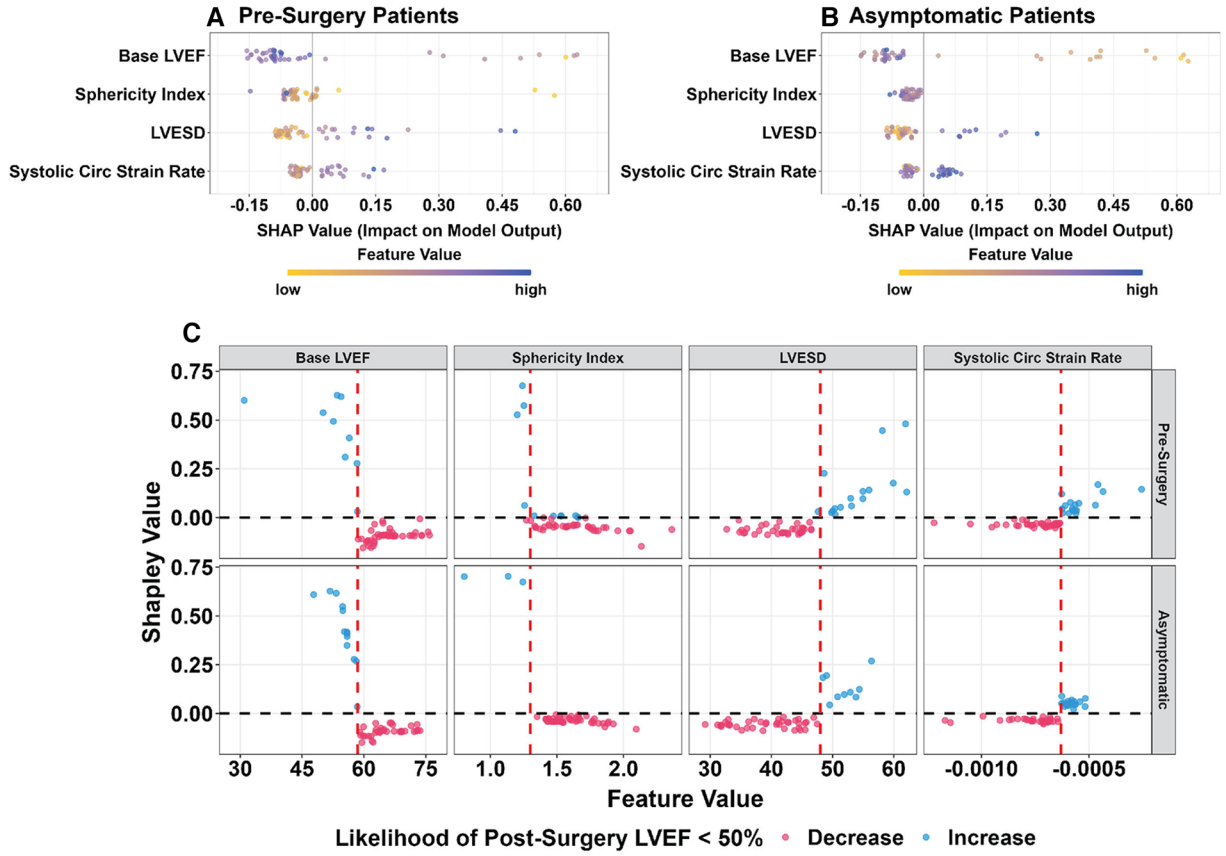

FIGURE 4
SHAP values for pre-surgery (A) and asymptomatic (B) PMR patients. Color value of each feature: highest blue and lowest yellow. Negative SHAP value (left side of 0.0) is a negative impact on the odds ratio, i.e., less likely to have post-surgical LVEF < 50%. Positive SHAP value (right side of 0.0) indicates a higher probability of post-surgical LVEF < 50%. (C) SHAP values for pre-surgery (top) & asymptomatic (bottom) PMR presented with potential cutoff values (red vertical dashed line) indicating the likelihood of post-surgical LVEF < 50%. A negative SHAP value (red) indicates a negative impact on the odds ratio, i.e., less likely to have post-surgical LVEF < 50%. A positive SHAP value (blue) indicates a higher probability of post-surgical LVEF < 50%. Each circle is representative of an individual patient.

impact on the probability of post-surgery LVEF < 50%. A negative SHAP value has a negative impact on the probability of post-surgery LVEF < 50%. The larger the absolute value of SHAP, the greater the contribution the feature has to the model prediction.

Figure 4C shows the SHAP value of the four features in the RF model with a data-driven cutoff value (red vertical dashed line) indicating the directional impact on the likelihood of post-surgical LVEF < 50% in pre-surgery (top graphs) and asymptomatic (bottom graphs) PMR patients. Each circle represents one patient, and the color denotes positive (blue) or negative (red) impact of the feature on the probability (or likelihood) of post-surgery LVEF < 50%. The higher the absolute baseline CMR derived LVEF (>58%) and sphericity index (>1.3), the less likely for post-surgical LVEF < 50% (negative SHAP values). Mid LV systolic circumferential strain rate is a negative quantity and more negative values represent a greater circumferential shortening rate. Thus, <−0.63 1/s (−0.00063 1/ms) suggests that it is less likely for post-surgical LVEF < 50% (negative SHAP values). In comparison, the higher the LVESD (>48 mm), the more likely to have a post-surgical LVEF < 50% (positive SHAP value).

Prediction of LVEF < 50% after mitral valve surgery in asymptomatic PMR

We address the important question of how many asymptomatic PMR patients would potentially be at risk for LVEF < 50% if they had gone to surgery. Therefore, we retrained the optimal RF model with the four selected features in all 51 pre-surgery PMR patients, and applied it to asymptomatic PMR patients (Figure 2). Random Forest predicted 14 out of 49 (28.57%) asymptomatic PMR patients would have LVEF < 50% post mitral valve surgery, had they gone to surgery.

Discussion

In the current study, we employed a combination of machine learning and regression methods with the intention of identifying a combination of CMR (and biomarker) predictors not accounted for by a linear model alone for predicting LVEF < 50% at 6 months after surgery. In addition to LVEF and LVESD, mid

LV systolic circumferential strain rate and LV sphericity index predict LVEF < 50% six months after surgery. **Figure 1** outlines the value of utilizing both machine learning and regression modeling to achieve an optimal analytical result in addressing this complicated question. Compared with classic regression models, machine learning: (1) integrates predictors extracted from multiple sources and models both linear and nonlinear interactions amongst them and; (2) identifies unexpected predictors not accounted for by linear models.

The RF model was most accurate when reducing the features to LVEF, LVESD, LV sphericity index and LV mid wall circumferential strain rate in comparison to linear regression modeling. CMR LV strain emanates from tissue tagging that allows for intramyocardial displacement and strain by motion of identifiable material points distributed throughout the myocardium (5, 6). The adverse spherical remodeling, increase in LV mid radius/wall thickness, and global decrease in LVED mass/volume elevates wall stress resulting in a detrimental effect on LV mid circumferential shortening. Models that determine the effect of LV shape on LVEF demonstrate the importance of circumferential strain over longitudinal strain in maintaining LVEF in the spherically dilated LV (20). However, these models do not account for the presence of mitral regurgitation. In this pilot study, the RF model captures the inescapable LV spherical remodeling characteristic of PMR (5, 6, 16, 21). This connection to circumferential strain rate rather than circumferential strain alone further underscores the confounding factors of PMR ejection dynamics in the face of ejection into the low pressure left atrium, increased preload, and increased adrenergic drive in patients with PMR and LVEF > 60% (22, 23). The decrease in contractile velocity at the LV mid wall can be attributed to the loss of sarcomeres in the PMR heart (5, 6, 16, 21).

Regurgitant volume and plasma XO activity are other features identified more than once in the four models. However, the regurgitant volume calculated from the difference of LV and RV stroke volumes is an underestimate due to the 30% incidence of significant tricuspid regurgitation in the pre-surgical PMR patients. When calculated using phase velocity mapping for forward stroke volume, regurgitant volume may become a very powerful feature predictor as demonstrated in previous studies in PMR patients (24). We have reported an increase in LV and plasma XO, extensive mitochondrial damage, and breakdown of desmin in patients with moderate to severe PMR and LVEF > 60% (5, 6, 16). Xanthine oxidase can depress myofilament sensitivity to calcium and XO products like superoxide and hydrogen peroxide, can oxidatively influence mitochondria, myofilaments, calcium handling proteins, resulting in decreased LV strain rate (25).

An important addition to the interpretation of machine learning models is the SHAP (Shapley Additive exPlanations) (14) value, developed from the Shapley value in cooperative game theory. The SHAP value assigns each feature an importance value for a particular prediction to explain the decision made by the machine learning models. The SHAP value provides an *overall interpretation* of the machine learning models including a directional impact of each feature on the prediction (i.e., a positive or negative impact on the probability of post-surgical LVEF < 50%) and a *local interpretation* at the patient level (i.e., knowing how each feature contributes to an individual prediction for each patient). This provides cutoff values that in a larger sample size can comprise a risk score.

The relatively small sample size and the absence of an external validation set is a limitation in this preliminary study, in addition to the potential for overfitting in a small number of patients. To address this, feature selection *via* LASSO (linear model) or recursive feature elimination (machine learning models) reduces the number of features and model complexity. To eliminate the potential sampling bias and obtain a robust model performance, we iterate the splitting, training, and testing process 100 times (i.e., using a different testing patient set of $n = 8$ vs. the training set of $n = 43$), and record the averaged model performance.

To demonstrate the limitation of regression analysis, we employed univariate regression vs. multivariate regression for LVEF, LVESD, LV sphericity index and LV mid circumferential strain rate to predict LVEF < 50%. Coefficients for univariate regression with single features (**Supplementary Table S3**) produce a similar pattern to machine learning, and the four features except LVESD. Inclusion of the four features in a multivariate logistic regression, the coefficients still produce similar patterns as machine learning, however, all four features are no longer significant (**Supplementary Table S4**). **Supplementary Table S5** also shows the odds ratio of the top 4 and 8 features from the RF model (**Figure 3C**). Therefore, multivariate logistic regression is not adequate when multiple features are interacting in both linear and nonlinear relations with the outcome. Consequently, the use of machine learning models may provide a better method of accurately assessing the contribution of linear and non-linear features in predicting a post-surgical decline in LVEF < 50%. This is depicted in a representative tree in the random forest (**Supplementary Figure S1**) and variable dependence and partial dependence plots (**Supplementary Figure S2**) that show that the association of the top 4 features in the RF model are not linear to the outcome (LVEF < 50%). This underscores the analytical benefits of a combination of regression and machine learning models and the potential advantages of utilizing the latter (**Figure 1**).

The impetus for this study is the unreliability of an echocardiographic LVEF > 60% in the complicated context of increased preload and facilitation of LV ejection in patients with PMR. Machine learning and multiple testing most certainly increase the risk of drawing a false-positive conclusion. Nevertheless, the findings from this approach, in albeit a small number of patients present a cogent argument for the underpinnings of LV sphericity and mid LV circumferential strain rate in the pathophysiology of PMR. Whether these, or any combination of LV and biomarker features, can reliably identify the need for surgery with better LV functional recovery can only be confirmed in a longitudinal study that incorporates machine learning and statistical models that capture both linear and non-linear interactions in asymptomatic PMR patients with LVEF > 60%.

Data availability statement

The original contributions presented in the study are included in the article/**Supplementary Material**, further inquiries can be directed to the corresponding author.

Ethics statement

The studies involving human participants were reviewed and approved by University of Alabama at Birmingham IRB and Auburn University IRB. The patients/participants provided their written informed consent to participate in this study.

Author contributions

JZ—Involved in the concept design, development, methodology and in-depth analyses and interpretation of machine learning and statistical predictive models and critical review and final approval of the manuscript. YL—Involved in analyses of machine learning and statistical predictive models and approval of the manuscript. NB—Involved in the design and analyses of machine learning and statistical predictive models, critical review and approval of the manuscript. MA—Involved in the recruitment and retention of subjects and critical manuscript review and approval pertaining to the mechanisms of the disease pathology. YF—Involved in the development of machine learning predictive models and provided critical review of methodologies, analyses and interpretation in the manuscript. BP—Involved in data collection, analyses, interpretation, critical review, preparation and final approval of manuscript. TD—Involved in design, analysis and interpretation of magnetic resonance data, critical review and approval of the manuscript. LD—Corresponding author conceived the idea and design of the manuscript, subject recruitment and retention. Spearheaded data analyses, and interpretation of the predictive models based on physiological mechanism of disease. Drafted and critically revised all contents of the manuscript and gave final approval of the manuscript for publication. All authors contributed to the article and approved the submitted version.

Funding

This work was supported by the National Heart, Lung, and Blood Institute and Specialized Centers of Clinically Oriented Research grant [P50HL077100 to L.J.D] in cardiac dysfunction; Department of Veteran Affairs for Merit Review grant [1CX000993-01 to L.J.D]; and National Institutes of Health Grant [P01 HL051952 to L.J.D]. No relationships to industry.

Conflict of interest

The authors declare that the research was conducted in the absence of any commercial or financial relationships that could be construed as a potential conflict of interest.

Publisher's note

All claims expressed in this article are solely those of the authors and do not necessarily represent those of their affiliated organizations, or those of the publisher, the editors and the reviewers. Any product that may be evaluated in this article, or claim that may be made by its manufacturer, is not guaranteed or endorsed by the publisher.

Supplementary material

The Supplementary Material for this article can be found online at: https://www.frontiersin.org/articles/10.3389/fcvm.2023.1112797/full#supplementary-material.

References

1. Miller JD, Suri RM. Left ventricular dysfunction after degenerative mitral valve repair: a question of better molecular targets or better surgical timing? *J Thorac Cardiovasc Surg*. (2016) 152(4):1071–74. doi: 10.1016/j.jtcvs.2016.07.018

2. Quintana E, Suri RM, Thalji NM, Daly RC, Dearani JA, Burkhart HM, et al. Left ventricular dysfunction after mitral valve repair-the fallacy of "normal" preoperative myocardial function. *J Thorac Cardiovasc Surg*. (2014) 148:2752–62. doi: 10.1016/j.jtcvs.2014.07.029

3. Enriquez-Sarano M, Suri RM, Clavel MA, Mantovani F, Michelena HI, Pislaru S, et al. Is there an outcome penalty linked to guideline-based indications for valvular surgery? Early and long-term analysis of patients with organic mitral regurgitation. *J Thorac Cardiovasc Surg*. (2015) 150(1):50–8. doi: 10.1016/j.jtcvs.2015.04.009

4. Otto CM, Nishimura RA, Bonow RO, Carabello BA, Erwin JP 3rd, Gentile F, et al. ACC/AHA guideline for the management of patients with valvular heart disease: a report of the American college of cardiology/American heart association joint committee on clinical practice guidelines. *Circulation*. (2021) 143(5):e35–71. doi: 10.1161/CIR.0000000000000932

5. Ahmed MI, Guichard JL, Soorappan RN, Ahmad S, Mariappan N, Litovsky S, et al. Disruption of desmin-mitochondrial architecture in patients with regurgitant mitral valves and preserved ventricular function. *J Thorac Cardiovasc Surg*. (2016) 152:1059–70. doi: 10.1016/j.jtcvs.2016.06.017

6. Ahmed MI, Gladden JD, Litovsky SH, Lloyd SG, Gupta H, Inusah S, et al. Increased oxidative stress and cardiomyocyte myofibrillar degeneration in patients with chronic isolated mitral regurgitation and ejection fraction >60%. *J Am Coll Cardiol*. (2010) 55:671–79. doi: 10.1016/j.jacc.2009.08.074

7. Quer G, Arnaout R, Henne M, Arnaout R. Machine learning and the future of cardiovascular care. *J Am Coll Cardiol*. (2021) 77(3):300–13. doi: 10.1016/j.jacc.2020.11.030

8. Goldstein BA, Navar AM, Carter RE. Moving beyond regression techniques in cardiovascular risk prediction: applying machine learning to address analytic challenges. *Europ Heart J*. (2017) 38:1805–14. doi: 10.1093/eurheartj/ehw302

9. Arevalillo J, Navarro H. *Using random forests to uncover bivariate interactions in high dimensional small data sets. Proceedings of the ACM SIGKDD workshop on statistical and relational learning in bioinformatics*; (2009). p. 3–6

10. Xie X, Yang M, Xie S, Wu X, Jiang Y, Liu Z, et al. Early prediction of left ventricular reverse remodeling in first-diagnosed idiopathic dilated cardiomyopathy: a comparison of linear model, random forest, and extreme gradient boosting. *Front Cardiovasc Med*. (2021) 4(8):684004. doi: 10.3389/fcvm.2021.684004

11. Breiman L. Random forests. *Mach Learn Arch*. (2001) 45(1):5–32. doi: 10.1023/A:1010933404324

12. Chen T, Guestrin C. *XGBoost: a scalable tree boosting system. Proceedings of the 22nd ACM SIGKDD international conference on knowledge discovery and data mining*; San Francisco, CA, USA (2016). p. 785–94

13. Burges CJC. A tutorial on support vector machines for pattern recognition. *Data Min Knowl Discov*. (1998) 2(2):121–67. doi: 10.1023/A:1009715923555

14. Lundberg SM, Lee S-I. *A unified approach to interpreting model predictions. Proceedings of the 31st international conference on neural information processing systems (NIPS'17)*;. Curran Associates Inc., Long Beach, CA, USA (2017). p. 4768–77

15. Hosner DW, Lemeshow S. *Applied logistic regression. Vol 581*. New York: Jhon Wiley & Son (1989).

16. Ahmed MI, Andrikopoulou E, Zheng J, Ulasova E, Pat B, Kelley EE, et al. Interstitial collagen loss, myocardial remodeling and function in primary mitral regurgitation. *J Am Coll Cardiol Basic Trans Sci*. (2022) 7(10):973–81. doi: 10.1016/j.jacbts.2022.04.014

17. Ahmed MI, Aban I, Lloyd SG, Gupta H, Howard G, Inusah S, et al. A randomized controlled Phase IIb trial of Beta-1 receptor blockade in isolated degenerative mitral regurgitation. *J Am Coll Cardiol*. (2012) 60:833–38. doi: 10.1016/j.jacc.2012.04.029

18. Huang X, Zhang L, Wang B, Li F, Zhang Z. Feature clustering based support vector machine recursive feature elimination for gene selection. *Appl Intell*. (2018) 48:594–607. doi: https://doi.org/10.1007/s10489-017-0992-2

19. Darst BF, Malecki KC, Engelman CD. Using recursive feature elimination in random forest to account for correlated variables in high dimensional data. *BMC Genet*. (2018) 19(Supplement 1):65. doi: 10.1186/s12863-018-0633-8

20. Stokke TM, Hasselberg NE, Smedsrud MK, Sarvari SI, Haugaa KH, Smiseth OA, et al. Geometry as a confounder when assessing ventricular systolic function. Comparison between ejection fraction and strain. *J Am Coll Cardiol*. (2017) 70(8):942–54. doi: 10.1016/j.jacc.2017.06.046

21. Schiros CG, Dell'Italia LJ, Gladden JD, Clark D 3rd, Aban I, Gupta H, et al. Magnetic resonance imaging with 3-dimensional analysis of left ventricular remodeling in isolated mitral regurgitation: implications beyond dimensions. *Circulation*. (2012) 125:2334–42. doi: 10.1161/CIRCULATIONAHA.111.073239

22. Zheng J, Yancey DM, Ahmed MI, Wei CC, Powell PC, Shanmugam M, et al. Increased sarcolipin expression and adrenergic drive in humans with preserved left ventricular ejection fraction and chronic isolated mitral regurgitation. *Circ Heart Fail*. (2014) 7(1):194–202. doi: 10.1161/CIRCHEARTFAILURE.113.000519

23. Grossman PM, Linares OA, Supiano MA, Oral H, Mehta RH, Starling MR. Cardiac-specific norepinephrine mass transport and its relationship to left ventricular size and systolic performance. *Am J Physiol Heart Circ Physiol*. (2004) 287(2):H878–88. doi: 10.1152/ajpheart.00007.2003

24. Myerson SG, d'Arcy J, Christiansen JP, et al. Determination of clinical outcome in mitral regurgitation with cardiovascular magnetic resonance quantification. *Circulation*. (2016) 133(23):2287–96. doi: 10.1161/CIRCULATIONAHA.115.017888

25. Perez NG, Gao WD, Marban E. Novel myofilament Ca^{2+}-sensitizing property of xanthine oxidase inhibitors. *Circ Res*. (1998) 83:423–30. doi: 10.1161/01.RES.83.4.423

frontiers | Frontiers in Cardiovascular Medicine

TYPE Original Research
PUBLISHED 25 April 2023
DOI 10.3389/fcvm.2023.1129990

OPEN ACCESS

EDITED BY
Matteo Cameli,
University of Siena, Italy

REVIEWED BY
Matthew Parker,
UMass Memorial Medical Center, United States
Pompilio Faggiano,
Fondazione Poliambulanza Istituto Ospedaliero, Italy

*CORRESPONDENCE
Greet Kerckhofs
✉ greet.kerckhofs@uclouvain.be

SPECIALTY SECTION
This article was submitted to Cardiovascular Imaging, a section of the journal Frontiers in Cardiovascular Medicine

RECEIVED 22 December 2022
ACCEPTED 03 April 2023
PUBLISHED 25 April 2023

CITATION
Pestiaux C, Pyka G, Quirynen L, De Azevedo D, Vanoverschelde J-L, Lengelé B, Vancraeynest D, Beauloye C and Kerckhofs G (2023) 3D histopathology of stenotic aortic valve cusps using *ex vivo* microfocus computed tomography.
Front. Cardiovasc. Med. 10:1129990.
doi: 10.3389/fcvm.2023.1129990

3D histopathology of stenotic aortic valve cusps using *ex vivo* microfocus computed tomography

Camille Pestiaux[1,2], Grzegorz Pyka[1,2], Louise Quirynen[1], David De Azevedo[3,4], Jean-Louis Vanoverschelde[3,4], Benoît Lengelé[2], David Vancraeynest[3,4], Christophe Beauloye[3,4] and Greet Kerckhofs[1,2,5,6]*

[1]Mechatronic, Electrical Energy and Dynamic Systems, Institute of Mechanics, Materials and Civil Engineering, UCLouvain, Louvain-la-Neuve, Belgium, [2]Pole of Morphology, Institute of Experimental and Clinical Research, UCLouvain, Brussels, Belgium, [3]Pole of Cardiovascular Research, Institute of Experimental and Clinical Research, UCLouvain, Brussels, Belgium, [4]Division of Cardiology, University Hospital Saint-Luc, Brussels, Belgium, [5]Department of Materials Engineering, KU Leuven, Heverlee, Belgium, [6]Prometheus, Division for Skeletal Tissue Engineering, KU Leuven, Leuven, Belgium

Background: Calcific aortic stenosis (AS) is the most prevalent heart valve disease in developed countries. The aortic valve cusps progressively thicken and the valve does not open fully due to the presence of calcifications. *In vivo* imaging, usually used for diagnosis, does not allow the visualization of the microstructural changes associated with AS.
Methods: *Ex vivo* high-resolution microfocus computed tomography (microCT) was used to quantitatively describe the microstructure of calcified aortic valve cusps in full 3D. As case study in our work, this quantitative analysis was applied to normal-flow low-gradient severe AS (NF-LG-SAS), for which the medical prognostic is still highly debated in the current literature, and high-gradient severe AS (HG-SAS).
Results: The volume proportion of calcification, the size and number of calcified particles and their density composition was quantified. A new size-based classification considering small-sized particles that are not detected with *in vivo* imaging was defined for macro-, meso- and microscale calcifications. Volume and thickness of aortic valve cusps, including the complete thickness distribution, were also determined. Moreover, changes in the cusp soft tissues were also visualized with microCT and confirmed by scanning electron microscopy images of the same sample. NF-LG-SAS cusps contained lower relative amount of calcifications than HG-SAS. Moreover, the number and size of calcified objects and the volume and thickness of the cusps were also lower in NF-LG-SAS cusps than in HG-SAS.
Conclusions: The application of high-resolution *ex vivo* microCT to stenotic aortic valve cusps provided a quantitative description of the general structure of the cusps and of the calcifications present in the cusp soft tissues. This detailed description could help in the future to better understand the mechanisms of AS.

KEYWORDS

aortic stenosis, microstructural characterization, ex vivo imaging, microfocus computed tomography, 3D histopathology

1. Introduction

Calcific aortic stenosis (AS) is the most prevalent heart valve disease in developed countries, as it affects about 29% of the population over 65 (1). It is characterized by the thickening of the aortic valve (AV) and is associated with the growth of calcifications within the extracellular matrix of the valve cusps. The preliminary stage of the disease corresponds to sclerosis, in which the valve is thickened and contains focal areas of calcification while the mobility of the cusps is considered normal. With time, the disease impairs the proper functioning of the valve by decreasing its aperture. This results in stenosis, left ventricular (LV) hypertrophy and finally heart failure. Advanced AS causes clinical symptoms such as decreased exercise tolerance, syncope and dyspnea (2, 3).

Severity of stenosis is evaluated based on *in vivo* parameters such as the mean pressure gradient (MPG) across the AV, the AV area and the peak aortic jet velocity. This is mostly measured using *in vivo* ultrasound imaging, such as transthoracic two-dimensional and Doppler echocardiography. This allows verification of the integrity and motion of the valve and the blood flow parameters, respectively (4, 5). However, several characteristics of AS remain unclear. For instance, the complex mechanism resulting in calcifications is not fully understood yet. Several studies suggest that calcifications arise from a succession of events, involving endothelial damage, lipid infiltration, inflammation, fibrosis and finally mineralization (2, 5–8). However, no preventive treatment has successfully been applied to slow down the AS progression (9, 10). Moreover, the spatial distribution, size and shape of the calcifications have been scarcely and inconsistently described, although they are the predominant feature causing the AV narrowing (2, 11, 12). Refining the pathogenesis of AS and of calcifications might thus open the way for new treatment strategies. In addition to the presence of calcifications, thickening of the cusps is also recognized as a major step in the disease (13). Some rare studies mention the preferential thickening and/or calcification of the non-coronary cusp compared to the other two (7, 14, 15). However, current literature contains few studies about the normal value of the AV thickness and the threshold values for sclerosis and stenosis (14, 16).

To be able to better characterize the microstructure of heart valves (i.e., the complex arrangement of the extracellular matrix components at the microscale and the presence of calcification), especially in case of stenosis, X-ray computed tomography (CT) is a valuable solution. It has already been extensively used *in vivo* (XCT) (17, 18) and *ex vivo* (microCT) (11, 19–21) to image mineralized tissues. In the particular case of calcific AS, it was used to quantify the volume fraction of calcification and to demonstrate the correlation between the aortic valve calcium score and the hemodynamic parameters obtained from Doppler echocardiography both *in vivo* and *ex vivo* (17, 19). However, despite being successfully used to define the severity of AS, with a better accuracy than echocardiography alone (17, 22–24), high-resolution microCT has never been applied to quantitatively compare the microstructural properties and composition of the valve and of the calcifications in different diagnosis groups of AS.

The aim of this study was to obtain a quantitative description of the microstructure and composition of calcified AV cusps using high-resolution microCT, for a better understanding of the calcification mechanism within the AV. In addition to the volume proportion of calcification, which is usually obtained from microCT, we examined the calcifications in terms of size, amount, number of particles and density composition. Changes in the soft tissues of the cusp were also described. Finally, our imaging technique was applied to different clinical diagnoses of AS.

2. Materials and methods

2.1. Description of AS severity

The severity of AS is evaluated based on echocardiographic parameters. High-gradient severe AS (HG-SAS) corresponds to MPG $\geq$ 40 mmHg, AV area $<$ 1 cm^2 and peak aortic jet velocity $\geq$ 4 m/s while moderate AS is defined by MPG $<$ 40 mmHg, AV area $\geq$ 1 cm^2 and peak aortic jet velocity from 2 to 4 m/s (25). However, some intermediate cases exist, as described in **Table 1**. This study contains three diagnosis groups: HG-SAS, moderate AS, and normal-flow low-gradient severe AS (NF-LG-SAS).

2.2. Patient selection

Patients were selected, as described in Boulif et al., (23), after a diagnosis of NF-LG-SAS, moderate AS or HG-SAS. AS caused by radiotherapy or irradiation were part of the exclusion criteria. For this retrospective study, only 14 patients for whom the number of samples collected at surgery was equal to three cusps per valve, were included. Among them, 5 were diagnosed as NF-LG-SAS, 2 as moderate AS and 7 as HG-SAS. One non-stenotic aortic valve cusp was included as non-calcified sample. It was provided by the donor bank and not used for transplantation because of a subtle commissural fusion. The study protocol was approved by the local ethical committee (2014/21NOV/560 and 2021/13JAN/014) and all patients gave informed consent prior to inclusion into the study.

TABLE 1 Classification of AS with reduced AV area opening ($\leq$1 cm^2) based on parameters measured *in vivo* using ultrasound imaging, according to (**2**, **26**).

		High-gradient (MPG $\geq$ 40 mmHg)	Low-gradient (MPG $<$ 40 mmHg)
Normal-flow (SVi $>$ 35 ml/m^2)	Preserved LVEF ($>$ 50%)	High-gradient severe AS (HG-SAS)	Normal-flow low-gradient severe AS (NF-LG-SAS)
Low-flow (SVi $<$ 35 ml/m^2)	Preserved LVEF ($>$ 50%)	High-gradient severe AS (HG-SAS)	Paradoxical low-flow low-gradient severe AS (PLG-SAS)
	Reduced LVEF ($<$ 50%)	High-gradient severe AS (HG-SAS)	Classical low-flow low-gradient AS

AS, aortic stenosis; LVEF, left ventricular ejection fraction; MPG, mean pressure gradient; SVi, stroke volume index.

2.3. High-resolution microfocus X-ray computed tomography imaging

All samples were preserved at −80 °C until sample preparation. They were thawed at room temperature and slightly dried on a paper tissue. Then, they were mounted in a sample holder, including a borosilicate bead to normalize the gray values in the reconstructed images. All samples were imaged using a Phoenix Nanotom M (GE Measurement and Control Solutions, Germany) equipped with a 180 kV/15 W energy nanofocus X-ray tube and a diamond-coated tungsten target. The voxel size was 14 µm. For one NF-LG-SAS cusp, zoom images at two different spatial resolutions were performed after cutting a region of interest from the sample. All acquisition and reconstruction parameters are listed in **Table 2**.

All microCT datasets were reconstructed with the Datos|x software (GE Measurement and Control Solutions, Germany) and exported as XY slices (.tiff). For one sample, an in-house developed MATLAB (The MathWorks, Massachusetts, USA) script was used to convert the 16-bit slices (.tiff) to 8-bit slices (.bmp), while simultaneously normalizing the histogram range to the dynamic range of the dataset. All the other datasets were normalized to that one using a second in-house developed MATLAB script with the borosilicate bead and the sample holder as reference materials. MATLAB scripts are available on github (27, 28).

2.4. Image segmentation and structural analysis of the entire cusp

For each dataset, the valvular tissue was segmented from the background using Avizo (Thermo Fisher Scientific, Bordeaux, France). Briefly, a region-of-interest was defined to remove the sample holder, and the cusp was then binarized using a manually selected threshold (25–255). For this, CTAn was used (Bruker MicroCT, Kontich, Belgium). Then, a closing step was performed to remove the small holes (square of size 5) and 3D analysis was performed (i.e., volume and thickness distribution, 3D analysis module) on the entire cusp (including both soft tissues and calcifications).

TABLE 2 Microct acquisition and reconstruction parameters, cusp N4.1 corresponds to the NF-LG-SAS cusp that was imaged at two higher resolutions after the selection of a region of interest.

	All cusps	Cusp N4.1	
Voxel size (µm)	14	5	1.2
Filter material	0.5 mm Al	0.5 mm Al	0.5 mm Al
Source voltage (kV)	90	90	90
Tube current (µA)	400	230	170
Exposure time (ms)	500	500	1,250
Tube focus mode	0	0	1
Number of images	800	1,600	1,600
Average	1	3	3
Skip	0	1	1
Fast scan mode	Yes	No	No
Acquisition time (min)	6'40"	57'	2 h17'
Beam hardening correction	9	9	9

2.5. Image segmentation and structural analysis of calcifications

Within the entire cusp, the calcifications were segmented using a multilevel Otsu segmentation (3 levels, CTAn). To have the same threshold values for all samples, the mean from the multi-level segmentation was selected (i.e., 75 ± 4.05, 139 ± 6.11 and 197 ± 5.94 for low, moderate and high density, respectively) and applied to all samples. The volume fraction of all calcifications within the cusp (all densities included, gray values from 75 to 255) was quantified (CTAn). All voxels identified as calcification (no distinction of density) and connected to each other were defined as one calcified particle (labeling module from Avizo). All particles of 10 voxels or less were not considered. The number of calcified particles and their volume were then computed. Three categories of volume were defined. The first category corresponds to particles up to 1×10^{-3} mm^3, the second one includes particles from 1×10^{-3} mm^3 to 1 mm^3 and the third category contains particles from 1 mm^3 and above. Then, to compensate the partial volume effect (PVE) observed when segmenting the calcifications with different densities, an in-house protocol was developed (CTAn). First, the high-density calcifications (HD, gray values 197–255) were segmented. This volume was dilated by two voxels and removed from the entire cusp. Then, the moderate and low-density calcifications were successively segmented (gray values 139–255 and 75–255 respectively). Additionally, an opening step (square of size two) was performed on both selections (MD and LD). Finally, each of the three selections (HD, MD and LD) were individually dilated by one voxel to compensate the volume loss and the final volumes were quantified for each density. This PVE correction resulted in a final volume loss of 11.02% ± 1.47% (**Supplementary Figure S1**), but eliminated wrongly assigned edge voxels of calcifications to another density class. 2D and 3D renderings were performed using Avizo.

2.6. Scanning electron microscopy (SEM) imaging

The region of interest cut from sample N4.1, and previously imaged at higher resolution with microCT, was embedded in paraffin in a home-made cylindrical shape holder. It was then cut with a micro-precision saw (Accutom 50, Struers LLC, USA) at the specific location determined based on the high-resolution microCT data. After mounting on a SEM holder, the top surface was sputtered with gold to make the sample conductive. The images were generated with the backscattered electron detector on the Ultra 55 FEG SEM (Zeiss, Germany) at a voltage of 15 kV.

2.7. Statistical analysis

GraphPad Prism 9 (GraphPad Software, California, USA) was used for the statistical analysis and data visualization. To compare

the NF-LG-SAS and HG-SAS groups, Mann-Whitney tests were performed for each structural parameter. Depending on the normality of the datasets, correlations were evaluated with Pearson or Spearman tests. To assess the effect of the diagnosis and of the density on the volume quantified for each density calcification, a multiple 2-way ANOVA test was performed. p-values below 0.05 were considered to be significant; *: $p < 0.05$, **: $p < 0.01$, ***: $p < 0.001$ and ****: $p < 0.0001$. In the bar graphs, the mean value of the different samples is indicated by the height of the bars. Error bars represent the standard deviation and the individual datapoints are given.

3. Results

3.1. *Ex vivo* microCT provides the 3D spatial localization of calcifications and reveals that the volume fraction of calcification is significantly lower in case of NF-LG-SAS than in HG-SAS

The volume fraction of calcification present in the soft tissues of calcified AV cusps explanted from human patients was computed both per valve and per cusp, based on *ex vivo* microCT images (**Figure 1**). First, we were capable of assessing the spatial distribution of the calcifications. Although calcifications are sometimes described as extrinsic (11), the 3D visualization obtained in our work demonstrated that calcifications were located inside the cusp soft tissues, with some rare particles visible on the subendothelial surface. They were mainly located on the adherent edges of the cusp, along the attachment to the anulus, while for the most calcified samples, not only the edges of the cusp were calcified, but the midportion of the cusp, between free and adherent edges, was affected as well (**Figures 1A–F**). Then, the volume fraction of calcification was assessed. It ranged from 9.8% to 50.9%, which demonstrates the wide variation among patients, but also among the three cusps of the same patient (**Figure 1G**). The volume fraction was significantly lower for the NF-LG-SAS cusps than for the HG-SAS ones (**Figure 1H**). The volume fraction of calcification was correlated with the mean pressure gradient across the AV. This correlation was stronger when both NF-LG-SAS and HG-SAS groups were considered compared to each group taken individually (**Figure 1I**). While the severity of NF-LG-SAS is still under discussion, in this case, most of the samples corresponding to NF-LG-SAS had a lower relative amount of calcification than the moderate AS samples. Since only 2 patients (corresponding to 6 cusps) had a moderate AS diagnosis, they were excluded from the statistical analyses.

3.2. The number and size of the particles constituting the calcifications is related to the severity of AS

Apart from a volumetric assessment of the calcifications, this study aimed at structurally describing the calcifications present in the cusp in an effort to investigate calcification formation mechanism. A calcified particle was defined as a cluster of voxels previously identified as calcification and connected to each other (**Figures 2A,B**). A significantly higher number of particles per volume unit were present in case of HG-SAS than in NF-LG-SAS (**Figure 2D**). Although the absolute volume of the largest particle in HG-SAS cusps was significantly higher than in NF-LG-SAS cusps (**Figure 2E**), for all cusps, it represented more than 50% of the calcification volume present in the sample (**Figure 2C**). The classification of the particles in three categories according to their size demonstrated that the increased number per volume unit observed in HG-SAS was mainly due to the presence of many small-sized particles (**Figures 2F–H**). Indeed, NF-LG-SAS cusps and HG-SAS cusps contained on average 157 and 519 particles, respectively, in the first category (corresponding to particles up to 1×10^{-3} mm^3). In the second category (from 1×10^{-3} mm^3 to 1 mm^3), these numbers dropped to 27 and 79, respectively, and the third category (from 1 mm^3 and above) only contained on average two particles for both NF-LG-SAS and HG-SAS diagnoses (**Figures 2F–H**). Consequently, both the number of particles per volume unit and the size of the largest particle were increased in case of HG-SAS. Moreover, the difference in the number of particles mainly relied on the quantity of the smallest ones, while the largest particles were equally present for both diagnoses.

3.3. *Ex vivo* microCT allows to distinguish and quantify different densities in the calcifications, but they did not differ between the different diagnosis groups

In addition to the number of calcified particles, we also investigated the density composition of the calcifications. The visualization of the calcifications in normalized gray scale allowed the distinction of different densities that were divided into three categories corresponding to low, moderate and high density (**Figure 3**). The spatial distribution of densities within the calcifications was highly heterogeneous for both NF-LG-SAS and HG-SAS diagnoses (**Figures 3A,B** and **Supplementary Movie S1**). The high-density calcifications had the highest relative volume in all cusps, while low- and moderate-densities were less, but equally, present (**Figure 3C**). The volume fraction of each density group could not be used to discern the NF-LG-SAS from the HG-SAS diagnosis groups. Both the diagnosis and the density groups had a strong effect on the absolute volume quantified for each density group (**Figure 3D**).

3.4. Cusp volume and thickness correlate with the degree of calcification

Calcific AS is not only characterized by the growth of calcifications within the cusp of the AV, but it is also associated with valve thickening and an increased cusp volume (**Figure 4**). The simultaneous visualization of the calcifications and the

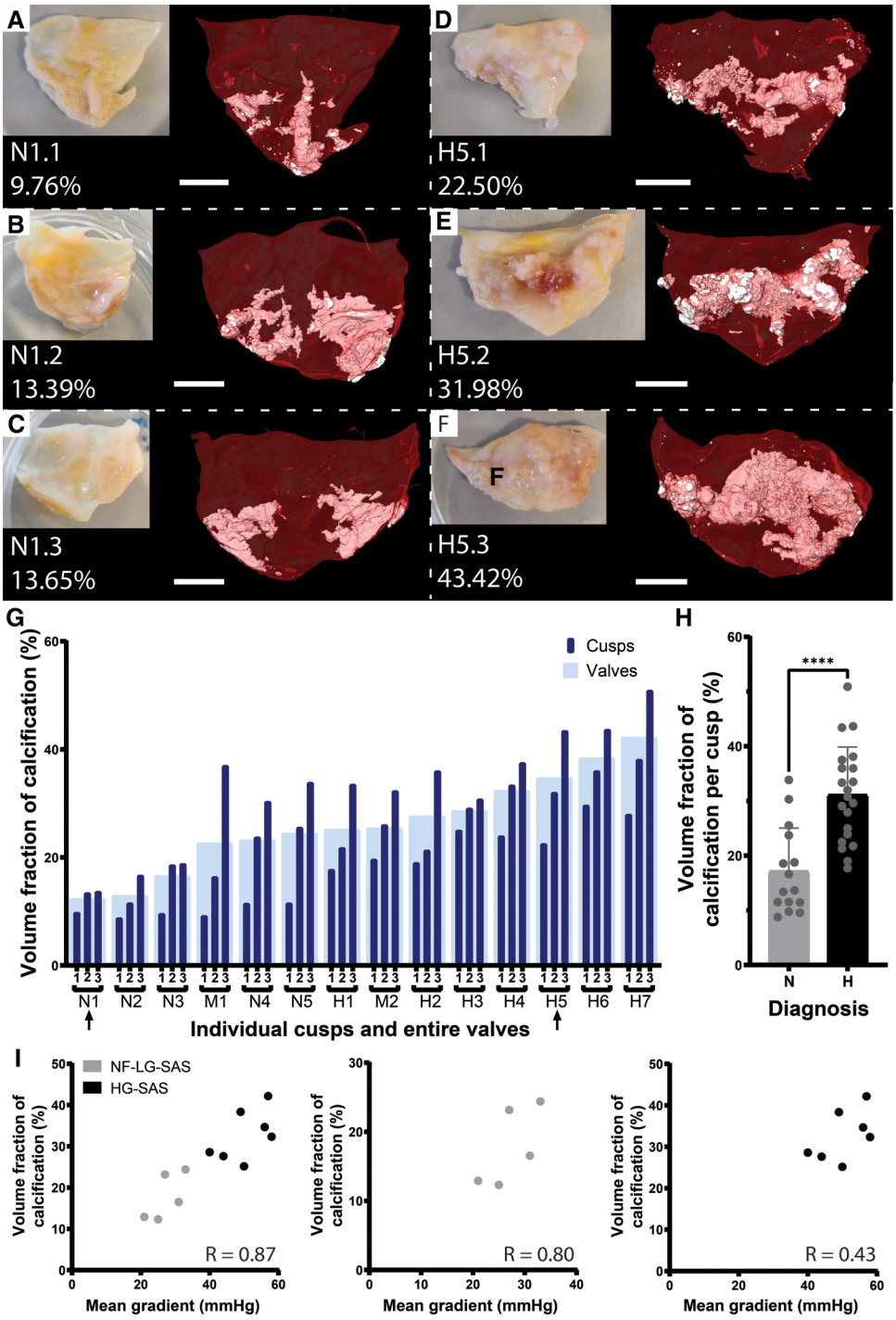

FIGURE 1
Quantification of the volume fraction of calcification per cusp and per valve. (A–F) Photographs and microCT-based 3D renderings of the three cusps for patient N1, diagnosed with NF-LG-SAS (A–C) and patient H5, diagnosed with HG-SAS (D–F). For the 3D renderings, soft tissue is shown in red and calcification in white. Scale bars = 5 mm. (G) Volume fraction of calcification for each cusp (dark blue) and for the entire valve (light blue). Arrows indicate the samples illustrated in (A–F). (H) Bar graph comparing the mean volume fraction of calcification for the NF-LG-SAS and HG-SAS groups. Individual datapoints are given for each cusp ($n = 15$ and $n = 21$ per group respectively). (I) Correlation between the volume fraction of calcification and the mean pressure gradient across the aortic valve for all patients (left), NF-LG-SAS patients (center) and HG-SAS patients (right). N, NF-LG-SAS; M, moderate AS; H, HG-SAS, ****: p-value < 0.0001.

thickness of the cusps revealed that the thickest area of the cusp corresponds to the large calcifications (Figure 4A and Supplementary Movie S2). While the mean thickness of the NF-LG-SAS and the HG-SAS cusps was about 1.6 mm and 2.2 mm respectively, the mean thickness of the non-calcified cusp was about 0.7 mm. The presence of a higher amount of calcification,

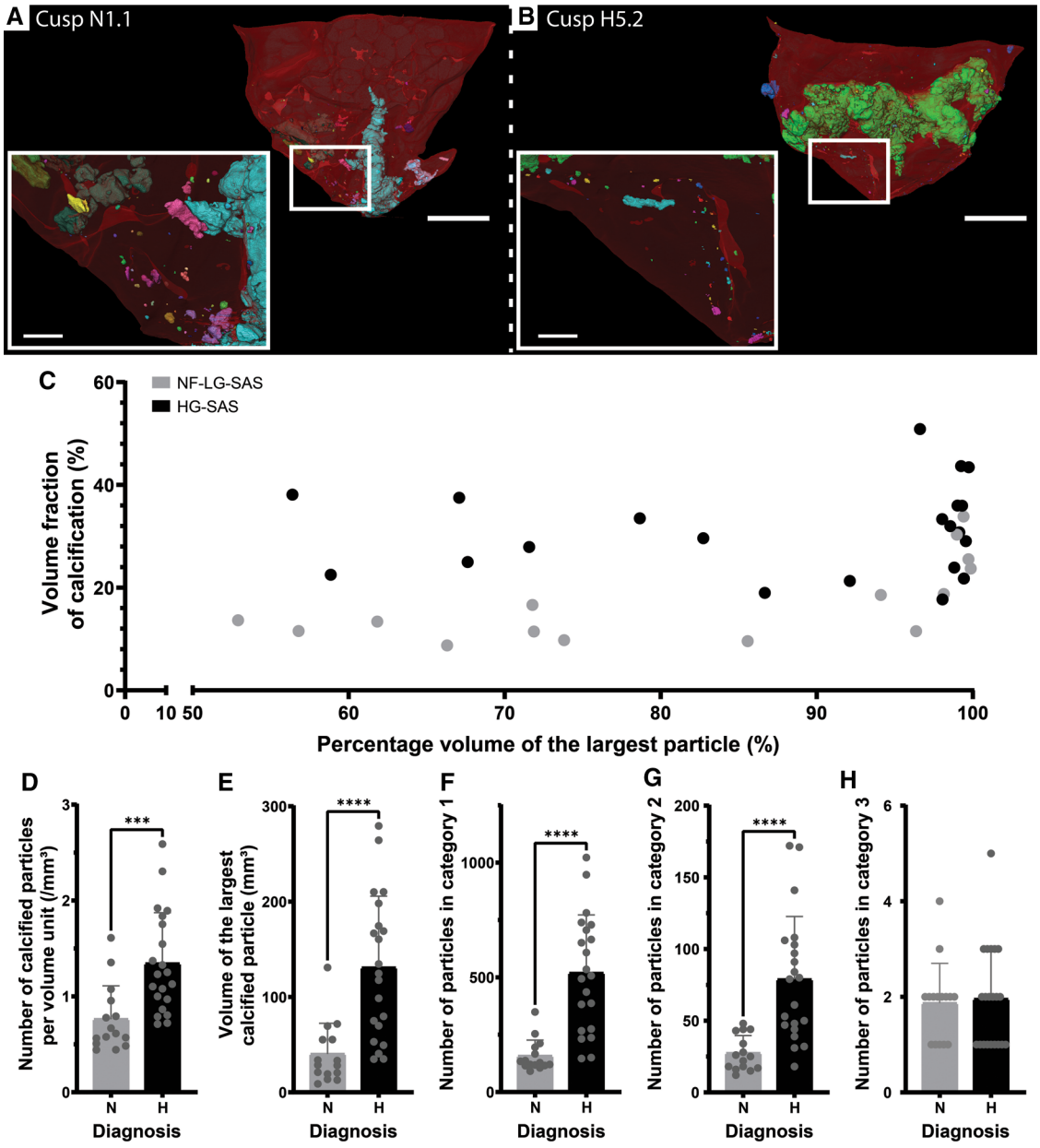

FIGURE 2
Quantification of the number and volume of calcified particles. (A,B) 3D renderings of the cusp N1.1 (A) and cusp H5.2 (B). Clusters of voxels identified as calcification and connected to each other are considered as one particle and displayed in the same color. Colors of particles are independent of any morphometrical quantification. Soft tissue is shown in red. A magnification (white square) is shown in the inset. Scale bars = 5 mm for the overview images and 1 mm for the inset. (C) Percentage volume of the largest particle in function of the volume fraction of calcification present in the cusp for the NF-LG-SAS samples and the HG-SAS samples. (D–H) Bar graphs comparing the number of calcified particles per volume unit (D), the volume of the largest particle (E), the number of particles in category 1 (F), category 2 (G) and category 3 (H), respectively for the NF-LG-SAS and HG-SAS groups. N, NF-LG-SAS; H, HG-SAS, ***: p-value < 0.001, ****: p-value < 0.0001.

such as in HG-SAS samples, resulted in a significant increase of the cusp thickness and volume, compared to the NF-LG-SAS group (Figures 4B,C). Moreover, the volume proportion of the cusp that still has a thickness corresponding to a healthy valve, defined by the mean thickness of the non-calcified cusp (0.7 mm), was significantly different between NF-LG-SAS and HG-SAS diagnoses. On average, 13.9% of the cusp volume from NF-LG-SAS samples and 7.0% from HG-SAS samples still had a normal thickness (< 0,7 mm). The volume proportion of the non-calcified cusp with a thickness below 0.7 mm was equal to 64.6% (Figure 4D). This suggests that the cusp continues to thicken as the mineralization progresses. Both the thickness and volume were correlated with the volume fraction of calcification present in the cusp (Figures 4E,F). Unlike gross evaluation-based studies, imaging the samples in 3D at high spatial resolution provided the full distribution of the thickness along the cusp (Figure 4G), allowing the observation of local variations.

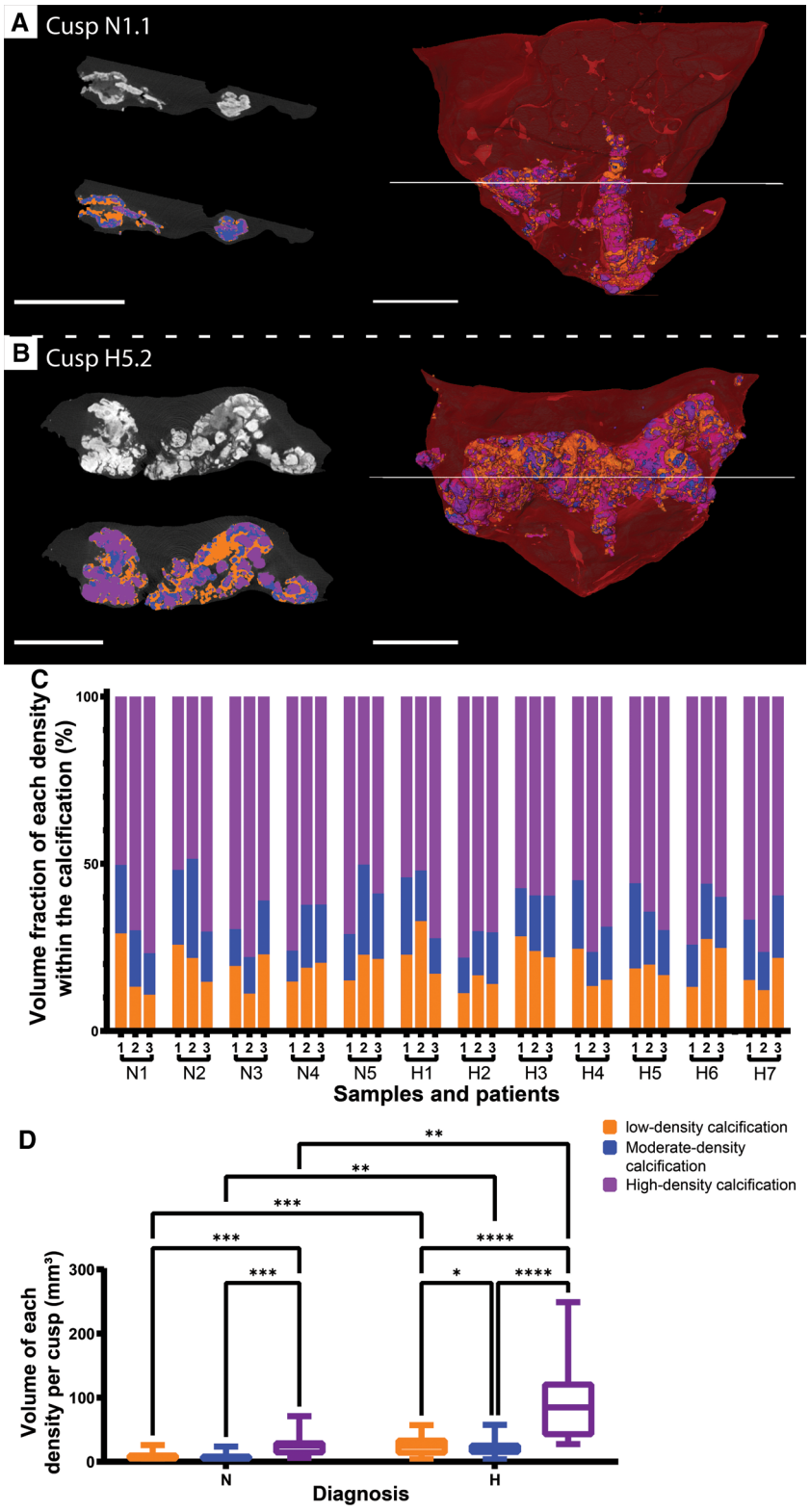

FIGURE 3
Distinction of three levels of density within the calcifications. (**A**,**B**) Ortho-slices in gray scale (top left) and after segmentation (bottom left) and 3D renderings (right) for cusp N1.1 (**A**) and cusp H5.2 (**B**). Low-density is shown in orange, moderate-density is shown in blue and high-density is shown in purple. Soft tissue is shown in dark gray on ortho-slices and in red on 3D renderings. Scale bars = 5 mm. (**C**) Volume fraction of each density group within the calcification for every cusp. (**D**) Box plots comparing the impact of the diagnosis within a density group, as well as of the density within a diagnosis group on the absolute volume of each density group. *: p-value < 0.05, **: p-value < 0.01, ***: p-value < 0.001, ****: p-value < 0.0001, N, NF-LG-SAS; H, HG-SAS.

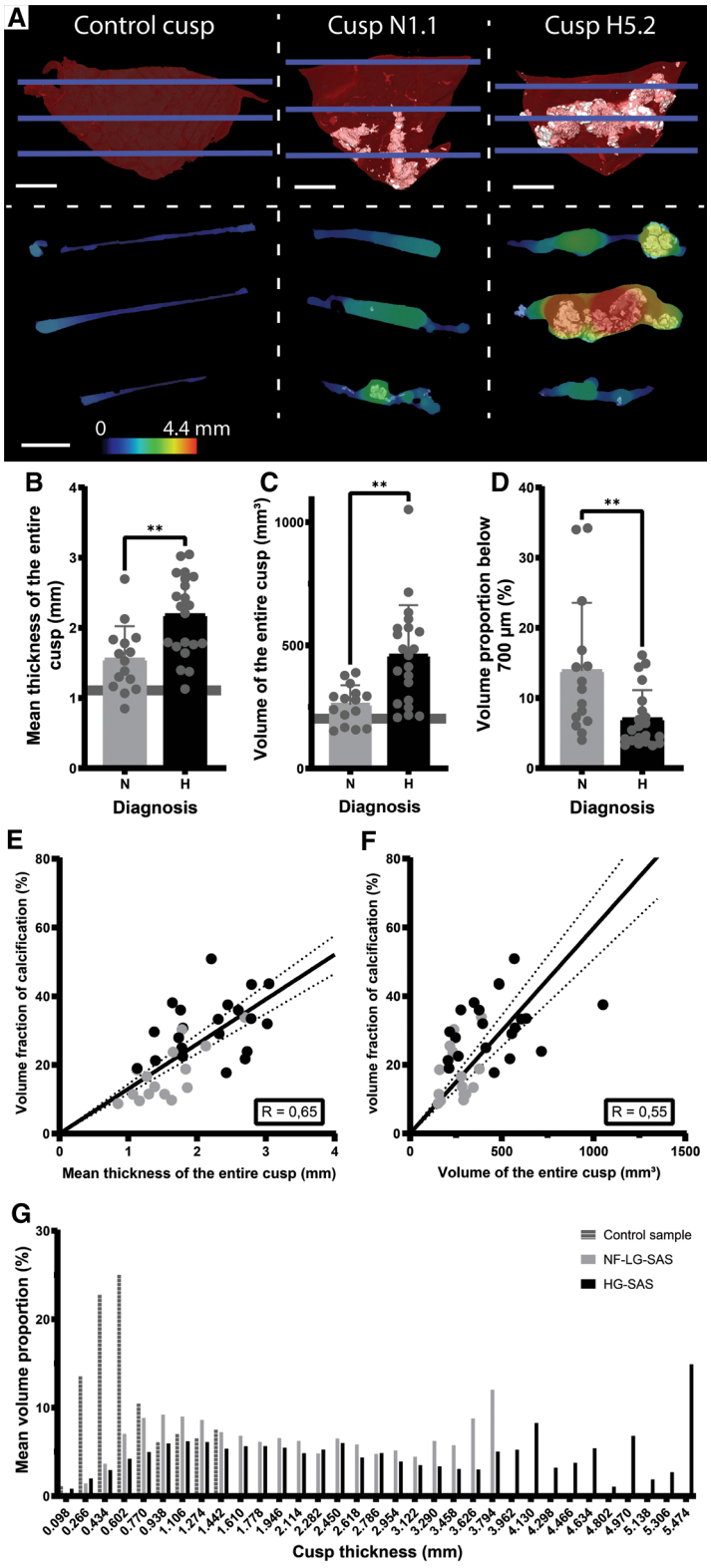

FIGURE 4
Quantification of the volume and thickness of the entire cusp. (**A**) 3D renderings (top) of the control cusp, sample N1.1 and H5.2 and ortho-slices (bottom) showing simultaneously the calcifications and the thickness values at three heights corresponding to the blue lines in the 3D renderings. For the 3D renderings, soft tissue is shown in red and calcification in white. Scale bars = 5 mm. Thickness is represented by the color scale bar. (**B–D**) Bar graphs comparing the mean thickness of the entire cusp (**B**), the volume of the entire cusp (**C**) and the volume proportion of the cusp with a thickness below 700 µm (**D**) for the NF-LG-SAS and HG-SAS groups. The horizontal line indicates the value for the control cusp, not shown on D for clarity (corresponding to 64.6%). (**E,F**) Correlations between the volume fraction of calcification and the mean thickness of the entire cusp (**E**) and the volume of the entire cusp (**F**), respectively. Dotted lines indicate the 95% confidence bands. (**G**) Average histogram of the thickness distribution in terms of volume proportion for the control cusp, the NF-LG-SAS and HG-SAS cusps. N, NF-LG-SAS; H, HG-SAS, **: p-value < 0.01.

3.5. *Ex* vivo high-resolution imaging revealed micro-sized calcifications

Another indication of pathology was also visualized by changes in the gray values of the soft tissues surrounding dense calcifications (**Figure 5**). Although being recognized as more attenuating areas, they were not identified as calcifications due to the limited spatial resolution and the partial volume effect (**Figure 5A**). Higher resolution imaging performed with microCT provided more accurate visualization of the dense calcification and of surrounding tissues, but it did not allow to distinguish individual micro-sized particles (**Figures 5B,C**). Only the SEM examination revealed that the more attenuating areas actually correspond to clusters of small calcification islets in the vicinity of dense calcifications (**Figures 5D,F** and **Supplementary Movie S3**). The composition analysis obtained from EDX proved that main and micro-sized calcifications were composed of calcium and phosphate while carbon was located in the surrounding soft

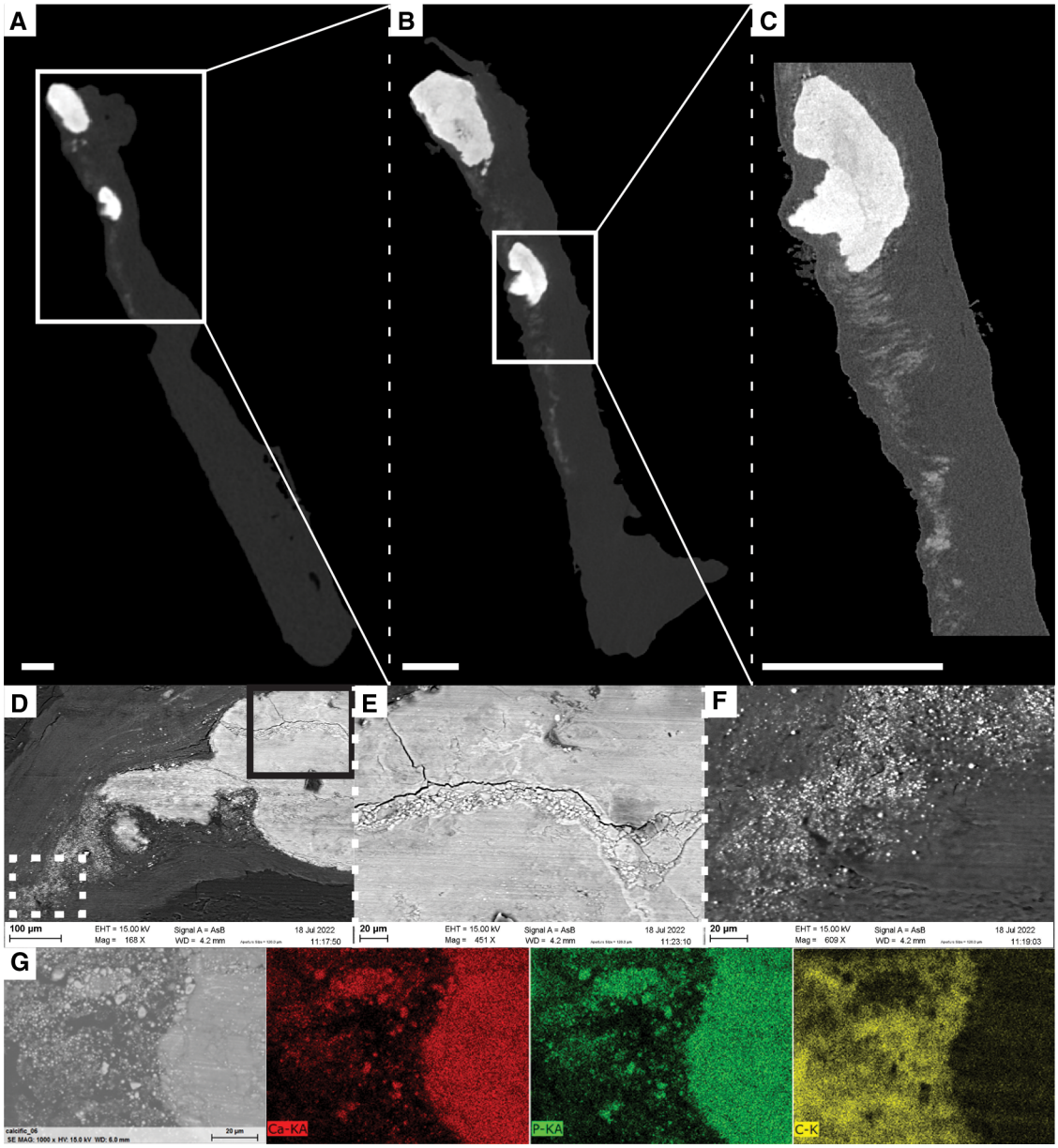

FIGURE 5
Visualization of soft tissue changes next to dense calcifications in sample N4.1. (**A–D**) Ortho-slices from *ex vivo* microCT obtained with different voxel sizes: 14 µm (**A**), 5 µm (**B**) and 1.2 µm (**C**). Scale bars = 0.5 mm. White squares correspond to the location of magnification. (**D–F**) SEM images with accumulation of particles within a dense calcification (**E**) and visualization of micro-sized particles in the soft tissue (**F**) obtained with backscattered electron detector, and different magnifications: x168 (**D**), x451 (**E**), and x609 (**F**). Solid black square and dotted white square in D correspond to the location of magnifications in the dense calcification and in soft tissues, respectively. (**G**) EDX analysis obtained at the border between the soft tissue and the dense calcification demonstrating that dense and micro-sized calcifications are composed of Calcium and Phosphate, while soft tissue is composed of Carbon.

tissues (Figure 5G). The micro-sized particles present in the soft tissues were mainly visualized in the least calcified samples. In addition to the observations made within the soft tissues, SEM also allowed to visualize the accumulation of small particles within dense calcifications (Figure 5E).

4. Discussion

In this study, a quantitative structural description of both the entire cusp and the calcifications was obtained using *ex vivo* microCT. The clear visualization of the cusp and the distinction of calcifications from the soft tissues allowed the quantification of several structural parameters, such as the volume fraction of calcification, the number and volume of calcified particles, and the distinction and quantification of the amount of different densities within the calcification in full 3D. Moreover, the volume and thickness of the entire cusp could be quantified, and changes in the soft tissues were observed, demonstrating the alteration of the extracellular matrix of the cusp. The observations and hypotheses of this study have been illustrated in a summary scheme (Figure 6). This structural characterization has the capability to provide a better description of the microstructural changes due to AS.

In vivo computed tomography and *ex vivo* microCT are two well-known X-ray-based techniques to visualize mineralized tissues (24, 29). *In vivo*, the degree of AV calcification is usually used in atypical cases of aortic stenosis (if hemodynamic and anatomic parameters are controversial). It is evaluated by the Agatston score (based on density weighting) or, less frequently, the calcium volume score (based on the volume quantification) (30). Both electron-beam computed tomography (EBCT) and multidetector computed tomography (MDCT) have been used to quantify AV calcification *in vivo*. Although EBCT was the first modality to have a sufficient temporal resolution to image the heart, MDCT, which was developed more recently, has a better signal-to-noise ratio and spatial resolution (31–33). These are two important parameters allowing the exclusion of non-valvular calcifications in the examination. In comparison with the microCT method presented in this study, *in vivo* techniques are used with a totally different purpose of diagnosis and quantification of the degree of calcification to assess the need for heart valve replacement. Although *ex vivo* microCT does not provide radiodensity measures in standardized units (Hounsfield

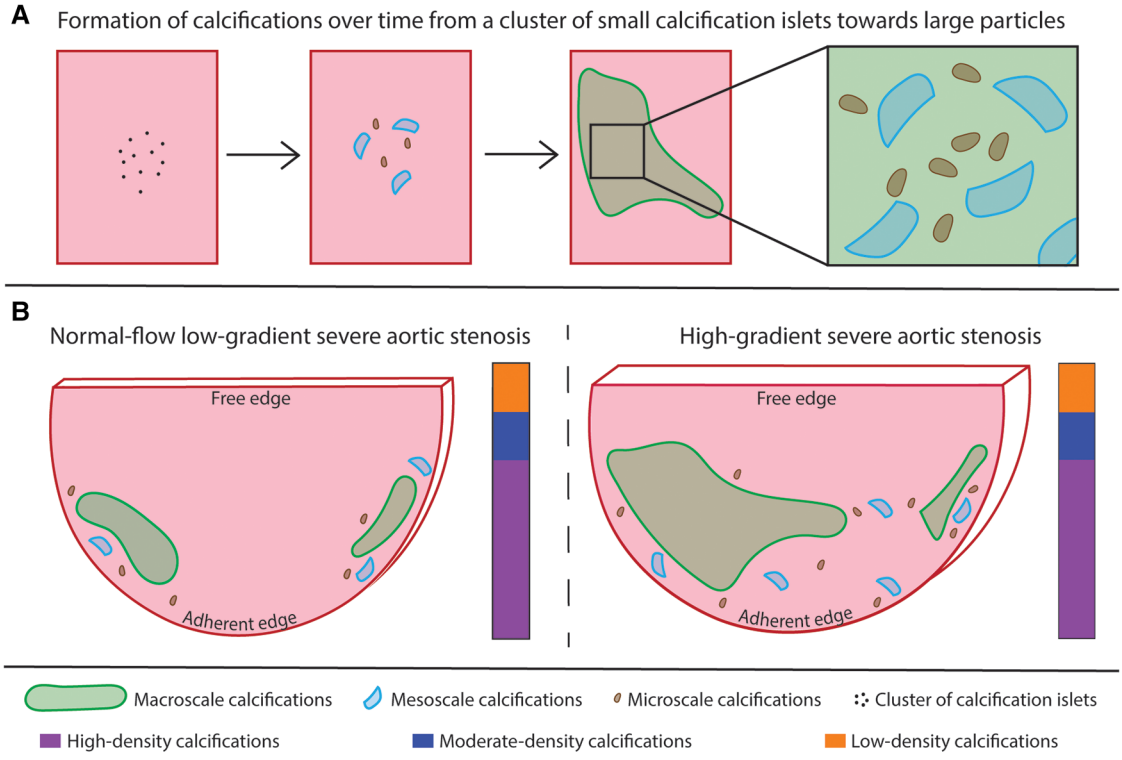

FIGURE 6
Summary scheme. (A) illustration of the hypothesis about the evolution of a cluster of small calcification islets into dense calcifications over time. Large calcifications correspond to the accumulation of small particles. (B) comparison of the two patterns of calcification. The calcifications are present in higher relative amount and the cusp is thicker in the HG-SAS group than in NF-LG-SAS. In the less calcified samples, the calcifications are mainly located at the adherent edges of the cusp, while for the most calcified samples, the midportion of the cusp is affected as well. The absolute volume of the largest calcified particle is higher in the HG-SAS group than in NF-LG-SAS, but it corresponds to at least 50% of the total calcification volume in all cases. The macroscale particles are present in equal number in both groups while the meso- and microscale particles are both present in higher number in the HG-SAS groups than in NF-LG-SAS. The calcification density is evenly heterogeneous in both diagnosis groups (illustrated by the vertical bar).

units used in clinical CT), which requires advanced calibration of the equipment, it produces high-resolution images. In comparison with *in vivo* CT approaches, for which the voxel's largest dimension corresponds to the 3mm-slice thickness, in this study, microCT has an isotropic voxel size of 14 µm. It enables the extraction of detailed microstructural information of explanted samples that could not be collected without organ removal and high radiation dose. *Ex vivo* microCT could be used in a multiscale manner in combination with for example MDCT to provide complementary data and better characterize AV calcifications.

E*x vivo* microCT is thus an already described tool that provides a detailed visualization of the AV cusps and an accurate quantification of the amount of calcification present in the soft tissues in case of calcified AS (11, 19–21). Nevertheless, the mean volume of calcification obtained in our study, in average 316 mm^3 per valve, is lower than the value published previously, which was 600 mm^3 (19). This difference might be explained by the amount of tissue collected during surgery and by different imaging strategies: (i) imaging per cusp in our case and the valve as a whole in the previous one, (ii) use of different voxel size (14 µm and 76 µm, respectively for our study and the study of Chitsaz et al.).

Our results demonstrated that it was possible not only to quantify the volume fraction of calcifications, but also to describe their 3D spatial distribution. Although the spatial distribution of the calcifications among the cusp does not correspond to a clear pattern, most of the calcification cores have an attachment to the adherent edge of the cusp, along the insertion to the aortic wall, while the free edge is usually free of calcification. This is especially visible in the less calcified samples and confirms what was reported before (6, 11). As the calcification increases, the midportion of the cusp becomes affected as well. Although Orzechowska et al. reported that minerals were mainly present on the surface of the cusp and corresponded to extrinsic mineralization, our data clearly shows that calcifications are mostly located inside the cusp (11).

We showed a variation in the volume fraction of calcification among the three cusps from a single valve, which suggests that they are affected differently by the disease. This confirms the results from Raman spectroscopy previously performed on one valve (15). Current literature often describes one cusp that would be especially more calcified than the other two, identified as the non-coronary cusp (7, 14, 15). The preferential growth of calcifications in one of the histological layers, identified as the fibrosa layers, located on the aortic side of the cusp, has also been mentioned (2, 7, 8). Nevertheless, such identification was not possible in our study because the true anatomy of the cusps and their *in vivo* position was not indicated during excision. Interestingly, both the non-coronary cusp, which is deprived of coronary artery, and the aortic side of the cusp are thought to be prone to decreased shear stress compared to the other two cusps and to the ventricular side of AV, respectively. Shear stress is therefore a determinant parameter in the initiation of AS. It is described as a continuous stimulus for the endothelium that should inhibit pathological changes such as calcifications, however without direct proof (2, 7, 34). The distinction of the three cusps and their orientation (i.e ventricular and aortic sides) could help to validate and to better understand the role of shear stress. We therefore recommend to use a systematic annotation of the cusps during surgery for future studies, which could easily overcome this limitation. The application of the detailed analysis presented in this study to bicuspid aortic valves might provide more information regarding the role of the shear stress in the calcification mechanism. Moreover, to fully characterize the process of calcification growth, it would have been necessary to include samples at an earlier stage of the disease.

Using high resolution *ex vivo* microCT, the volume of calcifications can be quantified, but they can also be clearly visualized. Unlike *in vivo* and/or low-resolution imaging, the technique presented here permits the observation of small-sized calcified particles, which are a key element to understand the formation of larger size calcifications. Indeed, small-sized calcified particles can be interpreted as onsets of calcifications. Our results showed that all AS samples contain one or two main calcified particles and that some onsets of calcifications are present in a variable amount. As the calcification increases, both the volume of the main calcified particles and the number of onsets of calcifications rise. This quantitative structural analysis could reveal different phases of AS. From this perspective, the first pattern (one or two relatively small main calcified particles and some onsets of calcifications) defines a quiescent form of valvular disease and the second one (one or two large calcified particles and many onsets of calcifications) corresponds to an active form of AS. In the second case, the numerous onsets of calcifications are expected to evolve quickly into larger calcified particles, which would further hinder the opening and closing of the valve and, consequently, the proper functioning of the heart. The distinction of such onsets of calcification could reveal the initial location of calcifications and help to determine the link between calcification growth, blood flow and shear stress. The inability of *in vivo* imaging to identify the small-sized particles, although they are present in high number and correspond to onsets of calcifications, highlights the need for high resolution *ex vivo* imaging when investigating the calcification mechanisms resulting in AS. The presence of calcified particles of different sizes in AS cusps was previously described by Razzolini and colleagues. As they performed a macroscopic evaluation, the size threshold used was 4 mm. Calcified particles were named microaggregates (below 4 mm) or macroaggregates (above 4 mm) (12). According to our results, we propose a new nomenclature based on *ex vivo* high-resolution imaging such as microCT. Macroscale calcifications are defined by a volume of 1 mm^3 or above, microscale calcifications have a volume below or equal to 1×10^{-3} mm^3 and, in between these two categories, calcified objects are qualified as mesoscale calcifications with a volume from 1×10^{-3} to 1 mm^3. Our examination reveals that both the volume of the largest macroscale calcification and the number of micro- and mesoscale calcifications are increased when the proportion of calcification rises.

In addition to the number and size of calcified particles, different normalized gray values were also distinguished within the calcifications. The distinction of different densities within the

calcifications was demonstrated in a previous study (11). However, previous studies did not assess the spatial distribution of densities in 3D and did not link it to the clinical diagnosis of the pathology. In our study, the examination of the spatial distribution for each density group confirms the heterogeneity observed by Orzechowska et al. However, it does not demonstrate that small-sized calcifications are particularly less dense than the larger ones or whether they would evolve into high-density calcifications. Cusps with a less advanced stage of AS should also be analyzed to better understand the presence of different densities within the calcifications. We foresee potential applications in animal models, such as the Reversa mice model (35), allowing the analysis at different time points.

To investigate the changes in thickness of the cusps due to AS, *in vivo* ultrasound imaging is mostly used (14) or *ex vivo* gross evaluation is performed (36). However, the absolute volume of the individual cusps is rarely assessed due to technical limitations. The 3D imaging technique that we present here provided quantitative values for the volume and the mean thickness of the cusp. Moreover, the full thickness distribution, including local variations, could also be quantified. It allowed us to observe that the thickened areas correspond to the location of large calcifications. As thickening is recognized as a precursor sign of AS, local thickening of the cusp might be an indication for future calcifications (13, 14). Moreover, we also assessed the thickness distribution of a non-calcified cusp, whereas this information is scarcely available in the current literature. Studying the volume and thickness distributions of both healthy and calcified cusps would provide a better description of the native structure of the valve and would help to determine precise thresholds for pathological variations. Since thickening is an indication for tissue remodeling, this quantification might also be used to detect an abnormality within the soft tissues and to indicate a region-of-interest for further investigations.

In addition to the change in thickness and volume of the cusp, we were also capable of visualizing changes in the soft tissues of the AV cusp with the presence of more-attenuating areas corresponding to micro-sized particles in the extracellular matrix. Initial visualization obtained with microCT allowed to locate a region of interest that could be investigated at higher resolution with microCT and, as demonstrated on one sample in our case, with other imaging modalities, such as SEM. Although microCT did not allow to visualize individual particles, it was used to indicate where the sample should be cut to be imaged with SEM. SEM images revealed that the previously defined region of interest contained small calcification islets located next to dense calcifications. This area would correspond to the location of future dense calcifications. Two different processes have been previously described to explain the formation of calcifications (2, 37). First, the osteogenic process is initiated by the differentiation of valvular cells into osteoblast-like cells. In this case, a highly organized bone-like mineral matrix is the basis for the nucleation of minerals. The second process is an apoptotic process of the valvular interstitial cells that is promoted by several stimuli and results in apoptotic cell aggregates. They consist of amorphous deposits of calcium and phosphorus crystals. The visualization of extracellular matrix changes such as the ones shown in our results, before the formation of dense calcifications, could help to better describe these two processes and to clarify their role in the calcification formation. Moreover, assessing the microstructure of extracellular components around these onsets of calcification could provide a detailed description of the remodeling associated with cusp thickening and calcification growth, such as excessive production and disorganization of collagen fibers (2, 7).

As case study in our work, the quantitative structural analysis we performed was applied to two patient groups: NF-LG-SAS and HG-SAS to determine whether they were structurally different from each other and to evaluate whether *ex vivo* microCT could be used to better understand the particular case of NF-LG-SAS diagnosis. The medical prognosis of NF-LG-SAS is still under discussion and it is still not clear whether NF-LG-SAS is a truly severe AS, as calcified as HG-SAS or whether it is an intermediate stage of AS in which calcifications will still increase and result in high pressure gradient (26, 38–42). The summary scheme outlines the main differences observed between the two diagnosis groups (**Figure 6B**). First, our quantification of the calcification volume demonstrated that NF-LG-SAS cusps were less calcified than the HG-SAS ones. In case of HG-SAS, the main calcified particle was significantly larger than that of NF-LG-SAS and the onsets of calcifications were more numerous, thus corresponding to an active form of AS. However, due to the low number of samples included in our study, it was not possible to determine whether the diagnosis alone could explain the different patterns of calcification (one or two relatively small main particles and few onsets of calcification vs. few large main particles and many onsets of calcifications) or whether the two patterns could be observed in each patient group. The quantification of the volume and spatial distribution of the different densities observed within the calcification did not permit to distinguish specific characteristics for NF-LG-SAS compared to HG-SAS. The thickness and volume of NF-LG-SAS cusps were significantly lower than those of HG-SAS. Consequently, all the structural parameters quantified in our work support several previously published studies that evaluate NF-LG-SAS as a less advanced AS progression than other severe AS cases (39, 42–46). Since AS classification contains several controversial subgroups, the imaging approach described in this study could be used to better characterize and understand each AS phenotype.

The technique presented in this study presents some limitations. The need for *ex vivo* imaging to obtain high-resolution images prevents the possibility for time-lapsed follow-up of the calcified cusps. This would help to investigate the evolution of the amount and spatial distribution of calcifications, the evolution of the calcified particles, as well as the different densities within the calcifications. It could also validate that changes observed in the extracellular matrix of the cusp correspond to future dense calcifications. Moreover, tissue shrinkage was observed on sample N4.1, which underwent longer scan time (more than 3 h in total). This limitation could be easily overcome by using an environmental stage to control the scanning atmosphere. Although our study allowed to distinguish different densities within the calcification based on normalized grey values, it was not possible to determine true density values. This would require the use of

reference materials with known density. As mentioned previously, our conclusions were also limited by the number of cusps and the absence of cusps affected by an earlier stage of AS.

As the technique presented here is non-destructive, it can be combined with other imaging modalities to investigate the components of the extracellular matrix. For instance, it was used as a preliminary imaging step to indicate where to cut the sample for SEM analysis. It could also be done prior to classical 2D histology, which could help to describe the endothelial damage, lipid infiltration, inflammation and fibrosis preceding mineralization. It was not possible in this study to combine both SEM imaging and classical 2D histology after microCT because the sample was embedded in paraffin in a home-made cylindrical sample holder and covered with gold. As a future perspective, we are convinced that combining *ex vivo* microCT with high-atomic number contrast-enhancing staining agents (CESAs), corresponding to contrast-enhanced computed tomography or CECT, could allow the visualization of the different histological layers in the cusp. This technique can also be applied in cryogenic conditions, corresponding to cryo-CECT, which was successfully used to perform histopathological analysis of entire mouse hearts (28). Such 3D imaging techniques have the potential to better define the microstructure of the extracellular matrix of healthy aortic valve and the disorganization induced by AS. Unlike classical 2D histology, they do not require any demineralization step. It could for example validate the preferential growth of calcifications within the fibrosa layer or the presence of neovascularization in case of AS (2, 47). It could also be used to quantify the excessive production of collagen fibers associated with the cusp thickening.

5. Conclusion

In conclusion, we used high resolution *ex vivo* microCT to provide a new quantitative description of the general structure of calcified cusps in case of AS and of the calcifications present in the cusp soft tissues. In the future, the results presented here can be used to further improve *in vivo* imaging protocols and the interpretation of clinical data. The detailed description of the stenotic AV cusps provided in our results could also help to better understand the mechanism of AS.

Data availability statement

The raw data supporting the conclusions of this article will be made available by the authors, without undue reservation.

Ethics statement

The studies involving human participants were reviewed and approved by comité éthique hospitalo-facultaire Saint-Luc - UCLouvain. The patients/participants provided their written informed consent to participate in this study.

Author contributions

Research conception and design: CP, LQ and GK; experiments realization: CP, GP and LQ; data analysis: CP, GP and LQ; interpretation of results: CP, GP, LQ, DDA and BL; interpretation of clinical data: DDA, J-LV, DV and CB; preparation of figures and draft of the manuscript: CP; editing and revision of the manuscript: DDA, BL and GK. All authors contributed to the article and approved the submitted version.

Funding

CP, BL and GK acknowledge the Action de Recherche Concertée (ARC 19/24-097)-Fédération Wallonie-Bruxelles and acknowledge the support from ASBL Jean Degroof-Marcel Van Massenhove funding and the Foundation Saint-Luc (RM2A project). GP and GK acknowledge the support from the SBO project of the Research Foundation Flanders (FWO; grant S007219N). DDA acknowledges the grant support from the Fondation Nationale de la Recherche Scientifique of the Belgian Government (FRSM PDR T.0237.21). Avizo 2022.1 (ThermoFisher Scientific, France) software acquisition was supported by the Fonds de la Recherche Scientifique – (FNRS - EQP - Tomo4D-U.N069.20).

Acknowledgments

We would like to thank the cardiology department from the *Cliniques Universitaires Saint-Luc* and Jamila Boulif for providing the samples, Sandrine Horman, Luc Bertrand and Catherine Behets for their guidance throughout the study. The X-ray microCT images were generated at the KU Leuven XCT Core Facility (supported by Jeroen Soete, research expert). This research benefited from the help of Catherine Rasse, statistical consultant of the Service de Méthodologie Statistique et de Calcul, technological platform of the UCLouvain - SMCS/LIDAM, UCLouvain.

Conflict of interest

The authors declare that the research was conducted in the absence of any commercial or financial relationships that could be construed as a potential conflict of interest.

Publisher's note

Supplementary material

The Supplementary Material for this article can be found online at: https://www.frontiersin.org/articles/10.3389/fcvm.2023.1129990/full#supplementary-material.

SUPPLEMENTARY FIGURE 1
Partial volume effect (PVE) correction for each density group. A–B: ortho-slices of sample N1.1 showing the classification of calcification into low, moderate and high-density before (A) and after (B) the PVE correction. C: absolute volume of each density group within the calcification for every cusp. Two bars are given for each cusp, before PVE correction (left) and after PVE correction (right).

SUPPLEMENTARY MOVIE S1
Distinction of three levels of density within the calcifications. Ortho-slices (right) and 3D renderings (left) of cusps N1.1 and H5.2. The horizontal white lines present in the 3D renderings correspond to the location of the ortho-slices. Soft tissue is shown in dark gray on ortho-slices and in red in the 3D renderings.

SUPPLEMENTARY MOVIE S2
Thickness distribution in 3D in cusps N1.1 and H5.2. Soft tissue is shown in red and calcification in white. The thickness distribution is shown on the ortho-slice progressively cutting the 3D renderings and is represented by the color scale bar.

SUPPLEMENTARY MOVIE S3
Visualization of micro-sized calcifications on microCT ortho-slices successively obtained at a voxel size of 14 µm, 5 µm and 1.2 µm. In the 3D renderings, the location of the ortho-slice is shown by the orange line, soft tissue is shown in red and calcification in white.

References

1. Pujari SH, Agasthi P. Aortic stenosis. In: Abai B, editor. *Statpearls*. Treasure Island, FL: StatPearls Publishing (2022).

2. Lindman BR, Clavel MA, Mathieu P, Iung B, Lancellotti P, Otto CM, et al. Calcific aortic stenosis. *Nat Rev Dis Prim*. (2016) 2:1–28. doi: 10.1038/nrdp.2016.6

3. Grimard BH, Larson JM. Aortic stenosis: diagnosis and treatment. *Am Fam Physician*. (2008) 78(6):717–24. PMID: 18819236.

4. Price S. Transthoracic echocardiography: normal two-dimensional and Doppler imaging. In: de Backer D, Cholley B, Slama M, Vieillard-Baron A, Vignon P, editors. *Hemodynamic monitoring using echocardiography in the critically ill* Berlin, Heidelberg: Springer (2011). p. 13–29. doi: 10.1007/978-3-540-87956-5_2

5. Izquierdo-Gómez MM, Hernández-Betancor I, García-Niebla J, Marí-López B, Laynez-Cerdeña I, Lacalzada-Almeida J. Valve calcification in aortic stenosis: etiology and diagnostic imaging techniques. *Biomed Res Int*. (2017) 2017. doi: 10.1155/2017/5178631

6. Somers P, Knaapen M, Mistiaen W. Histopathology of calcific aortic valve stenosis. *Acta Cardiol*. (2006) 61(5):557–62. doi: 10.2143/AC.61.5.2017772

7. Dweck MR, Boon NA, Newby DE. Calcific aortic stenosis: a disease of the valve and the myocardium. *J Am Coll Cardiol*. (2012) 60(19):1854–63. doi: 10.1016/j.jacc.2012.02.093

8. Aikawa E, Libby P. A rock and a hard place chiseling away at the multiple mechanisms of aortic stenosis. *Circulation*. (2017) 135(20):1951–5. doi: 10.1161/CIRCULATIONAHA.117.027776

9. Afshar M, Yazdan-Ashoori S, Engert JC, Thanassoulis G. Drugs for prevention and treatment of aortic stenosis: how close are we? *Can J Cardiol*. (2021) 37(7):1016–26. doi: 10.1016/j.cjca.2021.02.017

10. Lindman BR, Sukul D, Dweck MR, Madhavan MV, Arsenault BJ, Coylewright M, et al. Evaluating medical therapy for calcific aortic stenosis: jACC state-of-the-art review. *J Am Coll Cardiol*. (2021) 78(23):2354–76. doi: 10.1016/j.jacc.2021.09.1367

11. Orzechowska S, Wróbel A, Goncerz G, Podolec P, Rokita E. Physicochemical and micro-tomographic characterization of inorganic deposits associated with aortic stenosis. *J Heart Valve Dis*. (2014) 23(1):40–7. PMID: 24779327.

12. Razzolini R, Longhi S, Tarantini G, Rizzo S, Napodano M, Abate E, et al. Relation of aortic valve weight to severity of aortic stenosis. *Am J Cardiol*. (2011) 107(5):741–6. doi: 10.1016/j.amjcard.2010.10.052

13. Cosmi JE, Kort S, Tunick PA, Rosenzweig BP, Freedberg RS, Katz ES, et al. The risk of the development of aortic stenosis in patients with "benign" aortic valve thickening. *Arch Intern Med*. (2002) 162(20):2345–7. doi: 10.1001/archinte.162.20.2345

14. Cujec B, Pollick C. Isolated thickening of one aortic cusp: preferential thickening of the noncoronary cusp. *J Am Soc Echocardiogr*. (1988) 1(6):430–2. doi: 10.1016/S0894-7317(88)80025-7

15. Cheng CL, Chang HH, Huang PJ, Wang WC, Lin SY. Different calcification stage in each cusp of a calcified tricuspid aortic valve. *Circ J*. (2017) 81(12):1953–5. doi: 10.1253/circj.CJ-17-0129

16. Sahasakul Y, Edwards WD, Naessens JM, Tajik AJ. Age-related changes in aortic and mitral valve thickness: implications for two-dimensional echocardiography based on an autopsy study of 200 normal human hearts. *Am J Cardiol*. (1988) 62(7):424–30. doi: 10.1016/0002-9149(88)90971-X

17. Cowell SJ, Newby DE, Burton J, White A, Northridge DB, Boon NA, et al. Aortic valve calcification on computed tomography predicts the severity of aortic stenosis. *Clin Radiol*. (2003) 58(9):712–6. doi: 10.1016/S0009-9260(03)00184-3

18. Cueff C, Serfaty JM, Cimadevilla C, Laissy JP, Himbert D, Tubach F, et al. Measurement of aortic valve calcification using multislice computed tomography: correlation with haemodynamic severity of aortic stenosis and clinical implication for patients with low ejection fraction. *Heart*. (2011) 97(9):721–6. doi: 10.1136/hrt.2010.198853

19. Chitsaz S, Gundiah N, Blackshear C, Tegegn N, Yan KS, Azadani AN, et al. Correlation of calcification on excised aortic valves by micro-computed tomography with severity of aortic stenosis. *J Heart Valve Dis*. (2012) 21(3):320–7. PMID: 22808832.

20. Mazur P, Wypasek E, Gawęda B, Sobczyk D, Kapusta P, Natorska J, et al. Stenotic bicuspid and tricuspid aortic valves: micro-computed tomography and biological indices of calcification. *Circ J*. (2017) 81(7):1043–50. doi: 10.1253/circj.CJ-16-1166

21. Solache-Berrocal G, Barral-Varela AM, Areces-Rodríguez S, Junco-Vicente A, Vallina-Álvarez A, Corte-Torres MD, et al. Correlation of micro-computed tomography assessment of valvular mineralisation with histopathological and immunohistochemical features of calcific aortic valve disease. *J Clin Med*. (2019) 9(1):29. doi: 10.3390/jcm9010029

22. Awtry E, Davidoff R. Low-flow/low-gradient aortic stenosis. *Circulation*. (2011) 124(23):739–41. doi: 10.1161/CIRCULATIONAHA.111.075853

23. Boulif J, Gerber B, Slimani A, Lazam S, de Meester C, Piérard S, et al. Assessment of aortic valve calcium load by multidetector computed tomography. Anatomical validation, impact of scanner settings and incremental diagnostic value. *J Cardiovasc Comput Tomogr*. (2017) 11(5):360–6. doi: 10.1016/j.jcct.2017.07.004

24. Pawade T, Clavel MA, Tribouilloy C, Dreyfus J, Mathieu T, Tastet L, et al. Computed tomography aortic valve calcium scoring in patients with aortic stenosis. *Circ Cardiovasc Imaging*. (2018) 11(3):1–11. doi: 10.1161/CIRCIMAGING.117.007146

25. Messika-Zeitoun D, Lloyd G. Aortic valve stenosis: evaluation and management of patients with discordant grading. *E-journal Cardiol Pr*. (2018) 15:26. https://www.escardio.org/Journals/E-Journal-of-Cardiology-Practice/Volume-15/Aortic-valve-stenosis-evaluation-and-management-of-patients-with-discordant-grading

26. Dandel M, Hetzer R. Severe low-gradient aortic stenosis: impact of inadequate left ventricular responses to high afterload on diagnosis and therapeutic decision-making. *Heart Fail Rev*. (2022) 27(6):2017–31. doi: 10.1007/s10741-022-10240-y

27. Maes A. Cryogenic contrast-enhanced microCT enables nondestructive 3D quantitative histopathology of soft biological tissues (2022). GitHub.

28. Maes A, Pestiaux C, Marino A, Balcaen T, Leyssens L, Vangrunderbeeck S, et al. Cryogenic contrast-enhanced microCT enables nondestructive 3D quantitative histopathology of soft biological tissues. *Nat Commun*. (2022) 13(1):1–14. doi: 10.1038/s41467-022-34048-4

29. Rawson SD, Maksimcuka J, Withers PJ, Cartmell SH. X-ray computed tomography in life sciences. *BMC Biol*. (2020) 18(1):21. doi: 10.1186/s12915-020-0753-2

30. Pawade T, Sheth T, Guzzetti E, Dweck MR, Clavel MA. Why and how to measure aortic valve calcification in patients with aortic stenosis. *JACC Cardiovasc Imaging*. (2019) 12(9):1835–48. doi: 10.1016/j.jcmg.2019.01.045

31. Messika-Zeitoun D, Aubry MC, Detaint D, Bielak LF, Peyser PA, Sheedy PF, et al. Evaluation and clinical implications of aortic valve calcification measured by electron-beam computed tomography. *Circulation*. (2004) 110(3):356–62. doi: 10.1161/01.CIR.0000135469.82545.D0

32. Messika-Zeitoun D, Bielak LF, Peyser PA, Sheedy PF, Turner ST, Nkomo VT, et al. Aortic valve calcification: determinants and progression in the population. *Arterioscler Thromb Vasc Biol*. (2007) 27(3):642–8. doi: 10.1161/01.ATV.0000255952.47980.c2

33. Kulkarni S, Rumberger JA, Jha S. Electron beam CT: a historical review. *Am J Roentgenol*. (2021) 216(5):1222–8. doi: 10.2214/AJR.19.22681

34. Fernández Esmerats J, Heath J, Jo H. Shear-sensitive genes in aortic valve endothelium. *Antioxidants Redox Signal*. (2016) 25(7):401–4. doi: 10.1089/ars.2015.6554

35. Miller JD, Weiss RM, Serrano KM, Brooks RM, Berry CJ, Zimmerman K, et al. Lowering plasma cholesterol levels halts progression of aortic valve disease in mice. *Circulation*. (2009) 119(20):2693–701. doi: 10.1161/CIRCULATIONAHA.108.834614

36. Jatene MB, Monteiro R, Guimarães MH, Veronezi SC, Koike MK, Jatene FB, et al. Aortic valve assessment. Anatomical study of 100 healthy human hearts. *Arq Bras Cardiol*. (1999) 73(1):81–6. doi: 10.1590/S0066-782X1999000700007

37. Bonucci E. Bone mineralization. *Front Biosci*. (2012) 17(1):100–28. doi: 10.2741/3918

38. Dumesnil JG, Pibarot P, Carabello B. Paradoxical low flow and/or low gradient severe aortic stenosis despite preserved left ventricular ejection fraction: implications for diagnosis and treatment. *Eur Heart J*. (2010) 31(3):281–9. doi: 10.1093/eurheartj/ehp361

39. Pibarot P, Dumesnil JG. Paradoxical low-flow, low-gradient aortic stenosis: new evidence, more questions. *Circulation*. (2013) 128(16):1729–32. doi: 10.1161/CIRCULATIONAHA.113.005718

40. Kang DH, Jang JY, Park SJ, Kim DH, Yun SC, Song JM, et al. Watchful observation versus early aortic valve replacement for symptomatic patients with normal flow, low-gradient severe aortic stenosis. *Heart*. (2015) 101(17):1375–81. doi: 10.1136/heartjnl-2015-307528

41. Clavel M-A, Guzzetti E, Annabi M-S, Salaun E, Ong G, Pibarot P. Normal-flow low-gradient severe aortic stenosis: myth or reality? *Struct Hear*. (2018) 2(3):180–7. doi: 10.1080/24748706.2018.1437934

42. Chadha G, Bohbot Y, Lachambre P, Rusinaru D, Serbout S, Altes A, et al. Progression of normal flow low gradient "severe" aortic stenosis with preserved left ventricular ejection fraction. *Am J Cardiol*. (2020) 128(2):151–8. doi: 10.1016/j.amjcard.2020.05.003

43. Hachicha Z, Dumesnil JG, Bogaty P, Pibarot P. Paradoxical low-flow, low-gradient severe aortic stenosis despite preserved ejection fraction is associated with higher afterload and reduced survival. *Circulation*. (2007) 115(22):2856–64. doi: 10.1161/CIRCULATIONAHA.106.668681

44. Lancellotti P, Magne J, Donal E, Davin L, O'Connor K, Rosca M, et al. Clinical outcome in asymptomatic severe aortic stenosis: insights from the new proposed aortic stenosis grading classification. *J Am Coll Cardiol*. (2012) 59(3):235–43. doi: 10.1016/j.jacc.2011.08.072

45. Herrmann HC, Pibarot P, Hueter I, Gertz ZM, Stewart WJ, Kapadia S, et al. Predictors of mortality and outcomes of therapy in low-flow severe aortic stenosis: a placement of aortic transcatheter valves (PARTNER) trial analysis. *Circulation*. (2013) 127(23):2316–26. doi: 10.1161/CIRCULATIONAHA.112.001290

46. Yamashita E, Takeuchi M, Seo Y, Izumo M, Ishizu T, Sato K, et al. Prognostic value of paradoxical low-gradient severe aortic stenosis in Japan: Japanese multicenter aortic stenosis study, retrospective (JUST-R) registry. *J Cardiol*. (2015) 65(5):360–8. doi: 10.1016/j.jjcc.2014.12.019

47. Katsi V, Magkas N, Antonopoulos A, Trantalis G, Toutouzas K, Tousoulis D. Aortic valve: anatomy and structure and the role of vasculature in the degenerative process. *Acta Cardiol*. (2021) 76(4):335–48. doi: 10.1080/00015385.2020.1746053

frontiers | Frontiers in Cardiovascular Medicine

TYPE Original Research
PUBLISHED 30 May 2023
DOI 10.3389/fcvm.2023.1153814

OPEN ACCESS

EDITED BY
Konstantinos Papadopoulos,
Interbalkan Medical Center, Greece

REVIEWED BY
Andreea Calin,
Carol Davila University of Medicine and Pharmacy, Romania
Didem Oguz,
Harvard Medical School, United States

*CORRESPONDENCE
Mayooran Namasivayam
✉ mayooran.namasivayam@unsw.edu.au

RECEIVED 30 January 2023
ACCEPTED 15 May 2023
PUBLISHED 30 May 2023

CITATION
Namasivayam M, Meredith T, Muller DWM, Roy DA, Roy AK, Kovacic JC, Hayward CS and Feneley MP (2023) Machine learning prediction of progressive subclinical myocardial dysfunction in moderate aortic stenosis. Front. Cardiovasc. Med. 10:1153814. doi: 10.3389/fcvm.2023.1153814

Machine learning prediction of progressive subclinical myocardial dysfunction in moderate aortic stenosis

Mayooran Namasivayam[1,2,3]*, Thomas Meredith[1,2,3], David W. M. Muller[1,2], David A. Roy[1,2], Andrew K. Roy[1], Jason C. Kovacic[1,2,4,5], Christopher S. Hayward[1,2,6] and Michael P. Feneley[1,2,6]

[1]Department of Cardiology, St Vincent's Hospital, Sydney, NSW, Australia, [2]Faculty of Medicine and Health, University of New South Wales, Sydney, NSW, Australia, [3]Heart Valve Disease and Artificial Intelligence Laboratory, Victor Chang Cardiac Research Institute, Sydney, NSW, Australia, [4]Vascular Biology Laboratory, Victor Chang Cardiac Research Institute, Sydney, NSW, Australia, [5]Icahn School of Medicine at Mount Sinai, Cardiovascular Research Institute, New York, NY, United States, [6]Cardiac Mechanics Laboratory, Victor Chang Cardiac Research Institute, Sydney, NSW, Australia

Background: Moderate severity aortic stenosis (AS) is poorly understood, is associated with subclinical myocardial dysfunction, and can lead to adverse outcome rates that are comparable to severe AS. Factors associated with progressive myocardial dysfunction in moderate AS are not well described. Artificial neural networks (ANNs) can identify patterns, inform clinical risk, and identify features of importance in clinical datasets.

Methods: We conducted ANN analyses on longitudinal echocardiographic data collected from 66 individuals with moderate AS who underwent serial echocardiography at our institution. Image phenotyping involved left ventricular global longitudinal strain (GLS) and valve stenosis severity (including energetics) analysis. ANNs were constructed using two multilayer perceptron models. The first model was developed to predict change in GLS from baseline echocardiography alone and the second to predict change in GLS using data from baseline and serial echocardiography. ANNs used a single hidden layer architecture and a 70%:30% training/testing split.

Results: Over a median follow-up interval of 1.3 years, change in GLS (≤ or >median change) could be predicted with accuracy rates of 95% in training and 93% in testing using ANN with inputs from baseline echocardiogram data alone (AUC: 0.997). The four most important predictive baseline features (reported as normalized % importance relative to most important feature) were peak gradient (100%), energy loss (93%), GLS (80%), and DI < 0.25 (50%). When a further model was run including inputs from both baseline and serial echocardiography (AUC 0.844), the top four features of importance were change in dimensionless index between index and follow-up studies (100%), baseline peak gradient (79%), baseline energy loss (72%), and baseline GLS (63%).

Conclusions: Artificial neural networks can predict progressive subclinical myocardial dysfunction with high accuracy in moderate AS and identify features of importance. Key features associated with classifying progression in subclinical myocardial dysfunction included peak gradient, dimensionless index, GLS, and hydraulic load (energy loss), suggesting that these features should be closely evaluated and monitored in AS.

KEYWORDS

aortic stenosis, echocadiography, machine learning, LV dysfunction, neural network

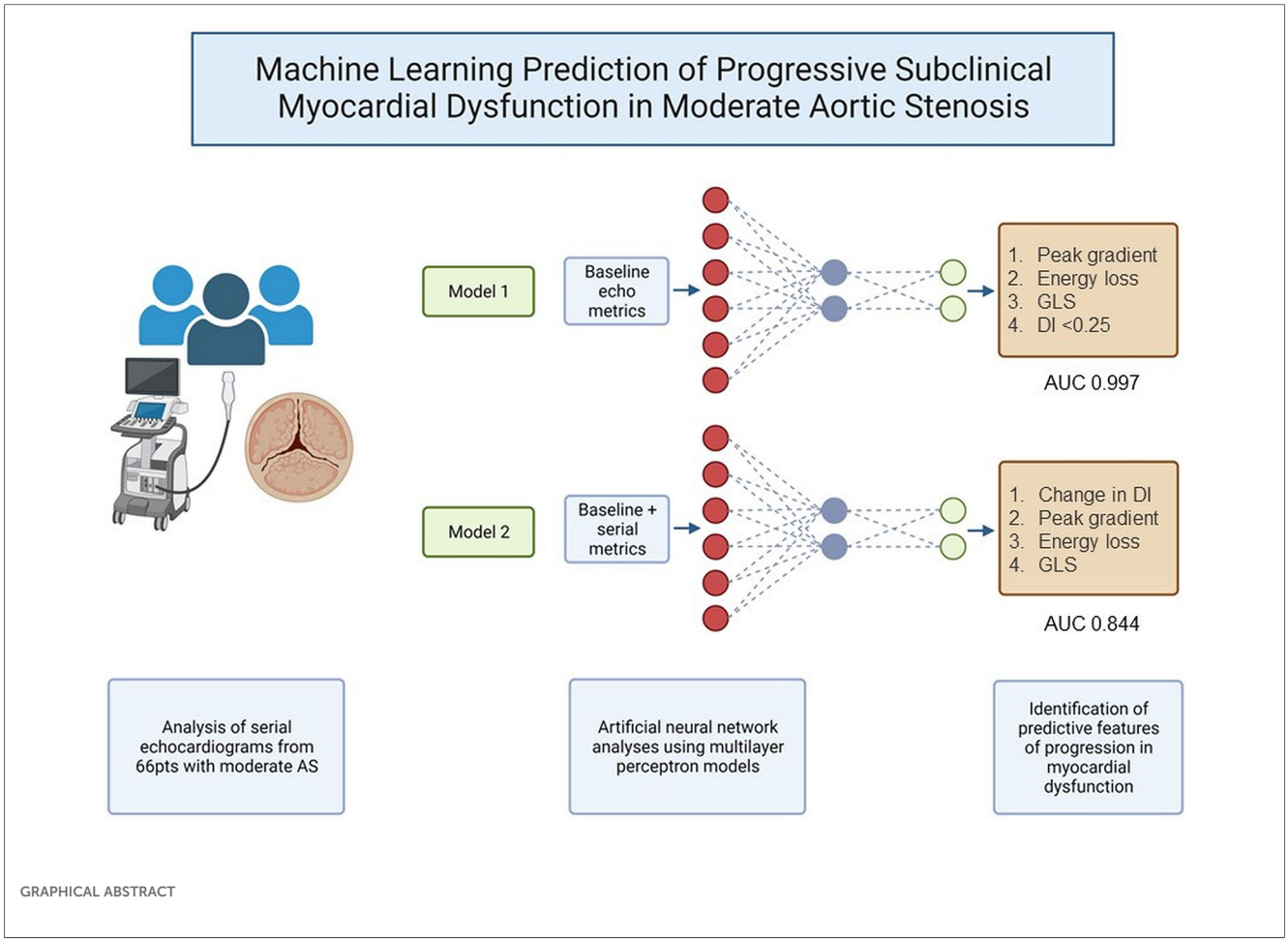

GRAPHICAL ABSTRACT

Introduction

The understanding of aortic stenosis (AS) is rapidly evolving. "Moderate severity" AS is actually a complex and poorly understood entity (1–7). It involves hydraulic load on the left ventricle, leading to fibrosis and adverse clinical outcomes, with rates approaching those of severe AS (5). Moderate severity aortic stenosis is no longer considered a benign, early stage of disease, as was once thought (1–4). The importance of subclinical myocardial dysfunction in moderate AS has recently been highlighted (6). However, factors associated with the progression of subclinical myocardial dysfunction in moderate AS are not well understood. Mechanistically, myocardial dysfunction is related to hydraulic load, which, in turn, relates to valve stenosis severity (7). Metrics of valve stenosis severity are challenging to interpret even in truly severe AS, let alone in moderate AS when metrics can be more uncertain and discordant (8, 9). Machine learning, and specifically artificial neural networks (ANNs), can identify patterns in datasets to predict risk and identify features of importance. We sought to use machine learning to identify whether metrics of valve stenosis severity could accurately predict the progression of subclinical myocardial dysfunction in moderate AS, and we additionally sought to identify which valve stenosis metrics were most important to this progression. We believe that such analyses could provide insights into the basis for progressive deterioration and adverse outcome in what is traditionally considered "early stage" disease.

Methods

Subjects

We evaluated the St. Vincent's Hospital and Clinic Echocardiography databases to identify studies between 2016 and 2021 with moderate severity AS, as determined by a text-search of report conclusions [reports are finalized by an imaging cardiologist or a senior cardiology fellow (minimum PGY7)] and confirmation of mean gradient <40 mmHg. A total of 336 patients were identified with baseline imaging of adequate quality for strain analysis in apical 2, 3, and 4-chamber views, of whom 100 had serial imaging but only 66 had serial imaging of adequate quality for strain analysis at both index and follow-up.

Echocardiographic analysis

A reanalysis of raw echocardiographic images was performed at the Heart Valve Disease and Artificial Intelligence Laboratory at the Victor Chang Cardiac Research Institute. Left ventricular

global longitudinal strain (GLS) analysis was performed by using TomTec Arena software, with the apical 2, 3, and 4-chamber views (10, 11). Studies were included for analysis only if the left ventricular endocardium could be visualized and endocardial tracking was accurate in the apical 2, 3, and 4-chamber views throughout the cardiac cycle. Aortic valve stenosis severity was assessed using aortic valve area (AVA) (as determined by continuity equation), mean and peak transvalvular gradients, and dimensionless index (DI). Valvular hydraulic load was assessed using energy loss, modified from the method first described by Garcia et al. (12). Information on body surface area was not available in our database, and therefore, we evaluated total (rather than indexed) energy loss. As flow conditions are important for the metrics of aortic valve stenosis severity, transvalvular flow rate (Q) was also measured as the ratio of stroke volume to ejection time (13, 14).

Neural network analysis

We utilized ANN analysis with multilayer perceptron models to identify features of valve stenosis severity from both baseline and serial echocardiography that could predict change in GLS between the index and the follow-up studies. We defined the target of models as change in GLS (classified by ≤ or > cohort median change). We constructed two models. The first used only inputs from baseline echocardiography. The second included additional inputs requiring data from serial echocardiography to account for the effects of dynamic change in metrics. We encoded inputs to optimize model efficiency, for example by binarizing key metrics at established diagnostic thresholds (such as AVA 1.0 cm^2, DI at 0.25. Q ≤ 210 ml/s) (13, 15, 16). Inputs for the first model included the following: AVA ≤ 1.0 cm^2, DI < 0.25, transvalvular flow rate ≤210 ml/s, peak gradient, mean gradient, left ventricular GLS, and energy loss. Inputs for the second model included model 1 inputs and additionally included the following: time between studies, change in AVA between studies, change in mean gradient between studies, change in dimensionless index between studies, change in energy loss between studies, and change in flow rate between studies. Both models used a single hidden layer architecture and a 70%:30% training/testing structure. This meant that models were trained on 70% of the cohort that was randomly selected and tested on the remaining unseen 30% of the cohort for validation, in order to avoid overfitting (17).

Model performance was assessed using prediction accuracy (% correct predictions), area under the receiver operating curve (AUC), and gain and lift functions. Features of importance were assessed using normalized importance scoring, with the most important feature scoring 100%, and other features were scaled accordingly as a proportion of importance.

Analyses were conducted using IBM SPSS Version 26.0 (IBM, Armonk, NY).

TABLE 1 Baseline characteristics.[a]

Age (years)	79 ± 10
Male/female	44 (66%)/22 (33%)
Peak gradient (mmHg)	39 (33–44)
Mean gradient (mmHg)	23 (20–27)
Aortic valve area (cm^2)	1.1 (0.8–1.5)
Dimensionless index	0.34 (0.26–0.40)
Transvalvular flow rate (ml/s)	256 (199–297)
Energy loss (cm^2)	1.2 (0.8–1.5)
Global longitudinal strain (%)	−16.7 ± 4.3
Left ventricular ejection fraction (%)	61 ± 8
Left atrial dimension (mm, parasternal long axis)	42 ± 7
Interventricular septal thickness (mm)	11 (10–13)
Posterior wall thickness (mm)	11 (10–12)
Estimated pulmonary artery systolic pressure (mmHg)	27 (23–34)

[a]Data presented as mean ± SD if normally distributed based on the skewness statistic between −0.5 and +0.5, aside from age and LVEF which, while not normally distributed, are reported here as mean ± SD per convention. Non-normal data presented as median (IQR).

Results

After exclusion criteria were implemented, 66 subjects (44 males, 22 females), aged 79 ± 10 years, with serial, strain-quality imaging over a median follow-up interval of 1.3 years (IQR: 0.8–2.0 years), remained. Baseline AS severity metrics are outlined in Table 1. Key valve severity metric changes from baseline to follow-up are noted in Table 2. All metrics of severity trended worse over time, with statistical significance reached by peak gradient, mean gradient, and peak velocity. GLS worsened over follow-up (baseline mean GLS −16.7%, mean change in GLS +0.74%, median change +0.48%), although the change in GLS was of borderline significance ($p = 0.06$, paired t-test).

As described, multilayer perceptron models were created initially from the metrics of AS severity from baseline echocardiogram alone (Model 1), and subsequently, incorporating parameters accounting for dynamic change in variables between the index and the follow-up studies (Model 2). The inputs and architecture for Model 1 are shown in Figure 1.

Model 1 yielded a prediction accuracy rate of 95% in training and 93% in testing, with an AUC of 0.997, while Model 2 yielded a prediction accuracy rate of 84% in training and 68% in testing, with an AUC of 0.844. Receiver operating curves for both models are shown in Figure 2. Gain and lift functions are shown in Figure 3. The relative feature importance in each model is shown in Figure 4. In Model 1, the four most important predictive baseline features (reported

Table 2 Changes in the metrics of AS severity at follow-up.[a]

Metric of severity	Follow-up	*p*-Value[b]
AVA (cm^2)	1.00 (0.77–1.26)	0.057
Peak gradient (mmHg)	43 (34–49)	0.02
Mean gradient (mmHg)	25.1 (21.0–29.9)	0.031
Peak velocity (m/s)	3.3 (2.9–3.5)	0.02
Dimensionless index	0.30 (0.23–0.36)	0.12

[a]Results are median (IQR).
[b]As compared with baseline.

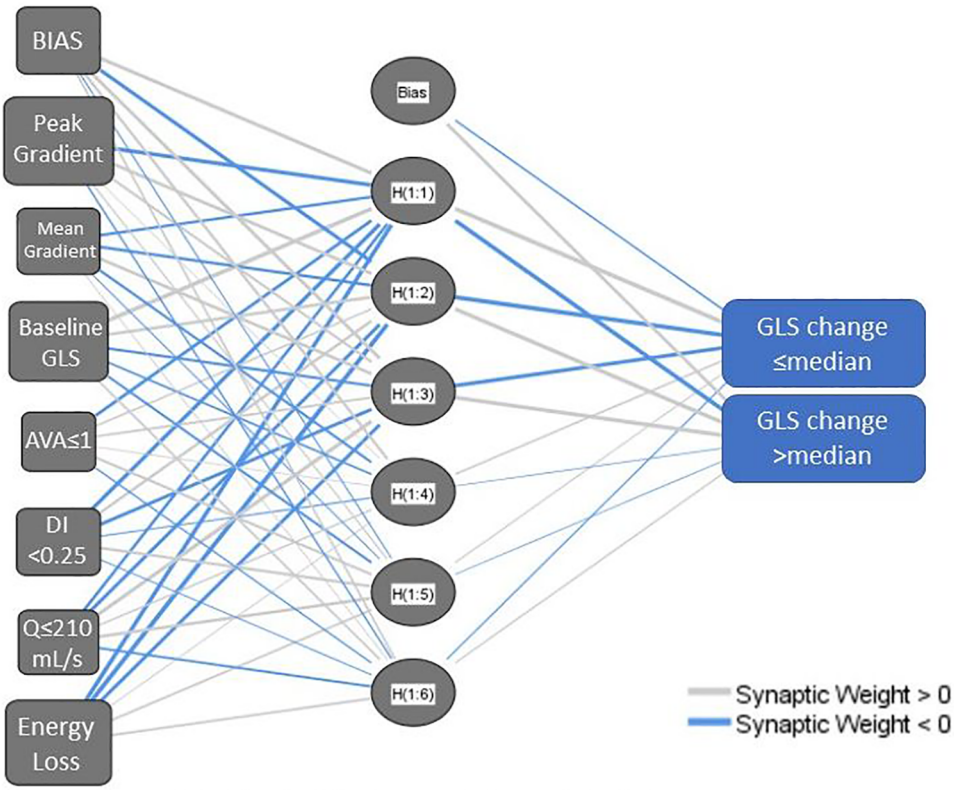

FIGURE 1
Network diagram for a multilayer perceptron neural network model using baseline aortic stenosis severity metrics (model 1). AVA, aortic valve area; DI, dimensionless index; GLS, left ventricular global longitudinal strain; Q, transvalvular flow rate. The network structure includes a bias node at the input layer and hidden layer and has multiple nodes in the hidden layer, hence H(1:1), H(1:2) etc.

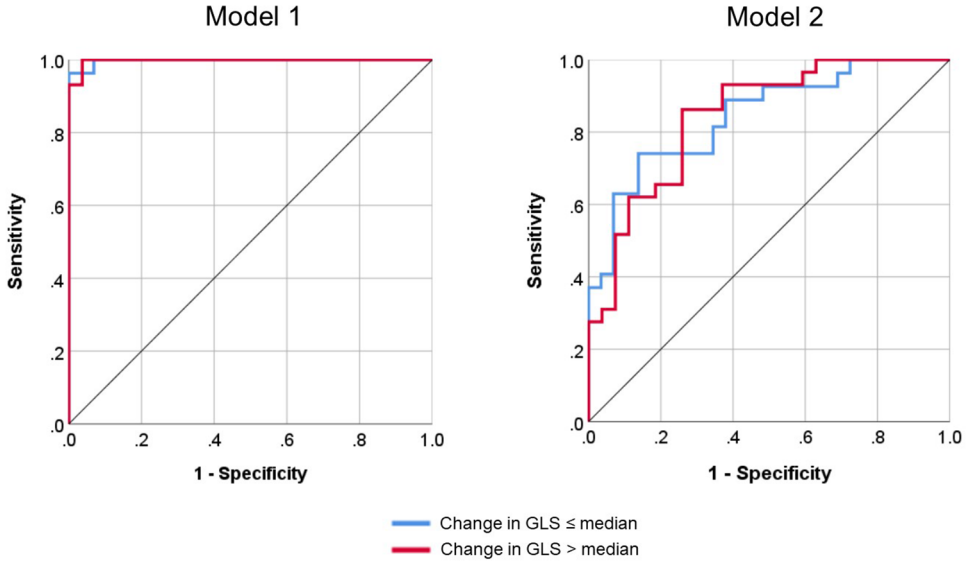

FIGURE 2
Receiver operating curves for Model 1 (baseline metrics only) and Model 2 (baseline metrics and dynamic change) for the classification of global longitudinal strain (GLS) progression.

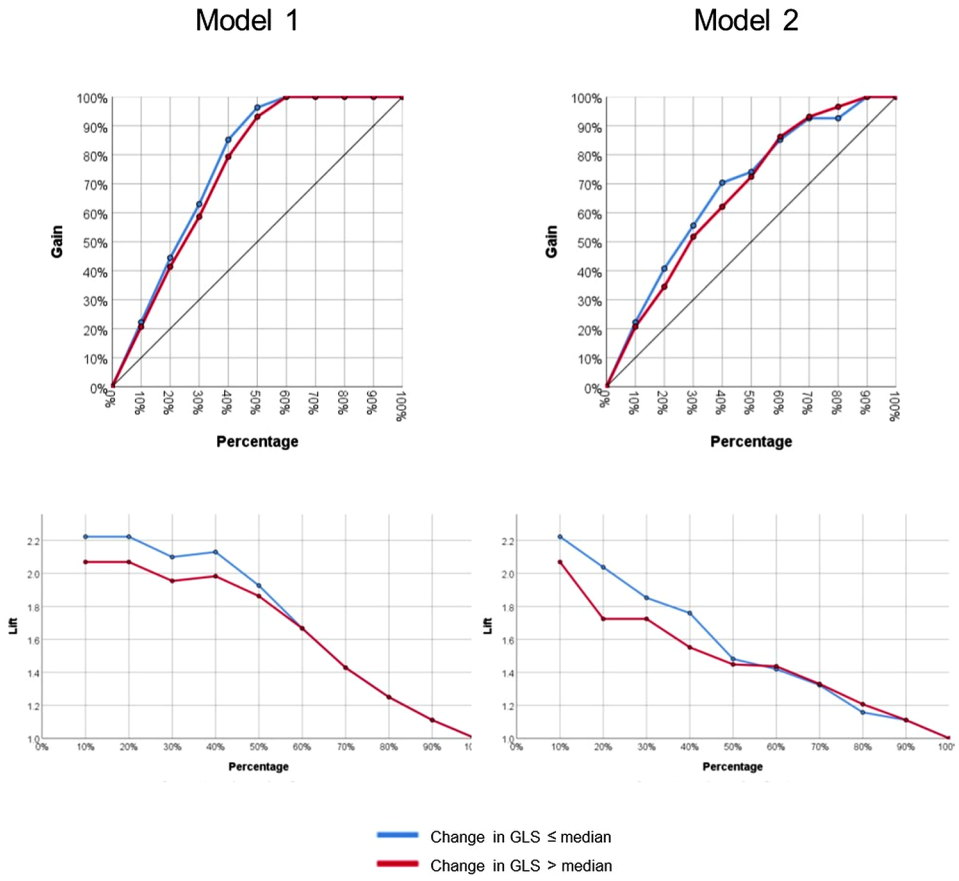

FIGURE 3
Gain and lift functions for Model 1 (baseline metrics only) and Model 2 (baseline metrics and dynamic change).

as normalized % importance relative to the most important feature) were peak gradient (100%), energy loss (93%), GLS (80%), and DI < 0.25 (50%). In Model 2, the top four features of importance were change in dimensionless index (100%), baseline peak gradient (79%), baseline energy loss (72%), and baseline GLS (63%).

Discussion

Studies have shown that patients with moderate AS have poor overall survival (1–5) that is comparable to patients with severe AS (5), suggesting that current classification systems are inaccurate and understanding of the disease and its progression are limited.

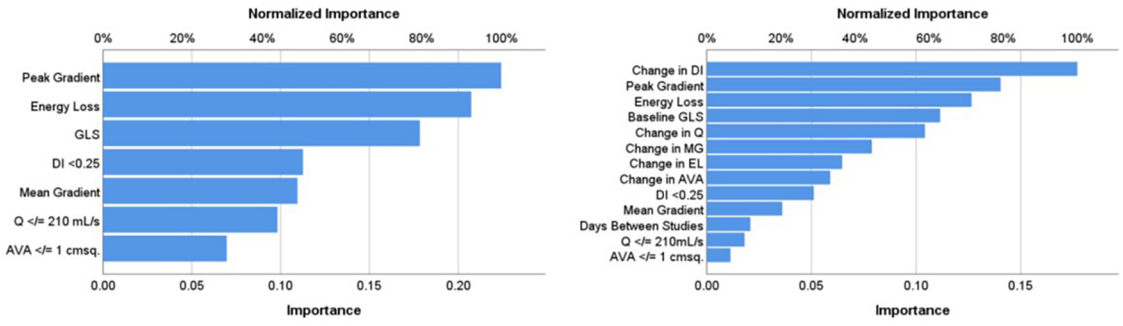

FIGURE 4
Relative importance of input features in Model 1 (baseline metrics) and Model 2 (baseline metrics and dynamic change). AA, aortic area at sinuses of Valsalva; AVA, aortic valve area (in cm^2); DI, dimensionless index; EL, energy loss; GLS, left ventricular global longitudinal strain; MG, mean gradient; Q, transvalvular flow rate.

Moreover, studies have shown that the subclinical myocardial dysfunction in AS is associated with adverse clinical prognosis (6). AS quantification is challenging, even when disease is severe, but is particularly challenging in earlier, moderate stages of disease. Knowing which features are most important can inform echocardiographic assessment, clinical decision-making, and overall patient management. In this study of moderate AS, we have shown that progression in subclinical myocardial dysfunction can be accurately predicted, using neural networks, by simple echocardiographic metrics of AS severity. Moreover, we have shown that some features of AS severity are considerably more important than others in predicting change in myocardial function. The most important features are peak gradient, baseline GLS, DI, and energy loss.

These findings are important because they highlight that aortic valve stenosis severity is a major contributing factor to the load faced by the left ventricular myocardium, even in moderate stages of the disease. Moreover, this load and subsequent myocardial dysfunction can progress with time, even over a relatively short follow-up interval (median time 1.3 years). This is important because it means that ongoing exposure to load, even at moderate AS severity, is likely to have a continued and progressive adverse impact upon myocardial function, which may be irreversible (18, 19).

Our findings also highlight which key parameters are important to progression in myocardial dysfunction in moderate AS. The importance of DI in both our models affirms recent literature demonstrating the value of this metric (20). Of note, AVA did not rank highly in importance in either of our models. This finding of superiority of DI to AVA in our models, most likely reflects the flow dependency of AVA and relative flow independency of DI (13). As expected, baseline GLS was an important feature relevant to the degree of GLS progression. This finding supports the increasing calls to better quantify myocardial dysfunction using tissue deformation in AS, both in moderate and in severe disease (6, 21). Early detection of myocardial dysfunction could identify those at high risk of progression. Finally, energy loss, a marker of valvular hydraulic load, featured as important in our analysis. This metric is not routinely used in clinical practice but has a strong research foundation and has been shown to identify clinical risk in previous studies (12, 22, 23). Energy loss accounts for the changes in the composition of total energy (comprised of kinetic and static pressure energy that interchange, as well as gravitational potential energy that remains stable) as blood traverses a stenotic aortic valve. Energy loss accounts for the phenomenon of pressure recovery that occurs in the proximal aorta, whereby static pressure energy is "recovered" as blood enters the proximal aorta and kinetic energy reduces. Incomplete pressure recovery contributes to hydraulic load, and the degree of this recovery, and hence energy loss, is itself dependent on the ratio of effective aortic valve orifice area and aortic area. Conceptually, it is the best physiologic marker of hydraulic load faced by the ventricle as a result of aortic valve stenosis (12, 24), and its importance in contributing to deteriorating strain affirms that it adds clinical value. Our findings support increasing the role of energy loss quantification, which is easily measured from standard echocardiography, in assessment of AS. A particularly interesting finding was that peak gradient outperformed mean gradient as an input feature. Traditionally, mean gradient has served as the more frequently evaluated metric in AS; however, the spread of data in peak gradient (IQR: range 11 mmHg vs. 7 mmHg for peak vs. mean gradient) likely allowed a greater resolution to detect differences in moderate stages of the disease, where gradients are lower. This finding has potential implications for low-gradient severe AS, where the focus on mean gradient perhaps should be shifted to peak gradient.

Another important finding in our study was the demonstration of the power of machine learning in the assessment of echocardiographic data (25–30). We have shown that prediction models with high accuracy and explainability (i.e., the ability to explain the basis of model formulation and identify which features are of particular importance in generating the model) can be developed using easily acquired echocardiographic metrics. Machine learning approaches can identify nonlinear and interaction patterns more ably than conventional statistical modeling, allowing these approaches to provide a greater insight into the understanding of disease processes and progression from existing clinical data repositories. Our findings support other data, which has strengthened the calls to improve diagnosis and phenotyping of AS through novel machine learning approaches (31–34).

While our findings are important and add to the body of literature supporting the need for greater advanced image phenotyping and risk prediction in moderate AS, some limitations should be discussed. First, our study is a single center, retrospective observation of prospectively collected, longitudinal data. To mitigate the limitation of a single-center approach, we used sample splitting to create an independent training and testing set, to avoid overfitting models to the trained dataset (17). It is important to note that the limitations of a single center machine learning approach are less relevant to our study because the goal of this study was not to create a broadly usable risk calculator. Rather, the motivation of this work was to (1) demonstrate that baseline echocardiographic metrics of AS severity can be used to predict change in myocardial function in moderate AS and (2) identify which parameters were most important to this change. In this sense, external validation is less important, as the study was intended to disclose key concepts in the understanding of disease progression in moderate AS, rather than create an externally usable model that would benefit from an external validation of generalizability. Having said this, the general inherent biases of a single-center study and reliance on subjects with a single-center follow-up must be acknowledged. With regard to the comparatively small sample size, we used a cohort that is well phenotyped and individually reanalyzed serial images with strict quality control. We took this approach in contrast to using a large-sized cohort with a shallow phenotyping approach (e.g., automated data repository metric extraction), which while important in its own right, can introduce noisy, missing, and/or inaccurate data in an initial survey. Our work demonstrates an early experience with this approach, which has

yielded valuable insights, and we encourage larger studies using database mining that could validate our findings. Our follow-up time was relatively short (median 1.3 years). This partly explains the modest changes in GLS over the study period. Indeed, our observed GLS change over the study period falls within the range of inter- and intraobserver variability reported elsewhere for GLS (35). Nevertheless, we demonstrated a clear trend in worsening GLS, and it is unlikely that random distribution of error would obscure the overall trend. Hence, despite this relatively short time interval, we were able to show that baseline AS metrics could accurately predict change in myocardial function over time, suggesting that the results would only have been amplified with a longer follow-up. Prospective studies with longer follow-up times could confirm and extend the findings of this study.

Conclusions

Moderate AS is a high-risk clinical entity, and subclinical myocardial dysfunction is important for this risk. Factors important to the progression of myocardial dysfunction in moderate AS are not well known. In this study, we have shown that neural network analysis could accurately predict change in subclinical myocardial dysfunction in moderate AS and identify which features were most important to this change. The key features included peak gradient, DI, baseline GLS, and energy loss, suggesting that these parameters should be evaluated carefully while assessing patients with moderate AS.

Data availability statement

The datasets presented in this article are not readily available because IRB restrictions prohibit sharing of data beyond our institution but can be considered upon reasonable request. Requests to access the datasets should be directed to mayooran.namasivayam@unsw.edu.au

Ethics statement

The studies involving human participants were reviewed and approved by St Vincent's Hospital HREC (Human Research Ethics Committee). Written informed consent for participation was not required for this study in accordance with the national legislation and the institutional requirements.

Author contributions

MN, CH, DM, and MF conceived and designed the study. MN and TM collected the data. MN performed analyses. All authors contributed to the article and approved the submitted version.

Funding

MN has received the National Heart Foundation of Australia Postdoctoral Fellowship, St Vincent's Clinic Foundation/St Vincent's Applied Medical Research Institute Clinician Grant, the New South Wales Ministry of Health Early-Mid Career Investigator Award, the Ramaciotti Foundation Health Investment Grant, and the Nvidia Corporation Academic Hardware Grant. MN's laboratory has received the Nvidia Corporation Academic Hardware Grant, but the company had no role in the study design, data collection, data analysis, or manuscript writeup. TM has received the Cardiac Society of Australia and New Zealand Research Scholarship and the National Heart Foundation of Australia PhD Scholarship. JK is the recipient of the Agilent Thought Leader Award (January 2022), which includes funding for research that is unrelated to the current manuscript.

Conflict of interest

The authors declare that the research was conducted in the absence of any commercial or financial relationships that could be construed as a potential conflict of interest.

Publisher's note

References

1. Delesalle G, Bohbot Y, Rusinaru D, Delpierre Q, Maréchaux S, Tribouilloy C. Characteristics and prognosis of patients with moderate aortic stenosis and preserved left ventricular ejection fraction. *J Am Heart Assoc*. (2019) 8(6):e011036. doi: 10.1161/JAHA.118.011036

2. Coisne A, Scotti A, Latib A, Montaigne D, Ho EC, Ludwig S, et al. Impact of moderate aortic stenosis on long-term clinical outcomes: a systematic review and meta-analysis. *JACC Cardiovasc Interv*. (2022) 15(16):1664–74. doi: 10.1016/j.jcin.2022.06.022

3. Narins CR. Implications of moderate aortic stenosis. *JACC Cardiovasc Interv*. (2022) 15(16):1675–7. doi: 10.1016/j.jcin.2022.07.003

4. Oh JK, Ito S. Severity of aortic stenosis: a moving target. *J Am Coll Cardiol*. (2022) 80(7):677–80. doi: 10.1016/j.jacc.2022.05.037

5. Strange G, Stewart S, Celermajer D, Prior D, Scalia GM, Marwick T, et al. Poor long-term survival in patients with moderate aortic stenosis. *J Am Coll Cardiol*. (2019) 74(15):1851–63. doi: 10.1016/j.jacc.2019.08.004

6. Stassen J, Pio SM, Ewe SH, Singh GK, Hirasawa K, Butcher SC, et al. Left ventricular global longitudinal strain in patients with moderate aortic stenosis. *J Am Soc Echocardiogr*. (2022) 35(8):791–800.e4. doi: 10.1016/j.echo.2022.03.008

7. Weyman AE, Scherrer-Crosbie M. Aortic stenosis: physics and physiology – what do the numbers really mean? *Rev Cardiovasc Med*. (2005) 6(1):23–32.

8. Stassen J, Ewe SH, Singh GK, Butcher SC, Hirasawa K, Amanullah MR, et al. Prevalence and prognostic implications of discordant grading and flow-gradient patterns in moderate aortic stenosis. *J Am Coll Cardiol*. (2022) 80(7):666–76. doi: 10.1016/j.jacc.2022.05.036

9. Pio SM, Amanullah MR, Butcher SC, Sin KY, Ajmone Marsan N, Pibarot P, et al. Discordant severity criteria in patients with moderate aortic stenosis: prognostic implications. *Open Heart*. (2021) 8(1):e001639. doi: 10.1136/openhrt-2021-001639

10. Yang H, Wright L, Negishi T, Negishi K, Liu J, Marwick TH. Research to practice: assessment of left ventricular global longitudinal strain for surveillance of cancer chemotherapeutic-related cardiac dysfunction. *JACC Cardiovasc Imaging*. (2018) 11(8):1196–201. doi: 10.1016/j.jcmg.2018.07.005

11. Amzulescu MS, De Craene M, Langet H, Pasquet A, Vancraeynest D, Pouleur AC, et al. Myocardial strain imaging: review of general principles, validation, and sources of discrepancies. *Eur Heart J Cardiovasc Imaging*. (2019) 20(6):605–19. doi: 10.1093/ehjci/jez041

12. Garcia D, Pibarot P, Dumesnil JG, Sakr F, Durand LG. Assessment of aortic valve stenosis severity: a new index based on the energy loss concept. *Circulation*. (2000) 101(7):765–71. doi: 10.1161/01.cir.101.7.765

13. Namasivayam M, He W, Churchill TW, Capoulade R, Liu S, Lee H, et al. Transvalvular flow rate determines prognostic value of aortic valve area in aortic stenosis. *J Am Coll Cardiol*. (2020) 75(15):1758–69. doi: 10.1016/j.jacc.2020.02.046

14. Namasivayam M, Picard MH. Flow rate in aortic stenosis: clinical tool, hemodynamic insight, or both? *J Am Soc Echocardiogr*. (2020) 33(4):449–51. doi: 10.1016/j.echo.2020.01.015

15. Obaid HS, Dheyab SA, Sabry SS. *The impact of data pre-processing techniques and dimensionality reduction on the accuracy of machine learning. 2019 9th Annual Information Technology, Electromechanical Engineering and Microelectronics Conference (IEMECON)* (2019). p. 279–83. doi: 10.1109/IEMECONX.2019.8877011

16. Alswaitti M, Siddique K, Jiang S, Alomoush W, Alrosan A. Dimensionality reduction, modelling, and optimization of multivariate problems based on machine learning. *Symmetry*. (2022) 14(7):1282. doi: 10.3390/sym14071282

17. Vabalas A, Gowen E, Poliakoff E, Casson AJ. Machine learning algorithm validation with a limited sample size. *PLoS One*. (2019) 14(11):e0224365. doi: 10.1371/journal.pone.0224365

18. Bing R, Cavalcante JL, Everett RJ, Clavel MA, Newby DE, Dweck MR. Imaging and impact of myocardial fibrosis in aortic stenosis. *JACC Cardiovasc Imaging*. (2019) 12(2):283–96. doi: 10.1016/j.jcmg.2018.11.026

19. Vassiliou VS, Perperoglou A, Raphael CE, Joshi S, Malley T, Everett R, et al. Midwall fibrosis and 5-year outcome in moderate and severe aortic stenosis. *J Am Coll Cardiol*. (2017) 69(13):1755–6. doi: 10.1016/j.jacc.2017.01.034

20. Altes A, Thellier N, Rusinaru D, Marsou W, Bohbot Y, Chadha G, et al. Dimensionless index in patients with low-gradient severe aortic stenosis and preserved ejection fraction. *Circ Cardiovasc Imaging*. (2020) 13(10):e010925. doi: 10.1161/CIRCIMAGING.120.010925

21. Vollema EM, Sugimoto T, Shen M, Tastet L, Ng ACT, Abou R, et al. Association of left ventricular global longitudinal strain with asymptomatic severe aortic stenosis: natural course and prognostic value. *JAMA Cardiol*. (2018) 3(9):839–47. doi: 10.1001/jamacardio.2018.2288

22. Bahlmann E, Gerdts E, Cramariuc D, Gohlke-Baerwolf C, Nienaber CA, Wachtell K, et al. Prognostic value of energy loss index in asymptomatic aortic stenosis. *Circulation*. (2013) 127(10):1149–56. doi: 10.1161/CIRCULATIONAHA.112.078857

23. Yoshida H, Seo Y, Ishizu T, Izumo M, Akashi YJ, Yamashita E, et al. Prognostic value of energy loss coefficient for predicting asymptomatic aortic stenosis outcomes: direct comparison with aortic valve area. *J Am Soc Echocardiogr*. (2019) 32(3):351–8.e3. doi: 10.1016/j.echo.2018.10.016

24. Garcia J, Barker AJ, Markl M. The role of imaging of flow patterns by 4D flow MRI in aortic stenosis. *JACC Cardiovasc Imaging*. (2019) 12(2):252–66. doi: 10.1016/j.jcmg.2018.10.034

25. Davis A, Billick K, Horton K, Jankowski M, Knoll P, Marshall JE, et al. Artificial intelligence and echocardiography: a primer for cardiac sonographers. *J Am Soc Echocardiogr*. (2020) 33(9):1061–6. doi: 10.1016/j.echo.2020.04.025

26. Gandhi S, Mosleh W, Shen J, Chow CM. Automation, machine learning, and artificial intelligence in echocardiography: a brave new world. *Echocardiography*. (2018) 35(9):1402–18. doi: 10.1111/echo.14086

27. Samad MD, Ulloa A, Wehner GJ, Jing L, Hartzel D, Good CW, et al. Predicting survival from large echocardiography and electronic health record datasets: optimization with machine learning. *JACC Cardiovasc Imaging*. (2019)12(4):681–9. doi: 10.1016/j.jcmg.2018.04.026

28. Shrestha S, Sengupta PP. The mechanics of machine learning: from a concept to value. *J Am Soc Echocardiogr*. (2018) 31(12):1285–7. doi: 10.1016/j.echo.2018.10.003

29. Tseng AS, Lopez-Jimenez F, Pellikka PA. Future guidelines for artificial intelligence in echocardiography. *J Am Soc Echocardiogr*. (2022) 35(8):878–82. doi: 10.1016/j.echo.2022.04.005

30. Namasivayam M. Machine learning in cardiac imaging: exploring the art of cluster analysis. *J Am Soc Echocardiogr*. (2021) 34(8):913–5. doi: 10.1016/j.echo.2021.05.011

31. Sengupta PP, Shrestha S, Kagiyama N, Hamirani Y, Kulkarni H, Yanamala N, et al. A machine-learning framework to identify distinct phenotypes of aortic stenosis severity. *JACC Cardiovasc Imaging*. (2021) 14(9):1707–20. doi: 10.1016/j.jcmg.2021.03.020

32. Namasivayam M, Myers PD, Guttag JV, Capoulade R, Pibarot P, Picard MH, et al. Predicting outcomes in patients with aortic stenosis using machine learning: the aortic stenosis risk (ASteRisk) score. *Open Heart*. (2022) 9(1):e001990. doi: 10.1136/openhrt-2022-001990

33. Dai W, Nazzari H, Namasivayam M, Hung J, Stultz CM. Identifying aortic stenosis with a single parasternal long axis video using deep learning. *J Am Soc Echocardiogr*. (2023) 36(1):116–8. doi: 10.1016/j.echo.2022.10.014

34. Kwak S, Lee Y, Ko T, Yang S, Hwang IC, Park JB, et al. Unsupervised cluster analysis of patients with aortic stenosis reveals distinct population with different phenotypes and outcomes. *Circ Cardiovasc Imaging*. (2020) 13(5):e009707. doi: 10.1161/CIRCIMAGING.119.009707

35. Donal E, Thebault C, O'Connor K, Veillard D, Rosca M, Pierard L, et al. Impact of aortic stenosis on longitudinal myocardial deformation during exercise. *Eur J Echocardiogr*. (2011) 12(3):235–41. doi: 10.1093/ejechocard/jeq187

frontiers | Frontiers in Cardiovascular Medicine

TYPE Case Report
PUBLISHED 20 July 2023
DOI 10.3389/fcvm.2023.1171226

OPEN ACCESS

EDITED BY
Konstantinos Papadopoulos,
Interbalkan Medical Center, Greece

REVIEWED BY
Özge Özden,
Memorial Bahçelievler Hospital, Türkiye
Irina Kotlar Velkova,
University Clinic of Cardiology,
North Macedonia

*CORRESPONDENCE
Constantinos Deltas
✉ Deltas@ucy.ac.cy

RECEIVED 21 February 2023
ACCEPTED 03 July 2023
PUBLISHED 20 July 2023

CITATION
Apostolou F, Ioannides M, Mitsis A, Koutsofti C, Deltas C and Avraamides P (2023) Case report: Aborted sudden cardiac death as a first presentation of severe mitral annulus disjunction—a case series and review of the literature.
Front. Cardiovasc. Med. 10:1171226.
doi: 10.3389/fcvm.2023.1171226

Case report: Aborted sudden cardiac death as a first presentation of severe mitral annulus disjunction—a case series and review of the literature

Fay Apostolou[1], Marios Ioannides[1], Andreas Mitsis[1], Constantina Koutsofti[2], Constantinos Deltas[2,3]* and Panayiotis Avraamides[1]

[1]Department of Cardiology, Nicosia General Hospital, Strovolos, Cyprus, [2]Biobank.cy Center of Excellence in Biobanking and Biomedical Research, University of Cyprus, Nicosia, Cyprus, [3]School of Medicine, University of Cyprus, Nicosia, Cyprus

Mitral annulus disjunction (MAD) is defined as a systolic displacement between the ventricular myocardium and the posterior mitral annulus supporting the posterior mitral leaflet. This structural abnormality is associated with the loss of mechanical annular function manifested as an abnormal systolic excursion of the leaflet hinge point into the left atrium but with maintained electrical function, separating the left atrium and ventricle electrophysiologically. The mitro-aortic fibrous continuity limits MAD anteriorly, between the aortic cusps and the anterior leaflet of the mitral valve. Consequently, MAD has been observed only at the insertion of the posterior leaflet. It can extend preferentially at the central posterior scallop. The first diagnostic modality aiding the diagnosis is transthoracic echocardiography (TTE), although in some cases adjunctive cardiac imaging modality might be suggested. MAD carries a strong association with malignant ventricular arrhythmogenesis and a profound predisposition for sudden cardiac death (SCD). In this context, a thorough investigation of this morphological and functional abnormality is vital in estimating the risk assessment and stratification for optimal management and elimination of the risk of the patient for SCD. Based on the current scientific data and literature, we will discuss the diagnosis, clinical implications, risk stratification, and therapeutic management of MAD.

KEYWORDS

mitral valve prolapse, mitral annulus disjunction, sudden cardiac death, ventricular arrhythmia, transthoracic echocardiography

Introduction

Mitral valve prolapse (MVP) is the most frequent cause of primary or degenerative mitral regurgitation (MR) with estimated prevalence up to 3% in the general population (1, 2). Mitral annulus disjunction (MAD) is frequently coexistent with MVP, although the reported prevalence of MAD varies due to the different imaging modalities, various cut-offs, heterogeneous subpopulations, and various MR-severity grades (3–5).

The clinical significance of MAD in the absence of mitral valve disease is unknown, although it has been shown that the prevalence of ventricular arrhythmias in MAD with

concomitant MVP and isolated MAD was not significantly different, which suggests the arrhythmogenicity of MAD alone (3, 6). MAD is currently considered an independent risk factor for ventricular arrhythmias and cardiac arrest independently of concomitant mitral valve abnormalities, suggesting the existence of a novel entity: MAD arrhythmic syndrome (7).

Epidemiology

At first, MAD was described in autopsy studies to be present in approximately 6% of human hearts (4, 8). The prevalence of MAD among patients with MVP varies between 20% and 58% (3, 9, 10). In a certain subset of patients with myxomatous MVP, MAD prevalence varies between 21.8% and 98% (3–5). In patients with MAD, the reported presence of MVP was 78% (6).

In arrhythmic MVP syndrome, MAD prevalence is reported between 34% (11) in patients with Marfan syndrome and 40% in carriers of Loeys–Dietz syndrome (12). In the abovementioned collagen vascular diseases, MAD appears as a marker of higher severity of arrhythmic event frequency, a higher number for mitral valve intervention needed, and among patients with extensive MAD, even more arrhythmic events (11, 12). In isolated MVP with systematic MAD assessment, generally in younger patients, the prevalence of 30% of MAD was reported (first large prospective cohort) (9). The strongest MAD-associated MVP feature was the advanced myxomatous-degeneration (marked leaflet-redundancy and bileaflet-MVP). The association was independent of all listed baseline characteristics, whereas MR severity was not independently associated with MAD (9).

Diagnostic criteria

The cornerstone for the diagnosis of MAD is cardiac imaging modalities. MAD can be detected easily in the long-axis views during end-systole using transthoracic echocardiography (TTE) (3–5, 10), and cardiac magnetic resonance (CMR) (13). As an adjunctive, cardiac computed tomography (CT) can also diagnose MAD. None of the abovementioned cardiac imaging modalities has been suggested in the present studies or guidelines as a gold standard method of diagnosis. In a study of 38 patients with myxomatous mitral valve disease, the authors described the recognition of MAD by using standard TTE using the length of the annular disjunction during end-systole on parasternal long-axis view, which was defined as the measurement from the junction of the left atrial wall and MV posterior leaflet to the basal LV posterior wall (4). With the use of a standardized intraoperative TEE protocol, MAD has also been described and defined as a separation between the P2 insertion into the left atrial wall and the atrioventricular attachment performed in a four-chamber mid-esophageal view. From this study, the significant correlation between the magnitude of disjunction and the number of segments with prolapse/flail was revealed (5), although according to a quantitative 3D echocardiographic study, more than one scallops of the posterior MVL may be involved (14).

MAD is widely known as a common abnormality in MVP. The disjunctive annulus is paradoxically functionally decoupled from the left ventricle and coupled more to the left atrium, consequently leading to paradoxical annulus dynamics with systolic expansion and annulus flattening. As a result, the abnormal mechanical stress and disjunctive annular dynamics exerted on the mitral valve and subvalvular apparatus accelerate the degenerative processes (14).

Excluding pseudo-MAD phenotype is of great importance. Pseudo-MAD refers to the juxtaposition of the posterior leaflet of the mitral valve on the atrial wall in systole mimicking MAD (15, 16). Particular attention is crucial for the recognition of MAD due to its strong correlation with life-threatening arrhythmic events. Therefore, high suspicion is suggested, especially in patients with concomitant MVP or myxomatous MV disease with arrhythmias or symptoms of arrhythmias. For the purpose of not underreporting such a potentially high arrhythmogenic entity, a multi-imaging modality approach may be necessary to raise the detection odds. Imaging modalities with superior spatial resolution such as cardiac CT or CMR may be used as adjunctive diagnostic tools for those with a lesser degree of MAD or high suspicion of MAD (17, 18). Cardiac CT can evaluate the mitral valve using a multiplanar reconstruction method, thereby providing detailed anatomic information, visualization of the entire circumference of the mitral valve attachment, and more sensitive detection of disjunction (17, 18). CMR is considered the gold standard imaging technique for evaluating myocardial function, quantifying chamber volumes, and detecting scar tissue/fibrosis (19) and may assist the risk stratification and prognostic information. Therefore, CMR may be an important adjunct to echocardiography as it can better define more subtle MAD and detect the markers of arrhythmia risk (13, 20).

Due to the high prevalence of MAD in normal subjects, an acceptable cut-off value of separation (≥5 mm) between the posterior leaflet insertion and the atrioventricular junction (basal LV free wall) is approved based on a histologic (7) and an echocardiographic description (5).

Arrhythmia substrate

The proposed mechanism of arrhythmias in MAD is related to a combination of papillary muscle fibrosis- anatomical substrate and mechanical stretch of the myocardium, which has been supported by CMR imaging findings (6, 21, 22).

SCD prevalence

All patients with MVP should be mandatory stratified for sudden cardiac death (SCD) risk. Risk stratification of patients with MVP includes focused history, 12-lead ECG, extended ECG monitoring, and detailed echocardiography. The use of CMR and

implantation of a loop recorder are more selective depending on the probability of VAs. Risk stratification involves two phases based on the clinical and imaging context and the detected arrhythmia (23). Even though the risk of malignant arrhythmias and SCD in MVP patients is low, estimated approximately 0.2%–0.4% per year, the real prevalence seems to be underestimated (24). A comprehensive clinical evaluation is mandatory to identify MVP patients with higher risk of arrhythmias. Family history of SCD is relevant to suggest the possibility of inherited arrhythmia syndromes (long-QT syndrome, arrhythmogenic right ventricular cardiomyopathy) as alternative diagnoses. Family history of MVP should also raise the attention to heritability, as either sporadic or familial forms.

Several phenotypic risk features of MVP have been identified including young age, female sex, high burden of ventricular ectopy (VE), bileaflet myxomatous MV degeneration, MR severity, and flail leaflet (8, 25).

More malignant risk factors of arrhythmia in MAD are younger age, high burden of VE, longer longitudinal distance of MAD, and evidence of papillary muscle fibrosis-anatomical substrate on CMR (6, 13). In addition to the arrhythmia risk, the presence of MAD has been shown to be associated with greater extent of mitral leaflet and chordae tendineae deformity and LV enlargement, and MR severity correlates with the degree of MAD. In other words, MAD may be a contributor to the progression of MR and may predispose to future degeneration and prolapse in patients without concomitant MV disease (9, 14). It still remains unclear whether MAD depth is a predictor of more frequent arrhythmic events, as it is proposed by the MAD-associated arrhythmia mechanism and the myocardial fibrosis as a hypothetic causative. Even though MAD presence in subjects with MVP has raised the VAs odds during follow-up, the first 10 years of follow-up did not confirm an association with excess mortality. As it is suggested by the risk stratification strategy in patients with MVP, the aim is to assess the risk of VAs and SCD according to the phenotypic risk features [T wave inversion in inferior leads, multiple polymorphic premature ventricular captures, MAD, redundant MV leaflets, enlarged left atrium, left ventricular ejection fraction (LVEF) < 50%, late gadolinium enlargement (LGE)] and the presence of high-risk ventricular tachycardia (VT). Based on the clinical and imaging context and the uncovered arrhythmia, Holter monitoring (periodic/diagnostic) and implantable loop recorder (ILR) are used for the risk stratification (23). MAD requires a deep and thorough understanding due to its apprehensive arrhythmogenic trait, and even the diagnosis of isolated MAD solely should instead raise awareness for a careful follow-up and not to acknowledge this as a high-risk factor for sudden death in all patients.

Case report 1

A 31-year-old Caucasian with a known medical history of bronchial asthma, mild MVP, autonomic dysregulation of sinus and atrioventricular node, smoking, and a family history with MVP and SCD was transferred to the emergency department of our hospital, following an episode of out-of-hospital cardiac arrest due to ventricular fibrillation. After the restoration of spontaneous circulation, a thorough clinical examination showed unremarkable findings, and a bedside FOCUS TTE on presentation showed a severely depressed LVEF and coronary angiography excluded obstructive coronary artery disease (CAD). Repeated TTE and TOE showed improved LV function (50% EF) and evidence of bileaflet MVP, severe mitral regurgitation, and MAD approximately 16 mm, not clearly visualized on initial imaging (**Figure 1**). The CMR showed significant annulus disjunction of the posterior leaflet of MV (**Figure 1**), measuring up to 16 mm, severe bileaflet MVP, and severe MR with posteriorly directed eccentric jet (**Supplementary Video S1**). Additional finding was an extensive, disseminated fibrosis of the mid lateral and inferolateral LV wall, posteromedial papillary muscle revealed by late gadolinium enhancement.

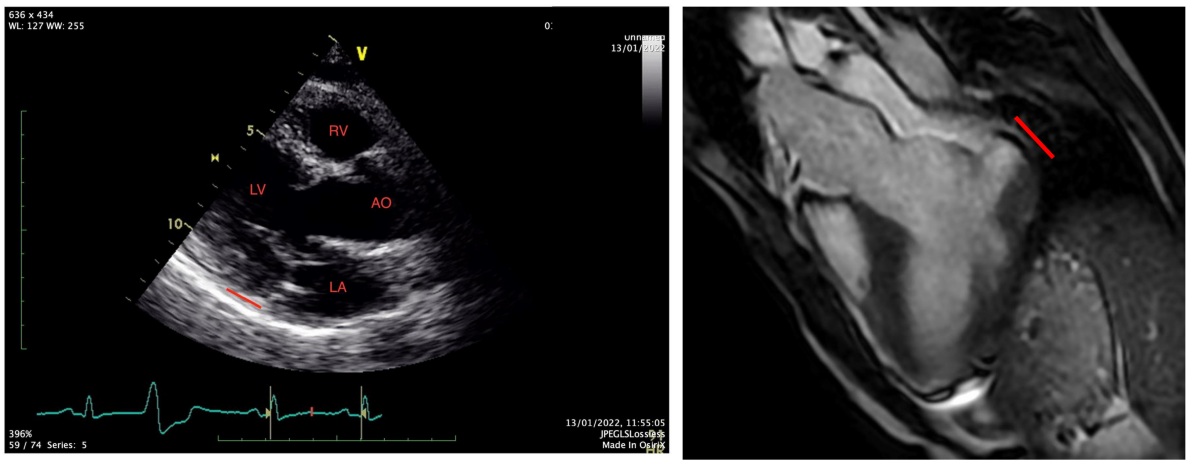

FIGURE 1
TTE and MRI, MAD noted with the red line.

A genetic test was performed with a next generation sequencing panel and revealed a very rare genetic variant in the *MYOM1* gene, classified as a variant of unknown significance (VUS). No specific relation between this mutation and MAD has been described.

The patient was discharged after receiving a secondary prevention implantable cardioverter defibrillator (ICD) and was referred for mitral valve repair. The post-operation follow-up with a cardiac event monitor showed a subtle arrhythmogenic activity VE burden (approximately 1.0%) and mild mitral regurgitation on transthoracic echocardiogram. He remained stable and asymptomatic.

Case report 2

A 50-year-old Caucasian man has been transferred to our clinic from another hospital, in an emergency manner for emergency coronary angiography due to persistent monomorphic ventricular tachycardia. While evaluating the patient, the patient collapsed abruptly due to ventricular fibrillation. He was successfully resuscitated from cardiac arrest and transferred fully consciousness for emergency coronary angiography. The clinical evaluation prior to the coronary angiography showed no significant clinical findings.

His past medical history was smoking in a habitual manner and former drug user (drug test upon admission was negative), reporting abstinence for 3 years now. He mentioned occasional palpitations without any further investigation. Collecting data from his family history, one case of sudden death was reported in the family at the age of 60 in a second-degree relative. Family history was negative for primary electrical diseases and MVP. He was not taking any medications or drugs at the time of presentation.

The coronary angiography excluded obstructive coronary artery disease as the cause of cardiac arrest and revealed a moderately impaired LV systolic function by left ventriculography.

The FOCUS echocardiographic assessment showed a moderately impaired LV systolic function, gross estimation LVEF: 40%, without pericardial effusion, and intact proximal ascending aorta. A complete TTE and TEE study that followed revealed a mildly dilated LV with borderline normal LVEF and MAD (**Figures 2**,**3**, **Supplementary Videos S2, S3**).

The cardiac magnetic resonance report an unveiled annular disjunction of the posterior LV wall, measuring a longitudinal MAD distance of 8 mm (**Figure 2**), with late gadolinium enhancement due to fibrosis in the anterolateral papillary muscle and basal posterolateral left ventricle. The left ventricular ejection fraction was borderline normal (LVEF: 50%), with mildly dilated left ventricular dimensions (LVESD: 36 mm/LVEDD: 53 mm short axis).

A multidisciplinary heart team suggested an ICD implantation as a secondary prevention for SCD and no further surgical intervention due to limited data in the current literature.

A genetic investigation with next generation sequencing panel revealed two variants of unknown significance (VUS) in *ANK2* and *TTN*. Both variants have no specific relation with MAD.

The patient is currently asymptomatic and without any worrying arrhythmic findings on follow-up cardiac rhythm monitoring 2 months after. His ICD check is also without any remarkable arrhythmic activity.

Risk stratification

Beyond the first part of the diagnostic algorithm with clinical approach, imaging, electrocardiographic, and cardiac event monitoring, asymptomatic patients with MAD—with or without MVP—require a close follow-up with repeated 2D-transthoracic echocardiography over the years, to explore MAD development over time and for routine rhythm surveillance, as MAD is an independent risk factor for arrhythmias (21). Additional diagnostic modalities such as CMR and electrophysiological study might be necessary for further risk stratification in cases with known risk factors for malignant arrhythmia. CMR is an optimal method for evaluating cardiac and valvular structure and function and for assessing the presence and extent of myocardial fibrosis. The presence of LGE is most often observed in the

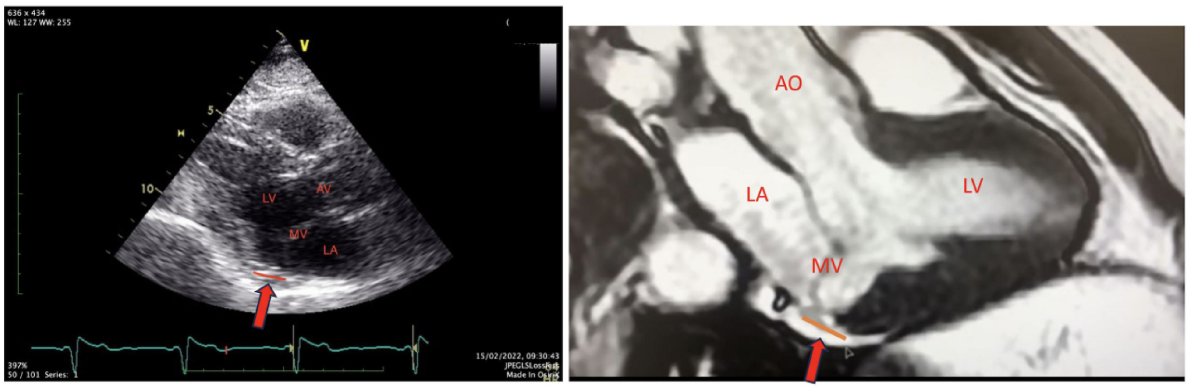

FIGURE 2
Transthoracic and MRI long-axis views. The red line and red arrow indicate the MAD area.

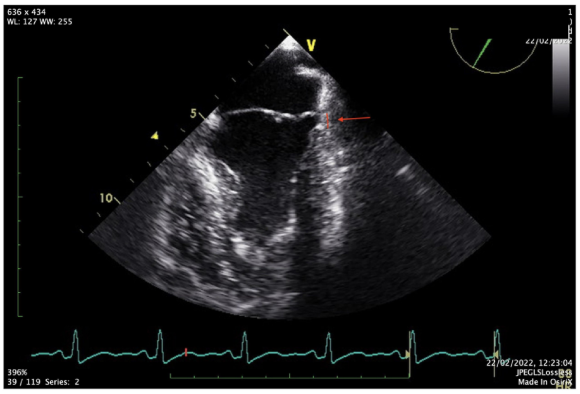

FIGURE 3
Transesophageal view of MAD (red line and red arrow).

papillary muscles or basal inferior wall and is highly linked with an increased risk of arrhythmias (26). The early detection of high-risk features is crucial in risk stratifying the patients and determining the necessity for more extensive evaluation and appropriate therapeutic management.

Therapeutic management

Current literature regarding the medical management of AMVP patients is scanty. The medical management should be addressed to the specific presentation by aiming the symptomatic improvement and improving survival (23).

The American Heart Association/European Society of Cardiology guidelines for ventricular arrhythmias and SCD have no distinctive criteria or recommendations for the secondary prevention of SCD and the management of ventricular arrhythmias in significant mitral valvulopathy (27, 28).

The pivotal challenge of SCD prevention mandates the establishment of primary and secondary preventive methods such as screening programs, technological measures (ECG, echocardiogram), and a fundamental risk stratification strategy with the use of CMR, treadmill exercise test, and a serial rhythm monitoring. In the case where MVP had been diagnosed in a random order or screening (relatives of SCD victims or athletes), a risk stratification strategy may be essential depending on the existence of high-risk criteria. It is essential to thoroughly evaluate with electrophysiological study, CMR, and echocardiography, particularly the young individuals, for the proper selection of candidates for ICD implantation (27).

According to the latest data from the expert consensus, patients with AMVP and a documented history of VF or hemodynamically not tolerated VT, in the absence of reversible causes, should receive an ICD. MVP with LVEF <35% and symptomatic HF despite ≥3 months of OMT should receive an ICD.

Ablation of PVCs in patients with frequent PVCs who are symptomatic or have decreased LV function is advised. Ablation of VA in MVP patients should be performed in experienced centers with expertise in VA ablation and interventional and surgical treatment of MV regurgitation. Ablation of PVCs is reasonable if triggering VF, particularly if not controlled by medications. Ablation of sustained monomorphic VT despite antiarrhythmic treatment or if antiarrhythmic treatment is not desired, or contraindicated, should be performed in MVP patients with recurrent ICD therapies. Mitral valve surgery may reduce the burden of malignant VAs in MVP patients and severe MR (23).

The promising potential of biomarkers and genetic studies for the determination of high-risk individuals, particularly after the latest correlating with familial clustering, is likely to be further tested in the coming future (29, 30).

A case report emphasized and illustrated the need to maintain alertness in malignant MVP patients and signified the role of mitral valve repair in the treatment of ventricular arrhythmias resulting from malignant MVP as a potential treatment option and secondary preventive method for SCD (31). Currently, there is no preferable surgical approach (valve repair or replacement), and as with the available data, none of them appears superior in terms of the reduction of ventricular arrhythmia burden. Despite this, a complete resolution of the disjunction can be achieved in both procedures and, subsequently, the reduction of malignant arrhythmias (13).

Conclusion

MAD is an anatomical, congenital variation associated frequently with MVP. Distinct anatomic characteristics of this potentially lethal entity may increase the risk of malignant ventricular arrhythmia and SCD. A suggestive therapeutic approach with ICD implantation and mitral valve repair might be necessary for this appropriate group. Large cohorts with long-term follow-up are required to better define MAD without MVP and its outcome and consequences. Future prospective studies evaluating ECG features, ventricular arrhythmia burden and morphology, and electrophysiological findings may provide further information. In individuals with different MAD phenotypes, further evidence could clarify its arrhythmogenic role and specify the effectiveness of antiarrhythmic therapy, the potential use of early catheter ablation in refractory ventricular arrhythmias, and the surgical approach in managing ventricular arrhythmia in patients with MVP (32).

Data availability statement

The raw data supporting the conclusions of this article will be made available by the authors, without undue reservation.

Ethics statements

Written informed consent was obtained from the individual(s) for the publication of any potentially identifiable images or data included in this article.

Author contributions

FA, MI, AM, and PA contributed in the clinical and imaging investigation. CK and CD acted as collaborating genetic consultants. All authors contributed to the article and approved the submitted version.

Conflict of interest

The authors declare that the research was conducted in the absence of any commercial or financial relationships that could be construed as a potential conflict of interest.

Publisher's note

Supplementary material

The Supplementary Material for this article can be found online at: https://www.frontiersin.org/articles/10.3389/fcvm.2023.1171226/full#supplementary-material.

References

1. Freed LA, Levy D, Levine RA, Larson MG, Evans JC, Fuller DL, et al. Prevalence and clinical outcome of mitral-valve prolapse. *N Engl J Med.* (1999) 341(1):1–7. doi: 10.1056/NEJM199907013410101

2. Dziadzko V, Dziadzko M, Medina-Inojosa JR, Benfari G, Michelena HI, Crestanello JA, et al. Causes and mechanisms of isolated mitral regurgitation in the community: clinical context and outcome. *Eur Heart J.* (2019) 40(27):2194–202. doi: 10.1093/eurheartj/ehz314

3. Konda T, Tani T, Suganuma N, Nakamura H, Sumida T, Fujii Y, et al. The analysis of mitral annular disjunction detected by echocardiography and comparison with previously reported pathological data. *J Echocardiogr.* (2017) 15 (4):176–85. doi: 10.1007/s12574-017-0349-1

4. Carmo P, Andrade MJ, Aguiar C, Rodrigues R, Gouveia R, Silva JA. Mitral annular disjunction in myxomatous mitral valve disease: a relevant abnormality recognizable by transthoracic echocardiography. *Cardiovasc Ultrasound.* (2010) 8:53. doi: 10.1186/1476-7120-8-53

5. Eriksson MJ, Bitkover CY, Omran AS, David TE, Ivanov J, Ali MJ, et al. Mitral annular disjunction in advanced myxomatous mitral valve disease: echocardiographic detection and surgical correction. *J Am Soc Echocardiogr.* (2005) 18(10):1014–22. doi: 10.1016/j.echo.2005.06.013

6. Dejgaard LA, Skjølsvik ET, Lie ØH, Ribe M, Stokke MK, Hegbom F, et al. The mitral annulus disjunction arrhythmic syndrome. *J Am Coll Cardiol.* (2018) 72 (14):1600–9. doi: 10.1016/j.jacc.2018.07.070

7. Hutchins GM, Moore GW, Skoog DK. The association of floppy mitral valve with disjunction of the mitral annulus fibrosus. *N Engl J Med.* (1986) 314(9):535–40. doi: 10.1056/NEJM198602273140902

8. Basso C, Perazzolo Marra M, Rizzo S, De Lazzari M, Giorgi B, Cipriani A, et al. Arrhythmic mitral valve prolapse and sudden cardiac death. *Circulation.* (2015) 132 (7):556–66. doi: 10.1161/CIRCULATIONAHA.115.016291

9. Essayagh B, Sabbag A, Antoine C, Benfari G, Batista R, Yang LT, et al. The mitral annular disjunction of mitral valve prolapse: presentation and outcome. *JACC Cardiovasc Imaging.* (2021) 14(11):2073–87. doi: 10.1016/j.jcmg.2021.04.029

10. Mantegazza V, Tamborini G, Muratori M, Gripari P, Fusini L, Italiano G, et al. Mitral annular disjunction in a large cohort of patients with mitral valve prolapse and significant regurgitation. *JACC Cardiovasc Imaging.* (2019) 12(11 Pt 1):2278–80. doi: 10.1016/j.jcmg.2019.06.021

11. Demolder A, Timmermans F, Duytschaever M, Muiño-Mosquera L, De Backer J. Association of mitral annular disjunction with cardiovascular outcomes among patients with Marfan syndrome. *JAMA Cardiol.* (2021) 6(10):1177–86. doi: 10.1001/jamacardio.2021.2312

12. Chivulescu M, Krohg-Sørensen K, Scheirlynck E, Lindberg BR, Dejgaard LA, Lie ØH, et al. Mitral annulus disjunction is associated with adverse outcome in Marfan and Loeys–Dietz syndromes. *Eur Heart J Cardiovasc Imaging.* (2021) 22(9):1035–44. doi: 10.1093/ehjci/jeaa324

13. Essayagh B, Iacuzio L, Civaia F, Avierinos JF, Tribouilloy C, Levy F. Usefulness of 3-Tesla cardiac magnetic resonance to detect mitral annular disjunction in patients with mitral valve prolapse. *Am J Cardiol.* (2019) 124(11):1725–30. doi: 10.1016/j.amjcard.2019.08.047

14. Lee APW, Jin CN, Fan Y, Wong RHL, Underwood MJ, Wan S. Functional implication of mitral annular disjunction in mitral valve prolapse: a quantitative dynamic 3D echocardiographic study. *JACC Cardiovasc Imaging.* (2017) 10 (12):1424–33. doi: 10.1016/j.jcmg.2016.11.022

15. Faletra FF, Leo LA, Paiocchi VL, Schlossbauer SA, Pavon AG, Ho SY, et al. Morphology of mitral annular disjunction in mitral valve prolapse. *J Am Soc Echocardiogr.* (2022) 35(2):176–86. doi: 10.1016/j.echo.2021.09.002

16. Niarchou P, Prappa E, Liatakis I, Vlachos K, Chatziantoniou A, Nyktari E, et al. Mitral valve prolapse and mitral annular disjunction arrhythmic syndromes: diagnosis, risk stratification and management. *Rev Cardiovasc Med.* (2022) 23 (9):295. doi: 10.31083/j.rcm2309295

17. Toh H, Mori S, Izawa Y, Fujita H, Miwa K, Suzuki M, et al. Prevalence and extent of mitral annular disjunction in structurally normal hearts: comprehensive 3D analysis using cardiac computed tomography. *Eur Heart J Cardiovasc Imaging.* (2021) 22(6):614–22. doi: 10.1093/ehjci/jeab022

18. Delgado V, Tops LF, Schuijf JD, de Roos A, Brugada J, Schalij MJ, et al. Assessment of mitral valve anatomy and geometry with multislice computed tomography. *JACC Cardiovasc Imaging.* (2009) 2(5):556–65. doi: 10.1016/j.jcmg.2008.12.025

19. Salerno M, Sharif B, Arheden H, Kumar A, Axel L, Li D, et al. Recent advances in cardiovascular magnetic resonance: techniques and applications. *Circ Cardiovasc Imaging.* (2017) 10(6):e003951. doi: 10.1161/CIRCIMAGING.116.003951

20. Mantegazza V, Volpato V, Gripari P, Ghulam Ali S, Fusini L, Italiano G, et al. Multimodality imaging assessment of mitral annular disjunction in mitral valve prolapse. *Heart.* (2021) 107(1):25–32. doi: 10.1136/heartjnl-2020-317330

21. Basso C, Iliceto S, Thiene G, Perazzolo Marra M. Mitral valve prolapse, ventricular arrhythmias, and sudden death. *Circulation.* (2019) 140(11):952–64. doi: 10.1161/CIRCULATIONAHA.118.034075

22. Basso C, Perazzolo Marra M. Mitral annulus disjunction: emerging role of myocardial mechanical stretch in arrhythmogenesis. *J Am Coll Cardiol.* (2018) 72 (14):1610–2. doi: 10.1016/j.jacc.2018.07.069

23. Sabbag A, Essayagh B, Barrera JDR, Basso C, Berni A, Cosyns B, et al. EHRA expert consensus statement on arrhythmic mitral valve prolapse and mitral annular disjunction complex in collaboration with the ESC council on valvular heart disease and the European Association of Cardiovascular Imaging endorsed by the Heart Rhythm Society, by the Asia Pacific Heart Rhythm Society, and by the Latin American Heart Rhythm Society. *Europace* (2022) 24(12):1981–2003. doi: 10.1093/europace/euac125

24. Basso C, Calabrese F, Corrado D, Thiene G. Postmortem diagnosis in sudden cardiac death victims: macroscopic, microscopic and molecular findings. *Cardiovasc Res.* (2001) 50(2):290–300. doi: 10.1016/S0008-6363(01)00261-9

25. Sriram CS, Syed FF, Ferguson ME, Johnson JN, Enriquez-Sarano M, Cetta F, et al. Malignant bileaflet mitral valve prolapse syndrome in patients with otherwise idiopathic out-of-hospital cardiac arrest. *J Am Coll Cardiol.* (2013) 62(3):222–30. doi: 10.1016/j.jacc.2013.02.060

26. Perazzolo Marra M, Basso C, De Lazzari M, Rizzo S, Cipriani A, Giorgi B, et al. Morphofunctional abnormalities of mitral annulus and arrhythmic mitral valve prolapse. *Circ Cardiovasc Imaging.* (2016) 9(8):e005030. doi: 10.1161/CIRCIMAGING.116.005030

27. Ahmed M, Roshdy A, Sharma R, Fletcher N. Sudden cardiac arrest and coexisting mitral valve prolapse: a case report and literature review. *Echo Res Pract.* (2016) 3(1):D1–8. doi: 10.1530/ERP-15-0020

28. Priori SG, Blomström-Lundqvist C, Mazzanti A, Blom N, Borggrefe M, Camm J, et al. ESC guidelines for the management of patients with ventricular arrhythmias and the prevention of sudden cardiac death: the task force for the management of patients

with ventricular arrhythmias and the prevention of sudden cardiac death of the European Society of Cardiology (ESC). Endorsed by: Association for European Paediatric and Congenital Cardiology (AEPC). *Eur Heart J.* (2015) 36 (41):2793–867. doi: 10.1093/eurheartj/ehv316

29. Narayanan K, Uy-Evanado A, Teodorescu C, Reinier K, Nichols GA, Gunson K, et al. Mitral valve prolapse and sudden cardiac arrest in the community. *Heart Rhythm.* (2016) 13(2):498–503. doi: 10.1016/j.hrthm.2015.09.026

30. Missov E, Cogswell R. Sudden cardiac death, mitral valve prolapse, and long QT syndrome. *Am J Med.* (2015) 128(10):e37–8. doi: 10.1016/j.amjmed.2015.05.030

31. Abbadi DR, Purbey R, Poornima IG. Mitral valve repair is an effective treatment for ventricular arrhythmias in mitral valve prolapse syndrome. *Int J Cardiol.* (2014) 177(1):e16–8. doi: 10.1016/j.ijcard.2014.07.174

32. Chatterjee NA, Rea TD. Secondary prevention of sudden cardiac death. *Heart Rhythm O2.* (2020) 1(4):297–310. doi: 10.1016/j.hroo.2020.08.002

frontiers | Frontiers in Cardiovascular Medicine

TYPE Brief Research Report
PUBLISHED 21 July 2023
DOI 10.3389/fcvm.2023.1211322

OPEN ACCESS

EDITED BY
Konstantinos Papadopoulos,
Interbalkan Medical Center, Greece

REVIEWED BY
Ythan H. Goldberg,
Lenox Hill Hospital, United States
Daniel Lovric,
University Hospital Centre Zagreb, Croatia

*CORRESPONDENCE
Mark J. Schuuring
✉ M.J.Schuuring-19@umcutrecht.nl

RECEIVED 24 April 2023
ACCEPTED 03 July 2023
PUBLISHED 21 July 2023

CITATION
Molenaar MA, Bouma BJ, Coerkamp CF, Man JP, Išgum I, Verouden NJ, Selder JL, Chamuleau SAJ and Schuuring MJ (2023) The impact of valvular heart disease in patients with chronic coronary syndrome.
Front. Cardiovasc. Med. 10:1211322.
doi: 10.3389/fcvm.2023.1211322

The impact of valvular heart disease in patients with chronic coronary syndrome

Mitchel A. Molenaar[1,2,3], Berto J. Bouma[2,3], Casper F. Coerkamp[2,3], Jelle P. Man[2,3], Ivana Išgum[3,4,5], Niels J. Verouden[1,3], Jasper L. Selder[1,3], Steven A. J. Chamuleau[1,2,3] and Mark J. Schuuring[2,3,6]*

[1]Department of Cardiology, Amsterdam UMC Location Vrije Universiteit Amsterdam, Amsterdam, Netherlands, [2]Department of Cardiology, Amsterdam UMC Location University of Amsterdam, Amsterdam, Netherlands, [3]Amsterdam Cardiovascular Sciences, Amsterdam UMC, Amsterdam, Netherlands, [4]Department of Biomedical Engineering and Physics, Amsterdam UMC Location University of Amsterdam, Amsterdam, Netherlands, [5]Department of Radiology and Nuclear Medicine, Amsterdam UMC Location University of Amsterdam, Amsterdam, Netherlands, [6]Department of Cardiology, University Medical Center Utrecht, Utrecht, Netherlands

Background: The European Society of Cardiology 2019 Guidelines on chronic coronary syndrome (CCS) recommend echocardiographic measurement of the left ventricular function for risk stratification in all patients with CCS. Whereas CCS and valvular heart disease (VHD) share common pathophysiological pathways and risk factors, data on the impact of VHD in CCS patients are scarce.
Methods: Clinical data including treatment and mortality of patients diagnosed with CCS who underwent comprehensive transthoracic echocardiography (TTE) in two tertiary centers were collected. The outcome was all-cause mortality. Data were analyzed with Kaplan-Meier curves and Cox proportional hazard analysis adjusting for significant covariables and time-dependent treatment.
Results: Between 2014 and 2021 a total of 1,984 patients with CCS (59% men) with a median age of 65 years (interquartile range [IQR] 57–73) underwent comprehensive TTE. Severe VHD was present in 44 patients and moderate VHD in 325 patients. A total of 654 patients (33%) were treated with revascularization, 39 patients (2%) received valve repair or replacement and 299 patients (15%) died during the median follow-up time of 3.5 years (IQR 1.7–5.6). Moderate or severe VHD (hazard ratio = 1.33; 95% CI 1.02–1.72) was significantly associated with mortality risk, independent of LV function and other covariables, as compared to no/mild VHD.
Conclusions: VHD has a significant impact on mortality in patients with CCS additional to LV dysfunction, which emphasizes the need for a comprehensive echocardiographic assessment in these patients.

KEYWORDS

coronary artery disease, valvular heart disease, prognosis, risk, mortality

1. Introduction

Chronic coronary syndrome (CCS) is characterized by stable atherosclerotic coronary plaques that build up over time. CCS affects more than 34 million adult Europeans and has a high mortality rate, despite advanced medical care and revascularization (1, 2).

The European Society of Cardiology (ESC) 2019 Guidelines on CCS recommend transthoracic echocardiographic (TTE) measurement of left ventricular (LV) function for risk stratification in all patients with CCS, as it is considered to be one of the strongest determinants of mortality (3–5). This is mainly based on the Coronary Artery Surgery

Study (CASS) registry (5). This CASS registry was performed in the 1970s, a long time before introduction of modern therapies and revascularization techniques.

It is unclear whether other echocardiographic findings provide additional information about the prognosis of patients with CCS. In particular data regarding the impact of valvular heart disease (VHD) on the mortality of patients with CCS are scarce. It is estimated that VHD affects more than 18 million Europeans (6, 7) and accounts for 10 to 20% of all cardiac surgery procedures (8, 9). As both VHD and CCS share common pathophysiological pathways and risk factors, a better understanding of the impact of VHD on mortality in patients with CCS is needed. Therefore, we performed a study in CCS patients and investigated the impact of VHD on mortality.

2. Methods

2.1. Design and patient population

In this retrospective cohort study, patients diagnosed by the treating physician with CCS between 2014 and 2021 were consecutively selected from electronic health records of the Amsterdam University Medical Center (two tertiary centers), the Netherlands. CCS patients (≥18 years) who underwent comprehensive transthoracic echocardiography (TTE) one year before or after the outpatient visit were eligible for inclusion. For patients with multiple studies, the TTE closest to the outpatient visit date was selected. This retrospective cohort study was approved by the local institutional review board, who waived the need for written consent.

2.2. Data collection and echocardiographic measurements

Baseline, treatment and mortality in follow-up data of patients with CCS were collected from pseudonymized electronic health records and stored in a registry. Two-dimensional TTE with Doppler tissue imaging (Vivid 9, GE Vingmed Ultrasound AS, Horten, Norway; Philips Epiq, Philips Affiniti and Philips IE33, Philips Medical Systems, Best, The Netherlands) was performed and assessed by clinical technicians or cardiology residents according to recommendations of the European Association of Cardiovascular Imaging (10), ESC guidelines (11, 12) and standard operating procedure (13). TTE images were digitized and analyzed using vendor-specific software (GE EchoPAC, GE Vingmed Ultrasound AS, Horten, Norway; Xcelera, Philips Medical Systems, Best, The Netherlands; TomTec 2D Cardiac Performance Analysis, Munich, Germany).

The initial assessment of the valves was performed qualitatively by a clinical technician or cardiology resident. Semi-quantitative and quantitative measurements of stenosis or regurgitation were obtained if indicated, especially if clinical decisions were based on these findings (11, 12). The results were documented in a TTE report (10), which were overseen by dedicated imaging cardiologists who made corrections if needed to maintain accuracy and completeness.

The Simpson's method of disks was used to estimate the LV volume at both end-diastolic and end-systolic phase from apical four- and two-chamber views. This method involved tracing the endocardial border on 2D echocardiographic images of the left ventricle during these phases, dividing the tracing into multiple disks (slices), and summing their volumes to obtain the total LV volume. The LV ejection fraction (LVEF) was calculated by subtracting the LV volume at end-systole from the LV volume at end-diastole, and dividing it by the LV volume at end-diastole. LV dysfunction was defined as mild to severe abnormal LV function (LVEF <51% for male and <53% for female). Moderately and severely abnormal LV function were defined as a LVEF of 30%–41% and <30%, respectively (14).

For the purpose of this study, the LV function and severity of aortic stenosis (AS), aortic regurgitation (AR), mitral stenosis (MS), mitral regurgitation (MR), tricuspid regurgitation (TR), pulmonary stenosis (PS), and pulmonary regurgitation (PR) were stored in the registry. Patients were excluded if TTE image acquisition was of poor quality or incomplete due to missing assessment of LV function or VHD (10). Multivalvular disease was defined as regurgitation and/or stenosis in two or more heart valves. Patients were categorized based on the most severe valve condition among the valves, which means that patients with both moderate and severe valvular lesions were classified as having severe VHD. Impaired renal function was defined as an estimated glomerular filtration rate (eGFR) < 60 ml/min/1.73 m^2. eGFR was calculated with the Chronic Kidney Disease Epidemiology Collaboration (CKD-EPI) creatinine equation (15). Obesity was defined as a body mass index of >30 kg/ m^2.

2.3. Outcome

The clinical endpoint was all-cause mortality. The end of follow-up was defined as the last recorded contact with the tertiary center or the date of mortality.

2.4. Statistical analysis

Results were expressed as mean values with standard deviation (SD) for normally distributed data, and median with interquartile range (IQR) for not normally distributed data. Nominal or ordinal data were expressed with numbers and percentages. The Shapiro-Wilk test was used to test for normality. The one-way ANOVA or Kruskal-Wallis test was performed for between group comparisons of continuous data, as appropriate. A Pearson's Chi-Square test was performed for categorical variables.

Missing values were imputed by multiple imputation by chained equation (MICE) with a linear regression model, which was iteratively performed for 10 iterations. The degree of multicollinearity between variables was assessed with the variance inflation factor (VIF) (16). Variables with a VIF greater than 10

were either dichotomized, centered by subtracting the mean value, or omitted from multivariable analysis to account for their collinearity with other variables. Variables with a p-value of $p \leq 0.05$ on univariable mortality analysis and time-dependent variables coronary revascularization and valve repair or replacement were entered into Cox proportional hazards (PH) models with backward selection procedure ($p \leq 0.05$) based on the Akaike information criterion. Cox PH analyses were conducted to examine the association between predictor variables and mortality. Predictor variables with a prevalence of at least 5% among the patients were included in multivariable analysis. To evaluate the assumption of PH, Kaplan Meier curves were inspected and Schoenfeld residuals were calculated (17). Analysis was performed for the predictor variables VHD, the number of valves affected and the specific subtypes of VHD (AS, AR, MS, MR, TR, PS and PR).

Statistical analyses were performed in Python V3.8 and RStudio V.2022.07.0 (RStudio Team, Boston, MA) using R-version 4.1.3. (R Core Team, Vienna, Austria). $P < 0.05$ was considered statistically significant.

3. Results

3.1. Study population

A total of 2,845 patients with CCS were screened. Among them, 861 patients were not eligible for inclusion, resulting in a study population of 1,984 patients, as shown in **Supplementary Figure S1**. The proportion of missing data was 3%, as shown in **Supplementary Table S1**. The median age of the study population was 65 years (IQR 57–73), 59% were men and 26% had a history of myocardial infarction (**Supplementary Table S2**). The majority, 54%, had a history of hypertension and 59% of the patients presented with chest pain at the outpatient visit. A minority of the patients presented with dyspnea (31%). The most common reported secondary prevention therapies were antiplatelet therapy (61%), statins (60%) and beta-blockers (52%). A total of 505 patients (25%) had LV dysfunction, which was severe in 39 patients (2%), as shown in **Supplementary Table S3**.

3.2. Concomitant valvular heart disease

No/mild, moderate and severe VHD were present in 1,615 (82%), 325 (16%) and 44 (2%) patients, respectively (**Supplementary Table S3**). MR was most the common VHD (moderate MR: 176 patients, severe MR: 3 patients) in patients with CCS, followed by TR (moderate TR: 128 patients, severe TR: 16 patients), and AS (moderate AS: 64 patients, severe AS: 24 patients). Multivalvular disease was present in 84 patients (4%). Compared to patients within the group with no/mild VHD, patients with moderate or severe VHD were significantly older and had more often hypertension, atrial fibrillation or flutter, and chronic obstructive pulmonary disease (COPD), used more often cardiovascular medication (anticoagulants, renin-angiotensin system inhibitors, beta-blockers, and diuretics), had a lower eGFR, and more often LV dysfunction (**Supplementary Tables S2, S3**). Patients with moderate or severe VHD had more often surgical aortic valve replacement (SAVR) in medical history. Patients with no/mild VHD were more often a current or former smoker and had more often a family history of coronary artery disease. Chest pain was more often reported in patients with no/mild VHD, while dyspnea was more frequently reported in patients with moderate or severe VHD.

3.3. Follow-up

The median follow-up time of patients was 3.5 years (IQR 1.7–5.6). During the follow-up period, a total of 654 patients (33%) received revascularization by coronary artery bypass grafting (CABG) and/or percutaneous coronary intervention (PCI). Follow-up data are shown in **Table 1**. Patients with severe VHD received revascularization by CABG (11%) more often compared to patients with moderate (3%) or no/mild VHD (3%) during follow-up. Valve repair or replacement was performed in 39 patients (2%) during follow-up. Transcatheter aortic valve replacement (TAVR) was most often performed (26 patients) followed by SAVR (10 patients). One patient with mild VHD and 14 patients with moderate VHD received valve repair or replacement during follow-up due to multivalvular disease, increase in severity, or combined with CABG.

A total of 299 patients (15%) died, of which 91 patients had moderate VHD and 13 patients had severe VHD. The mortality curves of patients with moderate and severe VHD showed a significant overlap and had both higher mortality rates compared to those with no/mild VHD (**Supplementary Figure S2**). Based on the overlap in the mortality curves and low number of patients with severe VHD ($n = 44$), it was decided to combine moderate and severe in further analysis (**Figure 1**).

3.4. Determinants of mortality

In univariable analysis, a number of variables were associated with mortality, as shown in **Table 2**. In multivariable analysis, moderate and severe combined VHD [hazard ratio (HR) = 1.33; 95% CI 1.02–1.72] remained associated with mortality independent of age (HR = 1.04; 95% CI 1.02–1.05), diabetes (HR = 1.58; 95% CI 1.24–2.00), current or former smoking (HR = 1.48; 95% CI 1.16–1.88), valve repair or replacement (HR = 1.50; 95% CI 1.02–2.20), COPD (HR = 1.96; 95% CI 1.42–2.70), chest pain (HR = 0.68; 95% CI 0.54–0.85), impaired renal function (HR = 1.61; 95% CI 1.27–2.04) and LV dysfunction (HR = 1.96; 95% CI 1.55–2.48). Details are shown in **Table 2** and **Supplementary Figure S3**.

Moderate VHD was associated with increased mortality (HR = 1.4; 95% CI 1.05–1.78), while severe VHD did not show a significant association with mortality (HR = 0.99; 95% CI 0.52–1.87, **Supplementary Table S4**).

TABLE 1 Follow-up of study population.

	All patients ($n = 1,984$)	No/mild VHD ($n = 1,615$)	Moderate VHD ($n = 325$)	Severe VHD ($n = 44$)	*p*-value
Revascularization[a], *n* (%)	654 (33.0)	517 (32.0)	120 (36.9)	17 (38.6)	0.165
CABG, *n* (%)	56 (2.8)	41 (2.5)	10 (3.1)	5 (11.4)	0.002
PCI, *n* (%)	622 (31.4)	492 (30.5)	116 (35.7)	14 (31.8)	0.179
Isolated or concomitant valve repair or replacement[b], *n* (%)	39 (2.0)	1 (0.1)	14 (4.3)	24 (54.5)	<0.001
SAVR, *n* (%)	10 (0.5)	0 (0.0)	4 (1.2)	6 (13.6)	<0.001
TAVR, *n* (%)	26 (1.3)	1 (0.1)	8 (2.5)	17 (38.6)	<0.001
SMVR, *n* (%)	1 (0.1)	0 (0.0)	0 (0.0)	1 (2.3)	<0.001
TEER, *n* (%)	3 (0.2)	0 (0.0)	2 (0.6)	1 (2.3)	<0.001
STVR, *n* (%)	1 (0.1)	0 (0.0)	0 (0.0)	1 (2.3)	<0.001
SPVR, *n* (%)	0 (0.0)	0 (0.0)	0 (0.0)	0 (0.0)	NA
Outcome, *n* (%)					
Death	299 (15.1)	195 (12.1)	91 (28.0)	13 (29.5)	<0.001

Follow-up of study population.
[a]Some patients received both coronary artery bypass graft and percutaneous coronary intervention.
[b]One patient with mild and 14 patients with moderate valvular heart disease received valve repair or replacement during follow-up due to multivalvular disease, increase in severity, or combined with coronary artery bypass grafting.
CABG, coronary artery bypass grafting; PCI, percutaneous coronary intervention; SAVR, surgical aortic valve replacement; SMVR, surgical mitral valve replacement; SPVR, surgical pulmonary valve replacement; STVR, surgical tricuspid valve replacement; TAVR, transcatheter aortic valve replacement; TEER, transcatheter edge-to-edge repair; VHD, valvular heart disease.

3.5. Mortality and multivalvular disease

Patients with multivalvular disease (unadjusted HR = 3.2; 95% CI 2.4–4.9), had a higher mortality rate than patients with single valve heart disease (unadjusted HR = 1.9; 95% CI 1.5–2.5) and the group with no/mild VHD (Log-Rank $p < 0.005$, **Supplementary Figure S4**).

3.6. Mortality by VHD subtype

Moderate and severe combined AS (unadjusted HR = 1.8, 95% CI 1.2–2.7), AR (unadjusted HR = 1.9, 95% CI 1.1–3.1), MR (unadjusted HR = 2.3, 95% CI 1.7–3.1), TR (unadjusted HR = 2.6, 95% CI 1.9–3.5) were associated with mortality (**Figure 2**). In addition, moderate and severe combined MS ($n = 6$), PR ($n = 7$) and PS ($n = 1$) were associated with mortality. In multivariable analysis, only moderate TR remained a significant predictor of mortality (HR = 1.6; 95% CI 1.2–2.3, **Supplementary Table S5**).

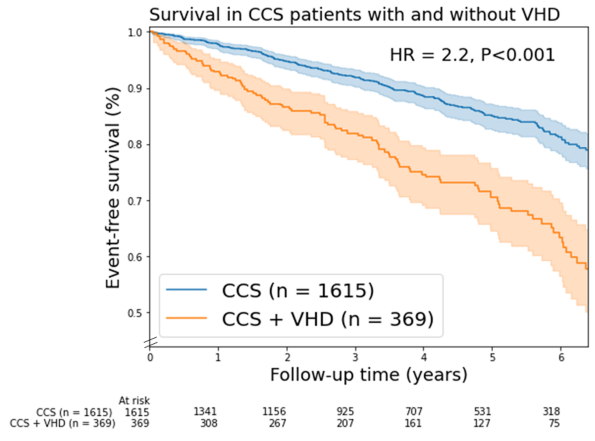

FIGURE 1
Kaplan-Meier mortality curves for chronic coronary syndrome (CCS) patients with/without valvular heart disease (VHD). In this figure, VHD is moderate and severe combined VHD. Shaded areas represent the 95% confidence intervals. HR, unadjusted hazard ratio.

4. Discussion

This study in patients with CCS showed that moderate or severe combined VHD was associated with mortality, independent of LV function and other covariables. In the 1,984 patients studied, patients with CCS and moderate or severe VHD had a higher risk of mortality compared to patients with CCS only, which increased with the number of valves affected. These findings demonstrate the importance of echocardiographic assessment of VHD, in addition to LV function, in CCS patients.

4.1. Valvular heart disease in patients with chronic coronary syndrome

To our knowledge, this is the first study that investigates the prognostic value of VHD in patients with CCS. Severe VHD is an established determinant of mortality for which valve repair or replacement is recommended by current guidelines (18, 19). We observed that severe VHD was not an independent determinant of mortality in patients with CCS. This finding may be explained by the number of patients with severe VHD ($n = 44$) that may have been too small to detect a significant effect. Moreover, a substantial proportion of CCS patients with severe VHD received a valvular intervention during follow-up (55%) which likely reduced their mortality risk.

TABLE 2 Univariable and multivariable Cox regression analysis of variables associated with mortality: moderate and severe combined.

Variable	Univariable analysis		Multivariable analysis	
	HR (95% CI)	*P*-value	HR (95% CI)	*P*-value
Age per year	1.1 (1–1.1)	<0.001	1.04 (1.02–1.05)	<0.001
Male	1.3 (1–1.7)	0.025		
Hypertension	1.4 (1.1–1.8)	0.0041		
Diabetes	1.5 (1.2–2)	<0.001	1.58 (1.24–2.00)	<0.001
Dyslipidaemia	0.98 (0.77–1.2)	0.85		
Current or former smoker	1.4 (1.1–1.7)	0.0083	1.48 (1.16–1.88)	0.001
Family history of CAD	0.63 (0.48–0.83)	0.0011		
Myocardial infarction	1.5 (1.2–1.9)	<0.001		
PCI	1.2 (0.95–1.5)	0.13		
CABG	1.9 (1.4–2.5)	<0.001		
Valve repair or replacement	2.4 (1.7–3.5)	<0.001	1.50 (1.02–2.20)	0.04
Atrial fibrillation/-flutter	2 (1.5–2.6)	<0.001		
Stroke	1.6 (1–2.4)	0.032		
COPD	3 (2.2–4.1)	<0.001	1.96 (1.42–2.70)	<0.001
Chest pain	0.59 (0.47–0.75)	<0.001	0.68 (0.54–0.85)	0.001
Dyspnea	1.3 (1–1.7)	0.019		
Obesity	1.0 (0.8–1.3)	0.76		
Impaired renal function	2.5 (2.0–3.1)	<0.001	1.61 (1.27–2.04)	<0.001
Cholesterol per mmol/l	0.95 (0.85–1.1)	0.31		
LDL per mmol/l	0.86 (0.76–0.97)	0.018		
Triglyceride per mmol/l	1.1 (1–1.2)	0.031		
Left ventricular dysfunction	2.7 (2.1–3.4)	<0.001	1.96 (1.55–2.48)	<0.001
Moderate or severe VHD	2.2 (1.8–2.8)	<0.001	1.33 (1.02–1.72)	0.03

Univariable and multivariable Cox analysis. Variables with a p-value of $p \leq 0.05$ on univariable mortality analysis were entered into the multivariable cox analysis with backward selection procedure. Moderate or severe VHD was a significant determinant of mortality independent of left ventricular dysfunction and other covariables.
CABG, coronary artery bypass grafting; CI, confidence interval; COPD, chronic obstructive pulmonary disease; HR, hazard ratio; LDL, low-density lipoprotein cholesterol; PCI, percutaneous coronary intervention; VHD, valvular heart disease.

We found that moderate VHD was independently associated with mortality. Potential benefit of intervention on mortality for patients with moderate VHD is currently subject of debate (20). Ongoing studies are investigating the impact of both moderate AS and LV dysfunction (21). The hypothesis that TAVR improves outcomes in these patients is currently being prospectively investigated in the TAVR UNLOAD trial (22). Further prospective investigations are warranted to confirm the prognostic value of VHD in patients with moderate CCS and evaluate the impact of early intervention of VHD on mortality (23). Our findings support the need for improvement of care in VHD patients, which might be achieved by early valve repair or replacement. However, the complexity of the interplay between CCS and VHD on symptoms (24), cardiac damage (25, 26), and clinical course (27) make appropriate timing of intervention difficult (28).

Previous studies have investigated the association between moderate to severe TR and mortality. In 85%–90% of the patients, TR is caused secondary by left-sided heart failure (18). We found that moderate TR was independently associated with mortality in patients with CCS. Several studies have confirmed that TR is a predictor of mortality independent of LV dysfunction, pulmonary pressures, and right ventricle dilatation and dysfunction (29–31). Our findings suggest that TR is a marker of advanced disease in patients with CCS, which has more value than merely reflecting the severity of right/left ventricular dysfunction and pulmonary hypertension (29).

In this study in two tertiary centers, a significantly higher number of CCS patients had moderate or severe AS ($n = 88$), TR ($n = 144$), and MR ($n = 179$) compared to the general population with the same or older age (32–34). These relatively high VHD rates were anticipated in these specialized care centers, in which more complex medical conditions are seen. Lower rates of VHD in CCS patients may be expected in non-tertiary centers.

4.2. Pathophysiology

Our study shows that VHD has an incremental prognostic role in patients with CCS, which may have several explanations. Firstly, our findings demonstrate that patients with both CCS and moderate or severe VHD have more often risk factors for mortality, including older age, COPD, atrial fibrillation/-flutter, and a lower eGFR. Secondly, patients with both CCS and VHD may have more advanced cardiovascular calcifications, which are observed in atherosclerotic plaque formation, mitral annular calcification, and aortic artery calcification (4). These calcifications are strong determinants of cardiovascular events (35). Thirdly, both CCS and VHD can cause LV dysfunction through ischemia and LV remodeling, which may accelerate detoriation of the LV function leading to end-stage heart failure (7). Further longitudinal research is necessary to investigate the pathophysiological mechanisms of VHD in patients with CCS.

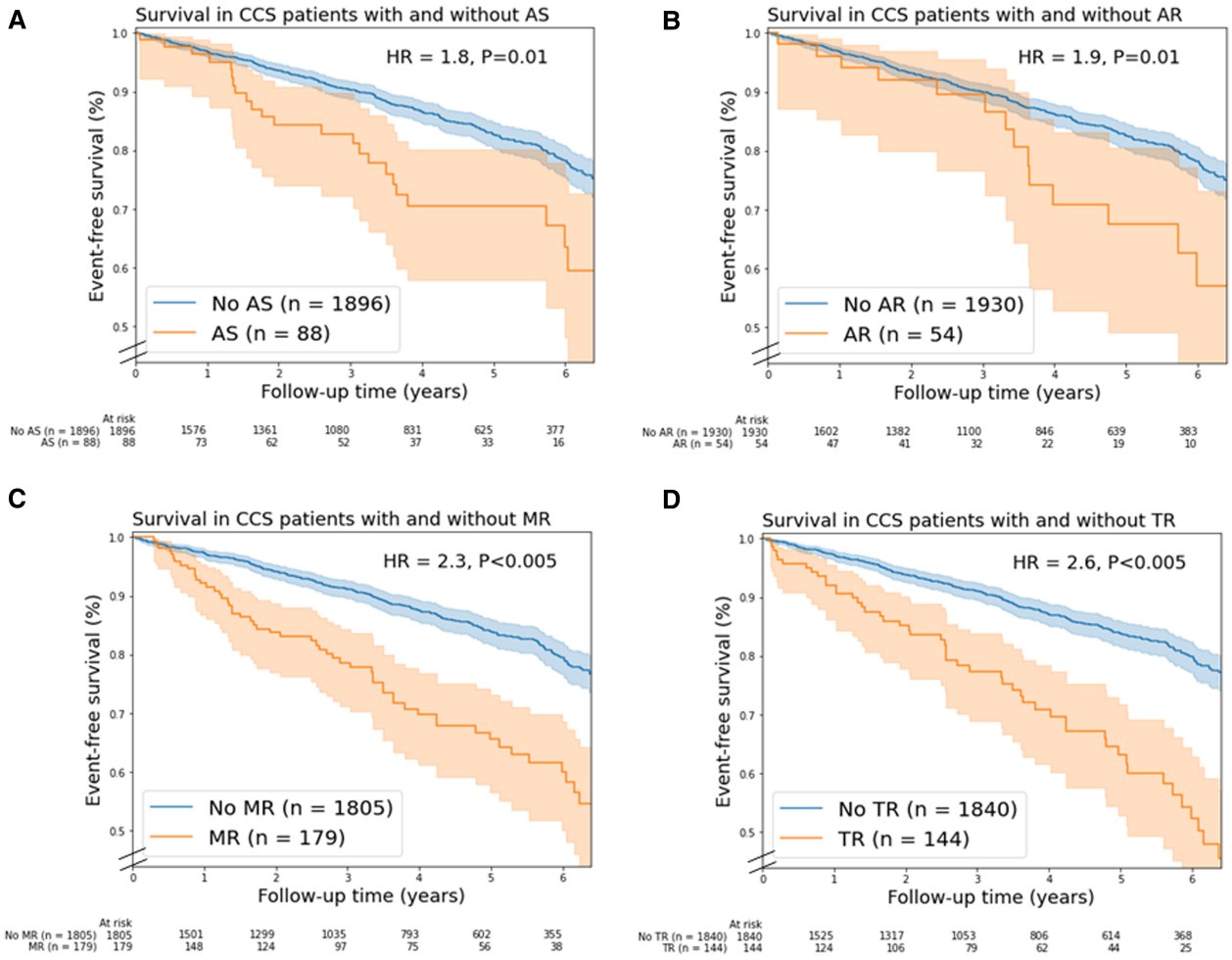

FIGURE 2
Kaplan-Meier mortality curves for chronic coronary syndrome (CCS) patients with/without (A) aortic stenosis, (B) aortic regurgitation, (C) mitral regurgitation, and (D) tricuspid regurgitation. In this figure, valvular heart disease (VHD) is moderate and severe combined VHD. Shaded areas represent the 95% confidence intervals. AR, aortic regurgitation; AS, aortic stenosis; HR, unadjusted hazard ratio; MR, mitral regurgitation; TR, tricuspid regurgitation.

4.3. Clinical implications

The observed independent prognostic value of VHD suggests that it could have a crucial role in the non-invasive risk stratification of patients with CCS. However, despite the advantages of TTE, such as low-costs, portability and absence of radiation (36), TTE may not be performed in all patients with CCS as recommended in current guidelines. A recent study by Neglia et al. (37) showed that the diagnostic process was not according to the ESC guideline in 44% of the patients with CCS. This finding may have detrimental implications for patients with (suspected) CCS since undiagnosed and untreated VHD is associated with heart failure and mortality (34). Therefore, echocardiography should be performed in all patients with (suspected) CCS to rule out VHD and other cardiac diseases (4, 38).

The LV function is currently the only recommended echocardiographic assessed feature for risk stratification in patients with CCS. The results of this study indicate that comprehensive echocardiographic assessment of VHD should be included in the standard clinical workup of patients with CCS, at least in those with a normal LV function.

4.4. Study limitations

Several remarks can be made about this study. Firstly, the study had a retrospective cohort study design that has inherent limitations. Secondly, to minimize the amount of missing data, information was extracted from textual notes in electronic medical records. The cause of mortality was not available for all patients and was therefore not further differentiated. Thirdly, valve calcifications and quantitative parameters of echocardiography were not evaluated in this study. Fourthly, there may have been a selection bias in this study as the patients who underwent TTE may have had a higher a-priori risk of VHD, which could have influenced the results. Nevertheless, the included patients reflect a real-life population that were seen at a tertiary center.

5. Conclusions

VHD was an independent determinant of mortality in patients with CCS. This finding demonstrates the need for a comprehensive echocardiographic assessment of VHD, in addition to LV function, in CCS patients. Moreover, it indicates that complete assessment of VHD should be included in the standard clinical workup of patients with CCS to improve risk stratification.

Data availability statement

The original contributions presented in the study are included in the article/**Supplementary Material**, further inquiries can be directed to the corresponding author.

Ethics statement

The studies involving human participants were reviewed and approved by the medical research Ethics Committee, Amsterdam UMC. Written informed consent for participation was not required for this study in accordance with the national legislation and the institutional requirements.

Author contributions

MM, CC, BB, and MS contributed to conception and design of the study. MM, CC, and MS organized the database. MM performed the statistical analysis and wrote the first draft of the manuscript. BB and MS revised sections of the manuscript. CC, JM, II, NV, JS, and SC commented on the manuscript. All authors contributed to the article and approved the submitted version.

Funding

The research was carried out with internal funding from the institute.

Acknowledgments

The authors thank Hafsah Rahimbaksh, Merijn Hofland, Tom Peper, Paulo Heemskerk and Björn van der Ster for their support in this project.

Conflict of interest

The authors declare that the research was conducted in the absence of any commercial or financial relationships that could be construed as a potential conflict of interest.

Publisher's note

All claims expressed in this article are solely those of the authors and do not necessarily represent those of their affiliated organizations, or those of the publisher, the editors and the reviewers. Any product that may be evaluated in this article, or claim that may be made by its manufacturer, is not guaranteed or endorsed by the publisher.

Supplementary material

The Supplementary Material for this article can be found online at: https://www.frontiersin.org/articles/10.3389/fcvm.2023.1211322/full#supplementary-material

References

1. Sorbets E, Fox KM, Elbez Y, Danchin N, Dorian P, Ferrari R, et al. Long-term outcomes of chronic coronary syndrome worldwide: insights from the international CLARIFY registry. *Eur Heart J.* (2020) 41:347–56. doi: 10.1093/eurheartj/ehz660

2. Timmis A, Townsend N, Gale CP, Torbica A, Lettino M, Petersen SE, et al. European Society of cardiology: cardiovascular disease statistics 2019. *Eur Heart J.* (2020) 41:12–85. doi: 10.1093/eurheartj/ehz859

3. Fihn SD, Gardin JM, Abrams J, Berra K, Blankenship JC, Dallas AP, et al. 2012 ACCF/AHA/ACP/AATS/PCNA/SCAI/STS guideline for the diagnosis and management of patients with stable ischemic heart disease. *J Am Coll Cardiol.* (2012) 60:e44–e164. doi: 10.1016/j.jacc.2012.07.013

4. Knuuti J, Wijns W, Saraste A, Capodanno D, Barbato E, Funck-Brentano C, et al. 2019 ESC guidelines for the diagnosis and management of chronic coronary syndromes. *Eur Heart J.* (2020) 41:407–77. doi: 10.1093/eurheartj/ehz425

5. Emond M, Mock MB, Davis KB, Fisher LD, Holmes DR, Chaitman BR, et al. Long-term survival of medically treated patients in the coronary artery surgery study (CASS) registry. *Circulation.* (1994) 90:2645–57. doi: 10.1161/01.CIR.90.6.2645

6. Benjamin EJ, Paul Muntner C, Chair Alvaro Alonso V, Marcio Bittencourt FS, Clifton Callaway MW, April Carson FP. Heart disease and stroke statistics—2019 update: a report from the American heart association. *Circulation.* (2019) 139:56–28. doi: 10.1161/CIR.0000000000000659

7. Coisne A, Scotti A, Latib A, Montaigne D, Ho EC, Ludwig S, et al. Impact of moderate aortic stenosis on long-term clinical outcomes: a systematic review and meta-analysis. *JACC Cardiovasc Interv.* (2022) 15:1664–74. doi: 10.1016/j.jcin.2022.06.022

8. Nkomo VT, Gardin JM, Skelton TN, Gottdiener JS, Scott CG, Enriquez-Sarano M. Burden of valvular heart diseases: a population-based study. *Lancet.* (2006) 368:1005–11. doi: 10.1016/S0140-6736(06)69208-8

9. Maganti K, Rigolin VH, Sarano ME, Bonow RO. Valvular heart disease: diagnosis and management. *Mayo Clin Proc.* (2010) 85:483–500. doi: 10.4065/mcp.2009.0706

10. Galderisi M, Cosyns B, Edvardsen T, Cardim N, Delgado V, Di Salvo G, et al. Standardization of adult transthoracic echocardiography reporting in agreement with recent chamber quantification, diastolic function, and heart valve disease recommendations: an expert consensus document of the European association of cardiovascular imaging. *Eur Heart J.* (2017) 18:1301–10. doi: 10.1093/ehjci/jex244

11. Vahanian A, Alfieri O, Andreotti F, Antunes MJ, Barón-Esquivias G, Baumgartner H, et al. Guidelines on the management of valvular heart disease (version 2012). *Eur Heart J.* (2012) 33:2451–96. doi: 10.1093/eurheartj/ehs109

12. Baumgartner H, Falk V, Bax JJ, De Bonis M, Hamm C, Holm PJ, et al. 2017 ESC/EACTS guidelines for the management of valvular heart disease. *Eur Heart J*. (2017) 38:2739–91. doi: 10.1093/eurheartj/ehx391

13. Bouma BJ, Riezenbos R, Voogel AJ, Veldhorst MH, Jaarsma W, Hrudova J, et al. Appropriate use criteria for echocardiography in The Netherlands. *Neth Heart J*. (2017) 25:330–4. doi: 10.1007/s12471-017-0960-9

14. Lang RM, Badano LP, Mor-Avi V, Afilalo J, Armstrong A, Ernande L, et al. Recommendations for cardiac chamber quantification by echocardiography in adults: an update from the American society of echocardiography and the European association of cardiovascular imaging. *J Am Soc Echocardiogr*. (2015) 28:1–39.e14. doi: 10.1016/j.echo.2014.10.003

15. Levey AS, Stevens LA, Schmid CH, Zhang Y, Castro AF, Feldman HI, et al. A new equation to estimate glomerular filtration rate. *Ann Intern Med*. (2009) 150:604–12. doi: 10.7326/0003-4819-150-9-200905050-00006

16. Kim JH. Multicollinearity and misleading statistical results. *Korean J Anesthesiol*. (2019) 72:558–69. doi: 10.4097/kja.19087

17. Hess KR. Graphical methods for assessing violations of the proportional hazards assumption in cox regression. *Stat Med*. (1995) 14:1707–23. doi: 10.1002/sim.4780141510

18. Vahanian A, Beyersdorf F, Praz F, Milojevic M, Baldus S, Bauersachs J, et al. 2021 ESC/EACTS guidelines for the management of valvular heart disease: developed by the task force for the management of valvular heart disease of the European society of cardiology (ESC) and the European association for cardio-thoracic surgery (EACTS). *Eur Heart J*. (2022) 43:561–632. doi: 10.1093/eurheartj/ehab395

19. Otto CM, Nishimura RA, Bonow RO, Carabello BA, Erwin JP, Gentile F, et al. 2020 ACC/AHA guideline for the management of patients with valvular heart disease: executive summary: a report of the American college of cardiology/American heart association joint committee on clinical practice guidelines. *Circulation*. (2021) 143:e35–71. doi: 10.1161/CIR.0000000000000932

20. Stassen J, Galloo X, van der Bijl P, Bax JJ. Focus on diagnosis and prognosis to guide timing of intervention in valvular heart disease. *Curr Cardiol Rep*. (2022) 24:1407–16. doi: 10.1007/s11886-022-01754-w

21. Samad MD, Ulloa A, Wehner GJ, Jing L, Hartzel D, Good CW, et al. Predicting survival from large echocardiography and electronic health record datasets: optimization with machine learning. *JACC Cardiovasc Imaging*. (2019) 12:681–9. doi: 10.1016/j.jcmg.2018.04.026

22. Spitzer E, Van Mieghem NM, Pibarot P, Hahn RT, Kodali S, Maurer MS, et al. Rationale and design of the transcatheter aortic valve replacement to UNload the left ventricle in patients with ADvanced heart failure (TAVR UNLOAD) trial. *Am Heart J*. (2016) 182:80–8. doi: 10.1016/j.ahj.2016.08.009

23. Khan KR, Khan OA, Chen C, Liu Y, Kandanelly RR, Jamiel PJ, et al. Impact of moderate aortic stenosis in patients with heart failure with reduced ejection fraction. *J Am Coll Cardiol*. (2023) 81:1235–44. doi: 10.1016/j.jacc.2023.01.032

24. Tastet L, Tribouilloy C, Maréchaux S, Vollema EM, Delgado V, Salaun E, et al. Staging cardiac damage in patients with asymptomatic aortic valve stenosis. *J Am Coll Cardiol*. (2019) 74:550–63. doi: 10.1016/j.jacc.2019.04.065

25. Bohbot Y, Renard C, Manrique A, Levy F, Maréchaux S, Gerber BL, et al. Usefulness of cardiac magnetic resonance imaging in aortic stenosis. *Circulation*. (2020) 13:e010356. doi: 10.1161/CIRCIMAGING.119.010356

26. Jansen R, Hart EA, Peters M, Urgel K, Kluin J, Tietge WJ, et al. An easy-to-use scoring index to determine severity of mitral regurgitation by 2D echocardiography in clinical practice. *Echocardiography*. (2017) 34:1275–83. doi: 10.1111/echo.13636

27. Padang R, Bagnall RD, Semsarian C. Genetic basis of familial valvular heart disease. *Circ: Cardiovasc Genet*. (2012) 5:569–80. doi: 10.1161/CIRCGENETICS.112.962894

28. Lancellotti P, Vannan MA. Timing of intervention in aortic stenosis. *N Engl J Med*. (2020) 382:191–3. doi: 10.1056/NEJMe1914382

29. Benfari G, Antoine C, Miller WL, Thapa P, Topilsky Y, Rossi A, et al. Excess mortality associated with functional tricuspid regurgitation complicating heart failure with reduced ejection fraction. *Circulation*. (2019) 140:196–206. doi: 10.1161/CIRCULATIONAHA.118.038946

30. Nath J, Foster E, Heidenreich PA. Impact of tricuspid regurgitation on long-term survival. *J Am Coll Cardiol*. (2004) 43:405–9. doi: 10.1016/j.jacc.2003.09.036

31. Wang N, Fulcher J, Abeysuriya N, McGrady M, Wilcox I, Celermajer D, et al. Tricuspid regurgitation is associated with increased mortality independent of pulmonary pressures and right heart failure: a systematic review and meta-analysis. *Eur Heart J*. (2019) 40:476–84. doi: 10.1093/eurheartj/ehy641

32. Cahill TJ, Prothero A, Wilson J, Kennedy A, Brubert J, Masters M, et al. Community prevalence, mechanisms and outcome of mitral or tricuspid regurgitation. *Heart*. (2021) 107:1003–9. doi: 10.1136/heartjnl-2020-318482

33. d'Arcy JL, Coffey S, Loudon MA, Kennedy A, Pearson-Stuttard J, Birks J, et al. Large-scale community echocardiographic screening reveals a major burden of undiagnosed valvular heart disease in older people: the OxVALVE population cohort study. *Eur Heart J*. (2016) 37:3515–22. doi: 10.1093/eurheartj/ehw229

34. Dziadzko V, Clavel M-A, Dziadzko M, Medina-Inojosa JR, Michelena H, Maalouf J, et al. Outcome and undertreatment of mitral regurgitation: a community cohort study. *Lancet*. (2018) 391:960–9. doi: 10.1016/S0140-6736(18)30473-2

35. Detrano R, Guerci AD, Carr JJ, Bild DE, Burke G, Folsom AR, et al. Coronary calcium as a predictor of coronary events in four racial or ethnic groups. *N Engl J Med*. (2008) 358:1336–45. doi: 10.1056/NEJMoa072100

36. Schuuring MJ, Išgum I, Cosyns B, Chamuleau SAJ, Bouma BJ. Routine echocardiography and artificial intelligence solutions. *Front Cardiovasc Med*. (2021) 8:648877. doi: 10.3389/fcvm.2021.648877

37. Neglia D, Liga R, Gimelli A, Podlesnikar T, Cvijić M, Pontone G, et al. Use of cardiac imaging in chronic coronary syndromes: the EURECA imaging registry. *Eur Heart J*. (2022) 44(2):142–58. doi: 10.1093/eurheartj/ehac640

38. Schuuring MJ, Tanis W. A remarkable exercise test leading to the diagnosis of left atrial myxoma. *Int J Cardiol*. (2015) 201:53–4. doi: 10.1016/j.ijcard.2015.08.002

frontiers | Frontiers in Cardiovascular Medicine

TYPE Original Research
PUBLISHED 03 November 2023
DOI 10.3389/fcvm.2023.1279687

OPEN ACCESS

EDITED BY
Francesco Ancona,
Ospedale San Raffaele (IRCCS), Italy

REVIEWED BY
Mayooran Namasivayam,
St Vincent's Hospital Sydney, Australia
Damiano Regazzoli,
Humanitas Research Hospital, Italy

*CORRESPONDENCE
Guangyuan Song
✉ songgy_anzhen@vip.163.com

†These authors have contributed equally to this work and share first authorship

RECEIVED 18 August 2023
ACCEPTED 23 October 2023
PUBLISHED 03 November 2023

CITATION
Xiao Z, Yao J, Liu X, Yuan F, Yan Y, Luo T, Wang M, Zhang H, Ren F and Song G (2023) Determinants of device success after transcatheter aortic valve replacement in patients with type-0 bicuspid aortic stenosis. Front. Cardiovasc. Med. 10:1279687. doi: 10.3389/fcvm.2023.1279687

Determinants of device success after transcatheter aortic valve replacement in patients with type-0 bicuspid aortic stenosis

Zhicheng Xiao[1†], Jing Yao[2†], Xinmin Liu[2], Fei Yuan[2], Yunfeng Yan[2], Taiyang Luo[2], Moyang Wang[3], Hongliang Zhang[3], Faxin Ren[1] and Guangyuan Song[2*]

[1]Department of Cardiology, Qindao University Medical College Affiliated Yantai Yuhuangding Hospital, Yantai, China, [2]Interventional Center of Valvular Heart Disease, Beijing Anzhen Hospital, Capital Medical University, Beijing, China, [3]Department of Cardiology, Fuwai Hospital, National Center for Cardiovascular Disease, Chinese Academy of Medical Science and Peking Union Medical College, Beijing, China

Background: Clinical evidence of transcatheter aortic valve replacement in patients with type-0 bicuspid aortic valve was relatively scarce.
Aims: Our goal was to explore determinants of device success after transcatheter aortic valve replacement in patients with type-0 bicuspid aortic valve morphology.
Methods: In this retrospective multicenter analysis, we included 59 patients with symptomatic severe aortic stenosis with type-0 bicuspid aortic valve morphology who underwent transcatheter aortic valve replacement. Type-0 bicuspid aortic valve was identified with multidetector computed tomography scans. The technical success rate was 89.8%, and the device success rate was 81.4%. Patients were divided into a device success group and a device failure group according to Valve Academic Research Consortium- 3 criteria.
Results: When we compared the two groups, we found that the ellipticity index of the aortic root and the presence of bulky calcifications at the commissure were statistically different (ellipticity index 35.7 ± 1.7 vs. 29.7 ± 1.1, $p = 0.018$; bulky calcification at the commissure, 54.5% vs. 4.5%, $p < 0.001$). Further multivariate logistic analysis showed that bulky calcification at the commissure had a negative correlation with device success (odds ratio 0.030, 95% confidence interval 0.003–0.285, $p = 0.002$). Yet there was no statistical correlation between the ellipticity index and device success (odds ratio 0.818, 95% confidence interval 0.667–1.003, $p = 0.053$).
Conclusions: The presence of bulky calcifications at the commissure is negatively correlated with device success after transcatheter aortic valve replacement in patients with type-0 bicuspid aortic valve.

KEYWORDS

transcatheter aortic valve replacement, bicuspid aortic valve, bulky calcification, device success, aortic stenosis

Introduction

Twenty-one years have passed since Dr. Alain Cribier performed the first transcatheter aortic valve replacement (TAVR) (1). TAVR has been shown to be an effective and safe treatment for low-to-high surgical risk patients with symptomatic aortic stenosis (AS) compared with surgical aortic valve replacement (2–4). Bicuspid aortic valve (BAV) occurs in 1%–2% of the population and accounts for 22%–28% of patients over 80 years

old with AS who need surgery. Due to their special anatomy, patients with BAV were excluded from previous randomized controlled trials (5). In 2017, Yoon et al. found BAV patients after TAVR had a similar 2-year mortality, lower procedural success, and a higher rate of paravalvular regurgitation (PVR) compared with patients with a tricuspid aortic valve (6). Forrest et al. found that the 1-year unadjusted risk of mortality was lower in BAV patients after TAVR (7), demonstrating that TAVR was effective and safe in BAV patients.

Type-0 BAV is an aortic valve (AV) morphology with only two equal cusps and two symmetric sinuses, absent any raphe or fusion between the leaflets. This classification of BAV was first introduced by Sievers through observation of 304 surgical specimens (8). Using the Sievers classification, two special phenotypes can be divided according to the direction of the cusps within the short axis of the heart plane, the laterolateral (side-to-side) or anteroposterior (front-and-back) BAV (9). Thus far, several classification methods for BAVs have been suggested but none of them have shown a correlation with clinical outcomes (9). Moreover, there is a paucity of data concerning type-0 BAV morphology, which is less frequently seen in Western populations. We sought to explore the determinants of device success after TAVR in BAV anatomy, with a particular focus on type-0 BAV morphology.

Methods

Study design and patients' selection

Consecutive patients with BAV with symptomatic AS from two Beijing centers, Fuwai Hospital and Anzhen Hospital, were included in the study between November 2020 and April 2022. All patients were diagnosed with severe AS by echocardiography if they met one of the following criteria: mean transvalvular pressure gradient (PGmean) of AV ≥40 mmHg; peak transvalvular velocity (Vmax) of AV ≥4 m/s, or AV area ≤1.0 cm^2. Fifty-nine patients were recognized as type-0 BAV through multidetector computed tomography scanning. All data were analyzed by the core laboratory, and therapeutic strategies were discussed by the cardiac multidisciplinary team before the operation. The therapeutic strategies were based on ESC/EACTS Guidelines and ACC/AHA Guidelines for valvular heart diseases. For patients who needed CABG or surgical intervention, they were mostly recommended and accepted cardiac surgery, except for patients who were judged moderate to severe frailty. For symptomatic patients with severe AS who were 65–80 years of age and had no anatomic contraindication to transfemoral TAVR, either SAVR or transfemoral TAVR was recommended after shared decision-making. For patients who were >80 years of age or for younger patients with a life expectancy <10 years and no anatomic contraindication to transfemoral TAVR, transfemoral TAVR was recommended in preference to SAVR. The study was conducted in accordance with the Code of Ethics of the World Medical Association (Declaration of Helsinki) for experiments involving humans.

TAVR procedures

The procedures were performed as described previously (10). All procedures were performed with the patients under local or general anesthesia, with intubation or laryngeal mask airway, in the hybrid catheterization laboratory. The means of inducing anesthesia was determined by the anesthetist, based on the patient's general condition and pulmonary function. Transfemoral access was the first choice when the femoral artery was of adequate caliber. Four types of prosthetic aortic valves were used for TAVR (**Supplementary Figure S1**), including the Venus-A (Venus Medtech, Inc. Hangzhou, China), Vitaflow (MicroPort Scientific Corporation, Shanghai, China), TaurusOne (Peijia Medical Co, Suzhou, China), and SAPIEN 3 (Edwards Lifesciences, Irvine, CA, USA). About half the self-expanding valves were implanted with the new generation of retrievable delivery systems.

Study end points

The end points of the study were defined according to Valve Academic Research Consortium- 3 criteria (11). Periprocedural mortality was defined as death occurring ≤30 days after the index procedure or >30 days but during the index hospitalization. Device success met all the criteria at 30 days: technical success; freedom from death; freedom from surgery or intervention related to the device or to a major vascular or access-related or cardiac structural complication; intended performance of the valve (mean gradient <20 mmHg, peak velocity <3 m/s, Doppler velocity index ≥0.25, and less than moderate aortic regurgitation).

Special notes

Calcification of the leaflet free edge referred to obvious calcification along the edge, over 2/3 the length of it. Bulky calcification at the commissure was determined by visual assessment using multidetector computed tomography transverse planes and maximum intensity projections. The ellipticity index of the aortic root was calculated as (long axis/short axis-1) × 100%, on the plane 5 mm above the annulus. The oversizing ratio was calculated as (prosthesis nominal perimeter/multislice computed tomography-derived annular perimeter-1) × 100%. A pacemaker was implanted if a high-degree of or complete atrioventricular blocking occurred and lasted for more than 24 h after the operation. Two special phenotypes of type-0 BAV were divided according to the direction of the cusps within the short axis of the heart plane, the laterolateral (side-to-side) or anteroposterior (front-and-back) BAV. Laterolateral indicates direction of the cusps is approximately parallel to the direction of the atrial septum within the short axis of the heart plane. Anteroposterior means cusps arranged in a front-and-back direction, with the orifice approximately perpendicular to the atrial septum.

Statistics

Continuous variables were described as mean ± standard deviation and compared using the unpaired Student t-test, in case they matched normal distribution. Categorical variables were described as numbers and percentages and were analyzed with the χ^2 test or the Fisher exact test. Variables with p-values < 0.1 on univariate analysis were entered into multivariate logistic regression models. All statistical analyses were performed using SPSS version 20.0 (IBM Inc., Armonk, NY, USA) with two-tailed significance set at 0.05.

Results

Baseline characteristics

Fifty-nine patients were included in the study; 25 of them (42.4%) were male. The mean Society of Thoracic Surgeons predicted risk of mortality score was 4.3 ± 1.7%. The PGmean of the AV before the operation was 62.7 ± 21.9 mmHg; the ejection fraction was 52.6 ± 15.4%. There were 17 patients (28.9%) who had moderate or severe mitral regurgitation, and 9 patients (15.3%) with moderate or severe tricuspid regurgitation. Most type-0 BAVs had an oval annulus with an ellipticity index of 30.8 ± 7.6%. Calcification of unilateral or bilateral leaflet free edges was found in up to 24 patients (40.7%). The ascending aorta was dilated in most patients, with an average diameter of 44.1 ± 7.0 mm at its widest plane. Two patients had ascending aorta diameters over 55 mm, but they were too fragile to undergo cardiac surgery, and we performed TAVR as a compromise formula. Nine patients' ascending aorta diameters ranged from 50 mm to 54 mm, without additional risk factors or coarctation. Thirteen patients had ascending aorta diameters from 45 mm to 49 mm, and the other patients had diameters less than 45 mm. In addition, the coronary ostial height of type-0 BAV patients was relatively high. The average left coronary ostial height was 15.5 ± 3.4 mm, and the right coronary ostial height was 16.9 ± 3.9 mm (Table 1).

TABLE 1 Baseline characteristics.

$N = 59$	
Male	25 (42.4%)
Age, year	69.3 ± 7.0
NYHA grading	
1	3 (5.1%)
2	16 (27.1%)
3	36 (61%)
4	4 (6.8%)
STS predicted risk of mortality score, %	4.3 ± 1.7
COPD	2 (3.4%)
DM	14 (23.7%)
HP	29 (49.2)
Cr level, μmol/L	84.4 ± 23.5
Prior PCI	3 (5.1%)
Prior CABG	0
Prior cardiac surgery	1 (1.7%)
Peripheral artery disease	3 (5.1%)
Prior stroke/TIA	2 (3.4%)
Atrial fibrillation	10 (16.9%)
Ejection fraction, %	52.6 ± 15.4
PGmean of AV, mmHg	62.7 ± 21.9
Vmax of AV, m/s	4.8 ± 1.0
LVEDD, mm	49.0 ± 7.5
Aortic regurgitation	4 (6.8%)
Mitral regurgitation	17 (28.9%)
Tricuspid regurgitation	9 (15.3%)
Laterolateral direction	47 (79.7%)
Calcification score, mm^3	664.4 ± 561.8
Bulky calcification at commissure	8 (13.6%)
Calcification of free edge	
None	35 (59.3%)
Unilateral	21 (35.6%)
Bilateral	3 (5.1%)
Maximum diameter, mm	37.0 ± 5.9
Minimum diameter, mm	25.5 ± 4.4
Ellipticity index, %	30.8 ± 7.6
Annulus diameter, mm	24.4 ± 3.1
LVOT diameter, mm	25.2 ± 5.0
STJ diameter, mm	33.0 ± 5.0
Ascending aorta diameter, mm	44.1 ± 7.0
Angle of heart, degree	53.4 ± 11.3
Height of LCA, mm	15.5 ± 3.4
Height of RCA, mm	16.9 ± 3.9

AV, aortic valve; CABG, coronary artery bypass grafting; COPD, chronic obstructive pulmonary disease; Cr, creatinine; DM, diabetes mellitus; HP, hypertension; LCA, left coronary artery; LVEDD, left ventricular end diastolic diameter; LVOT, left ventricular outflow tract; NYHA, New York Heart Association; PCI, percutaneous coronary intervention; PG, pressure gradient; RCA, right coronary artery; STJ, sinotubular junction; STS, Society of Thoracic Surgeons; TIA, transient ischemic attack.

Operative procedures and outcomes

In total, 96.6% of the patients were operated on via a transfemoral access. Two patients underwent TAVR via transcarotid and transaxillary accesses, respectively, since transfemoral access was not feasible. Only 1 patient had vascular complications. Based on the annular perimeters, calcification distribution and restriction above the annulus, we usually chose the "downsize strategy", with a 2.3 ± 8.1% oversizing ratio. Two patients died during the perioperative period, including 1 who had a valve-in-valve implantation because of paravalvular regurgitation and died of delayed occlusion of the left coronary artery after the operation. The other patient was discharged from the hospital in stable condition, and the cause of death was unknown. Valve-in-valve procedures were performed in 6 patients (10.2%) due to moderate to severe PVR after deployment of the first valve. Four patients (6.8%) had permanent pacemaker implants after the operation. The technical success rate was 89.8%, and the device success rate was 81.4%. Moderate-to-severe mitral regurgitation or tricuspid regurgitation was significantly reduced postoperatively (28.9% vs. 13.6%, 15.3% vs. 5.1%) (Table 2).

TABLE 2 Procedures and outcomes.

N = 59	
General anesthesia	24 (40.7%)
Femoral artery access	57 (96.6%)
Predilation	58 (98.3%)
Type of prosthetic valves	
Venus-A	27 (45.8%)
Vitaflow	22 (37.3%)
TaurusOne	7 (11.9%)
SAPIEN 3	3 (5.1%)
Size of prosthetic valves, mm	
23	24 (40.7%)
24	12 (20.3%)
26	9 (15.3%)
27	8 (13.6%)
29	3 (5.1%)
30	3 (5.1%)
Oversizing ratio, %	2.3 ± 8.1
Retrivable delivery system	28 (47.5%)
Vascular complications	1 (1.7%)
Structural complications of heart	0
Valve-in-valve	6 (10.2%)
Surgery	0
Permanent pacemaker	4 (6.8%)
Stroke	0
Technical success	53 (89.8%)
Device success	48 (81.4%)
Perioperative death	2 (3.4%)
Ejection fraction (post-TAVR), %	53.4 ± 12.0
PGmean of AV (post-TAVR), mmHg	16.5 ± 10.8
Vmax of AV (post-TAVR), m/s	2.2 ± 0.6
PVR (post-TAVR)	
1	20 (33.9%)
2	3 (5.1%)
3	1 (1.7%)
Mitral regurgitation (post-TAVR)	8 (13.6%)
Tricuspid regurgitation (post-TAVR)	3 (5.1%)

AV, aortic valve; PG, pressure gradient; PVR, paravalvular regurgitation.

Determinants of device success

Patients with device failure or device success were divided into 2 groups. When we compared the 2 groups, we found no significant differences in the STS score, medical history, ejection fraction, or PGmean of the aortic valve. The orientation of the aortic cusps also did not affect the device success rate. There was no statistical difference in unilateral or bilateral free edge calcification and overall calcification scores between the 2 groups. And we found no difference between early generation devices (unretrievable delivering systems) and retrievable delivering systems. It's worth pointing out 4 patients out of the 31 patients who used the unretrievable delivering systems underwent a second valve implantation. Two patients out of the 28 patients who used the retrievable delivering systems underwent a second valve implantation. However, bulky calcification at the commissure was found in 54.5% of the patients in the device failure group and in 4.5% in the device success group (**Table 3**), implying that bulky calcification had an inverse relationship with device success. In addition, the morphology of the aortic root was more elliptical in the device failure group than in the device success group (ellipticity 35.7 ± 1.7% vs. 29.7 ± 1.1%, $p = 0.018$) (**Table 3**).

Univariate logistic regression analysis, including age, STS score, and other factors, showed that bulky calcification at the commissure and the ellipticity index of the aortic root correlated with device success. Variables with p-values < 0.1 on univariate analysis were entered into multivariate logistic regression models. Multivariate logistic regression analysis, including bulky calcification at the commissure, the ellipticity index and oversizing ratio as covariates, showed that bulky calcification at the commissure negatively correlated with device success (odds ratio, 0.030, 95% confidence interval 0.003–0.285, $p = 0.002$) (**Table 4**). A total of 8 patients had bulky calcification at the commissure, with calcification mostly observed 6–8 mm above the annulus (**Figure 1**).

Discussion

TAVR in bicuspid AS has been an important focus of research in recent years. Due to the lack of evidence in BAV patients who have undergone TAVR in early large randomized controlled trials, the long-term prognosis of these patients is still under discussion. Sievers' classification can describe the morphology of the aortic valve but has poor clinical prognostic value. The BAV anatomical spectrum classification was developed by Michelena et al., who hoped to provide predictive value for clinical outcomes (9). Due to the complexity of its classification system, its clinical application is limited. The correlation with clinical outcomes needs to be further verified. Yoon et al. found that a calcified raphe and excess leaflet calcification were associated with increased risk of procedural complications and 2-year all-cause mortality (12). This research is the first to focus on the impact of calcification degree and calcification distribution of leaflets on clinical outcomes. Calcified raphe mainly exists in type-1 BAVs, yet for type-0 BAVs with no calcified raphe or excess leaflet calcification, which factors influence device success rate or prognosis of the patients is not well answered. Ielasi et al. compared type-0 BAV and type-1 BAV patients and observed a higher rate of mean transprosthetic gradient ≥20 mmHg in patients with type-0 BAV postoperatively (13). Compared with type-1 BAVs, type-0 BAVs are more likely to affect the prosthetic valve's well dilation. However, the study found no statistical difference of Valve Academic Research Consortium-2 device success rate between the two groups. Based on previous studies, we are interested in patients with type-0 bicuspid aortic stenosis, and wonder whether TAVR in these populations will differ from others.

Ascending aorta dilatation was common in our study. In 2022 ACC/AHA Aortic Disease Guideline (14), it is recommended that in patients with a BAV, a diameter of the aortic root or ascending aorta of 5.0 cm–5.4 cm, and an additional risk factor for aortic dissection, surgery to replace the aortic root, ascending aorta, or both is reasonable, when performed by experienced surgeons in a

TABLE 3 Characteristics of patients with device success.

	Device failure, $n = 11$	Device success, $n = 48$	P value
Male	6 (54.5%)	19 (39.6%)	0.37
Age, year	66.9 ± 2.3	69.9 ± 1.0	0.21
NYHA grading			0.56
1	0	3 (6.3%)	
2	4 (36.4%)	12 (25%)	
3	7 (63.6%)	29 (60.4%)	
4	0	4 (8.3%)	
STS predicted risk of mortality score, %	4.3 ± 0.4	4.3 ± 0.3	0.90
COPD	1 (9.1%)	1 (2.1%)	0.34
DM	3 (27.3%)	11 (22.9%)	1
HP	3 (27.3%)	26 (54.2%)	0.11
Cr level, μmol/L	76.7 ± 5.7	86.2 ± 3.5	0.23
Prior PCI	1 (9.1%)	2 (4.2%)	1
Peripheral artery disease	1 (9.1%)	2 (4.2%)	1
Prior stroke/TIA	0	2 (4.2%)	1
Atrial fibrillation	3 (27.3%)	7 (14.6%)	0.57
Ejection fraction, %	54.4 ± 5.3	52.1 ± 2.2	0.66
PGmean of AV, mmHg	64.3 ± 9.2	62.4 ± 2.9	0.8
Vmax of AV, M/s	5.0 ± 0.4	4.8 ± 0.1	0.7
LVEDD, mm	49.2 ± 2.7	49.0 ± 1.1	0.94
Aortic regurgitation			0.59
No	5 (45.5%)	22 (45.8%)	
Mild	6 (54.5%)	22 (45.8%)	
Moderate	0	4 (8.3%)	
Laterolateral direction	9 (81.8%)	38 (79.2%)	1
Calcification score, mm^3	825.6 ± 159.8	626.0 ± 88.5	0.32
Bulky calcification at commissure	6 (54.5%)	2 (4.5%)	<0.001
Calcification of free edge			0.51
None	8 (72.7%)	27 (56.3%)	
Unilateral	3 (27.3%)	18 (37.5%)	
Bilateral	0	3 (6.3%)	
Maximum diameter, mm	38.6 ± 1.0	36.6 ± 0.9	0.32
Minimum diameter, mm	24.9 ± 0.8	25.6 ± 0.7	0.61
Ellipticity index, %	35.7 ± 1.7	29.7 ± 1.1	0.018
Annulus diameter, mm	25.5 ± 0.9	24.2 ± 0.4	0.21
LVOT diameter, mm	26.7 ± 1.1	24.8 ± 0.7	0.26
STJ diameter, mm	32.9 ± 1.1	33.0 ± 0.8	0.94
Ascending aorta diameter, mm	43.2 ± 1.2	44.3 ± 1.1	0.67
Angle of heart, degree	53.1 ± 1.6	53.4 ± 1.6	0.93
Height of LCA, mm	16.0 ± 1.2	15.4 ± 0.5	0.61
Height of RCA, mm	17.8 ± 1.0	16.7 ± 0.6	0.42
General anesthesia	5 (45.5%)	19 (39.6%)	0.99
Type of prosthetic valves			0.77
Venus-A	5 (45.5%)	22 (45.8%)	
Vitaflow	4 (36.4%)	18 (37.5%)	
TaurusOne	2 (18.2%)	5 (10.4%)	
SAPIEN 3	0	3 (6.3%)	
Size of prosthetic valves, mm			0.29
23	3 (27.3%)	21 (43.8%)	
24	2 (18.2%)	10 (20.8%)	
26	4 (36.4%)	5 (10.4%)	
27	2 (18.2%)	6 (12.5%)	
29	0	3 (6.3%)	
30	0	3 (6.3%)	
Oversizing ratio	−1.5 ± 2.9	3.2 ± 1.1	0.079
Retrievable delivery system	6 (54.5%)	22 (45.8%)	0.60

AV, aortic valve; COPD, chronic obstructive pulmonary disease; Cr, creatinine; DM, diabetes mellitus; HP, hypertension; LCA, left coronary artery; LVEDD, left ventricular end diastolic diameter; LVOT, left ventricular outflow tract; NYHA, New York Heart Association; PCI, percutaneous coronary intervention; PG, pressure gradient; RCA, right coronary artery; STJ, sinotubular junction; TIA, transient ischemic attack.

Multidisciplinary Aortic Team. And in our study, patients with a diameter of the aortic root or ascending aorta of 5.0 cm–5.4 cm, were excluded from additional risk factors, such as aortic growth rate 0.3 cm/year, aortic coarctation or "root phenotype" aortopathy. So they don't meet the criteria of class 2a indication. The two patients with a diameter of the ascending aorta of >5.5 cm, who had an STS mortality risk score of >8, were too fragile to undergo SAVR and ascending aorta replacement, and eventually chose TAVR as a compromise formula. The therapeutic strategies were discussed by the cardiac multidisciplinary team before the final decision. BAV aortopathy can be divided into three dilatation phenotypes: ascending phenotype (70%), root phenotype (20%) and extended phenotype. And right-left fusion phenotype of BAV is thought associated with aortic root dilation (9). Whether type-0 BAV is associated with one of the dilatation phenotypes is still unknown. Most patients in our study had ascending aorta dilatation, but not aortic root dilatation. In fact, of the 11 patients with a diameter of the ascending aorta >5.0 cm, only one patient didn't achieve device success because of a second valve implantation. In Lei et al.'s study, long diameter of the sinus of valsalva is 37.1 ± 4.2 mm and short diameter is 26.7 ± 3.2 mm. Data of ascending aorta aren't shown in their study (15). In Yoon et al.'s study, the proportion of ascending aorta dilatation (≥5.0 cm) is 2.2%, smaller compared with our study (12). And ascending aorta-major diameter of type-0 BAV is 36.6 ± 4.0 mm, as shown in Ielasi et al.'s paper (13).

The device success rate was 81.4% in our study. Six patients needed a second valve implantation during the operation and one patient suffered from major vascular complication, leading to a technical success rate of 89.6%. Two patients had peak velocity of over 3 m/s 1 month after the operation, two patients had severe paravalvular leakage, and two patients died of sudden death within 1 month. It's worth pointing out that one of the patients who died and one of the patients with severe paravalvular leakage had undergone second valve implantation. The device success rates ranged from 83.4% to 96.5% in previous studies (6, 7, 13). Yoon et al. compared procedural and clinical outcomes in TAVR for bicuspid vs. tricuspid AS, and found TAVR in bicuspid AS had similar prognosis with tricuspid AS, but lower device success rate (6). Type-1 BAV was the major type in this study, and type-0 BAV accounted for only 12.8%. The proportion of self-expanding valves accounted for 34.4%, and balloon-expanding valves were used in more than half the

TABLE 4 Independent correlates with device success.

	Univariate logistic		Multivariate logistic	
	OR (95% CI)	*p*-value	OR (95% CI)	*p*-value
Male	0.55 (0.15–2.04)	0.369		
Age	1.07 (0.96–1.18)	0.211		
STS predicted risk of mortality score	1.03 (0.69–1.53)	0.895		
Atrial fibrillation	0.455 (0.097–2.146)	0.320		
Ejection fraction	0.99 (0.95–1.04)	0.655		
LVEDD	0.997 (0.91–1.09)	0.942		
Laterolateral direction	0.844 (0.157–4.545)	0.844		
Calcification score	0.999 (0.998–1.001)	0.325		
Bulky calcification at commissure	0.036 (0.006–0.230)	<0.001	0.030 (0.003–0.285)	0.002
Calcification of free edge	2.138 (0.570–8.019)	0.260		
Aortic regurgitation	1.243 (0.415–3.728)	0.697		
Ellipticity index	0.835 (0.720–0.967)	0.016	0.818 (0.667–1.003)	0.053
Annulus diameter	0.876 (0.712–1.076)	0.206		
LVOT diameter	0.922 (0.802–1.061)	0.258		
Angle of heart	1.003 (0.945–1.063)	0.931		
Oversizing ratio	1.080 (0.989–1.178)	0.086	1.028 (0.911–1.160)	0.657
Retrievable delivery system	0.705 (0.189–2.628)	0.603		

CI, confidence interval; LVEDD, left ventricular end diastolic diameter; LVOT, left ventricular outflow tract; OR, odds ratio; STS, Society of Thoracic Surgeons.

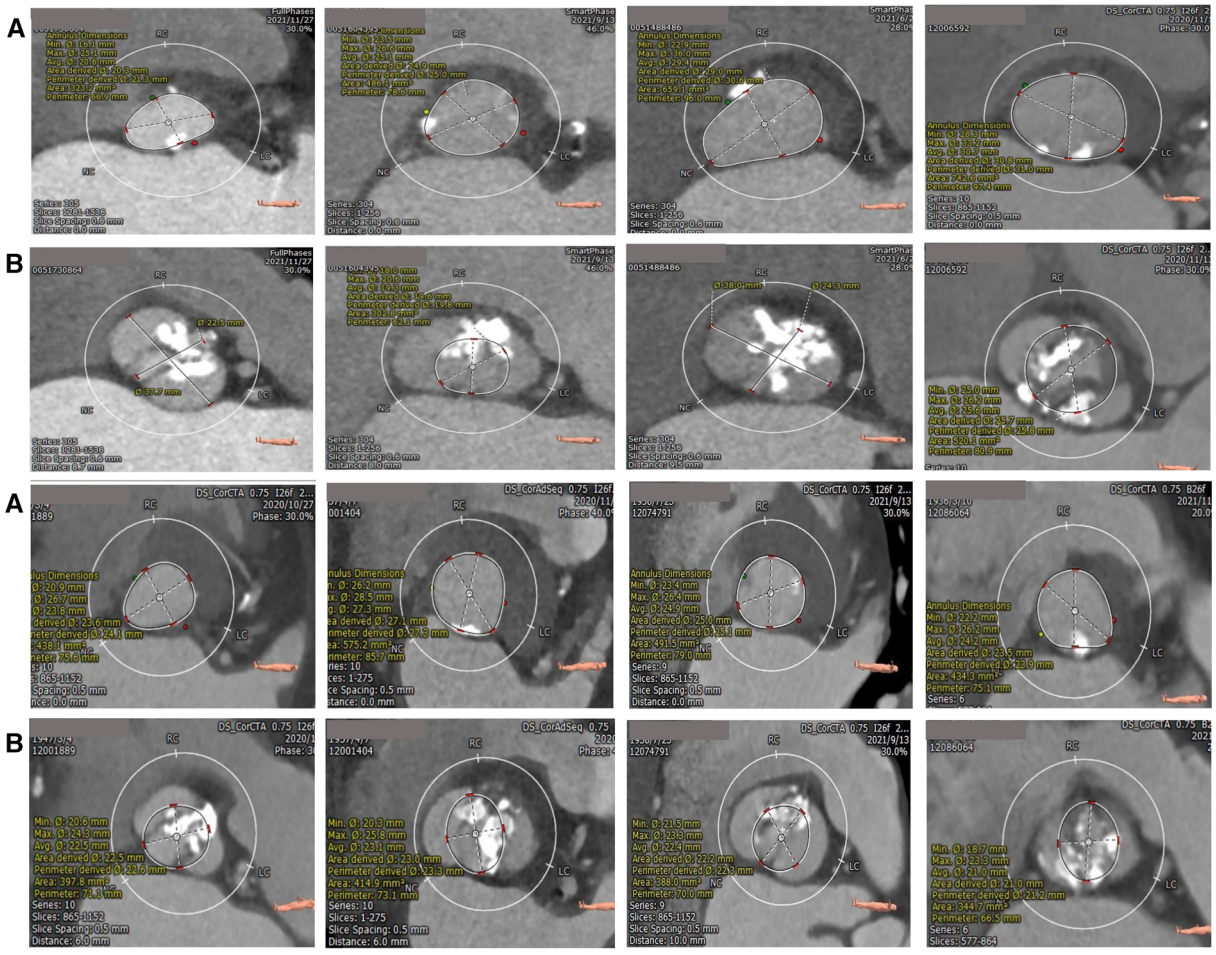

FIGURE 1
Calcification distribution of annulus (A) and bulky calcification at the commissure (B) superior and inferior are the same patients. The bulk calcification appeared primarily on the plane 6–8 mm above the annulus.

patients. Furtherly they found lower device success rates in bicuspid AS mainly appeared when using early generation devices, not suitable for new generation devices. Forrest et al. also compared outcomes in patients with bicuspid vs. tricuspid AS undergoing TAVR. The device success rate for type-0 BAV in the study was 96.5% and all-cause mortality was 1.7%, better results compared with previous studies (7). This might be partly due to improvements in devices and partly due to increased proficiency. Compared with their papers, our study showed similar all-cause mortality, but lower device success rate. Reasons for lower device success rate might be as follows: First, the study groups differed. We focused on patients of type-0 BAV, which accounted for about 10% of total BAV patients, and these patients had a trend toward a lower device success rate and a higher rate of mean trans prosthetic gradient $\geq$ 20mmHg, compared with type-1 BAV; Second, selecting patients of improper anatomy might be another reason. Third, using early generation unretrievable delivering system might lead to inappropriate placement of valves and increase the risk of a second valve implantation.

How to select a prosthetic valve of proper size is hard for patients of BAV. Annular-based sizing with minimal oversizing was thought accurate in BAV, meanwhile prosthesis under-expansion was common (16). Kim et al. compared annular vs. supra-annular sizing for TAVR in BAV patients. Supra-annular sizing might result in divergent size selection in approximately 40% of cases, with potential worsening in a large proportion of patients (17). Yet whether the discovery is fit for type-0 BAV needs further verification. In our paper, we also used annular-based sizing and the oversizing ratio was 2.3% ± 8.1%. Since annulus of most type-0 BAV is elliptical, we wonder supra-annular sizing based on intercommissure distance may not accurately reflect the structure.

Direction of cusps is an important parameter of type-0 BAV. Lei et al. assessed the procedural and clinical results of TAVR for nonraphe bicuspid aortic stenosis with coronary vs. mixed cusp fusion (15). Nonraphe BAV is similar to type-0 BAV, coronary and mixed cusp fusion morphology was analogous to anteroposterior and laterolateral classification. Thirty-day mortality was 7.0% in the study and had no relationship with cusp fusion morphology. Device success rates were not presented in the study, but they found need for a second valve was similar between the two groups. Our research demonstrated the direction of cusps was irrelevant with device success rates.

Type-0 BAV is different from type-1 BAV in many aspects. The absence of a raphe and 2 symmetric sinuses means that with TAVR in type-0 BAV, the prosthetic valve is rarely pushed to one sinus. In our study, the presence of bulky calcification was found to be an independent risk factor for device failure. The reasons may be as follows: The bulky calcification causes displacement or insufficient expansion of the prosthetic valve or poor adherence to the aortic wall, thus resulting in the use of a second valve, moderate-to-severe paravalvular regurgitation, or a high postoperative transvalvular pressure gradient. PVR is associated with an increased 5-year risk of mortality, and insufficient expansion of the prosthetic valve may impact device durability (18, 19). Probably due to the shear stress of the blood, we found that calcification was mainly present at the free edge of the leaflets, in a linear pattern. An elliptical aortic root may also lead to underexpansion of the prosthetic valve, thereby leading to the presence of paravalvular regurgitation and high transvalvular gradients. However, in multivariate logistic regression analysis, the elliptical index showed no statistical significance.

Study limitations

This is a retrospective observational study with limited sample, so the results need further confirmation. Besides, the population we focused on are type-0 BAV patients, which would reduce the generalizability of the conclusions. We discussed determinants of device success in our paper, while determinants of other endpoints, such as all-cause mortality, were not explored.

Conclusions

This is the first study focusing on patients with type-0 BAV who underwent TAVR. We found that bulky calcification at the commissure negatively correlated with device success. Our research provides a new aspect for cardiac interventionists, to evaluate the risk of the procedure in this special population. And retrievable delivering system should be considered once bulky calcification at the commissure is noticed. However, the sample size of this study is small and requires verification by larger samples.

Data availability statement

The original contributions presented in the study are included in the article/Supplementary Material, further inquiries can be directed to the corresponding author.

Ethics statement

The studies involving humans were approved by Ethics committee of Anzhen Hospital. The studies were conducted in accordance with the local legislation and institutional requirements. The Ethics Committee/institutional review board waived the requirement of written informed consent for participation from the participants or the participants' legal guardians/next of kin because data used in the study came from previously hospitalized patients.

Author contributions

ZX: Conceptualization, Writing – original draft. JY: Conceptualization, Writing – original draft. XL: Formal analysis, Writing – original draft. FY: Formal analysis, Writing – original draft. YY: Data curation, Writing – original draft. TL: Formal analysis, Writing – original draft. MW: Data curation, Writing –

original draft. HZ: Data curation, Writing – original draft. FR: Writing – review & editing. GS: Conceptualization, Writing – review & editing.

Funding

The authors declare that no financial support was received for the research, authorship, and/or publication of this article.

Conflict of interest

The authors declare that the research was conducted in the absence of any commercial or financial relationships that could be construed as a potential conflict of interest.

Publisher's note

Supplementary Material

The Supplementary Material for this article can be found online at: https://www.frontiersin.org/articles/10.3389/fcvm.2023.1279687/full#supplementary-material

References

1. Cribier A, Eltchaninoff H, Bash A, Borenstein N, Tron C, Bauer F, et al. Percutaneous transcatheter implantation of an aortic valve prosthesis for calcific aortic stenosis: first human case description. *Circulation*. (2002) 106(24):3006–8. doi: 10.1161/01.CIR.0000047200.36165.B8

2. Smith CR, Leon MB, Mack MJ, Miller DC, Moses JW, Svensson LG, et al. Transcatheter versus surgical aortic-valve replacement in high-risk patients. *N Engl J Med*. (2011) 364(23):2187–98. doi: 10.1056/NEJMoa1103510

3. Leon MB, Smith CR, Mack MJ, Makkar RR, Svensson LG, Kodali SK, et al. Transcatheter or surgical aortic-valve replacement in intermediate-risk patients. *N Engl J Med*. (2016) 374(17):1609–20. doi: 10.1056/NEJMoa1514616

4. Mack MJ, Leon MB, Thourani VH, Makkar R, Kodali SK, Russo M, et al. Transcatheter aortic-valve replacement with a balloon-expandable valve in low-risk patients. *N Engl J Med*. (2019) 380(18):1695–705. doi: 10.1056/NEJMoa1814052

5. Vincent F, Ternacle J, Denimal T, Shen M, Redfors B, Delhaye C, et al. Transcatheter aortic valve replacement in bicuspid aortic valve stenosis. *Circulation*. (2021) 143(10):1043–61. doi: 10.1161/CIRCULATIONAHA.120.048048

6. Yoon SH, Bleiziffer S, De Backer O, Delgado V, Arai T, Ziegelmueller J, et al. Outcomes in transcatheter aortic valve replacement for bicuspid versus tricuspid aortic valve stenosis. *J Am Coll Cardiol*. (2017) 69(21):2579–89. doi: 10.1016/j.jacc.2017.03.017

7. Forrest JK, Kaple RK, Ramlawi B, Gleason TG, Meduri CU, Yakubov SJ, et al. Transcatheter aortic valve replacement in bicuspid versus tricuspid aortic valves from the STS/ACC TVT registry. *JACC Cardiovasc Interv*. (2020) 13(15):1749–59. doi: 10.1016/j.jcin.2020.03.022

8. Sievers HH, Schmidtke C. A classification system for the bicuspid aortic valve from 304 surgical specimens. *J Thorac Cardiovasc Surg*. (2007) 133(5):1226–33. doi: 10.1016/j.jtcvs.2007.01.039

9. Michelena HI, Della Corte A, Evangelista A, Maleszewski JJ, Edwards WD, Roman MJ, et al. International consensus statement on nomenclature and classification of the congenital bicuspid aortic valve and its aortopathy, for clinical, surgical, interventional and research purposes. *J Thorac Cardiovasc Surg*. (2021) 162(3):e383–414. doi: 10.1016/j.jtcvs.2021.06.019

10. Wang M, Song G, Chen M, Feng Y, Wang J, Liu X, et al. Twelve-month outcomes of the TaurusOne valve for transcatheter aortic valve implantation in patients with severe aortic stenosis. *EuroIntervention*. (2022) 17(13):1070–6. doi: 10.4244/EIJ-D-21-00040

11. Varc-3 Writing C, Genereux P, Piazza N, Alu MC, Nazif T, Hahn RT, et al. Valve academic research consortium 3: updated endpoint definitions for aortic valve clinical research. *J Am Coll Cardiol*. (2021) 77(21):2717–46. doi: 10.1016/j.jacc.2021.02.038

12. Yoon SH, Kim WK, Dhoble A, Milhorini Pio S, Babaliaros V, Jilaihawi H, et al. Bicuspid aortic valve morphology and outcomes after transcatheter aortic valve replacement. *J Am Coll Cardiol*. (2020) 76(9):1018–30. doi: 10.1016/j.jacc.2020.07.005

13. Ielasi A, Moscarella E, Mangieri A, Giannini F, Tchetchè D, Kim WK, et al. Procedural and clinical outcomes of type 0 versus type 1 bicuspid aortic valve stenosis undergoing trans-catheter valve replacement with new generation devices: insight from the BEAT international collaborative registry. *Int J Cardiol*. (2021) 325:109–14. doi: 10.1016/j.ijcard.2020.10.050

14. Isselbacher EM, Preventza O, Hamilton Black J, Augoustides JG, Beck AW, Bolen MA, et al. 2022 ACC/AHA guideline for the diagnosis and management of aortic disease: a report of the American heart association/American college of cardiology joint committee on clinical practice guidelines. *Circulation*. (2022) 146(24):e334–482. doi: 10.1161/CIR.0000000000001106

15. Lei WH, Liao YB, Wang ZJ, Ou YW, Tsauo JY, Li YJ, et al. Transcatheter aortic valve replacement in patients with aortic stenosis having coronary cusp fusion versus mixed cusp fusion nonraphe bicuspid aortic valve. *J Interv Cardiol*. (2019) 2019:7348964. doi: 10.1155/2019/7348964

16. Tchetche D, de Biase C, van Gils L, Parma R, Ochala A, Lefevre T, et al. Bicuspid aortic valve anatomy and relationship with devices: the BAVARD multicenter registry. *Circ Cardiovasc Interv*. (2019) 12(1):e007107. doi: 10.1161/CIRCINTERVENTIONS.118.007107

17. Kim WK, Renker M, Rolf A, Fischer-Rasokat U, Wiedemeyer J, Doss M, et al. Annular versus supra-annular sizing for TAVI in bicuspid aortic valve stenosis. *EuroIntervention*. (2019) 15(3):e231–8. doi: 10.4244/EIJ-D-19-00236

18. Mack MJ, Leon MB, Smith CR, Miller DC, Moses JW, Tuzcu EM, et al. 5-year outcomes of transcatheter aortic valve replacement or surgical aortic valve replacement for high surgical risk patients with aortic stenosis (PARTNER 1): a randomised controlled trial. *Lancet*. (2015) 385(9986):2477–84. doi: 10.1016/S0140-6736(15)60308-7

19. Martin C, Sun W. Transcatheter valve underexpansion limits leaflet durability: implications for valve-in-valve procedures. *Ann Biomed Eng*. (2017) 45(2):394–404. doi: 10.1007/s10439-016-1738-8

frontiers | Frontiers in Cardiovascular Medicine

TYPE Original Research
PUBLISHED 14 November 2023
DOI 10.3389/fcvm.2023.1215826

OPEN ACCESS

EDITED BY
Konstantinos Papadopoulos,
Interbalkan Medical Center, Greece

REVIEWED BY
Alberto Guido Pozzoli,
Ospedale Regionale di Lugano, Switzerland
Vahid Sadri,
Georgia Institute of Technology, United States

*CORRESPONDENCE
Jose M. de la Torre Hernandez
✉ josemariadela.torre@scsalud.es;
✉ chematorre60@gmail.com

RECEIVED 02 May 2023
ACCEPTED 23 October 2023
PUBLISHED 14 November 2023

CITATION
de la Torre Hernandez JM, Veiga Fernandez G, Ben-Assa E, Iribarren J, Sainz Laso F, Lee D-H, Ruisanchez Villar C, Lerena P, Garcia Camarero T, Iribarren Sarrias JL, Cuesta Cosgaya JM, Maza Fernandez ME, Garilleti C, Fradejas-Sastre V, Benito M, Barrera S, Gil Ongay A, Vazquez de Prada JA and Zueco J (2023) First description and validation of a new method for estimating aortic stenosis burden and predicting the functional response to TAVI.
Front. Cardiovasc. Med. 10:1215826.
doi: 10.3389/fcvm.2023.1215826

First description and validation of a new method for estimating aortic stenosis burden and predicting the functional response to TAVI

Jose M. de la Torre Hernandez[1,2]*, Gabriela Veiga Fernandez[1], Eyal Ben-Assa[3], Julia Iribarren[4], Fermin Sainz Laso[1], Dae-Hyun Lee[1], Cristina Ruisanchez Villar[1], Piedad Lerena[1], Tamara Garcia Camarero[1], Jose L. Iribarren Sarrias[5], Jose M. Cuesta Cosgaya[1], Maria E. Maza Fernandez[6], Celia Garilleti[1], Victor Fradejas-Sastre[1], Mercedes Benito[1], Sergio Barrera[1], Aritz Gil Ongay[1], Jose A. Vazquez de Prada[1,2] and Javier Zueco[1]

[1]Cardiology Division, Hospital Universitario Marques de Valdecilla, IDIVAL, Santander, Spain, [2]Department of Cardiology, Medical School, University of Cantabria, Santander, Spain, [3]Cardiology Division, Assuta Ashdod University Hospital, Ben Gurion University, Ashdod, Israel, [4]School of Mathematics, Universidad de la Laguna, San Cristobal de la Laguna, Spain, [5]Intensive Care Unit, Complejo Hospitalario Universitario de Canarias, Santa Cruz de Tenerife, Spain, [6]Hydrodynamics and Coastal Infrastructures Group of IH Cantabria, Instituto de Hidraulica Ambiental, Universidad de Cantabria, Santander, Spain

Background: Up to one-fifth of patients continue to have poor quality of life after transcatheter aortic valve implantation (TAVI), with an additional similar proportion not surviving 1 year after the procedure. We aimed to assess the value of a new method based on an integrated analysis of left ventricular outflow tract flow velocity and aortic pressure to predict objective functional improvement and prognosis after TAVI.

Methods: In a cohort of consecutive patients undergoing TAVI, flow velocity–pressure integrated analysis was obtained from simultaneous pressure recordings in the ascending aorta and flow velocity recordings in the left ventricular outflow tract by echocardiography. Objective functional improvement 6 months after TAVI was assessed through changes in a 6-min walk test and NT-proBNP levels. A clinical follow-up was conducted at 2 years.

Results: Of the 102 patients studied, 82 (80.4%) showed objective functional improvement. The 2-year mortality of these patients was significantly lower (9% vs. 44%, $p = 0.001$). In multivariate analysis, parameter "(Pressure at Vmax – Pressure at Vo)/Vmax" was found to be an independent predictor for objective improvement. The C-statistic was 0.70 in the overall population and 0.78 in the low-gradient subgroup. All echocardiographic parameters and the valvuloarterial impedance showed a C-statistic of <0.6 for the overall and low-gradient patients. In a validation cohort of 119 patients, the C-statistic was 0.67 for the total cohort and 0.76 for the low-gradient subgroup.

10.3389/fcvm.2023.1215826

Conclusion: This new method allows predicting objective functional improvement after TAVI more precisely than the conventional parameters used to assess the severity of aortic stenosis, particularly in low-gradient patients.

KEYWORDS

aortic stenosis, transcatheter aortic valve implantation, clinical outcomes, aortic pressure, flow velocity, left ventricular outflow tract

Introduction

Transcatheter aortic valve implantation (TAVI) substantially improves survival and quality of life in most patients with severe aortic stenosis (AS). Nonetheless, up to one-fifth of patients continue to have poor quality of life after TAVI, with an additional similar proportion not surviving 1 year after the procedure (1). However, given the poor prognosis associated with non-procedural management of symptomatic severe AS, the decision will usually be made to proceed with TAVI, even if there is a concern for a sub-optimal result (2).

Nonetheless, it is important to explore and understand the factors associated with a sub-optimal outcome to inform decisions regarding the optimal timing of TAVI and/or adjunctive interventions that may improve the outcomes after TAVI such as particular medications and rehabilitation. Furthermore, the identification of such predictors is important to help in the decision-making when the indication for TAVI is uncertain because of the risk of futility due to frailty or relevant comorbidities and in certain cases of low-flow/low-gradient AS (3, 4).

AS represents a complex, multifaceted set of syndromes that may present in a range of manners and is not isolated to calcific degeneration of the aortic valve alone. Each component part of the system, from the ventricle proximal to the valve to the vasculature distal, can impact signs and symptoms (5–8). With such a more inclusive perspective, the indication for and timing of TAVI could be enhanced, adding precision to the decision-making process.

A previous study by our group identified a series of variables related to the aortic valve, left ventricle, cardiac rhythm, and arterial pulse wave that showed a high predictive value for functional recovery in patients undergoing TAVI (9).

Continuous cardiac afterload monitoring based on a combined analysis of flow velocity signal recorded by Doppler and aortic pressure, the velocity–pressure (VP) loops, has been suggested. This analysis appeared to provide insights into arterial mechanics with standard hemodynamic signals recorded in the operating room (10–12).

We designed an original diagnostic approach based on the integrated analysis of left ventricular outflow tract flow velocity–aortic pressure. In this study, we aimed to assess the value of this approach to predict the objective functional improvement after TAVI and thus to estimate the AS burden.

Methods

Population

The present study was performed in a subgroup of population included in a larger study previously published by our group (9).

All consecutive patients scheduled for TAVI in our institution who met the inclusion criteria were prospectively included in the study. The criteria for inclusion are as follows: (1) diagnosis of symptomatic severe AS (according to guidelines) without significant regurgitation, (2) indication for TAVI established by the institutional Heart Team, and (3) undergoing a TAVI procedure through femoral artery access. Patients who did not consent or who exhibited cognitive impairment that prevented them from properly understanding the investigational procedures were excluded.

Patients who were initially included but presenting severe periprocedural complications such as coronary obstruction, annulus rupture, or stroke were finally excluded from the analysis, given their relevant effect on physiologic measurements and functional recovery after the procedure. For the same reason, patients who required permanent pacemaker implantation after the procedure and showed pacemaker dependence were excluded.

All the procedures were performed in the appropriate setting of a catheterization laboratory dedicated to structural heart interventions. The local TAVI program was started in 2009 and was mostly based on balloon-expandable prosthetic valves. The study was approved by the corresponding Institutional Review Board, and all participating patients signed the informed consent after proper explanation of the investigational procedures. Database was completely anonymized.

All patients were monitored in a specific structural cardiology office, where the clinical follow-up was performed, tests were applied, and the medical treatment of each patient was optimized as much as possible.

Pre-procedural and post-procedural clinical and functional evaluation

The workflow of the study is shown in **Supplementary Figure 1**. Once the patients received the indication for TAVI by the Heart Team, they were evaluated in the outpatient office for structural heart interventions. In this visit, all the clinical information was collected, and the functional status of the

10.3389/fcvm.2023.1215826

patient including quality of life and frailty was assessed using accepted questionnaires [SF-36, EQ-5D, Barthel I, Essential Frailty Toolset, NYHA class, and the Kansas City Cardiomyopathy Questionnaire (KCCQ)], a 6-min walk test, and the determination of NT-proBNP (N-terminal pro-brain natriuretic peptide) levels in the baseline condition. All clinical and functional assessment was repeated 30 days, 6 months, and 12 months after the TAVI procedure by the same team and in the same setting. Transthoracic echocardiography was performed before TAVI and in subsequent visits after TAVI.

Intraprocedural investigational examinations

A systematic protocol-specific transesophageal and transthoracic echocardiographic examination was performed during the TAVI procedure in all patients before and after prosthetic valve implantation. The intraprocedural echocardiographic examinations were performed simultaneously with the invasive central pressure measurements. The following parameters are obtained: left ventricular ejection fraction (LVEF), stroke volume, maximal and mean aortic valve gradients, energy loss index, pulse Doppler recording at the left ventricular outflow tract (LVOT), and continuous Doppler recording through the aortic valve. The Doppler recordings were generally obtained from the transthoracic echocardiography except for those few cases in which the transgastric view provided a more adequate recording.

Invasive pressure measurements in the ascending aorta were performed with a 5- or 6-Fr pigtail catheter attached to a fluid-filled manometer system. The catheter was inserted through a femoral 6-Fr introducer sheath (contralateral to the femoral access for TAVI) with its tip steadily positioned in the middle portion of the ascending aorta, at least 3 cm over the cusps of the aortic valve. Invasive aortic pressure recordings were taken at two different intraprocedural moments, pre- and post-TAVI, simultaneously with the echocardiographic examinations. An average of 20 cardiac cycles was used to render the final pressure measurements.

Construction and analysis of the flow velocity in LVOT–pressure in ascending aorta loops

The first step was to align both simultaneous VP records and create a mesh to obtain the same number of coincident points in time for velocity and pressure (**Figure 1**). The resulting images were processed using the WebPlotDigitizer application (13). The resulting data were saved in two independent vectors to later face them and create the loops with a program developed in R. From the loops, the angles and distances between the points defined by the maximum and minimum pressure–velocity values were calculated.

Endpoints and definitions

The objective functional improvement of a patient with AS after the TAVI procedure was defined as the achievement at

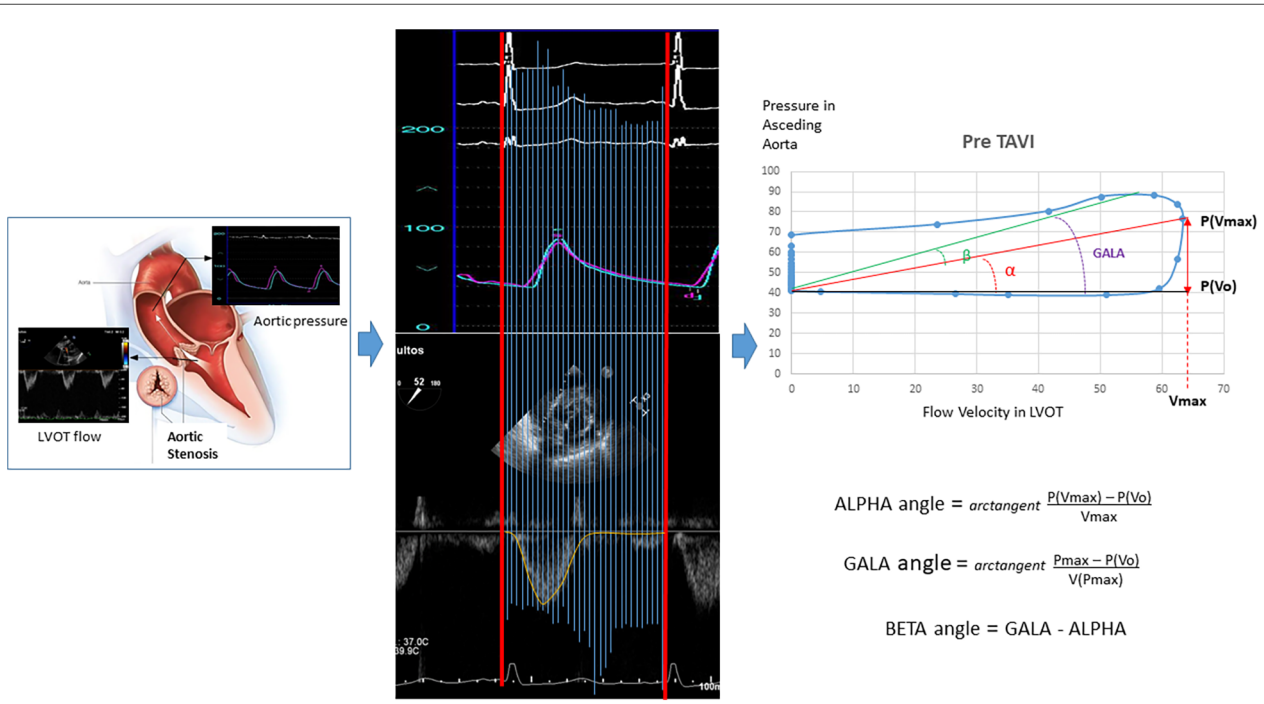

FIGURE 1
Construction and analysis of the loops for "flow velocity in left ventricular outflow tract/blood pressure in the aorta." LVOT, left ventricular outflow tract.

6 months of an increase of at least 10% in the distance covered during the 6-min walk test or a reduction of at least 50% in NT-proBNP blood levels with respect to pre-TAVI when this 10% increase was not evident. In this way, with both criteria, the potential presence of factors that limit the speed of gait and are not related to cardiovascular capacity was taken into consideration.

For those patients who died before the 6-month landmark and after the 30-day evaluation, improvement was based on this evaluation, but this was considered negative if the patients suffered from or died of heart failure afterward. Patients who died before the 30-day follow-up, patients who died because of heart failure were considered without improvement, and the rest of the patients who died from other causes were excluded from the analysis since no functional evaluation was available. Subjective improvement was considered if patients reported a positive change in at least one class of the NYHA classification and/or an increase in at least 10 points in the KCCQ. All patients underwent a systematic clinical follow-up at 2 years. Baseline staging of cardiac damage was conducted according to the classification proposed by Généreux et al. (14).

Statistical analysis

Continuous variables are presented as means ± standard deviations or medians (interquartile ranges) according to the type of distribution, and categorical variables are presented as percentages. Distribution was assessed for each variable with the Shapiro–Wilk test. Accordingly, continuous variables were compared using the Student's *t*-test if they followed a normal distribution and by non-parametric tests when this was not the case. The categorical variables were compared with the chi-squared test or Fisher's exact test, as required.

Multivariable logistic regression analysis identified independent predictors of objective functional improvement post-TAVI. Among all the clinical, echocardiographic, hemodynamic, and VP loop-related variables, those that showed a univariate relationship with an outcome ($p < 0.2$) were entered into the multivariable logistic regression model. Then, a stepwise elimination analysis was performed to define a useful subset of predictors.

The Hosmer–Lemeshow test or the likelihood ratio test was used to evaluate the goodness of fit, that is, the overall significance of the model. The Nagelkerke R^2 was used to determine the amount of variance of the dependent variable, which explains the estimated model. This indicates the degree of usefulness of the independent variables in predicting the dependent variable. When using prediction models, it is first necessary to differentiate two subsets of the original sample. One will be used to estimate the desired model (train data), and the other will be used to test the estimated model (test data). The R createDataPartition command allowed us to obtain these sets from the original sample.

In the presence of unbalanced samples, it is necessary to balance the set with which the model is to be estimated, that is, the train data set. To solve this problem, R function ROSE (*Random Over-Sampling Examples*), which allowed us to deal with binary classification problems in the presence of unbalanced samples, was used. Because the sample partitions used for the model estimation phase were random and different from each other, they led to different estimates of the prediction model. That is why, to finish with the model estimation phase, it is necessary to carry out machine learning techniques known as assembled models. There are different ways to obtain the assembled model, either by using different algorithms or by varying the training data obtained by bootstrapping, for the same algorithm. In this last procedure, each model has different parameters since it has been estimated from a different sample in each case. This is the method that has been chosen to solve the problem that was raised above. Assembled models are used to more robustly predict an outcome from multiple models.

The discriminating power of the parameters for predicting objective functional improvement was assessed by considering the area under the curve from the receiver operating characteristic (ROC) analysis. Box and whisker plots were built to show the baseline and post-TAVI evolution of variables according to improvement subgroups. Kaplan–Meier curves for event-free survival were obtained for each group and compared using the log-rank test and the hazard ratios with 95% confidence intervals. *p*-values of <0.05 were considered statistically significant. Statistical packages SPSS 25.0, R programs, and MedCalc Statistical Software version 19.6.4 (MedCalc Software Ltd., Ostend, Belgium) were used during the course of the study.

Results

Finally, among the 105 eligible patients, 102 consecutive patients who underwent TAVI and met the inclusion criteria were included in the study. The baseline characteristics of the patients are listed in **Supplementary Table S1**. Approximately 52% were women, and their mean age was 81 ± 6.6 years. Among these patients, 82 (80.4%) presented objective functional improvement 6 months after the intervention, whereas 93 (91%) reported a variable degree of subjective improvement. The changes in 6-min walk test results and NT-proBNP levels observed after the procedure are shown in **Supplementary Figure S2**. The group with objective improvement significantly increased the distance in the walk test and showed a significant decrease in biomarker levels. The group without improvement experienced no positive changes in these parameters.

The hemodynamic, echocardiographic, and VP loop-derived parameters at baseline for both groups, with and without objective functional improvement, are listed in **Table 1**. A lower central systolic blood pressure (SBP) was significantly associated with clinical improvement at 6 months. The variables that reflect characteristics of the arterial system, such as pulse pressure (PP), valve–aortic impedance (Zva), or total arterial distensibility (SVi/PP), did not show significant differences between the groups.

TABLE 1 Baseline parameters according to objective functional improvement after TAVI.

	No improvement	Improvement	*p*
	n = 20	*n* = 82	
SBP (mmHg)	136 ± 4	130 ± 3	0.03
MAP (mmHg)	95 ± 3	92 ± 2	0.16
PP (mmHg)	59 ± 4	58 ± 2	0.34
SVi/PP (ml/mmHg)	0.75 ± 0.23	0.8 ± 0.3	0.60
LVEF (%)	57 ± 2	56 ± 1	0.20
SVi (ml/kg/m^2)	42 ± 3	43 ± 2	0.46
Aortic maximal gradient (mmHg)	81 ± 6	86 ± 3	0.51
Aortic mean gradient (mmHg)	48 ± 4	49 ± 2	0.67
Energy loss index (cm^2/m^2)	0.48 (0.4–0.63)	0.44 (0.35–0.5)	0.29
Indexed aortic valve area (cm^2/m^2)	0.42 (0.34–0.54)	0.4 (0.32–0.5)	0.26
Zva (mmHg/ml/m^2)	4.6 ± 1.3	4.7 ± 1.7	0.87
VP analysis			
ALPHA angle (°)	4.21 (0.6–8)	9.6 (3.9–17)	0.027
BETA angle (°)	77.3 (23.63–86.8)	54.7 (25.4–84)	0.26
GALA angle (°)	80.78 (36.5–90)	64.6 (48.1–90)	0.61
P(Vmax) – P(Vo)	8.59 ± 1.9	16.6 ± 1.8	0.004
Vmax	83.01 ± 5.6	80.88 ± 3.3	0.78
Pmax – P(Vmax)	47 ± 27	35 ± 18	0.09
P(Vmax) – P(Vo)/Vmax	0.09 ± 0.08	0.23 ± 0.19	0.001

MAP, mean arterial pressure; Zva, valvuloarterial impedance, defined as (SBP + mean aortic gradient)/SVi.
Values are mean ± SD or medians (25th–75th interquartile ranges), depending on variable distribution.

The baseline values of the parameters derived from the VP loops are also listed in Table 1. A larger ALPHA angle or the closely related parameters "(Pressure at Vmax – Pressure at Vo)/Vmax" and "P(Vmax) – P(Vo)" were all significantly associated with objective functional improvement at 6 months.

The respective VP loops of patients with and without objective functional improvement, showing the remarkably larger values for the ALPHA angle and the P(Vmax) – P(Vo) difference in the patients experiencing improvement, are illustrated in Figure 2.

In the multivariate regression analysis, the only variable that resulted in an independent predictor of objective functional improvement was the ALPHA angle (OR 1.12, 95% CI 1.0064–1.2417; $p = 0.03$). Replacing the ALPHA angle value for the equivalent parameter, "P(Vmax) – P(Vo)/Vmax," resulted in this being a unique independent predictor.

The proportional changes observed for the different variables analyzed in the study after the TAVI procedure according to the reported objective improvement are presented in Table 2. The VP loops of one patient at baseline and after TAVI, in whom objective functional improvement was noted, are illustrated in Figure 3. The corresponding recordings for pressure and velocity showed changes in magnitude and time coupling after TAVI.

The discriminative performance of different parameters to predict the objective functional improvement after TAVI is described in Figure 4 and Supplementary Table S2. The AUC was significantly higher for the ALPHA angle and [P(Vmax) – P(Vo)]/Vmax and also for the closely related P(Vmax) – P(Vo)

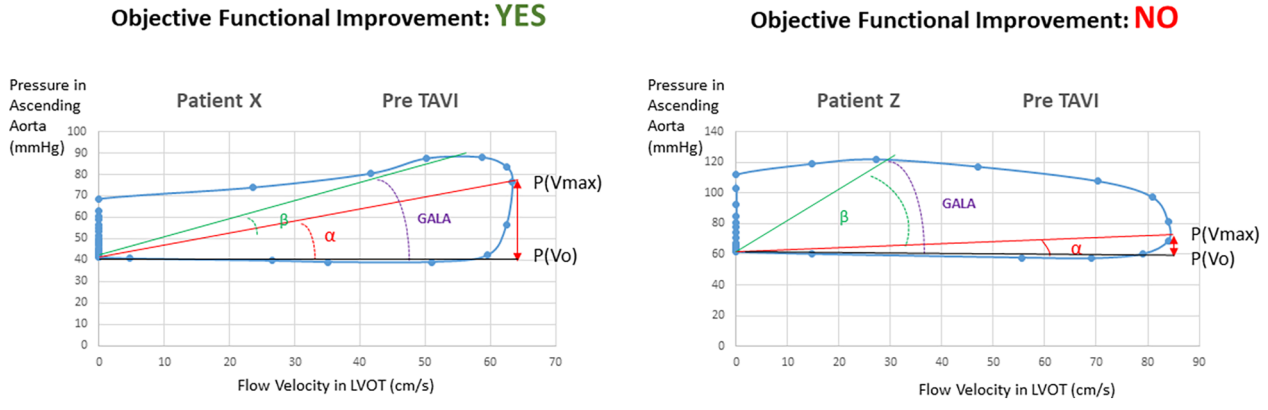

FIGURE 2
Velocity–pressure loops at baseline in patients with and without objective functional improvement after TAVI.

TABLE 2 Proportional variation of parameters from baseline to post-TAVI according to objective functional improvement.

	No improvement $n = 20$	Improvement $n = 82$	p
Variation pre–post			
SBP	0.29 ± 0.26	0.37 ± 0.27	0.32
MAP	−0.08 ± 0.14	−0.03 ± 0.16	0.25
PP	−0.14 (−0.26/0.01)	−0.06 (−0.24/0.1)	0.55
Aortic maximal gradient	−0.7 (−0.77/−0.61)	−0.73 (−0.8/−0.62)	0.36
Aortic mean gradient	−0.76 (−0.8/−0.69)	−0.78 (−0.83/−0.70)	0.49
SVi	0.08 (−0.02/0.24)	0.05 (−0.13/0.39)	0.55
Zva	−0.30 (−0.46/−0.16)	−0.28 (−0.46/−0.12)	0.55
ALPHA angle	0.09 (−0.45/0.71)	−0.60 (−0.84/0.28)	0.03
BETA angle	−0.26 (−0.40/0.86)	−0.01 (−0.29/1.04)	0.37
GALA angle	−0.19 (−0.35/0.52)	−0.05 (−0.35/0.56)	0.76
Pmax – P(Vmax)	0.34 ± 0.9	1.43 ± 2.7	0.006
P(Vmax) – P(Vo)	0.23 (−0.38/1.55)	−0.50 (−0.78/0.94)	0.04

The proportion of variation was calculated as (value post – value pre)/value pre. Values are means ± SDs or medians (25th–75th interquartile ranges), depending on the variable distribution.

compared with the other conventional parameters used in clinical practice to estimate the severity of AS. These differences were even more pronounced in the low-gradient AS subgroup, most of them with a low-flow condition (≤35 ml/m^2). The cutoff value for [P(Vmax) – P(Vo)]/Vmax was 0.1 in the overall and low-gradient groups.

In the long term, the group with objective functional improvement showed a significantly lower incidence or mortality (9% vs. 44% at the 2-year follow-up; $p = 0.001$) (Figure 5).

The predictive value of the VP loop-derived parameter [P (Vmax) – P(Vo)]/Vmax was assessed in a validation cohort of 119 patients. The clinical and procedural characteristics of the validation cohort are described in Supplementary Tables S3 and 4. Applying the same definition for objective functional improvement after TAVI, the parameter showed an AUC of 0.67 for the total cohort and 0.76 for the low-gradient subgroup (both $p < 0.001$).

The summarized results are graphically illustrated in Figure 6.

Discussion

In the present study, the parameters derived from the integrated analysis of LVOT flow velocity and ascending aorta pressure resulted in the only independent predictors for objective clinical improvement at 6 months in patients with severe aortic stenosis undergoing TAVI.

Namely, the parameter "[P(Vmax) – P(Vo)]/Vmax" resulted in a predictor for objective improvement in the overall population and was even more accurate in the low-gradient subgroup. This parameter outperformed all other conventional parameters used in clinical practice to estimate AS severity, particularly in the challenging subgroup of patients with low-gradient AS.

The calculation of this parameter is not complex since both aortic pressure and flow velocity recordings include a simultaneous electrocardiographic recording in the same lead. Thus, the pressure at Vmax is estimated through the time

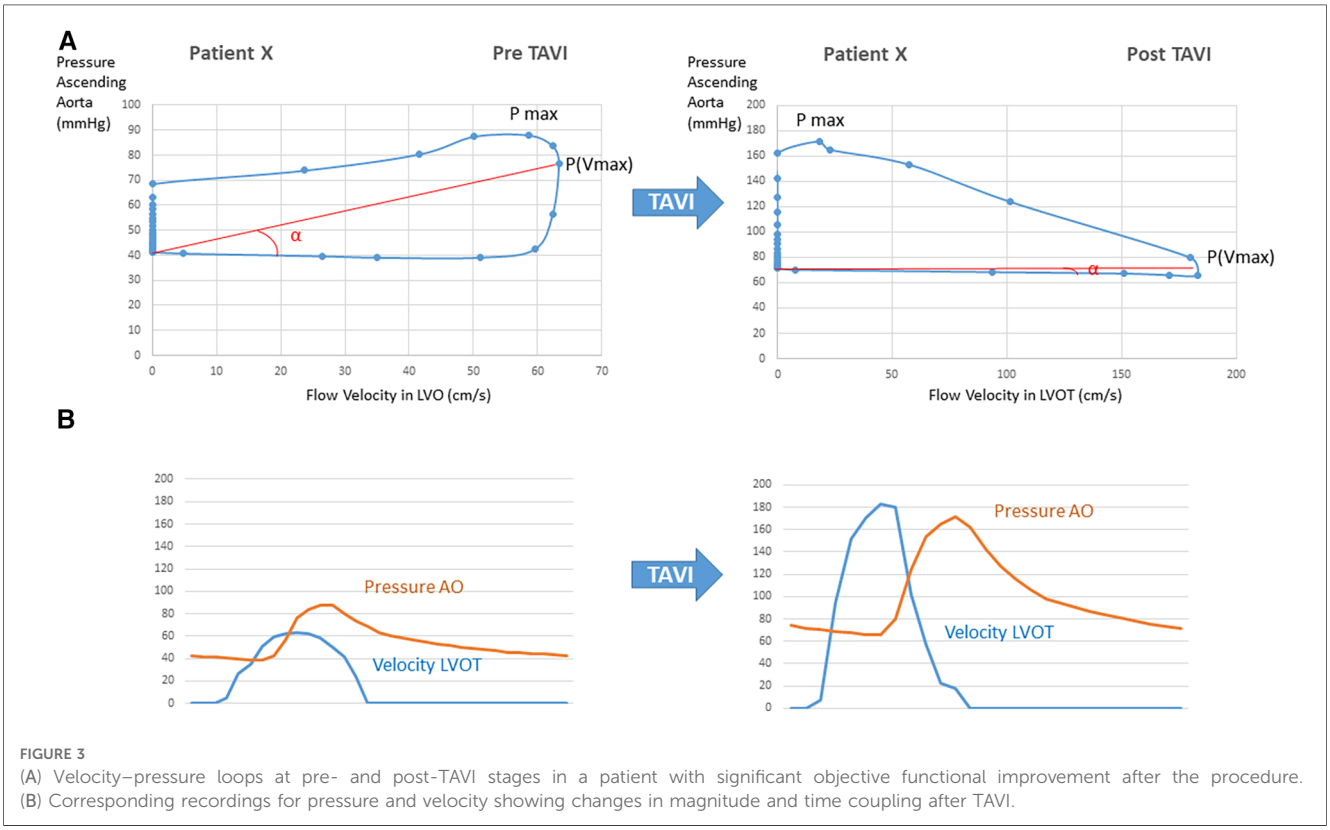

FIGURE 3
(A) Velocity–pressure loops at pre- and post-TAVI stages in a patient with significant objective functional improvement after the procedure. (B) Corresponding recordings for pressure and velocity showing changes in magnitude and time coupling after TAVI.

10.3389/fcvm.2023.1215826

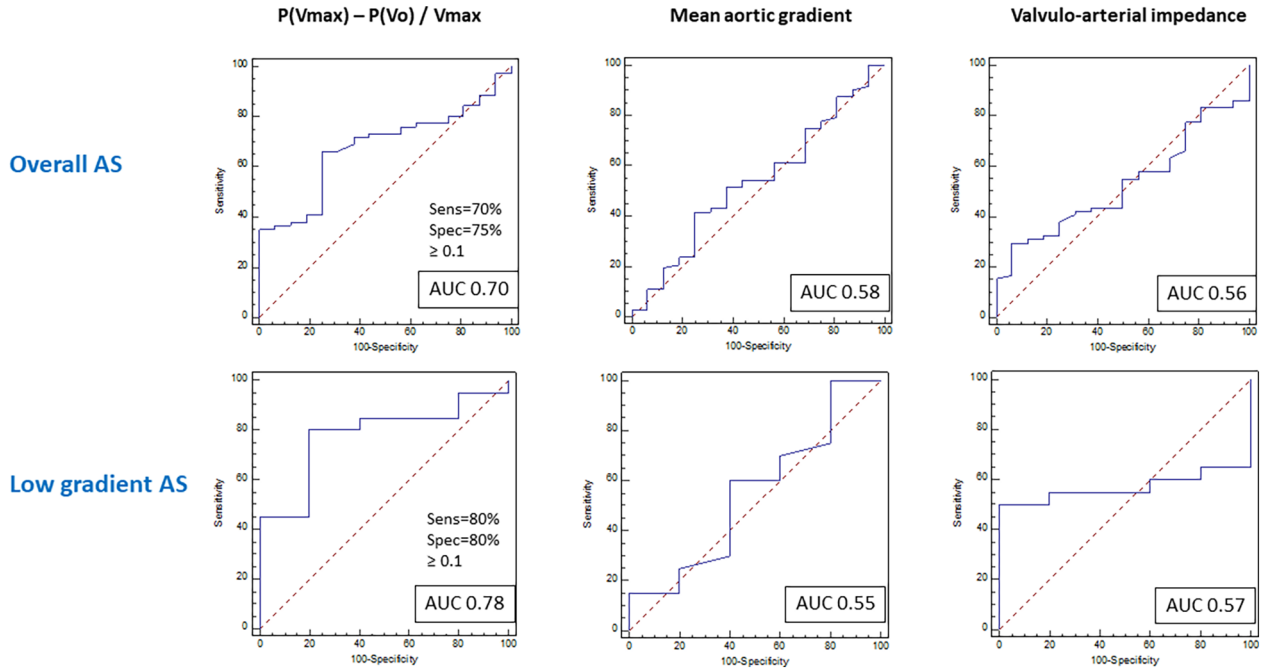

FIGURE 4
Receiver operating curves for prediction of functional improvement after TAVI in the general population with aortic stenosis and the low-gradient aortic stenosis subpopulation.

between peak R-wave and peak Doppler flow velocity applied to the pressure curve, and the pressure at Vo is equivalent to the diastolic pressure. We do not have a clear pathophysiological explanation for the relationship between this parameter and the true hemodynamic load imposed by aortic stenosis (estimated from the functional improvement patients experience after valve replacement). However, we are convinced that this parameter reflects the interaction, throughout the ventricular ejection phase, between the flow velocity proximal to the valve (at the LVOT) and the dynamics of pressure just distal to the valve (aortic root). This multidimensional integral nature, which contemplates pressure, velocity, and time, explains its additional value with respect to pressure parameters such as the gradient, which are unidimensional.

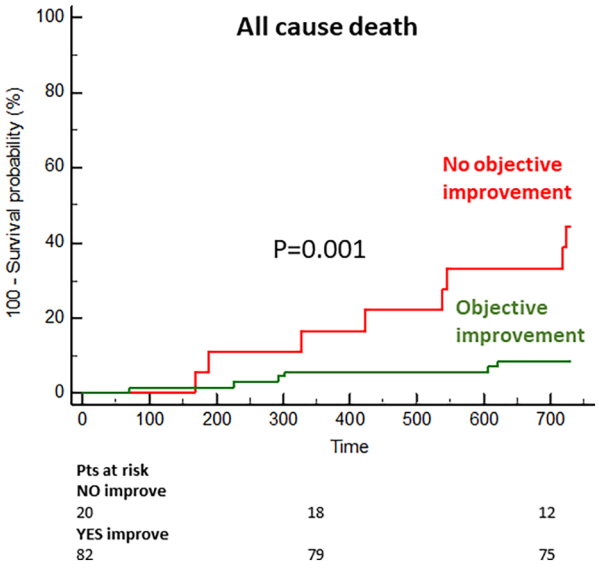

FIGURE 5
Cumulative incidence of mortality in the subgroups with and without objective functional improvement.

Vallée and colleagues described aortic velocity–pressure loops and a series of angles derived from them (ALPHA, BETA, and GALA) as an estimate of ventriculoaortic coupling that is easily monitored during surgical interventions, obtaining a continuous measurement of left ventricular afterload (10–12). In the study by Hong et al., to build the VP loop in the ascending aorta, the aortic velocity was measured immediately after the acquisition of invasive pressures at the center of the LVOT with close attention paid to obtaining an angle of the Doppler signal to aortic blood flow close to 0° (11). Noteworthy, in studies aimed to measure the valvuloarterial impedance in patients with AS using magnetic resonance imaging, flow measurement is routinely performed at the LVOT or just above the valve (15, 16). The flow measurement in the LVOT, where complex flow is less prominent, is thought to provide a more accurate measurement of forward flow (17).

In our study, an original new design was proposed to assess the effect of aortic stenosis in which flow is measured in the LVOT and pressure in the ascending aorta, so it is plausible that the ALPHA angle or [P(Vmax) – P(Vo)]/Vmax could be largely representing the effect of the valvular component of the

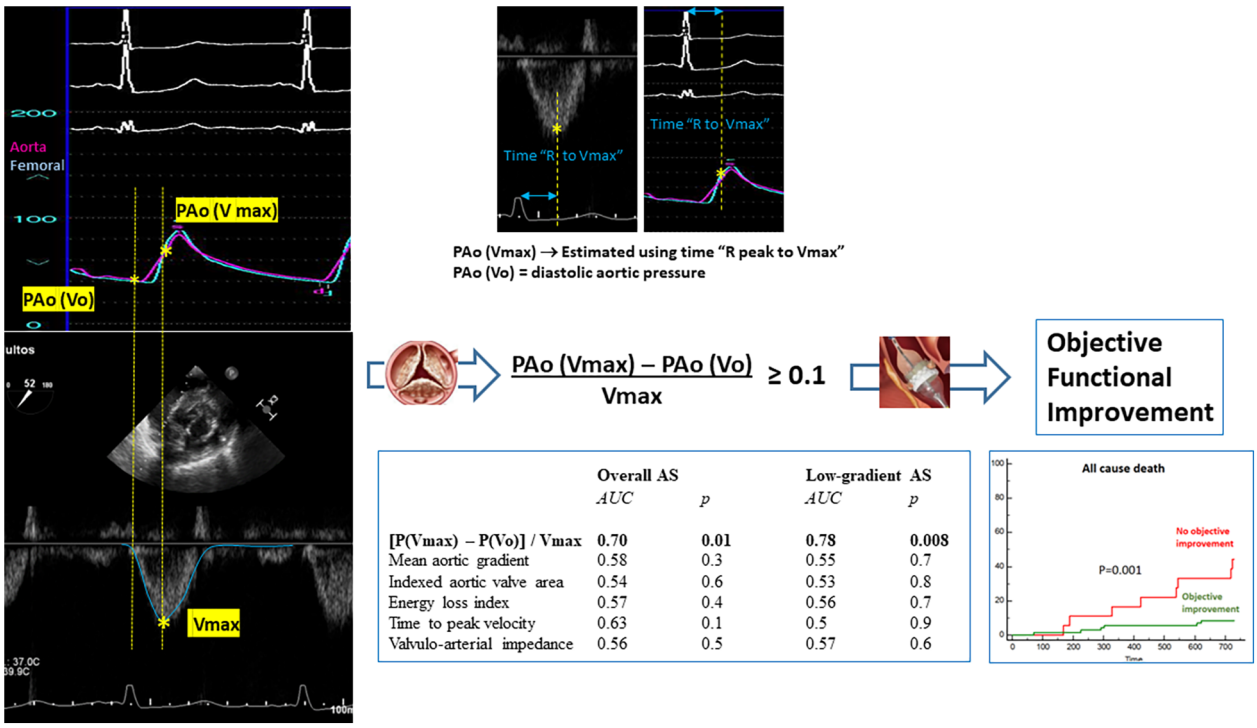

	Overall AS		Low-gradient AS	
	AUC	*p*	*AUC*	*p*
[P(Vmax) – P(Vo)] / Vmax	**0.70**	**0.01**	**0.78**	**0.008**
Mean aortic gradient	0.58	0.3	0.55	0.7
Indexed aortic valve area	0.54	0.6	0.53	0.8
Energy loss index	0.57	0.4	0.56	0.7
Time to peak velocity	0.63	0.1	0.5	0.9
Valvulo-arterial impedance	0.56	0.5	0.57	0.6

FIGURE 6
Parameter "(Pressure at Vmax – Pressure at Vo)/Vmax" derived from the integrated analysis of flow velocity in the left ventricular outflow tract and blood pressure in the aorta at baseline results in a more accurate predictive factor for objective functional improvement after TAVI in the general population with aortic stenosis and the low-gradient aortic stenosis subpopulation. The calculation of this parameter is simplified through the electrocardiographic recordings in simultaneous pressure and Doppler tracings. The objective functional improvement after TAVI portends a highly relevant prognostic effect.

afterload. Thus, patients with clinical improvement at 6 months had significantly higher values at baseline than those who did not improve.

The conventional echocardiographic parameters such as the indexed aortic valve area, energy loss index, and peak or mean aortic gradients were not significant predictors. The delayed time to peak velocity also did not show any independent predictive value (18).

Briand et al. described the concept of valvuloarterial impedance (Zva) to quantify the global afterload in aortic stenosis since this variable took into account the valve and arterial load components (5). However, the valvuloarterial impedance did not result in an independent predictor when entering the VP loop parameters in the regression model. Furthermore, its predictive value was poor compared with the VP loop-derived values.

Patients with low-gradient/low-flow AS, particularly with low ejection fraction, have a significantly worse medium-term to long-term survival compared with all other patients undergoing TAVI (19). In this setting, a low-dose dobutamine stress echocardiography is recommended to distinguish between true severe and pseudosevere aortic stenosis. However, after TAVI, the absence of contractile reserve at baseline in this test was not associated with any negative effect on clinical outcomes or LVEF changes at follow-up (19). Cardiac tomography assessment of the degree of valve calcification provides important additional information (20). Nonetheless, given the poor prognosis with medical treatment, TAVI should be considered an option in certain patients with low-gradient AS. Therefore, it is important to know the parameters that allow identifying patients who may benefit from the intervention.

In our study, the patients with low-gradient AS who underwent TAVI had had diagnostic confirmation of the severity of the stenosis, in some cases after dobutamine stress echo or after considering a high degree of valve calcification on tomography. Nonetheless, in these patients, valve calcification had no predictive value for functional improvement after TAVI. Remarkably, the VP loop parameters showed a notable discriminatory value in the low-gradient population regardless of the stroke volume, clearly better than the yielded by valve-related echocardiographic measurements or the valvuloarterial impedance.

The contribution of this study is original and provides an additional value with respect to the previous study of our group since this study investigates the value of an integrated analysis of LVOT flow velocity and aortic pressure, measured non-invasively and invasively, respectively, in the assessment of aortic stenosis. This true novel approach could have by itself a high potential value in defining the hemodynamic burden imposed by aortic stenosis. In contrast, the previous study included a series of

conventional parameters well known in clinical practice (9). Thus, the new proposed method seems to outperform any of those conventional parameters.

These findings should be prospectively validated in a larger population of patients currently treated with TAVI. The development of software capable of facilitating the integrated analysis of pressure and Doppler tracings would be welcome. In addition, the use of central pressure recordings estimated by non-invasive techniques would allow a broader implementation of this type of analysis (8, 21).

Limitations

This study contains several limitations. First, the sample size of the cohorts limits the statistical power of the study. The fact that most patients presented clinical improvement at 6 months has meant that the sample is unbalanced, which required machine learning techniques to try to correct the regression analysis outcomes. Anyway, the predictive superiority of the VP loop parameters over the conventional metrics used to estimate AS severity was evident in this study. In addition, the predictive power of these parameters was prospectively validated.

The definition of objective functional improvement was specific to the study and, although well thought out, may be questionable. However, it was sufficiently precise and, at the same time, conservative, as confirmed by seeing how the group considered without improvement showed even worse post-TAVI performance in the walking test and the absence of changes in heart failure biomarkers. In addition, the classification also showed important prognostic implications. The assessment time of 6 months can be discussed; however, we know from previous studies that the improvement after TAVI is rapid, being evident even at 30 days (22, 23). On the other hand, a later evaluation, especially in an elderly population, may be affected by the concurrence or progression of other unrelated pathological processes, such as coronary artery disease or certain comorbidities.

These results are certainly applicable to the profile of patients included in the study, who are patients with degenerative-calcified aortic stenosis, most of whom have tricuspid anatomy and a minority have bicuspid anatomy. Therefore, the results could obviously be applicable to patients undergoing aortic valve replacement surgery. The validity of the method in bicuspid stenosis or in rheumatic stenosis could be defended taking into account that the pathophysiological effects of aortic valve stenosis would be comparable.

In methods, it is indicated that patients who were initially included but presenting severe periprocedural complications such as coronary obstruction, annulus rupture, or stroke were finally excluded from the analysis, given their relevant effect on physiologic measurements and functional recovery after the procedure. The aim of the study was to establish pre-procedural predictors of objective functional improvement since these are the ones that would be of value to help in the decision-making when the indication for TAVI is uncertain. With regard to comorbidity and frailty, all were included in the predictive model. The fact is that the clinical selection process prior to indication already excludes those with very high frailty or severe comorbidities that seriously compromise the patient's short-term future and make the transcatheter aortic valve implantation (TAVI) procedure futile.

The rate of missing data was extremely low. This is a series of limited sizes, from a single center with a systematic prospective database. All patients belong to our regional public health system and are therefore perfectly traceable. In addition, all patients in the TAVI program are followed up in our department.

The application of this method in clinical practice would require the use of specific software, but it is not complex and could be developed without great difficulty.

Conclusion

The integrated analysis of the left ventricular outflow tract flow velocity and aortic pressure allows us to predict the degree of objective functional improvement after TAVI and thus to estimate the aortic stenosis burden more precisely than the conventional parameters used to assess the severity of aortic stenosis, particularly in low-gradient patients.

Data availability statement

The raw data supporting the conclusions of this article will be made available by the authors, without undue reservation.

Ethics statement

The studies involving humans were approved by the IDIVAL Comite de Ensayos Clinicos. The studies were conducted in accordance with the local legislation and institutional requirements. The participants provided their written informed consent to participate in this study.

Author contributions

JT, GV, and EB-A: research idea and study design. GV, JI, FS, D-HL, CR, PL, TG, JIS, JC, MM, CG, VF-S, MB, SB, and AG: data acquisition. JT, GV, EB-A, JI, and TG: data analysis/interpretation. JT, GV, EB-A, JI, TG, and JIS: statistical analysis. JV and JZ: supervision and mentorship. All authors contributed to the article and approved the submitted version.

Conflict of interest

JT received grants/research support from Abbott Medical, Biosensors, Bristol Myers Squibb, and Amgen and received honoraria or consultation fees from Boston Scientific, Medtronic, Biotronik, Astra Zeneca, and Daiichi-Sankyo.

The remaining authors declare that the research was conducted in the absence of any commercial or financial relationships that could be construed as a potential conflict of interest.

Publisher's note

All claims expressed in this article are solely those of the authors and do not necessarily represent those of their affiliated organizations, or those of the publisher, the editors and the reviewers. Any product that may be evaluated in this article, or claim that may be made by its manufacturer, is not guaranteed or endorsed by the publisher.

Supplementary material

The Supplementary Material for this article can be found online at: https://www.frontiersin.org/articles/10.3389/fcvm.2023.1215826/full#supplementary-material

SUPPLEMENTARY FIGURE S1
Protocol for the workflow of the study. TAVI = transcatheter aortic valve implantation; TT = transthoracic; TE = transesophageal.

SUPPLEMENTARY FIGURE S2
Baseline and 6 months post-TAVI values for the 6-minute walk test and for blood levels of NT-proBNP (Nitro-terminal-pro brain natriuretic peptide), according to the classification for objective functional improvement.

References

1. Arnold SV, Cohen DJ, Dai D, Jones PG, Li F, Thomas L, et al. Predicting quality of life at 1 year after transcatheter aortic valve replacement in a real-world population. *Circ Cardiovasc Qual Outcomes*. (2018) 11:e004693. doi: 10.1161/circoutcomes.11.suppl_1.190

2. Leon MB, Smith CR, Mack M, Miller DC, Moses JW, Svensson LG, et al. Transcatheter aortic-valve implantation for aortic stenosis in patients who cannot undergo surgery. *N Engl J Med*. (2010) 363:1597–607. doi: 10.1056/NEJMoa1008232

3. Saybolt MD, Fiorilli PN, Gertz ZM, Herrmann HC. Low-flow severe aortic stenosis: evolving role of transcatheter aortic valve replacement. *Circ Cardiovasc Interv*. (2017) 10:e004838. doi: 10.1161/CIRCINTERVENTIONS.117.004838

4. Eugène M, Duchnowski P, Prendergast B, Wendler O, Laroche C, Monin JL, et al. Contemporary management of severe symptomatic aortic stenosis. *J Am Coll Cardiol*. (2021) 78:2131–43. doi: 10.1016/j.jacc.2021.09.864

5. Briand M, Dumesnil JG, Kadem L, Tongue AG, Rieu R, Garcia D, et al. Reduced systemic arterial compliance impacts significantly on left ventricular afterload and function in aortic stenosis: implications for diagnosis and treatment. *J Am Coll Cardiol*. (2005) 46:291–8. doi: 10.1016/j.jacc.2004.10.081

6. Pibarot P, Dumesnil JG. Improving assessment of aortic stenosis. *J Am Coll Cardiol*. (2012) 60:169–80. doi: 10.1016/j.jacc.2011.11.078

7. Yotti R, Bermejo J, Gutiérrez-Ibañes E, Pérez del Villar C, Mombiela T, Elízaga J, et al. Systemic vascular load in calcific degenerative aortic valve stenosis: insight from percutaneous valve replacement. *J Am Coll Cardiol*. (2015) 65:423–33. doi: 10.1016/j.jacc.2014.10.067

8. Ben-Assa E, Brown J, Keshavarz-Motamed Z, de la Torre Hernandez JM, Leiden B, Olender M, et al. Ventricular stroke work and vascular impedance refine the characterization of patients with aortic stenosis. *Sci Transl Med*. (2019) 11: eaaw0181. doi: 10.1126/scitranslmed.aaw0181

9. De la Torre Hernandez JM, Veiga Fernandez G, Ben-Assa E, Sainz Laso F, Lee DH, Ruisanchez Villar C, et al. A new integrative approach to assess aortic stenosis burden and predict objective functional improvement after TAVR. *Front Cardiovasc Med*. (2023) 10:1118409. doi: 10.3389/fcvm.2023.1118409

10. Vallée F, Le Gall A, Joachim J, Passouant O, Matéo J, Mari A, et al. Beat-by-beat assessment of cardiac afterload using descending aortic velocity-pressure loop during general anesthesia: a pilot study. *J Clin Monit Comput*. (2018) 2:23–32. doi: 10.1007/s10877-017-9982-5

11. Joachim J, Vallée F, Le Gall A, Matéo J, Lenck S, Millasseau S, et al. Velocity-pressure loops for continuous assessment of ventricular afterload: influence of pressure measurement site. *J Clin Monit Comput*. (2018) 32:833–40. doi: 10.1007/s10877-017-0082-3

12. Hong A, Joachim J, Buxin C, Levé C, Le Gall A, Millasseau S, et al. Using velocity-pressure loops in the operating room: a new approach of arterial mechanics for cardiac afterload monitoring under general anesthesia. *Am J Physiol Heart Circ Physiol*. (2019) 317:H1354–62. doi: 10.1152/ajpheart.00362.2019

13. Rohatgi A. WebPlotDigitizer. Available at: https://automeris.io/WebPlotDigitizer. (Accessed May 15, 2021).

14. Généreux P, Pibarot P, Redfors B, Mack MJ, Makkar RR, Jaber WA, et al. Staging classification of aortic stenosis based on the extent of cardiac damage. *Eur Heart J*. (2017) 38:3351–8. doi: 10.1093/eurheartj/ehx381

15. Kilner PJ, Gatehouse PD, Firmin DN. Flow measurement by magnetic resonance: a unique asset worth optimising. *J Cardiovasc Magn Reson*. (2007) 9:723–8. doi: 10.1080/10976640701465090

16. Muzzarelli S, Monney P, O'Brien K, Faletra F, Moccetti T, Vogt P, et al. Quantification of aortic flow by phase-contrast magnetic resonance in patients with bicuspid aortic valve. *Eur Heart J Cardiovasc Imaging*. (2014) 15:77–84. doi: 10.1093/ehjci/jet129

17. Soulat G, Kachenoura N, Bollache E, Perdrix L, Diebold B, Zhygalina V, et al. New estimate of valvuloarterial impedance in aortic valve stenosis: a cardiac magnetic resonance study. *J Magn Reson Imaging*. (2017) 45:795–803. doi: 10.1002/jmri.25399

18. Kamimura D, Hans S, Suzuki T, Fox ER, Hall ME, Musani SK, et al. Delayed time to peak velocity is useful for detecting severe aortic stenosis. *J Am Heart Assoc*. (2016) 5(10):e003907. doi: 10.1161/JAHA.116.003907

19. Ribeiro HB, Lerakis S, Gilard M, Cavalcante JL, Makkar R, Herrmann HC, et al. Transcatheter aortic valve replacement in patients with low-flow, low-gradient aortic stenosis: the TOPAS-TAVI registry. *J Am Coll Cardiol*. (2018) 71:1297–308. doi: 10.1016/j.jacc.2018.01.054

20. Clavel MA, Pibarot P, Messika-Zeitoun D, Capoulade R, Malouf J, Aggarval S, et al. Impact of aortic valve calcification, as measured by MDCT, on survival in patients with aortic stenosis: results of an international registry study. *J Am Coll Cardiol*. (2014) 64:1202–13. doi: 10.1016/j.jacc.2014.05.066

21. De la Torre Hernández JM, Veiga Fernandez G, Brown J, Sainz Laso F, Lee DH, Fradejas V, et al. Validation study to determine the accuracy of central blood pressure measurement using the SphygmoCor XCEL cuff device in patients with severe aortic stenosis undergoing transcatheter aortic valve replacement. *J Clin Hypertens*. (2021) 23:1165–75. doi: 10.1111/jch.14245

22. Arnold SV, Reynolds MR, Lei Y, Magnuson EA, Kirtane AJ, Kodali SK, et al. Predictors of poor outcomes after transcatheter aortic valve replacement: results from the PARTNER (placement of aortic transcatheter valve) trial. *Circulation*. (2014) 129:2682–90. doi: 10.1161/CIRCULATIONAHA.113.007477

23. Arnold SV, Afilalo J, Spertus JA, Tang Y, Baron SJ, Jones PG, et al. Prediction of poor outcome after transcatheter aortic valve replacement. *J Am Coll Cardiol*. (2016) 68:1868–77. doi: 10.1016/j.jacc.2016.07.762

frontiers | Frontiers in Cardiovascular Medicine

TYPE Case Report
PUBLISHED 26 January 2024
DOI 10.3389/fcvm.2024.1263905

OPEN ACCESS

EDITED BY
Konstantinos Papadopoulos,
Interbalkan Medical Center, Greece

REVIEWED BY
Faizus Sazzad,
National University of Singapore, Singapore
Jamshid Karimov,
Cleveland Clinic, United States

*CORRESPONDENCE
Katharina Huenges
✉ Katharina.Huenges@uksh.de

RECEIVED 20 July 2023
ACCEPTED 08 January 2024
PUBLISHED 26 January 2024

CITATION
Huenges K, Langguth P, Grothusen C, Hoffmann G, Kapahnke J, Haneya A, Strotmann J and Cremer J (2024) Case Report: The woman with the big heart—an imaging-guided attempt of surgical reduction. Front. Cardiovasc. Med. 11:1263905. doi: 10.3389/fcvm.2024.1263905

Case Report: The woman with the big heart—an imaging-guided attempt of surgical reduction

Katharina Huenges[1]*, Patrick Langguth[2], Christina Grothusen[1,3], Grischa Hoffmann[1], Julia Kapahnke[1], Assad Haneya[1], Jörg Strotmann[4] and Jochen Cremer[1]

[1]Department of Cardiovascular Surgery, UKSH Kiel, Kiel, Germany, [2]Department of Radiology and Neuroradiology, UKSH Kiel, Kiel, Germany, [3]Internal Medicine I, St. Johannes Hospital Dortmund, Dortmund, Germany, [4]Department of Cardiology, Städtisches Krankenhaus Kiel, Kiel, Germany

In a female patient with acute cardiac decompensation, an auxiliary finding of a giant left atrium emerged. The surgical therapy of the atrial reduction, in addition to a mitral valve replacement and a coronary artery bypass grafting, is hereby presented.

KEYWORDS
mitral, mitral valve, atrial, cardiac surgery, imaging

Introduction

Atrial reduction surgery is not commonly performed in the daily cardiac surgery routine. There have been only very scarce data of cases and techniques published so far (1–3). In this patient, the preoperative imaging provided a safe surgical planning, and a relevant reduction of the atrial size was possible.

Case description

A 72-year-old female patient with a giant left atrium was presented to our department. Permanent atrial fibrillation has been known for the past 13 years. Due to severe cardiac decompensation, the patient had to be admitted to an external cardiology clinic. The chest x-ray at the admission date showed a severe mediastinal enlargement (Figures 1A, B). Echocardiography revealed a massive biatrial dilatation, with a pronounced dilatation of the left atrium and intra-atrial thrombus masses were detectable. The left ventricle (LV) function was normal. Transthoracic and transesophageal echocardiography were not able to reliable measure the atrial dimensions possibly due to beam width limitations. Further examinations revealed a severe mitral regurgitation with secondary pulmonary hypertension, a moderate tricuspid regurgitation, and a two-vessel coronary artery disease. A significant left anterior descending (LAD) stenosis was treated interventionally with a drug eluting stent (DES) implantation, but a moderate circumflex artery stenosis remained untreated. The decision for the LAD intervention was made by the external cardiologist due to the decompensated condition of the patient. Anticoagulation was performed with edoxaban, but still, left atrial thrombus formation was detectable (Figure 2A, Supplementary Video S1). The mitral regurgitation was due to degeneration of the anterior and posterior leaflets (Carpentier IIIa, Figure 2B), and an additional annular calcification was notable. Optimized heart failure medication was given, and after careful recompensation, the patient was transferred to our department for surgical therapy. Anticoagulation therapy was switched to therapeutic low-molecular-weight heparin.

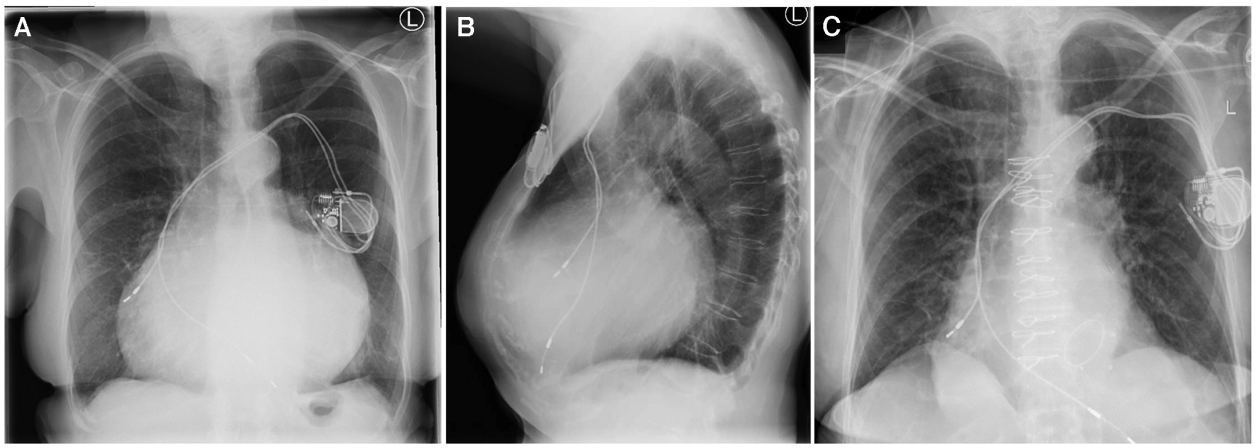

FIGURE 1
(A) Chest x-ray prior to surgery, (B) lateral chest x-ray prior to surgery, and (C) chest x-ray after surgery.

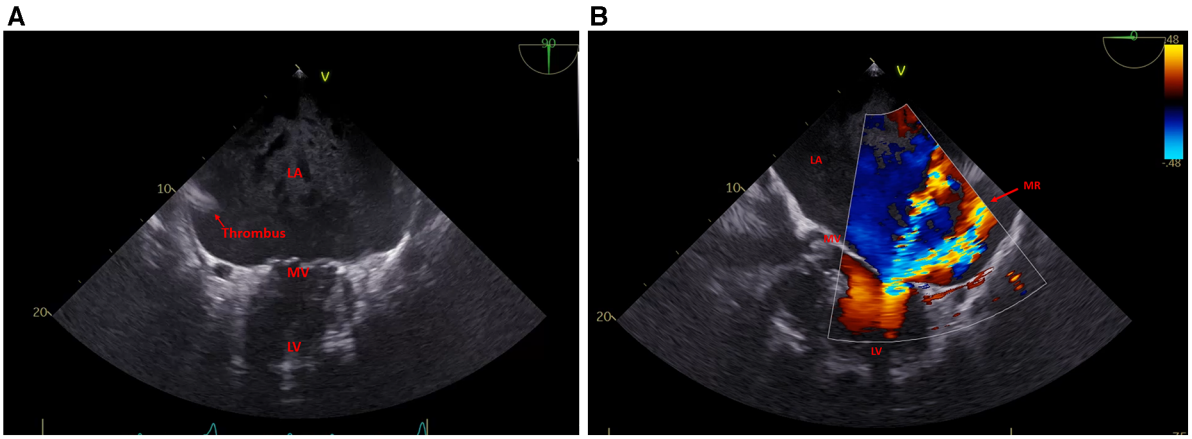

FIGURE 2
(A) Left atrium (LA) with thrombus formation two-chamber view and (B) mitral regurgitation.

Computed tomography (CT) with additional CT angiography was performed for better understanding of the cardiac structures. With the CT scan, the left atrial dimensions were measurable, the axial diameter was 12.5 cm × 15 cm, and the volumetric calculation showed 1,204 ml (Syngo.via VB60A, Siemens Healthineers, Erlangen, Germany) (Figure 3).

Case report timeline

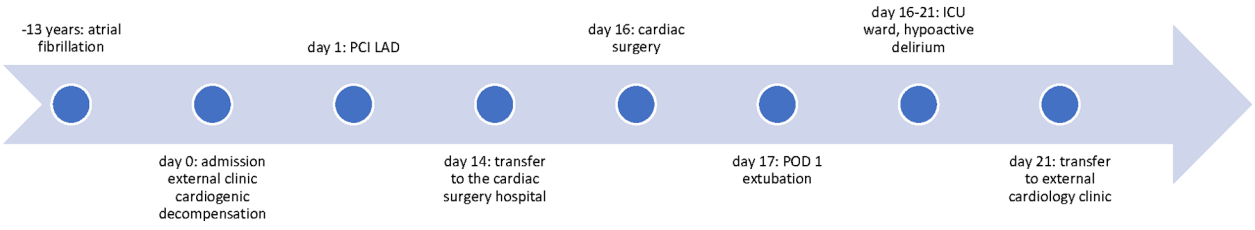

Surgical technique

Cardiac surgery was performed in standard fashion with general anesthesia, using median sternotomy as the approach. For the heart–lung machine, bicaval venous cannulation and aortic direct cannulation were applied. In moderate aortic atherosclerosis, cautious aortic cannulation and cross-clamping were necessary. Antegrade and retrograde blood cardioplegia were used as it is our standard cardioplegic approach.

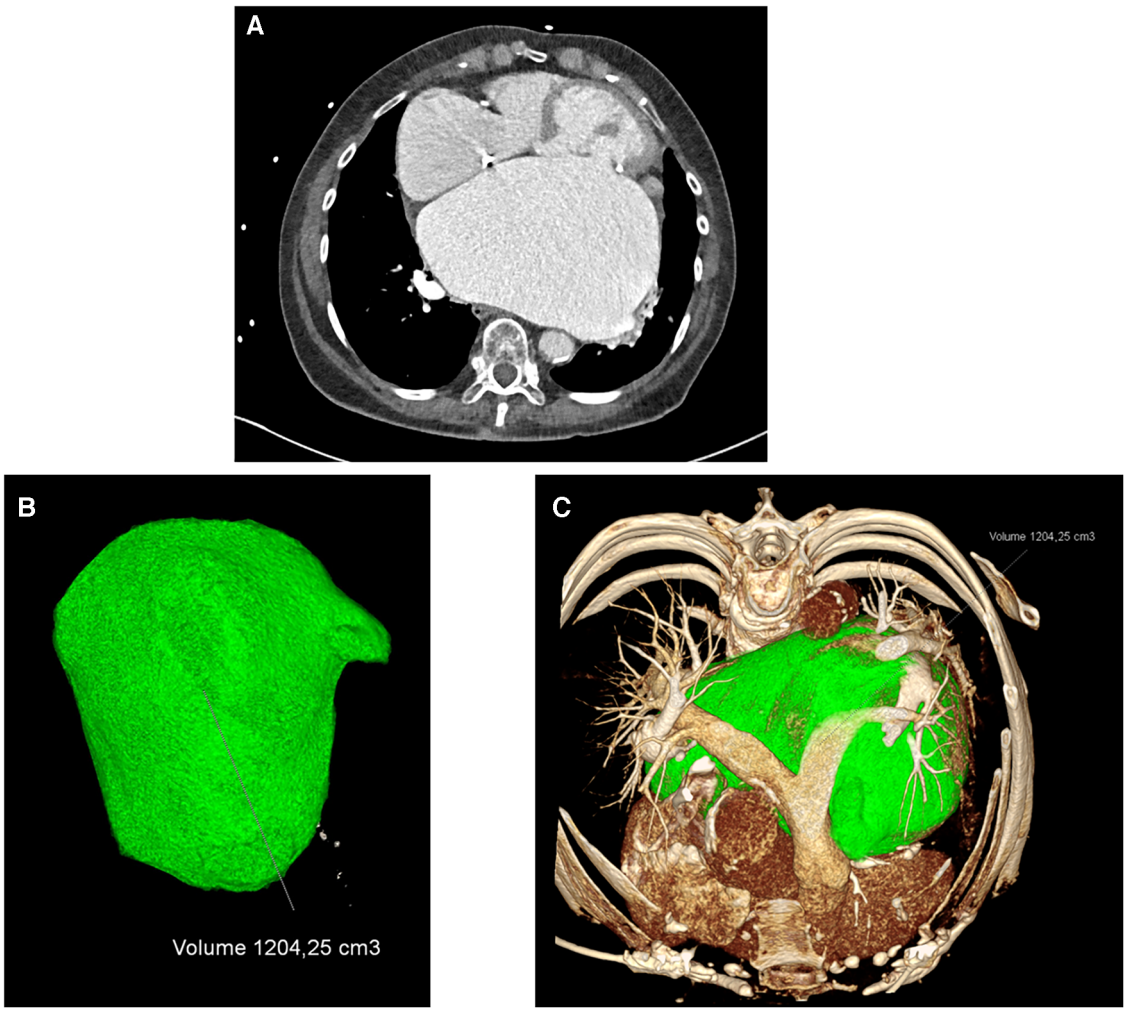

FIGURE 3
(A) CT scan prior surgery, (B) left atrial 3D volumetric measurements, and (C) left atrial (green) intrathoracic 3D dimensions.

The left atrium was opened via the interatrial sulcus. For improved vision, a retractor was inserted. The distance between the left and right pulmonary veins was over 10 cm. Close to the left atrial appendage, a 2 cm × 1.5 cm × 1.5 cm white thrombus was found and extracted. For reduction of the atrium, a longitudinal incision was made between the area of the coronary sinus until the middle line between the pulmonary veins and a tissue reduction of 3–4 cm was performed and with a 4-0 Prolene suture using the double-running technique. A second oblique oval-shaped excision of 6 cm × 7 cm of tissue parallel to the atrioventricular grove was performed with the same suturing. With these two incisions and steps of tissue removal, a relevant reduction of the atrial dimension was possible. The surgery was continued by aortocoronary bypass grafting of the first marginal branch of the circumflex coronary artery using a venous graft. It was followed by a mitral biologic valve replacement (33 mm Hancock II, Medtronic) as reconstruction of the native mitral valve was not feasible due to severe annular sclerosis.

Under catecholamine and inotropic support, the patient was transferred to our intensive care unit. After careful weaning, extubation was possible on the first postoperative day. Due to a slight hypoactive delirium, ICU observation was necessary for the first 5 days, and in a stable hemodynamic situation, the patient was then transferred to the external cardiology department for further treatment.

Echocardiography revealed a competent mitral valve prosthesis without any paravalvular leakage, the left atrium seemed to be reduced, but still a reliable measurement was not possible.

A follow-up computed tomography was performed 2 weeks after the surgery due to still slightly impaired renal function, this time only as a native CT scan without contrast agent. The size of the left atrium was reduced optically, and careful estimation showed a 30%–40% reduction of the atrial size due to surgery. However, after the radiological analysis and reconstruction, the left atrial reduction was approximately over 50% of the atrial initial size (volume before: 1,205 ml; volume after: 582 ml).

After an initial very promising course after the surgery, the patient developed COVID-19 significantly 3 months after the surgery and had to be rehospitalized, but from the cardiac aspects, the patient showed no complications.

Discussion

Atrial reduction surgery is not commonly performed in the daily cardiac surgery routine. There have been only very scarce data of cases and techniques published so far (1–3). The main reason is that even if mitral valve regurgitation or tricuspid valve regurgitation is severe and ongoing for many years, it is not invariably leading to giant atria. After correction of the heart valve pathology, until a certain degree, an atrial re-remodeling can occur with an autonomous reduction of the atrial size.

In our patient, we did see a giant left atrium, and even after the mitral valve surgery, remodeling with a significant atrial reduction was not very likely. Since intra-atrial thrombus formation had already occurred despite anticoagulation therapy, we did see the need for an attempt of atrial reduction. With the CT reconstruction, a safe operative plan for the surgery was possible. The reduction technique applied in this case led to a relevant decrease in left atrial size. The choice of the tissue reduction line has the potential for a safe reduction without changing the native normal atrial configuration. Sparing the superior atrial wall (compared to the plication techniques) further reduces the risk of permanent atrioventricular node disorders.

Informed consent was obtained from the patient included in this study.

Data availability statement

The original contributions presented in the study are included in the article/**Supplementary Material**, further inquiries can be directed to the corresponding author.

Ethics statement

The studies involving humans were approved by the Christian-Albrechts-University, Ethikkommission. The studies were conducted in accordance with the local legislation and institutional requirements. The participants provided their written informed consent to participate in this study. Written informed consent was obtained from the individual(s) for the publication of any potentially identifiable images or data included in this article.

Author contributions

KH: Conceptualization, Data curation, Investigation, Methodology, Writing – original draft. PL: Investigation, Visualization, Writing – review & editing. CG: Writing – review & editing. GH: Writing – review & editing. JK: Writing – review & editing. AH: Writing – review & editing. JS: Writing – review & editing. JC: Writing – review & editing.

Funding

The author(s) declare financial support was received for the research, authorship, and/or publication of this article.

We acknowledge financial support by DFG within the funding programme Open Access-Publikationskosten.

Conflict of interest

The authors declare that the research was conducted in the absence of any commercial or financial relationships that could be construed as a potential conflict of interest.

Publisher's note

Supplementary material

The Supplementary Material for this article can be found online at: https://www.frontiersin.org/articles/10.3389/fcvm.2024.1263905/full#supplementary-material

References

1. Xie X, Bai J. Giant left atrium. *J Card Surg.* (2018) 33:97–8. doi: 10.1111/jocs.13527

2. Shimamura J, Saito A, Kinoshita O, Ono M. Giant left atrium. *J Card Surg.* (2013) 28:719–20. doi: 10.1111/jocs.12225

3. Apostolakis E, Shuhaiber JH. The surgical management of giant left atrium. *Eur J Cardiothorac Surg.* (2008) 33(2):182–90. doi: 10.1016/j.ejcts.2007.11.003

frontiers | Frontiers in Cardiovascular Medicine

TYPE Case Report
PUBLISHED 27 March 2024
DOI 10.3389/fcvm.2024.1366444

OPEN ACCESS

EDITED BY
Emmanuel Androulakis,
Royal Brompton & Harefield NHS Foundation Trust, United Kingdom

REVIEWED BY
Krunoslav Michael Sveric,
Technical University Dresden, Germany
Anikó Ilona Nagy,
Semmelweis University, Hungary

*CORRESPONDENCE
Konstantinos Papadopoulos
papadocardio@gmail.com

RECEIVED 06 January 2024
ACCEPTED 13 March 2024
PUBLISHED 27 March 2024

CITATION
Papadopoulos K, Ikonomidis I and Vannan MA (2024) The added value of three-dimensional transthoracic echocardiography in mitral annular disjunction: a case report. Front. Cardiovasc. Med. 11:1366444. doi: 10.3389/fcvm.2024.1366444

The added value of three-dimensional transthoracic echocardiography in mitral annular disjunction: a case report

Konstantinos Papadopoulos[1]*, Ignatios Ikonomidis[2] and Mani A. Vannan[3]

[1]Echocardiography Laboratory, European Interbalkan Medical Center, Thessaloniki, Greece, [2]Echocardiography Laboratory, 2nd Cardiology Department, Medical School, Attikon University Hospital, National and Kapodistrian University of Athens, Athens, Greece, [3]Structural and Valvular Center of Excellence, Marcus Heart Valve Center, Piedmont Heart Institute, Atlanta, GA, United States

Background: Mitral annular disjunction (MAD) refers to the arrhythmic mitral valve prolapse (MVP) syndrome associated with ventricular arrhythmias and sudden cardiac death. Although the pathophysiology of this disease is still under investigation, specific imaging criteria that establish the diagnosis have been recognized. In this article, we demonstrate most of these criteria using three-dimensional transthoracic echocardiography (3D-TTE) and provide added value in the management of MAD syndrome.
Case presentation: A 50-year-old male patient with recent syncope and a history of mitral regurgitation (MR) and MAD was admitted to our clinic for further investigation. According to our protocol, the patient underwent a complete 3D-TTE, laboratory blood exams, and 24 h ambulatory electrocardiogram (ECG). Our investigation confirmed the presence of MAD syndrome with bileaflet prolapse, severe MR, and non-sustained ventricular tachycardia, necessitating an implantable cardioverter defibrillator (ICD) and surgical mitral valve repair. The 3D-TTE analysis of the mitral valve demonstrated mitral annular systolic expansion and systolic flattening of the saddle-shaped annulus and quantified the extent of the disjunction arc. Additionally, four-dimensional (4D) strain analysis of the left ventricle revealed the presence of fibrosis of the posteromedial papillary muscle and basal inferolateral wall, which are variables that are required for the diagnosis and therapeutic management of MAD syndrome.
Conclusions: 3D-TTE and 4D strain offer valuable insights for diagnosing and managing patients with MAD syndrome. This method seems to correlate well with the other imaging modalities and could be included in the management protocol of MAD syndrome.

KEYWORDS

MAD syndrome, 4D strain, 3D echocardiography, arrhythmic mitral valve prolapse, case report

Introduction

MVP is one of the most common valvulopathies with a normally benign course. It affects 2%–3% of the general population and surgical repair is the gold standard treatment (1–3). Less than 1% of the patients with MVP present with malignant arrhythmias and experience sudden cardiac death (4, 5). Extent research from autopsies

has recognized an entity that correlates with ventricular arrhythmias called mitral annular disjunction (MAD). MAD is characterized by the separation of the hinge point of the posterior mitral leaflet from the posterior ventricular wall, systolic expansion and flattening of the annulus, curling motion of the basal inferolateral left ventricular (LV) wall, and the presence of segmental fibrosis of the posterior wall or the posteromedial papillary muscle (PM) (6, 7). The standard echocardiographic approach starts with a parasternal long-axis view for evaluation of the aforementioned findings. A distance of the posterior leaflet from the LV wall of >5 mm is considered pathognomonic for the presence of MAD. Typically, patients with MAD have Barlow's disease or bileaflet prolapse with myxomatous degeneration. Further TTE analysis should include tissue Doppler imaging for the "Pickelhaube" sign (high-velocity spike of the lateral mitral annulus, >16 cm/sec) and speckle tracking analysis for assessment of the mechanical dispersion of the LV (the standard deviation of contraction duration of LV segments, normal median values = 21 msec) (8, 9).

The gold standard method for diagnosing MAD syndrome is cardiac magnetic resonance imaging (CMR) due to its higher spatial resolution capable of detecting MAD of even >2 mm. Additionally, it can confirm the presence of fibrosis and scarring through late gadolinium enhancement (LGE) (10, 11). Echocardiography remains the first-line diagnostic method for patients with MVP. Several publications have already described the imaging findings of MAD using 3D transesophageal echocardiography (TEE), computed tomography (CT), and CMR (12–14). However, since 3D-TTE is less invasive than TEE and less costly than CMR and cardiac CT, it can be considered the preferred method when feasible. This study aims to give the methodology of how to evaluate the dynamic changes of mitral annulus in MAD syndrome with 3D-TTE and search for myocardial fibrosis with 4D strain. To our knowledge, this is the first described MAD case in the literature evaluated using 3D-TTE.

Case presentation

Patient clinical and echocardiographic characteristics

A 50-year-old male patient with mitral regurgitation (MR) and MAD previously diagnosed with CMR was referred to our clinic due to a recent syncopial episode. TTE revealed severely dilated left heart chambers (4D left ventricular end-diastolic volume (LVEDV) = 218 ml, left atrial volume index (LAVI) >48 ml/m^2) with an LVEF of 57%, bileaflet prolapse of the mitral valve, severe MR [effective regurgitant orifice area (EROA) 60 mm^2, regurgitant volume (RV) 117 ml], and a 12 mm displacement of the hinge point of the mitral annulus from the posterior ventricular wall (Figures 1A,B). Further complete 3D-TTE analysis of the patient was performed to demonstrate the imaging findings of MAD syndrome (Figures 1C,D). A previous CMR examination of the patient had reported LV dilatation with almost identical volumes and EF to TTE (EDV = 217 ml, EF = 59%), the presence of MAD of 10 mm displacement, and the presence of myocardial fibrosis of the basal inferolateral wall (Figure 2). Due to our protocol for patients with syncope, we performed a 24 h ambulatory electrocardiogram (ECG) that revealed episodes of monomorphic and polymorphic non-sustained ventricular tachycardia (Figure 2). In accordance with the management algorithm of the recently published EHRA and EACVI consensus document for MAD syndrome (15), the patient was treated with surgical mitral valve repair and implantable cardioverter defibrillator (ICD) implantation.

3D transthoracic echocardiography analysis

The 3D-TTE examination was performed with the GE Vivid E95 echo machine (GE Vingmed Ultrasound, Horten, Norway), using the 4Vc probe, and all data were stored in the EchoPAC v.203 workstation.

Advanced LV assessment and 4D strain analysis values were performed with the dedicated AutoLVQ application, using a full-volume apical four-chamber view, focused on the LV, with a frame rate of >25 vps. Global LV strain values were overall normal. The longitudinal strain was measured at −21%, circumferential strain at −20%, radial strain at 69%, and area strain at −40%. The strain values of the basal inferolateral segment were reduced, confirming the presence of the fibrosis detected in the MRI examination of the patient. The segmental radial strain was measured at 35% (normal values at 43.2 ± 4.5%), area strain at 24% (−36.5 ± 3.9%) (with adjacent segmental values of −47 and −56%), and circumferential strain at 18% (−30.3 ± 4.0%), while the longitudinal strain was preserved at −22% (−21 ± 0.6%) due to the hyperdynamic motion of the basal posterior wall (16) (Figure 3).

Advanced mitral valve assessment was performed with the AutoMVQ method that provided the measurements of the leaflets and the annulus, using an apical four-chamber view, focused on the mitral valve with 4D zoom and a frame rate of >12 vps. By default, AutoMVQ creates the mitral valve model using a middle reference frame between end-diastole and end-systole. Since the requested information for MAD syndrome is the dimension changes between diastole and systole, we had to manually adjust the systolic and diastolic frames twice and provide two different mitral valve quantification (MVQ) models. A direct comparison of the systolic and diastolic models allows us to understand the dynamic annulus changes in MAD syndrome. In our patient, this method confirmed (1) the flattening of the saddle-shaped annulus during the systole and (2) the systolic expansion. In particular, the annulus area increased from 14.6 cm^2 to 23.2 cm^2, the perimeter from 13.7 cm to 17.2 cm, the anteroposterior diameter from 3.4 cm to 4.8 cm, and the commissural diameter from 4.2 cm to 5.5 cm. Meanwhile, the annulus height decreased from 11.4 cm to 7.0 cm (Figure 4). The disjunction arc of the valve was easily demonstrated by an "en face" 3D ventricular view of the mitral valve where the extent of the arc was assessed by measuring the circumference of the posterior annulus involved within the disjunction. Volume

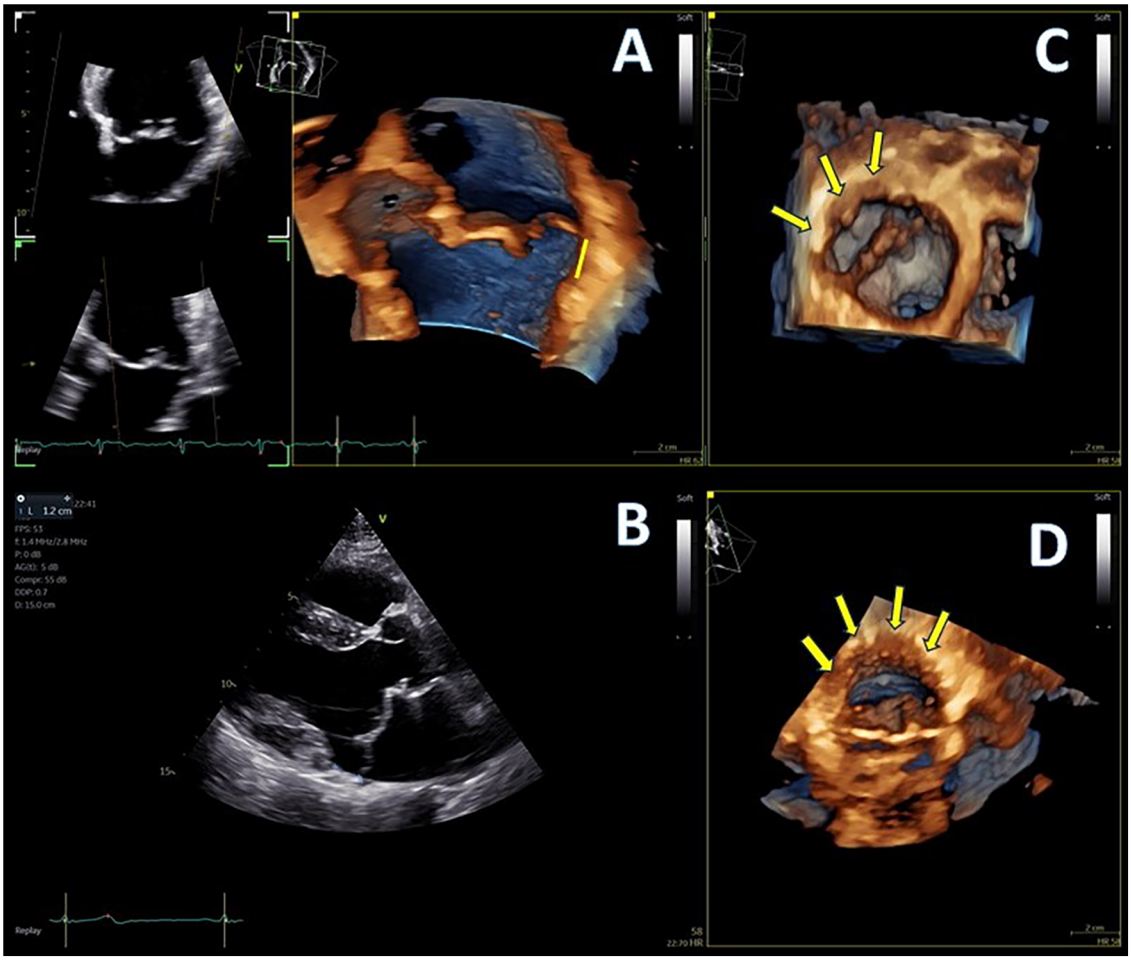

FIGURE 1
(A,B) Mitral annular disjunction (MAD) demonstrated by 4D and 2D transthoracic echocardiography (TTE), 12 mm of distance from posterior left ventricular (LV) wall, indicated with yellow line, and (C,D) extent of disjunction arc seen with two different orthogonal volume rendering views, indicated with yellow arrows.

rendering views can reveal the actual part of the free posterior wall of the left ventricle that is separated from the annulus and the atrium (Figures 1C,D).

Discussion

Recognition of MAD syndrome with myocardial fibrosis is of major importance, as it has been correlated with malignant arrhythmias and sudden cardiac death (4, 17). Patients with myxomatous mitral valve disease should be investigated for the presence of MAD (18). This information is also important when planning surgical repair for such patients, as the surgeon may need to use longer stitches and stabilize the annulus ring close to the posterior wall of the left ventricle (19, 20). The advantage of CMR with its high spatial resolution is the ability to simultaneously assess the morphology and the dynamics of the mitral valve, the volumes and performance of the left ventricle, and the presence of myocardial fibrosis (12, 13, 21). If it is feasible to appreciate most of these variables with the less invasive and costly 3D-TTE, then CMR might not be the first-line method in the future.

In this MAD case, we have presented the methodology of how to evaluate the dimensions and the dynamic changes of the mitral annulus with 3D-TTE. The MVQ method is widely recognized providing detailed information on the dimensions of the mitral valve, which correlates well with cardiac CT and has already proven its value in the management of MR (6, 22). 3D-TTE and 3D-TEE also correlate well (23), making transthoracic echocardiography reliable for giving accurate MVQ measurements. Previous published studies have only included MAD patients evaluated by TEE. Since our routine practice stands on transthoracic echocardiography and we aim to provide diagnosis with the minimum radiation exposure (instead of cardiac CT), cost (instead of CMR), and minimally invasive way (instead of TEE), 3D-TTE emerges as the most attractive alternative method. In our case, 3D-TTE was able to demonstrate most of the required imaging characteristics of MAD syndrome.

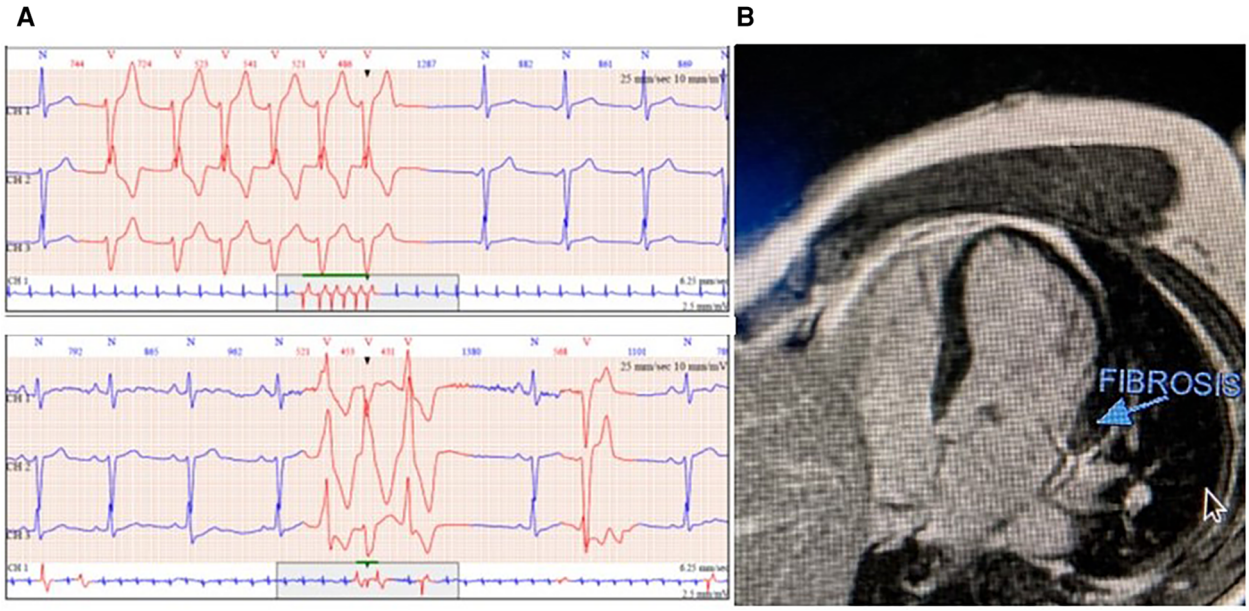

FIGURE 2
(A) Monomorphic and polymorphic ventricular tachycardia in 24 h ambulatory electrocardiogram (ECG) and (B) cardiac magnetic resonance imaging (CMR) with fibrosis detection of the basal inferolateral wall.

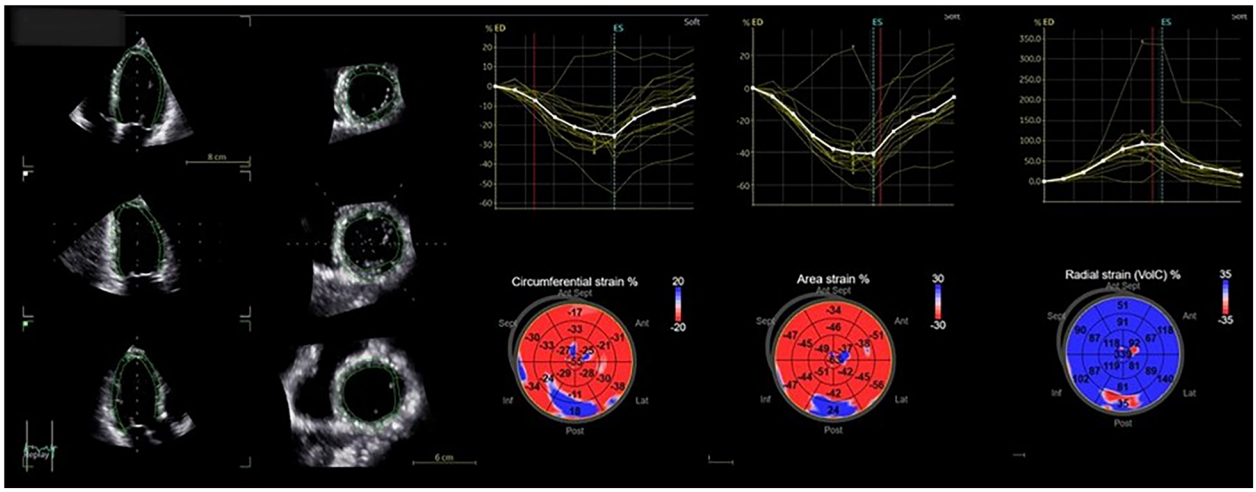

FIGURE 3
Four-dimensional strain analysis showing abnormal values of circumferential, area, and radial strain of the basal inferolateral wall.

A standard 2D parasternal long-axis view was the first image that was used to confirm the presence of MAD syndrome by the "uncoupling" of the posterior ventricular wall from the hinge point of the posterior mitral annulus. A distance of more than 5 mm is usually considered to be diagnostic for the presence of MAD (14). 3D-TTE was able to provide detailed information about the presence and extent of the disjunction arc, the systolic expansion, and the flattening of the saddle-shaped annulus. The extent of the disjunction arc correlates with the severity of MR and the abnormal dynamics of the valve (6). It is well established from previous publications (6, 13, 24) that at the end-diastole, the annulus dimensions are at their maximum, with the anteroposterior diameter and annulus area presenting the greater change. Physiologically, the annulus contracts rapidly at the early systole and then starts to expand. In normal subjects, the end-systolic annulus area is smaller than the end-diastolic one (6). Patients with myxomatous valve disease have larger annulus dimensions, the valve expands even more at the late-systolic

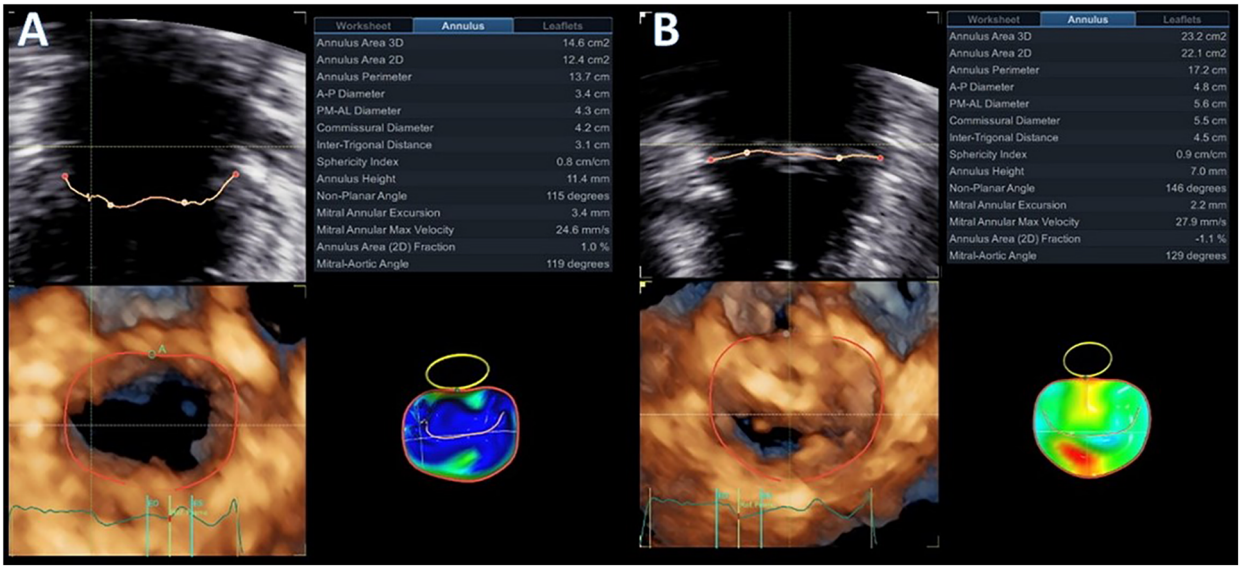

FIGURE 4
Diastolic (**A**) and systolic (**B**) mitral valve quantification (MVQ) models showing the dynamic changes and the systolic expansion and flattening of the mitral annulus.

period, but the overall annulus area does not reach the end-diastolic measurements (6, 25). In MAD syndrome, on the other hand, the baseline dimensions of the annulus are increased. There is still early systolic contraction of the valve, but, afterward, there is overexpansion of the annulus, with dimensions that exceed the diastolic ones (25). Manual adjustments of the standard MVQ methodology were able to appreciate the systolic expansion and flattening of the annulus by measuring all annulus dimensions and height changes throughout the cardiac cycle. The two frames that we used were the end-diastolic and end-systolic ones to be in agreement with previous publications that analyzed the annulus dynamics.

The 4D strain method was further used to give information about the presence of ventricular myocardial fibrosis and was included in the management algorithm of the patient (26). Segmental basal inferolateral wall strain values were significantly reduced especially the area strain which is a parameter that can be evaluated only with 4D strain. Since in MAD there is segmental hypercontractility of the basal inferolateral wall, 2D strain/speckle tracking evaluation of longitudinal strain is of limited value as longitudinal deformation is increased in this part of the LV and radial and circumferential 2D strain values are not reproducible since it is easy to make errors due to variable/off axis plane selection and through-plane motion (27). 4D strain, on the other hand, can simultaneously provide measurements for longitudinal, radial, circumferential, and area strain. In our patient, except for the longitudinal strain, which was unaffected, the presence of fibrosis and the systolic stretching of the basal inferolateral wall resulted in the reduction of the radial strain values and in positive values of circumferential and area strain that confirmed the presence of fibrosis and the lengthening of the fibers during systole due to the disjunction arc. From this point of view, 4D strain seems superior and may be the only echocardiographic method that can detect myocardial abnormalities in MAD cases. A limitation of this method that probably still makes CMR the gold standard diagnostic tool is the inability to detect fibrotic tissue on the posteromedial PM. Strain analysis by default excludes papillary muscles from tracking, and it is impossible with the present applications of 4D strain to extend our analysis to the PM.

Limitations

It has to be mentioned that this specific patient had excellent 2D and 3D images, which made possible all this extensive analysis of the annulus dimensions and dynamics. This method might have unreliable results in the case of suboptimal imaging and low frame rate acquisitions. It is common knowledge that we cannot provide reliable 3D volume-rendered images without decent baseline 2D images. Frame rate, on the other hand, is also very important since we need to determine precisely the true end-diastolic and end-systolic frame. Frame rate furthermore affects the 4D strain analysis. For accurate results, we need >25 volumes per second (vps), but this number is even quite low for information like mechanical dispersion. Mechanical dispersion analysis requires >50 vps; otherwise, the measurements in milliseconds will not be accurate. Currently, with the provided technology it is difficult to acquire full-volume images of the left ventricle, including the epicardial layer, with high frame rates. Next-generation vendors and the evolvement of the probes may overcome this issue.

Another restriction of this approach is the time that is needed for this extensive analysis. Previous publications have shown that

3D-TTE is a time-saver (28) and does not necessarily require big experience. However, the imager should be familiar with the MVQ application and 4D strain analysis in order to be able to include this approach in routine practice. Since MAD is not present in everyday practice though, in our opinion, it is worth it to spend some time on this detailed 3D analysis.

Conclusions

The MAD syndrome is not yet fully investigated. The first important step for the management of these patients is correct diagnosis. A complete 2D/3D-TTE protocol seems to be able to describe most of the required imaging features of this disease and detect the presence of fibrosis. This is the first MAD case in the literature, analyzed with 3D-TTE with results confirmed with CMR. Even though our initial experience is promising, this remains one single case reported and further investigation should be done to validate the method and routinely include 3D-TTE in our diagnostic protocols.

Data availability statement

The raw data supporting the conclusions of this article will be made available by the authors, without undue reservation.

Ethics statement

Written informed consent was obtained from the individual(s) for the publication of any potentially identifiable images or data included in this article.

Author contributions

KP: Conceptualization, Investigation, Methodology, Writing – original draft, Writing – review and editing. II: Methodology, Supervision, Writing – review and editing. MV: Conceptualization, Investigation, Methodology, Supervision, Writing – review and editing.

Funding

The authors declare that no financial support was received for the research, authorship, and/or publication of this article.

Conflict of interest

The authors declare that the research was conducted in the absence of any commercial or financial relationships that could be construed as a potential conflict of interest.

The authors declared that they were an editorial board member of Frontiers, at the time of submission. This had no impact on the peer review process and the final decision.

Publisher's note

References

1. Wu S, Siegel RJ. Mitral annular disjunction: a case series and review of the literature. *Front Cardiovasc Med*. (2022) 9:976066. doi: 10.3389/fcvm.2022.976066

2. Freed LA, Levy D, Levine RA, Larson MG, Evans JC, Fuller DL, et al. Prevalence and clinical outcome of mitral-valve prolapse. *N Engl J Med*. (1999) 341(1):1–7. doi: 10.1056/NEJM199907013410101

3. Dziadzko V, Dziadzko M, Medina-Inojosa JR, Benfari G, Michelena HI, Crestanello JA, et al. Causes and mechanisms of isolated mitral regurgitation in the community: clinical context and outcome. *Eur Heart J*. (2019) 40(27):2194–202. doi: 10.1093/eurheartj/ehz314

4. Basso C, Iliceto S, Thiene G, Perazzolo Marra M. Mitral valve prolapse, ventricular arrhythmias, and sudden death. *Circulation*. (2019) 140(11):952–64. doi: 10.1161/CIRCULATIONAHA.118.034075

5. Miller MA, Dukkipati SR, Turagam M, Liao SL, Adams DH, Reddy VY. Arrhythmic mitral valve prolapse: JACC review topic of the week. *J Am Coll Cardiol*. (2018) 72(23 Pt A):2904–14. doi: 10.1016/j.jacc.2018.09.048

6. Lee AP, Jin CN, Fan Y, Wong RHL, Underwood MJ, Wan S. Functional implication of mitral annular disjunction in mitral valve prolapse: a quantitative dynamic 3D echocardiographic study. *JACC Cardiovasc Imaging*. (2017) 10 (12):1424–33. doi: 10.1016/j.jcmg.2016.11.022

7. Faletra FF, Leo LA, Paiocchi VL, Schlossbauer SA, Pavon AG, Ho SY, et al. Morphology of mitral annular disjunction in mitral valve prolapse. *J Am Soc Echocardiogr*. (2022) 35(2):176–86. doi: 10.1016/j.echo.2021.09.002

8. van Wijngaarden AL, de Riva M, Hiemstra YL, van der Bijl P, Fortuni F, Bax JJ, et al. Parameters associated with ventricular arrhythmias in mitral valve prolapse with significant regurgitation. *Heart*. (2021) 107(5):411–8. doi: 10.1136/heartjnl-2020-317451

9. Aagaard EN, Kvisvik B, Pervez MO, Lyngbakken MN, Berge T, Enger S, et al. Left ventricular mechanical dispersion in a general population: data from the Akershus cardiac examination 1950 study. *Eur Heart J Cardiovasc Imaging*. (2020) 21 (2):183–90. doi: 10.1093/ehjci/jez210

10. Dejgaard LA, Skjølsvik ET, Lie ØH, Ribe M, Stokke MK, Hegbom F, et al. The mitral annulus disjunction arrhythmic syndrome. *J Am Coll Cardiol*. (2018) 72 (14):1600–9. doi: 10.1016/j.jacc.2018.07.070

11. Basso C, Perazzolo Marra M. Mitral annulus disjunction: emerging role of myocardial mechanical stretch in arrhythmogenesis. *J Am Coll Cardiol*. (2018) 72 (14):1610–2. doi: 10.1016/j.jacc.2018.07.069

12. Mantegazza V, Volpato V, Gripari P, Ghulam Ali S, Fusini L, Italiano G, et al. Multimodality imaging assessment of mitral annular disjunction in mitral valve prolapse. *Heart*. (2021) 107(1):25–32. doi: 10.1136/heartjnl-2020-317330

13. Levack MM, Jassar AS, Shang EK, Vergnat M, Woo YJ, Acker MA, et al. Three-dimensional echocardiographic analysis of mitral annular dynamics: implication for annuloplasty selection. *Circulation*. (2012) 126(11 Suppl 1):S183–8. doi: 10.1161/CIRCULATIONAHA.111.084483

14. Toh H, Mori S, Izawa Y, Fujita H, Miwa K, Suzuki M, et al. Prevalence and extent of mitral annular disjunction in structurally normal hearts: comprehensive 3D analysis using cardiac computed tomography. *Eur Heart J Cardiovasc Imaging*. (2021) 22(6):614–22. doi: 10.1093/ehjci/jeab022

15. Sabbag A, Essayagh B, Barrera JDR, Basso C, Berni A, Cosyns B, et al. EHRA expert consensus statement on arrhythmic mitral valve prolapse and mitral annular

disjunction complex in collaboration with the ESC council on valvular heart disease and the European association of cardiovascular imaging endorsed cby the heart rhythm society, by the Asia pacific heart rhythm society, and by the Latin American heart rhythm society. *Europace*. (2022) 24(12):1981–2003. doi: 10.1093/europace/euac125

16. Bernard A, Addetia K, Dulgheru R, Caballero L, Sugimoto T, Akhaladze N, et al. 3D echocardiographic reference ranges for normal left ventricular volumes and strain: results from the EACVI NORRE study. *Eur Heart J Cardiovasc Imaging*. (2017) 18 (4):475–83. doi: 10.1093/ehjci/jew284

17. Essayagh B, Sabbag A, Antoine C, Benfari G, Batista R, Yang LT, et al. The mitral annular disjunction of mitral valve prolapse: presentation and outcome. *JACC Cardiovasc Imaging*. (2021) 14(11):2073–87. doi: 10.1016/j.jcmg.2021.04.029

18. Toh H, Mori S, Izawa Y, Toba T, Watanabe Y, Kono AK, et al. Varied extent of mitral annular disjunction among cases with different phenotypes of mitral valve prolapse. *JACC Case Rep*. (2021) 3(10):1251–7. doi: 10.1016/j.jaccas.2021.06.038

19. Gray R, Indraratna P, Cranney G, Lam H, Yu J, Mathur G. Mitral annular disjunction in surgical mitral valve prolapse: prevalence, characteristics and outcomes. *Echo Res Pract*. (2023) 10(1):21. doi: 10.1186/s44156-023-00032-x

20. Maffessanti F, Marsan NA, Tamborini G, Sugeng L, Caiani EG, Gripari P, et al. Quantitative analysis of mitral valve apparatus in mitral valve prolapse before and after annuloplasty: a three-dimensional intraoperative transesophageal study. *J Am Soc Echocardiogr*. (2011) 24(4):405–13. doi: 10.1016/j.echo.2011.01.012

21. Perazzolo Marra M, Basso C, De Lazzari M, Rizzo S, Cipriani A, Giorgi B, et al. Morphofunctional abnormalities of mitral annulus and arrhythmic mitral valve prolapse. *Circ Cardiovasc Imaging*. (2016) 9(8):e005030. doi: 10.1161/CIRCIMAGING.116.005030

22. Coisne A, Pontana F, Aghezzaf S, Mouton S, Ridon H, Richardson M, et al. Utility of three-dimensional transesophageal echocardiography for mitral annular sizing in transcatheter mitral valve replacement procedures: a cardiac computed tomographic comparative study. *J Am Soc Echocardiogr*. (2020) 33(10):1245–1252.2. doi: 10.1016/j.echo.2020.04.030

23. Papadopoulos K, Ikonomidis I, Özden Ö, Tzikas A, Arampatzis CA, Vannan MA. Level of agreement between three-dimensional transthoracic and transesophageal echocardiography for mitral annulus evaluation: a feasibility and comparison study. *Echocardiography*. (2022) 39(12):1512–21. doi: 10.1111/echo.15481

24. Apor A, Nagy AI, Kovács A, Manouras A, Andrássy P, Merkely B. Three-dimensional dynamic morphology of the mitral valve in different forms of mitral valve prolapse—potential implications for annuloplasty ring selection. *Cardiovasc Ultrasound*. (2016) 14(1):32. doi: 10.1186/s12947-016-0073-4

25. Essayagh B, Mantovani F, Benfari G, Maalouf JF, Mankad S, Thapa P, et al. Mitral annular disjunction of degenerative mitral regurgitation: three-dimensional evaluation and implications for mitral repair. *J Am Soc Echocardiogr*. (2022) 35 (2):165–75. doi: 10.1016/j.echo.2021.09.004

26. Muraru D, Cucchini U, Mihăilă S, Miglioranza MH, Aruta P, Cavalli G, et al. Left ventricular myocardial strain by three-dimensional speckle-tracking echocardiography in healthy subjects: reference values and analysis of their physiologic and technical determinants. *J Am Soc Echocardiogr*. (2014) 27 (8):858–871.1. doi: 10.1016/j.echo.2014.05.010

27. Marwick TH, Leano RL, Brown J, Sun JP, Hoffmann R, Lysyansky P, et al. Myocardial strain measurement with 2-dimensional speckle-tracking echocardiography: definition of normal range. *JACC Cardiovasc Imaging*. (2009) 2 (1):80–4. doi: 10.1016/j.jcmg.2007.12.007

28. Miranda Castilho B, Campos G, Almeida J, Veiga R, Coelho C, Cotrim N, et al. Fully automated 3D echocardiographic algorithms: accurate and time saving—the answer for 3D in routine clinical practice? *Eur Heart J Cardiovasc Imaging*. (2023) 24(Supplement_1):jead119.143. doi: 10.1093/ehjci/jead119.143

Frontiers in
Cardiovascular Medicine

Innovations and improvements in cardiovascular treatment and practice

Focuses on research that challenges the status quo of cardiovascular care, or facilitates the translation of advances into new therapies and diagnostic tools.

Discover the latest Research Topics

See more →

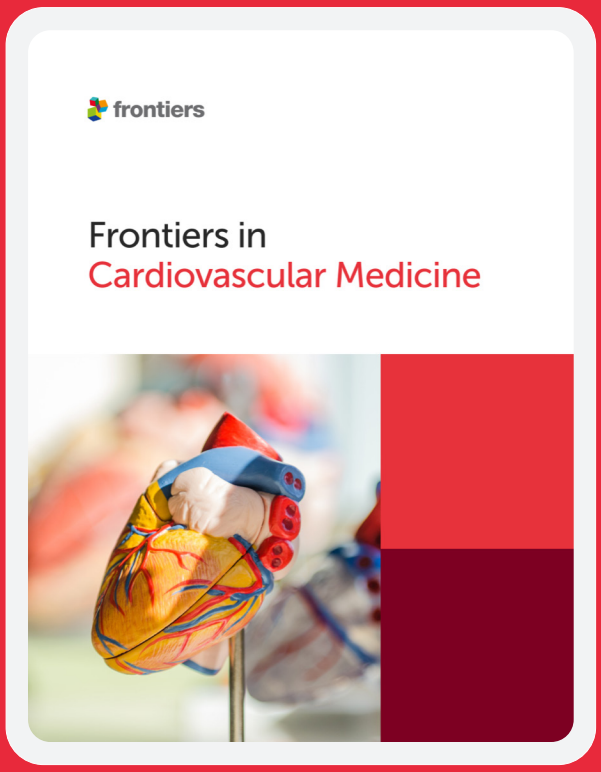

Frontiers

Avenue du Tribunal-Fédéral 34
1005 Lausanne, Switzerland
frontiersin.org

Contact us

+41 (0)21 510 17 00
frontiersin.org/about/contact